Ruthenium Arene Anticancer Complexes

A Thesis Submitted for the Degree of Doctor of Philosophy

by

Tijana Bugarčić

School of Chemistry
Faculty of Science and Engineering
The University of Edinburgh

November 2008

"Alice opened the door and found that it led into a small passage, not much larger than a rat-hole: she knelt down and looked along the passage into the loveliest garden you ever saw. How she longed to get out of that dark hall, and wander about among those beds of bright flowers and those cool fountains, but she could not even get her head though the doorway; 'and even if my head would go through,' thought poor Alice, 'it would be of very little use without my shoulders. Oh, how I wish I could shut up like a telescope! I think I could, if I only know how to begin.' For, you see, so many out-of-the-way things had happened lately, that Alice had begun to think that very few things indeed were really impossible."

from "Alice's Adventures in Wonderland"

by Lewis Carroll

Abbreviations

A	Adenine
ADF	Amsterdam Density Functional
ATD	Arrival Time Distribution
a.u.	atomic unit
bip	biphenyl
bipy	2,2′-bipyridine
bz	benzene
C	Cytosine
ca.	circa (about)
CCDC	Cambridge Crystallographic Data Center
CCS	Collision Cross Section
CD	Circular Dichroism
cisplatin	*cis*-diamminedichloroplatinum(II)
COSMO	COnductor-like Screening MOdel
Cp	Cyclopentadiene
CT	Calf Thymus
dha	dihydroanthracene
dien	diethylenetriamine
DFT	Density Functional Theory
dmpda	4,5-dimethyl-*ortho*-phenylenediamine
DMSO	Dimethyl Sulfoxide
DNA	Deoxyribonucleic acid

EDTA	Ethylenediaminetetraacetic acid
en	ethylenediamine
ESI	Electro-Spray Ionization
EtBr	Ethidium bromide
FAAS	Flameless Atomic Absorption Spectrometry
G	Guanine
GGA	Generalized Gradient Approximation
GSH	Glutathione
GSSG	oxidized glutathione
hha	hexahydroanthracene
hmb	hexamethylbenzene
HMG	High Mobility Group
IC_{50}	50% inhibitory concentration
ICD	Induced Circular Dichroism
ind	indane
IM	Ion Mobility
MS	Mass Spectrometry
m-terp	*meta*-terphenyl
N-MeIm	N-methylimidazole
NMR	Nuclear Magnetic Resonance
o-bqdi	*ortho*-bezoquinonediimine
o-pda	*ortho*-phenylenediamine
o-sqdi	*ortho*-semiquinonediimine

pda	1,3-propylenediamine
p-cym	*para*-cymene
phen	phenanthralene
ppm	parts per million
p-terp	*para*-terphenyl
SCF	Self-Consistent Field
T	Thymine
tha	tetrahydroanthracene
THF	Tetrahydrofuran
thn	tetrahydronaphthalene
t_m	melting temperature
UV-VIS	Ultraviolet-Visible
VDD	Veronoi Deformation Density
WATERGATE	WATER suppression by GrAdient Tailored Excitation
ZORA	Zero-Order Regular Approximation
9-EtG	9-Ehtylguanine

Abstract

Organoruthenium complexes of the type $[(\eta^6\text{-arene})Ru^{II}(YZ)Cl]^+$, where the arene is benzene or a benzene derivative, and YZ = chelating ligand exhibit anticancer activity, including activity against cisplatin resistant cancer cells. This thesis is concern with synthesis and characterization of novel Ru^{II} arene anti-cancer complexes, containing different arenes and chelating ligands (YZ). The mechanism of action and cytotoxic activity of these complexes are investigated.

Synthesis and characterization of complexes of the type $[(\eta^6\text{-arene})Ru(en)Cl]^+$, where the arene is *ortho-* , *meta-* or *para*-terphenyl (*o*-, *m*- or *p*-terp) are reported. $[(\eta^6\text{-}p\text{-terp})Ru(en)Cl]^+$ has a similar potency to cisplatin and much higher activity, against cancer cell lines, than *o*- and *m*-terp analogues. *p*-Terp complex binds to DNA rapidly and quantitatively and the experimental data are consistent with combined intercalative and monofunctional (coordination) binding mode of $[(\eta^6\text{-}p\text{-terp})Ru(en)Cl]^+$. The *o*- and *m*-terp analogues bind to DNA preferentially through the coordination. The *o*- and *m*-terp complexes have similar collision cross-sections as a result of similarities in size and shape. Therefore it is difficult to separate them using ion-mobility in combination with mass spectrometry. Both *o*- and *m*-terp complexes could be separated from the *p*-terp analogue.

The synthesis and characterization of Ru^{II} arene complexes containing 2,2′-bipyridine (bipy), 2,2′-bipyridine-3,3′-diol ($bipy(OH)_2$) or deprotonated 2,2′-bipyridine-3,3′-diol (bipy(OH)O) as chelating ligands and different arenes are reported as well, including several x-ray crystal structures. In aqueous solution only deprotonated (bipy(OH)O) form of the 2,2′-bipyridine-3,3′-diol are present. Hydrolyses of these complexes are relatively fast and when the arene is biphenyl, initial aquation is followed by partial

arene loss. Complexes with bipy(OH)O as chelating ligands, in general exhibit good cytotoxicity towards A2780 human ovarian cancer cells. These activity data can be contrasted with those of the parent bipy complex [(η^6-tha)Ru(bipy)Cl][PF_6], where tha = tetrahydroanthracene, which is inactive towards A2780 cells (IC_{50} > 100 μM). However [(η^6-ind)Ru(bipy(OH)$_2$)Cl][PF_6] and [(η^6-ind)Ru(bipy)Cl][PF_6], where ind = indane, bind only weakly to DNA and therefore DNA may not be the major target for these complexes.

Loss of cytotoxic activity was observed for Ru^{II} arene complexes containing different arenes, halides and *o*-phenylenediamine (*o*-pda) or *o*-benzoquinonediimine (*o*-bqdi) as chelating ligands, going from the amine complexes to its oxidized (imine) form (e.g. IC_{50} = 11 μM for [(η^6-*p*-cym)Ru(*o*-pda)Cl][PF_6] and IC_{50} > 100 μM for [(η^6-hmb)Ru(*o*-bqdi)Cl][PF_6], where *p*-cym = *para*-cymene and hmb = hexamethylbenzene, against A2780 cells). The loss of activity is contributed to the absence of hydrolysis or to the formation of the less stable adducts with 9-ethylguanine (9-EtG), which leads to the weakened binding to DNA. The x-ray crystal structures of [(η^6-*p*-cym)Ru(*o*-pda)Cl][PF_6] and [(η^6-hmb)Ru(*o*-bqdi)Cl][PF_6] are reported and their differences discussed.

Acknowledgments

I would like to thank my supervisor Professor Peter J. Sadler for giving me the opportunity to work in his group, supporting and leading me through my PhD. I would like to thank Professor Sadler for all his understanding and kindness. It has been a great pleasure to work for Professor Sadler, in the supportive and encouraging environment of his research group.

Very special thanks to Dr Abraha Habtemariam for all his support, motivation and encouragement, for all the useful discussions and for being a great friend. Without Dr Habtemariam's support the years of my PhD would have been a lot harder and less productive.

I would also like to thank all the other past and present members of the group, especially Dr Ana M. Pizarro, Dr Sarah Dougan and Dr Arindam Mukherjee for all their help and support during the past years. Thanks to Dr. Pieter C. A. Bruijnincx for all the useful discussions and special thanks for the help with PyMOL and all the other programs I was not familiar with.

Thanks to Professor Simon Parsons and his research group for solving all the crystal structures I used in my thesis. I would like to thank Professor Robert J. Deeth, Hui-Chung Tai and Dr Luca Salassa for all their help with molecular modeling. Special thanks to Dr Jonathan P. Williams and Kevin Gilles for carrying out the ion mobility experiments.

I would also like to thank Professor Viktor Brabec for his support during my stay in Brno (CR). Thanks to all the members of Professor Brabec's research group, especially to Dr Olga Novakova for all her patience and help.

I would like to thank Oncosence Ltd., Professor Viktor Brabec's group (Brno, CR) and Sabine van Rijt (Warwick University) for the cytotoxicity tests.

Finally I would like to thank my parents, my brother Filip and my sister Ivana, as well as all my friends for all their love and encouragement. A special thanks to Marc for all his patience and support.

At the end I would like to thank Oncosence Ltd., Overseas Research Students Awards Scheme (ORS), University of Edinburgh and Warwick University for financial support. A special thanks to COST Action D39 for financial support during my stay in Brno (CR).

Contents

Abbreviations.....iii

Abstract..... vi

Declaration.....viii

Acknowledgments.....ix

Contents.....xi

Chapter 1: Introduction.....1

1.1 Metals in medicine.....2

1.1.1 Metal-based drugs.....3

1.2 Statistics and history of cancer.....4

1.3 Platinum-based anticancer drugs.....4

1.4 Other metal based anti-cancer drugs.....5

1.5 Mechanism of action of cisplatin.....6

1.5.1 Apoptosis.....9

1.6 Ruthenium chemistry.....9

1.7 Ruthenium antitumour agents.....10

1.7.1 Ru^{III} complexes in clinical trials.....11

1.8 Ru^{II} arene anticancer complexes.....13

1.8.1 Hydrolyses of Ru^{II} arene complexes.....15

1.8.2 Interactions of Ru^{II} arene complexes with 9-ethylguanine (9-EtG).....17

1.8.3 Interaction of Ru^{II} arene complexes with oligonucleotides.....18

1.9 DNA binding of Ru^{II} arene complexes.....20

1.9.1 DNA as a potential target site.....20

1.9.2 Interaction with CT DNA.....20

1.9.3 Unwinding of plasmid DNA.....21

1.9.4 Melting of CT DNA.....22

1.9.5 Fluorescence experiments.....23

1.9.6 Circular dichroism.....23

1.10 Aims.....24

1.11 References.....25

Chapter 2: Experimental Section.....30

2.1 Instrumentation and techniques.....31

2.1.1 Nuclear magnetic resonance (NMR) spectroscopy.....31

2.1.1.1 Nuclear magnetism.....31

2.1.1.2 Chemical shift.....32

2.1.1.3 Pulsed-field gradients.....34

2.1.1.4 Experimental methods.....35

2.1.2 Ultraviolet-visible (UV-Vis) and fluorescence spectroscopy.....35

2.1.2.1 Experimental methods.....38

2.1.3 Electrospray ionization mass spectrometry (ESI-MS).....38

2.1.3.1 Experimental methods.....39

2.1.4 Elemental analysis.....39

2.1.4.1 Experimental methods.....39

2.1.5 X-ray crystallography.....40

2.1.5.1 Experimental methods.....40

2.1.6 Circular dichroism (CD).....40

2.1.6.1 CD of DNA.....41

2.1.6.2 Experimental methods.....42

2.1.7 Atomic absorption spectrometry (AAS).....42

2.1.7.1 Experimental methods.....43

2.1.8 Molecular modelling.....43

2.1.8.1 Density Functional Theory (DFT).....43

2.1.8.2 The Amsterdam Density Functional (ADF) program.....44

2.1.8.3 Experimental methods.....46

2.1.9 Cancer cell growth inhibition.....46

2.2 Synthesis and characterization of starting materials.....47

2.2.1 Materials.....47

2.2.2 Birch reduction.....47

2.2.3 Preparation of dimers.....53

2.3 References.....56

Chapter 3: Terphenyl Ru^{II} complexes.....58

3.1 Introduction.....59

3.2 Experimental section.....61

3.2.1 Materials.....61

3.2.2 Preparation of complexes.....62

3.2.3 X-ray crystallography.....64

3.2.4 Cytotoxicity.....65

3.2.5 Cellular ruthenium complex uptake.....66

3.2.6 Metalation reactions in cell-free media.....66

3.2.7 Fluorescence measurements.....67

3.2.8 DNA melting.....67

3.2.9 *Unwinding of negatively supercoiled DNA*.....68

3.2.10 *Other Physical Methods*.....68

3.3 ***Results***.....69

3.3.1 *Synthesis and characterization*.....69

3.3.2 *Crystal structures*.....72

3.3.3 *Cytotoxicity*.....78

3.3.4 *Cellular ruthenium complex uptake*.....79

3.3.5 *DNA binding in cell-free media*.....80

3.3.5.1 Kinetics of binding to calf thymus (CT) DNA.....81

3.3.5.2 Circular Dichroism (CD).....82

3.3.5.3 Ethidium bromide (EtBr) fluorescence.....86

3.3.5.4 DNA melting.....88

3.3.5.5 Unwinding of supercoiled DNA.....90

3.4 ***Discussion***.....92

3.5 ***Summary***.....98

3.6 ***References***.....99

Chapter 4: Bipyridine Ru^{II} arene complexes.....102

4.1 ***Introduction***.....103

4.2 ***Experimental section***.....105

4.2.1 *Materials*.....105

4.2.2 *Synthesis of ruthenium complexes*.....106

4.2.3 *X-ray crystallography*.....112

4.2.4 *pH measurement*.....114

4.2.5 *Hydrolysis*.....114

4.2.6 *Rate of arene loss*.....115

4.2.7 *Computation*.....115

4.2.8 *Metallation reactions*.....116

4.2.9 *Circular dichroism (CD)*.....116

4.2.10 *DNA melting*.....117

4.2.11 *Fluorescence measurements*.....117

4.3 ***Results***.....118

4.3.1 *Synthesis and characterization*.....118

4.3.2 *Crystal structures*.....120

4.3.3 *pH dependence*.....129

4.3.4 *Aqueous solution chemistry*.....129

4.3.5 *Interactions with 9-EtG*.....133

4.3.6 *Computation*.....135

4.3.7 *Cancer cell growth inhibition*.....137

4.3.8 *Binding to calf thymus (CT) DNA*.....139

4.3.8.1 Kinetics of binding.....139

4.3.8.2 Circular dichroism (CD).....140

4.3.8.3 DNA melting.....142

4.3.8.4 Ethidium bromide (EtBr) fluorescence.....142

4.4 ***Discussion***.....144

4.5 ***Summary***.....151

4.6 ***References***.....153

Chapter 5: Ru^{II} arene complexes with redox active diamine ligands.....157

5.1 ***Introduction***.....158

5.2 ***Experimental section***.....159

5.2.1 *Materials*.....159

5.2.2 *Synthesis of ruthenium complexes*.....160

5.2.3 *X-ray crystallography*.....163

5.2.4 *Hydrolysis*.....164

5.2.5 *Oxidation in methanol*.....164

5.2.6 *Reaction with GSH*.....165

5.2.7 *Computation*.....165

5.3 ***Results***.....166

5.3.1 *Syntheses and characterization*.....166

5.3.2 *Crystal structures*.....168

5.3.3 *Ligand based-oxidation*.....173

5.3.4 *Aquation*.....176

5.3.5 *Reaction with GSH*.....182

5.3.6 *Computation*.....184

5.3.7 *Cytotoxicity*.....186

5.4 ***Discussion***.....188

5.5 ***Summary***.....196

5.6 ***References***.....197

Chapter 6: Isomer separation by ion mobility mass spectrometry.....200

6.1 ***Introduction***.....201

6.1.1 *Ruthenium(II) terphenyl complexes*.....201

6.1.2 *Mass Spectrometry (MS)*.....202

6.1.3 *Ion mobility (IM)*.....203

6.1.4 Ion mobility (IM) in combination with mass spectrometry (MS) 203

6.2 Experimental Section.....206

6.2.1 Preparation of Complexes.....206

6.2.2 Preparation of samples.....207

6.2.3 Hybrid quadrupole/ion mobility/oa-ToF MS instrumentation.....207

6.2.4 Estimation of collision cross-section (CCS) measurement using the T-Wave based ion mobility device.....208

6.3 Results.....209

6.4 Discussion.....212

6.5 Summary.....213

6.6 References.....214

Chapter 7: Conclusions and Future work.....216

7.1 Conclusions.....217

7.2 Future work.....220

7.2.1 DNA structural distortion induced by terphenyl Ru^{II} arene complexes.....220

7.2.2 Sandwich bis-p-terp complex.....221

7.2.3 Dinuclear terphenyl complexes.....221

7.2.4 Cellular uptake studies of bipyridine complexes.....222

7.2.5 o-Semiquinonediimine (o-sqdi) as a possible intermediate in the oxidation of o-phenylenediamine.....223

7.2.5.1 Detection of the *o*-sqdi species.....223

7.2.5.2 The ability of *o*-phenylenediamine (*o*-pda) complexes to overcome cross-resistance towards A2780AD cell line.....224

7.2.6 Dinuclear mixed valent Ru complexes.....225

7.3 References.....226

Conferences attended.....228

Publications.....228

Chapter 1

Introduction

"There is no subject so old that something new cannot be said about it."

Fyodor Dostoyevsky

This thesis is concerned with the synthesis and characterization of Ru^{II} arene `piano-stool` complexes and their potential application as anti-cancer agents. The focus of this work is on development of structure-activity relationships with the view to design more promising anticancer agents. The focus of this Chapter is on general chemistry of ruthenium (Ru) and its complexes. Metal-based drugs used in the treatment of cancer are discussed as well.

1.1 Metals in medicine

The elements thought to be essential for human life are: H, C, N, O, F, Na, Mg, Si, P, S, Cl, K, Ca, V, Mn, Fe, Co, Ni, Cu, Zn, Se, Mo, Sn, and I. Still some of these biochemically essential elements can be toxic at high doses.

Metal excesses (poisonings) as well as deficiencies have been of a particular interest in medicine and health science disciplines for a long period of time.[1] Metals are not biodegradable and their toxicity determination is a problem caused by a complex nature of interactions of metals with biological systems.[2] Use of metals in medicine traces back in antiquity, and began with the use of Fe, Au and As in the treatment of different chronic dieses. However there is a subtle balance between the therapeutic benefit on the one hand and the side-effects on the other hand.

1.1.1 Metal-based drugs

The wide range of coordination numbers and geometries, as well as the wide range of accessible oxidation states and thermodynamic as well as kinetic characteristics of metal ions, leads to metal-based compounds offering possibilities for design of therapeutic agents. Therefore medicinal inorganic chemistry is an expanding field and discoveries in inorganic and bioinorganic chemistry have had a significant impact on modern clinical medicine.

In modern times, the first metal-based drug to find use in medicine was an arsenical, Salvarsan, used in the treatment of syphilis.[3] The later availability of penicillin made this drug redundant.

Therapeutic applications of metal compounds, such as the use of platinum complexes in cancer chemotherapy, gallium in hypercalcemia, bismuth as anti-ulcer medication, and sodium nitroprusside in hypertension have been described previously, as well as the use of metal radionuclides in diagnosis and radiotherapy and paramagnetic metal complexes as contrast agents in magnetic resonance imaging.[4]

Li salts are used in neurological disorders[1] and Au drugs have proven effectiveness in treating rheumatoid and psoriatic arthritis as well as bronchial asthma.[5] Vanadium compounds have been studied for use as insulin mimetics for treating diabetes.[6] Medical use of Co, Cs and Ra as gamma ray-emitters in radiotherapy for cancer, the use of Ag for treatment of burns and Hg in the form of calomel ointment as an antiseptic have been described.[1]

1.2 Statistics and history of cancer

Cancer is thought to be an old disease. Scientists now a day think that even dinosaurs may have had cancer. From looking at the remains of Egyptian mummies it has been found that they suffered from cancer as well.[7] The word cancer comes from the ancient Greek language and means crab. The Greeks thought that clusters of cancer cells looked like the legs of a crab.

Cancer is a second leading cause of death, after heart diseases, in the United States.[8] All type of cancers display characteristic uncontrolled cell division and these cells have the ability to invade healthy tissues. There are around 200 different types of cancer. Some are very common, others are rare. Development of cancer involves a series of complex mechanisms related to a genetic make up and exposure to certain risks.

1.3 Platinum-based anticancer drugs

The discovery of the biological activity of cisplatin[9] was followed by the extensive use of the drug in cancer chemotherapy. Cisplatin is highly effective in the treatment of testicular cancer, with a 90% cure-rate.[10] The use of cisplatin is restricted by its side-effects, which include nephrotoxicity, neurotoxicity and emetogenesis.

The most widely used drugs for treatment of various types of cancers are platinum-based drugs. A limiting factor in the use of platinum based drugs is resistance of cells to these drugs being developed with time.[11] More than 3000 platinum compounds have been synthesized and tested for biological activity.[12] Only four platinum drugs are registered as marketed drugs. These are cisplatin, carboplatin, oxaliplatin and

nedaplatin (Figure 1.1), oxaliplatin being the only one approved by the food and drug administration (FDA for colorectal cancer), since the release of cisplatin and carboplatin.[11, 13, 14]

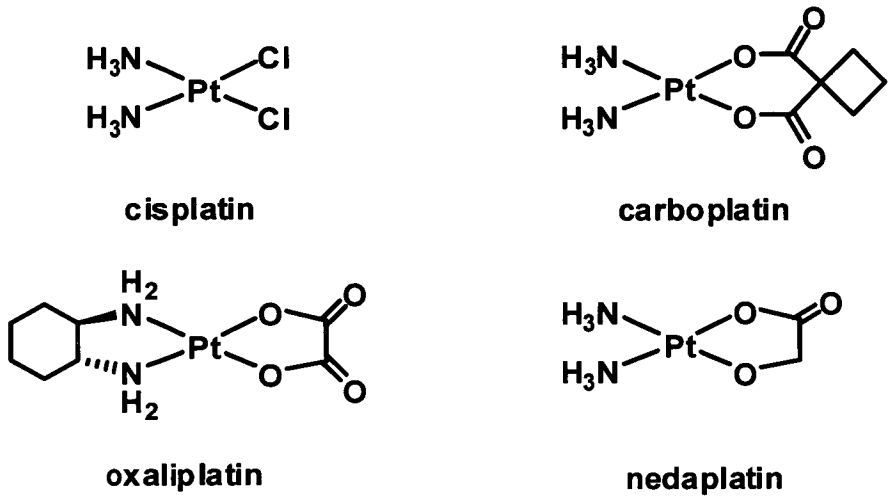

Figure 1.1 Chemical structures of marketed platinum anticancer drugs.

1.4 Other metal based anti-cancer drugs

Both the success and drawbacks of cisplatin as an anticancer drug prompted a search for analogous transition metal complexes. The anticancer activity of metallocene complexes [MCp_2Cl_2] is dependent on the metal ion, and it has been found that when M = Ti, V, Nb, or Mo complexes are active and when M = Ta and W complexes show marginal activity, while for M = Zr and Hf, complexes were found to be inactive.[15, 16] Titanocene and vanadocene dichloride were found to exhibit the best activity against lung, breast and gastrointestinal cancers in mice.

The tetrahedral organometallic Ti^{IV} complex titanocene dichloride [$TiCp_2Cl_2$] was one of the two Ti^{IV} complexes to enter clinical trials. The clinical trials of both budotitane and titanocene dichloride (Figure 1.2) have now been abandoned, whereas trials of some gallium complexes are still in progress.

Au^{I} and Au^{III} complexes have been tested for anti-cancer activity in different cell lines, and some of these were found to exhibit good activity but their cardiovascular toxicity prevented clinical use.[5]

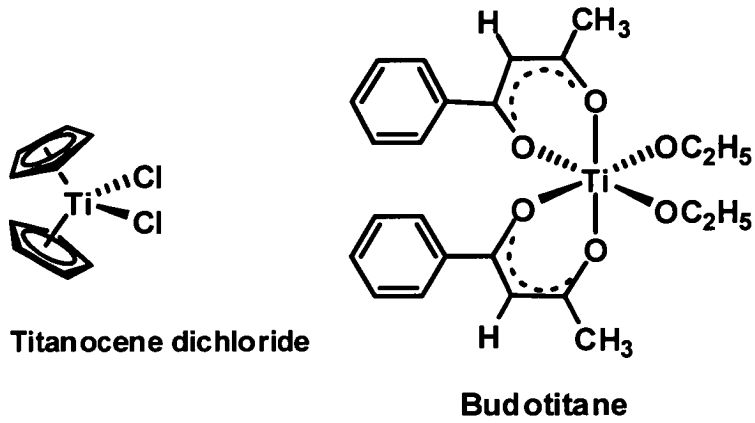

Figure 1.2 Ti^{IV} anticancer complexes, titanocene dichloride and budotitane.

1.5 Mechanism of action of cisplatin

Once in body fluids cisplatin can interact with various biomolecules,[17] but its antitumour activity derives from its capability to form bifunctional DNA cross-links after the activation through hydrolysis. The evidence that DNA is the primary target for cisplatin among many potential cellular targets has been extensively discussed.[18] The major target site for cisplatin on DNA is *N7* of guanine (G) nucleobase,[19] the

most electron-rich site on DNA and easily accessible to the drug in the major groove of B-DNA. Other binding sites include *N7* of adenine (A) nucleobase and *N3* of cytosine (C). 1, 2-Intrastrand cross-links that involve G and sometimes A are the most common platinated adducts of DNA from cancer cells treated with cisplatin.

In the GG intrastrand cross-linking pathway, aquation is followed by monofunctional adduct formation and then ring closure to give the bifunctional GG macrochelate.[19] H-bonding formation between NH protons of cisplatin and the phosphate backbone or C6O of G nucleobase can play a role in stabilizing such cross-links.[20] The GG platination causes B-DNA to bend (by about 35–40°), and this bend is recognized by proteins such as High Mobility Group (HMG) proteins. HMG proteins bind strongly to bent platinated DNA (Figure 1.3) and this causes shielding from repair and leads to apoptosis.[21-23] At the same time HMG proteins are hijacked from their normal function.[24]

Interstrand DNA cross-links can also cause major structural changes in DNA. These changes are rarer but could be important for cytotoxicity. The interstrand DNA cross-link made by cisplatin unwinds DNA close to the platination site and bends the helix toward the minor groove where Pt is bound.[10]

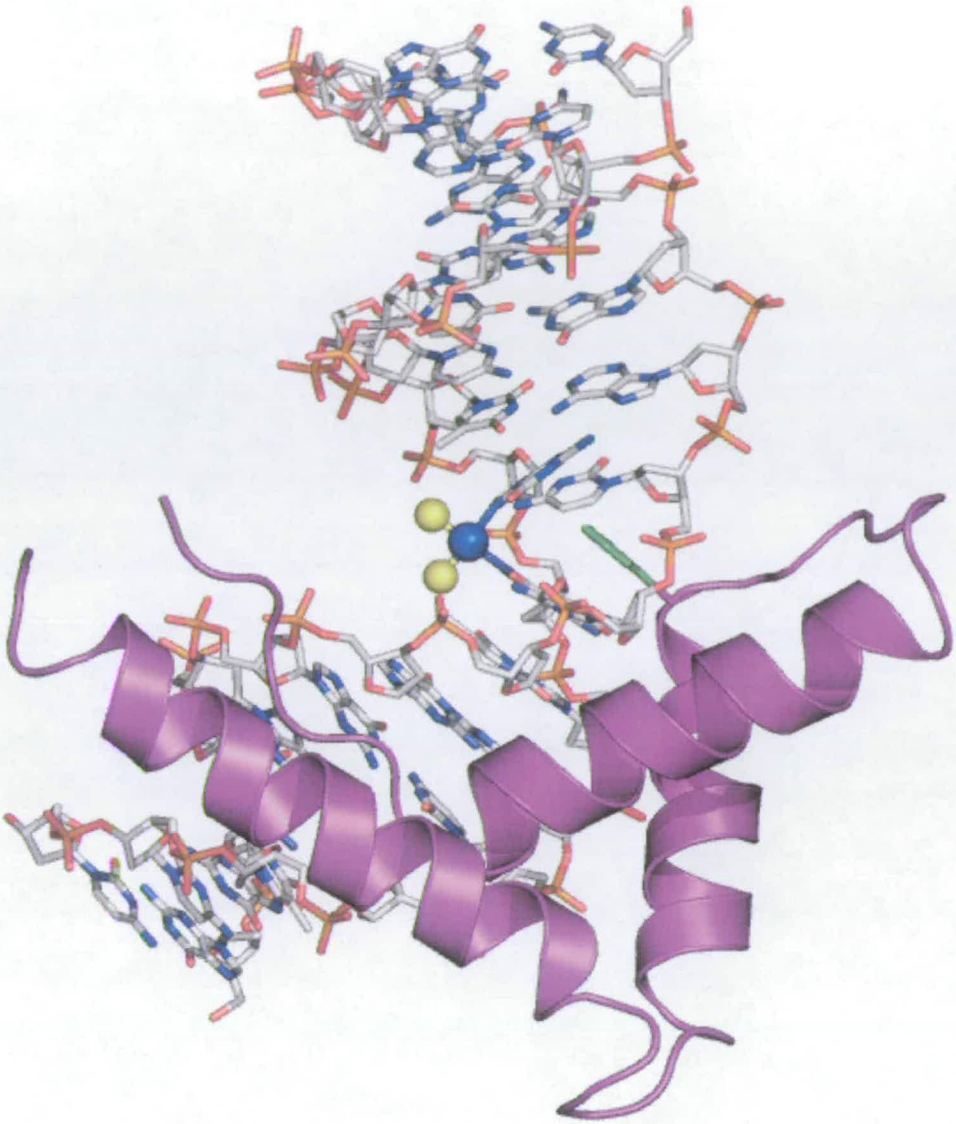

Figure 1.3 Adduct formed between the nonsequence-specific domain A of HMG1 and DNA modified by cisplatin. Colour code for cisplatin: Pt, deep blue and N of the NH_3 groups, yellow. Colour code for DNA: N, blue; O, red; P, orange and C, grey. Domain A of HMG1 is a purple ribbon with the intercalating phenylalanine highlighted in green (Coordinates are taken from the Protein Data Bank, 1CKT).[23]

1.5.1 Apoptosis

On one hand an extensive occurrence of cell death results in serious consequences for the whole organism and on the other hand low induction of apoptosis is connected to an increased cancer risk.[2] Insufficient apoptosis is common in diseases such as mononucleosis, diabetes and cancer, while excessive apoptosis is common in diseases such as AIDS (Acquired immune deficiency syndrome), Alzheimer's disease, Parkinson's disease and in rejection of transplanted organs.

1.6 Ruthenium chemistry

Ruthenium is a group 8 transition metal and together with Os, Rh, Ir, Pd and Pt forms the platinum metals group. Ru has atomic number 44 ($Kr5s^1 4d^7$) and the atomic weight 101.07. Ru has seven isotopes (^{96}Ru, ^{98}Ru, ^{99}Ru, ^{100}Ru, ^{101}Ru, ^{102}Ru and ^{104}Ru), ^{102}Ru being the most abundant at 31.6%. The oxidation states of Ru range from 0 to VIII, and the most common oxidation states in bioinorganic chemistry are II, III and IV.[25] Ru^{II} and Ru^{III} compounds usually have six-coordinated low-spin octahedral geometry. The three $(t_{2g})d$ orbitals are oriented towards the faces of the octahedron and are fully populated in Ru^{II} while in Ru^{III} $(t_{2g})d$ orbitals have a single electronic vacancy.[26, 27] The difference of one electron between the two oxidation states affects significantly their chemistry. Ru^{II} behaves as a relatively "soft",[28] π-donor metal ion while Ru^{III} behaves as borderline "hard" metal ion, which can function as a π-acceptor.[29]

The reduction potential for the Ru^{III}/Ru^{II} couple is a strong function of the ligand environment.[30-33] The effect of back donation of electron density from the metal

stabilizes Ru in lower oxidation state (Ru^{II}). Therefore the coordination of π-acceptor ligands increases the reduction potential, while the electron donor ligands cause its decrease.[29, 34]

1.7 Ruthenium antitumour agents

Different types of ruthenium complexes have been tested with the aim of discovering a behaviour similar to that of cisplatin, but it has been found that just a few exhibit this.[35] Metal complexes are often prodrugs and they undergo transformations before reaching the target. The transformation of the complex can include oxidation or reduction of the metal ion, ligand substitution or modification of the ligands that are still bound to the metal. Therefore, in structure–activity relationships the nature of the active species, the role of the metal itself, and the role of the ligands are of the great importance.

It has been found that Ru complexes are usually active against Pt-resistant tumours.[36] Ru and its complexes have several features which make them very good for pharmacological use. Due to strong ligand field stabilization energy, ruthenium complexes of the most common oxidation states (Ru^{II} and Ru^{III}) are octahedral in geometry (*vide infra*) and fairly inert to ligand substitution, especially Ru^{III} complexes.[37] This makes them attractive as drugs as they should ideally arrive at the target intact.

Ru^{III}, due to its similarity with Fe^{III}, is thought to be transported into tumour cells via transferrin. Tumour cells should have a higher density of transferrin receptors due to the increased requirements for nutrients, which provides selectivity for targeting

cancer cells over those that are not. When transferrin is bound to the receptor it releases the drug.

Fac-[$Ru^{III}Cl_3(NH_3)_3$] was found to induce filamentous growth of *E. coli* at concentrations comparable to cisplatin.[38] Both *fac*-[$Ru^{III}Cl_3(NH_3)_3$] and *cis*-[$Ru^{II}Cl_2(NH_3)_4$] Ru-ammine complexes have low solubility which makes them unsuitable as drugs.[37]

Several other Ru^{II} and Ru^{III} complexes have been reported to exhibit anticancer activity, including *mer*-[Ru(terpy)Cl_3] (terpy = 2,2′:6′,2″-terpyridine), *α*-[Ru(azpy)$_2$$Cl_2$] and *α*-[Ru(azpy)$_2$-O,O′] (azpy = 2-(phenylazo)pyridine; O,O′ = 1,1-cyclobutanedicarboxylate, oxalate, or malonate)[39, 40] as well as Ru^{IV} complex [Ru(H_2cdta)Cl_2] (cdta = 1,2-cyclohexanediaminetetraacetate).[41]

1.7.1 Ru^{III} complexes in clinical trials

The most significant was the entry of two Ru^{III} octahedral complexes into clinical trials for cancer treatment. One of them NAMI-A (imidazolium *trans*-tetrachlorodimethylsulfoxideimidazoleruthenate(III); Figure 1.4), has relatively low toxicity towards cancer cells, but is particularly effective against solid tumour metastases and the drug has completed phase I clinical trials.[42] DNA has been proposed as one of the biological targets of KP1019 (indazolium *trans*-tetrachlorobis(1*H*-indazole)ruthenate(III); Figure 1.4), and it has also been reported that the drug triggers apoptosis.[43] However, the cellular mechanism of the activation of apoptosis is still not understood.

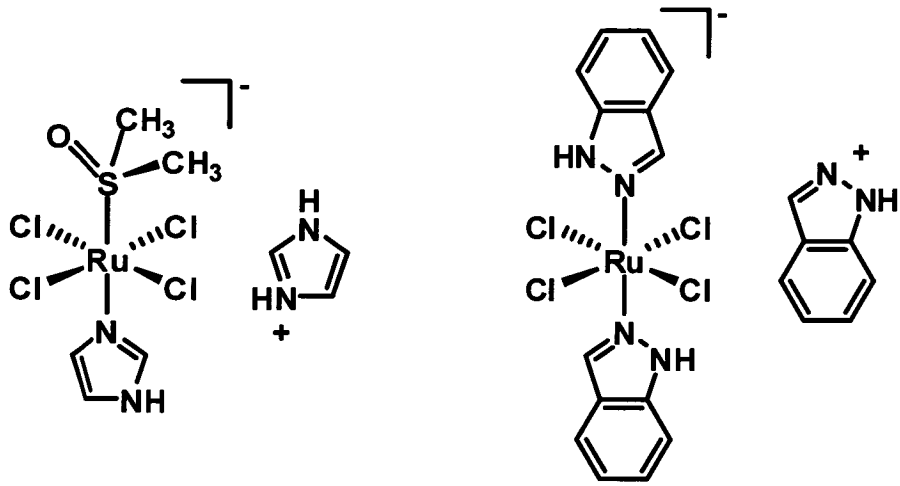

Figure 1.4 Chemical structures of NAMI-A and KP1019, Ru^{III} antimetastatic and cytotoxic potential anticancer agents, respectively.

It has been suggested that Ru^{III} complexes are "activated by reduction" *in vivo* to Ru^{II} and so they should coordinate more rapidly to biomolecules[44, 45] due to the increased lability of Ru^{II}-Cl bonds compared to that in Ru^{III} complexes, which tend to be more inert toward ligand substitution (*vide infra*). The reduction of Ru^{III} to Ru^{II} could occur by single-electron transfer from proteins which exist in the mitochondrial electron-transfer chain or proteins in microsomal electron-transfer systems. Microsomal proteins are believed to be more efficient.[37] Oxidation of Ru^{II} back to Ru^{III} could occur by reaction with molecular oxygen or cytochrome oxidaze,[46] as well as with other oxidants.

1.8 Ru^{II} arene anticancer complexes

Ru^{II} arene complexes with phosphine ligands have been reported to possess antitumour and DNA binding properties.[47-49] They include bifunctional Ru^{II} arene complexes of the general formula $[(\eta^6\text{-arene})Ru^{II}(pta)Cl_2]$, where pta = 1,3,5-triaza-7-phosphatricyclo[3.3.1.1]decane. These complexes showed pH dependent DNA damaging properties.

Organoruthenium complexes of the type $[(\eta^6\text{-arene})Ru^{II}(XY)Z]^+$, where arene is benzene (bz) or bz derivative, XY chelating ligand and Z halide (Figure 1.5) have been studied as potential anticancer agents.[50-52] The structure-activity relationships of these complexes have been discussed before.[50, 51, 53-55] Ru^{II} arene complexes in which the chelating ligand is ethylenediamine (en) and the leaving group is chloride are cytotoxic to cancer cells, including cell lines that are resistant to cisplatin.[50, 51] It has been found for chlorido en complexes that cytotoxicity against A2780 human ovarian cancer cells increases with the increase of the size of the arene.[50, 56]

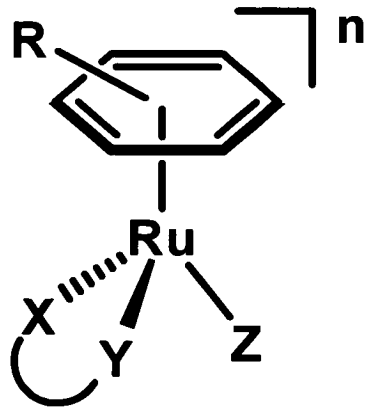

Figure 1.5 General chemical structure of Ru^{II} arene `piano-stool` complexes containing η^6 bound arene, a chelating ligand XY and a monodentate ligand Z.

In this type of complexes, the arene provides a hydrophobic face for the complex and stabilizes Ru in the +2 oxidation state so that oxidation to Ru^{III} is difficult. The structural and electronic features of metal–arene bonding have been previously discussed.[57] The arene is considered as a π-acceptor ligand towards Ru and the evidence for this comes from the arene proton resonances in ^1H NMR which, upon arene coordination to Ru^{II} shift to a lower frequency due to the increase in electron density.[58]

The substitution of chloride by other halides has only a small effect on the cytotoxicity of en complexes. It is believed that bromido and iodido ligands are exchanged with chlorido ligands in an extracellular biological media as the concentration of chloride is ~ 104 mM, so that the iodido and bromido complexes would act only as prodrugs.[59]

The chelating ligand provides additional stability. Complexes containing chelating ligands tend to be more active than those containing only mono-dentate ligands.[50] The

nature of the chelating ligand can play a crucial role in anticancer activity.[54] Changing the nature of the donor atoms in the chelating ligand (*e.g.* from N to O) has also been investigated and in this case the structure-activity relationships become complicated. The structure-activity relationships reported for Ru^{II} arene complexes containing N,N-chelating ligands show that although complexes containing en as chelating ligand were cytotoxic, complexes containing tetramethyl-en as chelating ligands showed no cytotoxicity. This suggests that NH groups on the chelating ligand play a role in the activity, possibly stabilizing G adducts on DNA via H-bonding (*vide supra*).

1.8.1 Hydrolyses of Ru^{II} arene complexes

The mechanism of cytotoxic action of Ru^{II} arene complexes is thought to involve hydrolysis of the Ru-Z bond generating reactive Ru-H_2O species (Figure 1.6) that can further bind to DNA and form the adducts. In general, Ru^{II} arene complexes that hydrolyse also exhibit cancer cell cytotoxicity, whereas those that do not hydrolyse exhibit usually no activity. Therefore the hydrolysis rates are of high importance in order to relate them to anti-cancer activity. The hydrolysis rates of en complexes $[(\eta^6\text{-bip})Ru(en)Cl]^+$ (3.95×10^{-3} s^{-1}, $t_{1/2}$ = 2.92 min), $[(\eta^6\text{-tha})Ru(en)Cl]^+$ (6.84×10^{-3} s^{-1}, $t_{1/2}$ = 1.69 min) and $[(\eta^6\text{-dha})Ru(en)Cl]^+$ (6.49×10^{-3} s^{-1}, $t_{1/2}$ = 1.78 min), where bip = biphenyl, tha = tetrahydroanthracene and dha = dihydroanthracene, are measured at 37°C, and are found to be relatively fast and independent of ionic strength.[60]

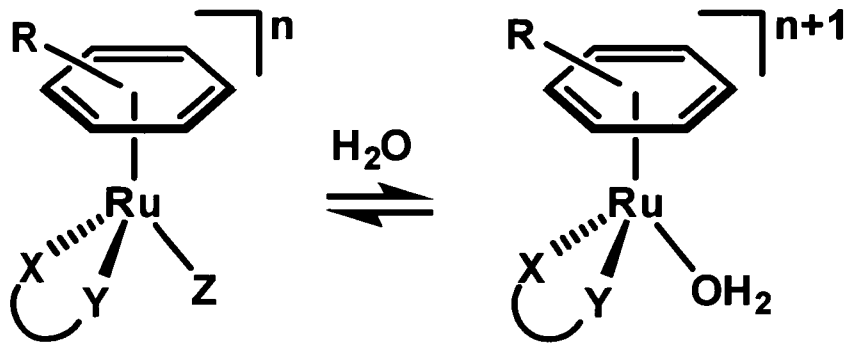

Figure 1.6 Hydrolysis of Ru^{II} arene complexes in aqueous solution and formation of the aqua adduct.

The presence of bipyridine (bipy) as a π-acceptor in [(η^6-arene)Ru(bipy)Cl]Cl complexes, where arene = bz, *p*-cymene (*p*-cym) and hexamethylbenzene (hmb), has been reported to decrease the rate of hydrolysis by 2 orders of magnitude compared to analogues in which bipy is replaced with two aqua ligands.[61] The π-acceptor ligand bipy withdraws electron density from Ru and increases the positive charge on the metal, making it less favourable for Cl^- to leave, slowing down the hydrolysis.

Density functional theory (DFT) calculations for aquation of complex [(η^6-bz)Ru(en)Z]$^+$, where Z = Cl^-, Br^-, I^- or N_3^- suggested that the aquation occurs via a concerted interchange pathway rather than a stepwise dissociacion/coordination process. The reaction barriers and overall reaction energies for aquation follow the order Br < Cl < I < N_3.[55] The reactions were found to occur closer to the I_a (interchange-associative) mechanism than to the I_d (interchange-dissociative) mechanism. On the basis of electronegativity, the azido complex would be expected to hydrolyse at a rate between the chlorido and bromido complexes, but a slower rate was observed. The lower hydrolysis rate in the case of azido complex is ascribed to the increased steric bulk in the case of this pseudohalide. Further evidence for the

mechanism is that I_a substitution is more influenced by steric factors than substitution via an I_d pathway.[55] The electron-accepting effect of the π-acid arenes is thought to be responsible for the shift of the pathway towards the more associative I_a mechanism as the Ru metal has more characteristics of Ru^{III} over those of Ru^{II}, and Ru^{III} complexes are known to react via associative pathways.[62]

1.8.2 Interactions of Ru^{II} arene complexes with 9-ethylguanine (9-EtG)

Intramolecular π-π arene-9-EtG (model nucleobase) stacking has been observed in the crystal structure of $[(\eta^6\text{-bip})Ru^{II}(en)(9\text{-EtG-}N7)][PF_6]_2$.[63] This together with the strong H-bonding between an NH of en and C6O from 9-EtG, observed in the same crystal structure was found to contribute to the G-specificity when this type of complexes binds to DNA.[64]

The x-ray crystal structures of $[(\eta^6\text{-dha})Ru^{II}(en)(9\text{-EtG-}N7)]^{2+}$ and $[(\eta^6\text{-tha})Ru^{II}(en)(9\text{-EtG-}N7)]^{2+}$ show again the presence of a strong intramolecular π–π arene-9-EtG stacking[65] (Figure 1.7). The outer ring of the arene (dha and tha, respectively) lies directly over the purine base. The outer arene ring is parallel to the purine ring and the centroid-centroid distance is 3.31 Å in the structure of dha, and 3.45 Å in the structure of tha 9-EtG adduct. Stereospecific H-bonding has also been observed between en NH···C6O of 9-EtG in $[(\eta^6\text{-dha})Ru^{II}(en)(9\text{-EtG-}N7)]^{2+}$ and $[(\eta^6\text{-tha})Ru^{II}(en)(9\text{-EtG-}N7)]^{2+}$, with distances of 2.1 Å and 1.9 Å, respectively.[65]

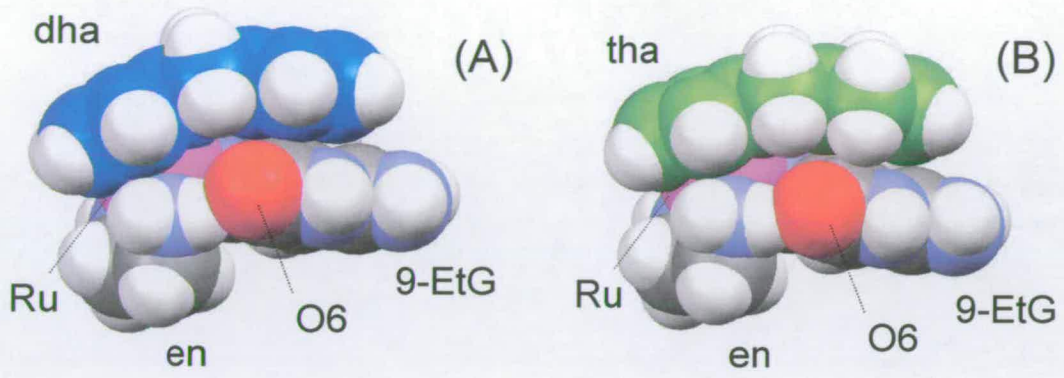

Figure 1.7 Space filling representation of the x-ray crystal structure of the cation of (**A**) $[(\eta^6\text{-dha})\text{Ru(en)(9-EtG-}N7)][PF_6]_2$ and (**B**) $[(\eta^6\text{-tha})\text{Ru(en)(9-EtG-}N7)][PF_6]_2$.

1.8.3 Interaction of Ru^{II} arene complexes with oligonucleotides

The interaction of $\{(\eta^6\text{-bip})\text{Ru(en)}\}^{2+}$ fragment with the d(ATACATGGTACATA)·d(TAT^{17}G^{18}TACCATGTAT) duplex has been studied by HPLC-ESI-MS as well as by 2D NOESY NMR. It has been found that ruthenation occurs at *N7* of every G residue of the 14-mer. At one site (T^{17}G^{18}) two different conformers were identified. In one conformer, intercalation of bip between G^{18} and adjacent thymine (T^{17}) is observed and in the second conformer, the bip arene is non-intercalated but it is stacked on the tilted T^{17}, lying on the surface of the major groove (Figure 1.8).[66]

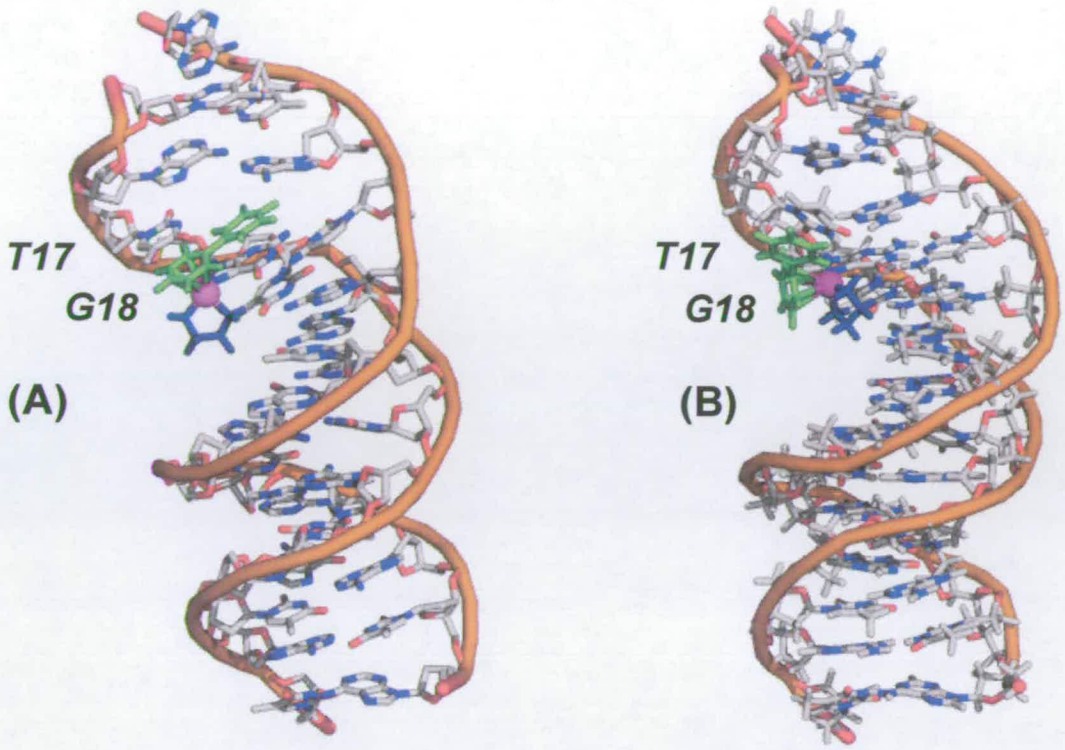

Figure 1.8 Molecular models of two conformers of 14-mer d(ATACATGGTACATA)·d(TAT^{17}G^{18}TACCATGTAT) ruthenated at *N7* of G^{18} with monofunctional $\{(\eta^6\text{-bip})\text{Ru(en)}\}^{2+}$ fragment (**A**) showing the intercalation of the arene between G^{18} and T^{17} and (**B**) bip is non-intercalated but stacked on a tilted T^{17}. Colour code: Ru shown in pink, en in deep blue and bip in green.[66]

1.9 DNA binding of Ru^{II} arene complexes

1.9.1 DNA as a potential target site

Platinum-based drugs that are in clinical use target DNA (*vide infra*), and these are believed to interact primarily with nucleic acid through coordination bond formation. As DNA is an important potential biological target for many metal-based anticancer agents,[67] distortions of DNA structure often correlate with anticancer activity.[68, 69] Therefore, it is of a great importance to understand DNA binding properties of potential anti-cancer agents.

Chlorido Ru^{II} arene complexes are the dominant species in blood plasma (pH = 7.4), where the chloride concentration is ca. 104 mM (*vide infra*). In the cell nucleus where the chloride concentration is lower (ca. 4–20 mM) increased concentration of aqua Ru^{II} species is more likely to occur. Once a Ru^{II} arene complex is activated through hydrolysis and the aqua species is formed, Ru is a potential centre for nucleophilic attack by biomolecules. The binding of Ru^{II} arene complexes to DNA is of special interest, as this may be the ultimate target for this type of agent.

1.9.2 Interaction with CT DNA

Ru^{II} arene complexes of the type $[(\eta^6\text{-arene})Ru(en)Cl]^+$, where arene = bip, dha, tha or *p*-cym have been found to interact with CT DNA in a cell-free medium and bind preferentially to *N7* of G residues. In addition to coordination to G *N7*, hydrophobic

(non-coordinative) interactions can occur between the arene and DNA.[56] The non-coordinative interactions relay on electrostatic interactions, shape and size molecular recognition, and hydrogen bonding. These interactions may include intercalation of the extended arene between DNA bases and minor groove binding. For more extended arenes the possibility of arene intercalation between the DNA bases arises.[70] The extent of ruthenation of double helical CT DNA by Ru^{II} arene complexes was followed, at an r_i (molar ratio of free ruthenium complex to nucleotide phosphates at the onset of incubation with DNA) value of 0.1 in 10 mM $NaClO_4$ at 37°C. The amount of ruthenium bound per DNA nucleotide phosphate increased with time and $t_{½}$ (the time at which binding reaches 50%) was found to be dependent on the arene. The $t_{½}$ obtained for $[(\eta^6\text{-bip})Ru(en)Cl]^+$ and $[(\eta^6\text{-tha})Ru(en)Cl]^+$ complexes was 10 and for $[(\eta^6\text{-dha})Ru(en)Cl]^+$ 15 min, while $t_{½}$ for $[(\eta^6\text{-}p\text{-cym})Ru(en)Cl]^+$ was 3.5 h. Under the same conditions $t_{½}$ for cisplatin was ca. 2 h. Thus for bip, dha and tha Ru^{II} complexes binding to CT DNA is for an order of magnitude faster compared to that of cisplatin. The binding of bip complex to DNA was nearly quantitative after ca. 3 h (ca. 90%).[56]

1.9.3 Unwinding of plasmid DNA

Ru^{II} arene complexes of the type $[(\eta^6\text{-arene})Ru(en)Cl]^+$, where arene = bip, tha or dha were reported to unwind negatively-supercoiled pSP73KB plasmid DNA by 14 ± 1°, while *p*-cym complex unwinds plasmid DNA by only 7 ± 0.5°.[56] The result suggested that the higher unwinding for bip, tha and dha complexes, compare to that of *p*-cym is a result of the intercalation of the extended arene (*vide infra*) into the DNA bases, upon mono-functional binding.

1.9.4 Melting of CT DNA

It has been found that at lower salt concentrations (0.01 M $NaClO_4$), Ru^{II} arene complexes of the type $[(\eta^6\text{-arene})Ru(en)Cl]^+$, where arene = bip, tha and dha increase the melting temperature (t_m) of CT DNA. The increase becomes more pronounced with increasing r_b value (r_b is a number of Ru atoms bound per nucleotide residue). When the ionic strength is increased (higher salt concentration), t_m was found to decrease. Lower electrostatic effects between the positively-charged complexes and CT DNA are expected with the increase of the concentration of Na^+ ions from $NaClO_4$. This electrostatic effect stabilizes the DNA and should increase its melting temperature (t_m) compared to the t_m of unmodified DNA. Hense at low ionic strengths the increase in t_m is due to the modification of DNA by bip, tha and dha complexes as the positive charges on Ru and the intercalation of the arenes increases the stability of DNA.[56]

The melting behavior of DNA modified by $[(\eta^6\text{-}p\text{-cym})Ru(en)Cl]^+$ decreases t_m even at low salt concentration indicating that the factors responsible for thermal stabilization of DNA are notably reduced.[56] The factor that can be involved in DNA stabilization is intercalation of the arene between the base residues (*vide infra*) and the separation of negative backbone charges caused by the intercalation (due to elongation and unwinding of DNA).

1.9.5 Fluorescence experiments

Ethidium bromide (EtBr) is an intercalator and is fluorescent when bound to DNA. EtBr can be used to distinguish intercalating from nonintercalating ligands on DNA by competition. The possible intercalation of the arene into double helical DNA has been probed by EtBr fluorescence experiment,[56] and it has been found that complexes of the type $[(\eta^6\text{-arene})Ru(en)Cl]^+$, when arene = bip, tha or dha are able to displace EtBr from DNA and quench its relative fluorescence more than the *p*-cym complex of the same type.

1.9.6 Circular dichroism

The binding of Ru^{II} arene complexes of the type $[(\eta^6\text{-arene})Ru(en)Cl]^+$, where arene = bip, tha, dha, *p*-cym or bz, to CT DNA has been studied by circular dichroism (CD).[56] An induced CD band at 350-410 nm was observed for the interaction of bip, tha and dha complexes with CT-DNA. On the other hand no induced band in this region was observed for *p*-cym and bz complexes. This induced CD band appears to be related to intercalation of the extended arenes into DNA or to groove binding. Similar bands were previously observed for other metal complexes.[71, 72]

1.10 Aims

The general aim of this thesis is to investigate the design, synthesis and anti-cancer activity of Ru^{II} arene complexes containing different arenes and N,N-chelating ligands. The studies are focused on changes in anti-cancer activity influenced by changing the physical and chemical properties of complexes through the changes in the steric and electronic effects of the ligands. The main focus is on studies of aqueous solution chemistry, solid state structures, reactivity towards nucleobases and DNA (as potential cellular targets). The first aim was to investigate the effect of the size and the shape of the arene ligand on the binding mode of Ru^{II} arene complexes to DNA and to relate this to the differences in anti-cancer activity. The second aim was to investigate the effects of π-acceptor and redox-active chelating ligands as well as the effects of their substituents on the chemical, physical and biological properties of Ru^{II} arene complexes. The overall aim of this thesis is to create possible candidates for development as anticancer agents.

1.11 References

(1) Yung, C. Y. *Pharmacol. Biochem. Behav.* **1984,** *21 Suppl 1*, 41-7.

(2) Krug, H. F. *Materialwiss. Werkst.* **2002,** *33*, 770-774.

(3) Ehrlich, P. *Wiener Medizin. Woch.* **1911,** *61*, 14-9.

(4) Abrams, M. J.; Murrer, B. A. *Science* **1993,** *261*, 725-30.

(5) Shaw, C. F., III *Chem. Rev.* **1999,** *99*, 2589-2600.

(6) Thompson, K. H.; McNeill, J. H.; Orvig, C. *Chem. Rev.* **1999,** *99*, 2561-2571.

(7) http://info.cancerresearchuk.org/youthandschools/latestfromthelab/.

(8) http://www.deathreference.com/Bl-Ce/Causes-of-Death.html.

(9) Rosenberg, B.; Vancamp, L.; Krigas, T. *Nature* **1965,** *205*, 698-9.

(10) Jung, Y.; Lippard, S. J. *Chem. Rev.* **2007,** *107*, 1387-1407.

(11) Fuertes, M. A.; Alonso, C.; Perez, J. M. *Chem. Rev.* **2003,** *103*, 645-662.

(12) Weiss, R. B.; Christian, M. C. *Drugs* **1993,** *46*, 360-77.

(13) Kelland, L. R.; Sharp, S. Y.; O'Neill, C. F.; Raynaud, F. I.; Beale, P. J.; Judson, I. R. *J. Inorg. Biochem.* **1999,** *77*, 111-115.

(14) Wong, E.; Giandomenico, C. M. *Chem. Rev.* **1999,** *99*, 2451-2466.

(15) Koepf-Maier, P.; Koepf, H. *Chem. Rev.* **1987,** *87*, 1137-52.

(16) Koepf-Maier, P.; Koepf, H. *Struct. Bond.* **1988,** *70*, 103-94.

(17) Reedijk, J. *Chem. Rev.* **1999,** *99*, 2499-2510.

(18) Jamieson, E. R.; Lippard, S. J. *Chem. Rev.* **1999,** *99*, 2467-2498.

(19) Caradonna, J. P.; Lippard, S. J.; Gait, M. J.; Singh, M. *J. Am. Chem. Soc.* **1982,** *104*, 5793-5.

(20) Hambley, T. W. *Drug. Des. Deliv.* **1988,** *3*, 153-8.

(21) Ohndorf, U. M.; Rould, M. A.; He, Q.; Pabo, C. O.; Lippard, S. J. *Nature* **1999,** *399*, 708-12.

(22) Huang, J. C.; Zamble, D. B.; Reardon, J. T.; Lippard, S. J.; Sancar, A. *Proc. Natl. Acad. Sci. U S A* **1994,** *91*, 10394-8.

(23) Ohndorf, U.-M.; Rould, M. A.; He, Q.; Pabo, C. O.; Lippard, S. J. *Nature* **1999,** *399*, 708-712.

(24) Kartalou, M.; Essigmann, J. M. *Mutat. Res.* **2001,** *478*, 1-21.

(25) Moyer, B. A.; Meyer, T. J. *J. Am. Chem. Soc.* **1978,** *100*, 3601-3.

(26) Taube, H. *Surv. Prog. Chem.* **1973,** *6*, 1-46.

(27) Taube, H. *Coord. Chem. Rev.* **1978,** *26*, 1-5.

(28) Huheey, J. E., *Principles of Structure and Reactivity. 2nd Ed.* Harper and Row, New York: **1978**; p 276.

(29) Krentzien, H.; Taube, H. *J. Am. Chem. Soc.* **1976,** *98*, 6379-80.

(30) Clarke, M. J.; Taube, H. *J. Am. Chem. Soc.* **1974,** *96*, 5413-19.

(31) Clarke, M. J.; Taube, H. *J. Am. Chem. Soc.* **1975,** *97*, 1397-403.

(32) Matsubara, T.; Ford, P. C. *Inorg. Chem.* **1976,** *15*, 1107-10.

(33) Isied, S. S.; Taube, H. *Inorg. Chem.* **1976,** *15*, 3070-5.

(34) Lim, H. S.; Barclay, D. J.; Anson, F. C. *Inorg. Chem.* **1972,** *11*, 1460-6.

(35) Clarke, M. J.; Zhu, F.; Frasca, D. R. *Chem. Rev.* **1999,** *99*, 2511-2533.

(36) Keppler, B. K.; Henn, M.; Juhl, U. M.; Berger, M. R.; Niebl, R.; Wagner, F. E. *Prog. Clin. Biochem. Med.* **1989,** *10*, 41-69.

(37) Clarke, M. J.; Bitler, S.; Rennert, D.; Buchbinder, M.; Kelman, A. D. *J. Inorg. Biochem.* **1980,** *12*, 79-87.

(38) Durig, J. R.; Danneman, J.; Behnke, W. D.; Mercer, E. E. *Chem.-Biol. Interact.* **1976,** *13*, 287-94.

(39) Velders, A. H.; Kooijman, H.; Spek, A. L.; Haasnoot, J. G.; de Vos, D.; Reedijk, J. *Inorg. Chem.* **2000,** *39*, 2966-7.

(40) Hotze, A. C. G.; Bacac, M.; Velders, A. H.; Jansen, B. A. J.; Kooijman, H.; Spek, A. L.; Haasnoot, J. G.; Reedijk, J. *J. Med. Chem.* **2003,** *46*, 1743-1750.

(41) Vilaplana, R. A.; Gonzalez-Vilchez, F.; Gutierrez-Puebla, E.; Ruiz-Valero, C. *Inorg. Chim. Acta* **1994,** *224*, 15-18.

(42) Rademaker-Lakhai, J. M.; Van Den Bongard, D.; Pluim, D.; Beijnen, J. H.; Schellens, J. H. M. *Clin. Cancer Res.* **2004,** *10*, 3717-3727.

(43) Kapitza, S.; Pongratz, M.; Jakupec, M. A.; Heffeter, P.; Berger, W.; Lackinger, L.; Keppler, B. K.; Marian, B. *J. Cancer Res. Clin. Onc.* **2005,** *131*, 101-110.

(44) Kelman, A. D.; Clarke, M. J.; Edmonds, S. D.; Peresie, H. J. *J. Clin. Hem. Onc.* **1977,** *7*, 274-88.

(45) Clarke, M. J. *Met. Complexes Cancer Chemother.* **1993**, 129-56.

(46) Stanbury, D. M.; Haas, O.; Taube, H. *Inorg. Chem.* **1980,** *19*, 518-24.

(47) Allardyce, C. S.; Dyson, P. J. *J. Cluster Sci.* **2001,** *12*, 563-569.

(48) Dorcier, A.; Dyson, P. J.; Gossens, C.; Rothlisberger, U.; Scopelliti, R.; Tavernelli, I. *Organometallics* **2005,** *24*, 2114-2123.

(49) Scolaro, C.; Bergamo, A.; Brescacin, L.; Delfino, R.; Cocchietto, M.; Laurenczy, G.; Geldbach, T. J.; Sava, G.; Dyson, P. J. *J. Med. Chem.* **2005,** *48*, 4161-4171.

(50) Aird, R. E.; Cummings, J.; Ritchie, A. A.; Muir, M.; Morris, R. E.; Chen, H.; Sadler, P. J.; Jodrell, D. I. *Br. J. Cancer* **2002,** *86*, 1652-1657.

(51) Morris, R. E.; Aird, R. E.; Murdoch, P. d. S.; Chen, H.; Cummings, J.; Hughes, N. D.; Parsons, S.; Parkin, A.; Boyd, G.; Jodrell, D. I.; Sadler, P. J. *J. Med. Chem.* **2001,** *44*, 3616-3621.

(52) Yan, Y. K.; Melchart, M.; Habtemariam, A.; Sadler, P. J. *Chem. Comm.* **2005**, 4764-4776.

(53) Dougan, S. J.; Melchart, M.; Habtemariam, A.; Parsons, S.; Sadler, P. J. *Inorg. Chem.* **2007,** *46*, 1508.

(54) Habtemariam, A.; Melchart, M.; Fernandez, R.; Parsons, S.; Oswald, I. D. H.; Parkin, A.; Fabbiani, F. P. A.; Davidson, J. E.; Dawson, A.; Aird, R. E.; Jodrell, D. I.; Sadler, P. J. *J. Med. Chem.* **2006,** *49*, 6858-6868.

(55) Wang, F.; Habtemariam, A.; van der Geer Erwin, P. L.; Fernandez, R.; Melchart, M.; Deeth Robert, J.; Aird, R.; Guichard, S.; Fabbiani Francesca, P. A.; Lozano-Casal, P.; Oswald Iain, D. H.; Jodrell Duncan, I.; Parsons, S.; Sadler Peter, J. *Proc. Natl. Acad. Sci. U. S. A.* **2005,** *102*, 18269-74.

(56) Novakova, O.; Chen, H.; Vrana, O.; Rodger, A.; Sadler, P. J.; Brabec, V. *Biochemistry* **2003,** *42*, 11544-11554.

(57) Muetterties, E. L.; Bleeke, J. R.; Wucherer, E. J.; Albright, T. *Chem. Rev.* **1982,** *82*, 499-525.

(58) Stebler-Roethlisberger, M.; Hummel, W.; Pittet, P. A.; Buergi, H. B.; Ludi, A.; Merbach, A. E. *Inorg. Chem.* **1988,** *27*, 1358-63.

(59) Kennedy, R. S.; Konok, G. P.; Bounous, G.; Baruchel, S.; Lee, T. D. G. *Anticancer Res.* **1995,** *15*, 2643-9.

(60) Wang, F.; Chen, H.; Parsons, S.; Oswald, I. D. H.; Davidson, J. E.; Sadler, P. J. *Chem.-A Eur. J.* **2003,** *9*, 5810-5820.

(61) Dadci, L.; Elias, H.; Frey, U.; Hoernig, A.; Koelle, U.; Merbach, A. E.; Paulus, H.; Schneider, J. S. *Inorg. Chem.* **1995,** *34*, 306-15.

(62) Fairhurst, M. T.; Swaddle, T. W. *Inorg. Chem.* **1979,** *18*, 3241-4.

(63) Chen, H. M.; Parkinson, J. A.; Parsons, S.; Coxall, R. A.; Gould, R. O.; Sadler, P. J. *J. Am. Chem. Soc.* **2002,** *124*, 3064-3082.

(64) Liu, H. K.; Berners-Price, S. J.; Wang, F. Y.; Parkinson, J. A.; Xu, J. J.; Bella, J.; Sadler, P. J. *Angew. Chem.-Int. Ed.* **2006,** *45*, 8153-8156.

(65) Chen, H.; Parkinson, J. A.; Parsons, S.; Coxall, R. A.; Gould, R. O.; Sadler, P. J. *J. Am. Chem. Soc.* **2002,** *124*, 3064-3082.

(66) Liu, H.-K.; Berners-Price, S. J.; Wang, F.; Parkinson, J. A.; Xu, J.; Bella, J.; Sadler, P. J. *Angew. Chem.-Int. Ed.* **2006,** *45*, 8153-8156.

(67) Zhang, C. X.; Lippard, S. J. *Curr. Opin. Chem. Bio.* **2003,** *7*, 481–489.

(68) Brabec, V. *Prog. Nucleic Acid Res. Mol. Biol.* **2002,** *71*, 1-68.

(69) Brabec, V.; Novakova, O. *Drug Resist. Updates* **2006,** *9*, 111-122.

(70) Chen, H.; Parkinson, J. A.; Morris, R. E.; Sadler, P. J. *J. Am. Chem. Soc.* **2003,** *125*, 173-186.

(71) Lyng, R.; Rodger, A.; Norden, B. *Biopolymers* **1991,** *31*, 1709-20.

(72) Long, E. C.; Barton, J. K. *Acc. Chem. Res.* **1990,** *23*, 271-3.

Chapter 2

Experimental Section

"We can't solve problems by using the same kind of thinking we used when we created them."

Albert Einstein

In this Chapter the general techniques and instrumentation used are described. The methods related to particular experiments and details of these experiments are described in appropriate chapters. The focus of this Chapter is as well on synthesis and characterization of the starting materials, dienes used in a preparation of dimers, and dimers used in further syntheses of Ru^{II} arene complexes. Syntheses of Ru^{II} arene complexes are described in following chapters.

2.1 Instrumentation and techniques

2.1.1 Nuclear magnetic resonance (NMR) spectroscopy[1]

2.1.1.1 Nuclear magnetism

Nuclear magnetic resonance (NMR) spectroscopy relies on the magnetic properties of nuclei. In general, NMR makes use of ^{1}H, ^{13}C, ^{15}N nuclei, which all possess spin 1/2. Only the ^{1}H (natural abundance 99.985) NMR was studied in this thesis and it was mainly used for characterization of synthesized complexes. When placed in a strong magnetic field (B_0; Figure 2.1) spins with a spin quantum number 1/2 will create a two-state distribution with different energies (α and β states) and precess at the Larmor frequency (ν_0) around B_0 defined as:

$$\nu_0 = \gamma B_0/2\pi$$

where γ is the gyromagnetic ratio of the nucleus.

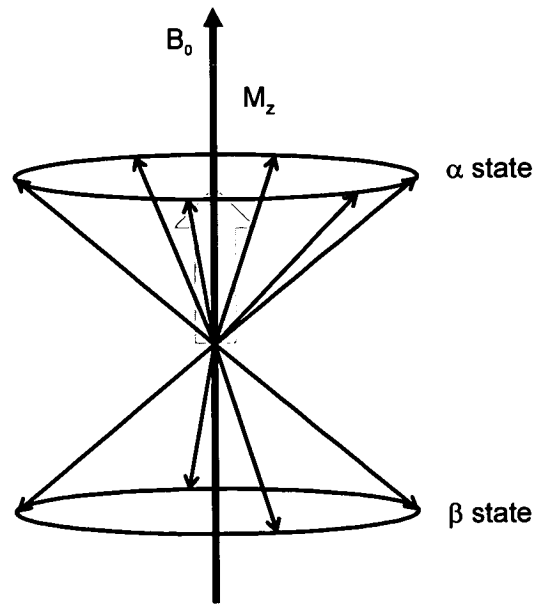

Figure 2.1 Bulk magnetisation (M_z) resulting from population difference of spins in state α and β placed in a static magnetic field B_0.

At a macroscopic level, the population difference between α and β states results in a bulk magnetization (M_z) co-linear to B_0. This magnetization is the source of the NMR signal and its size is related to the population difference between the two states. The manipulation of the M_z, using radiofrequency pulses, forms the basis of Fourier transform NMR spectroscopy.

2.1.1.2 Chemical shift

Each nucleus experiences a magnetic field that is a sum of external and local magnetic fields. Local magnetic field, resulting from shielding of nuclei, can be described as:

$$B_{local} = B_0(1-\sigma)$$

where σ is the shielding constant. The shielding constant is affected by surrounding atoms whose contribution can be divided into diamagnetic and paramagnetic components:

$$\sigma = \sigma_{diamagnetic} + \sigma_{paramagnetic}$$

For example, the magnetic field B_0 induces a current in the phenyl ring which produces a field (B_i) which opposes the external magnetic field above and below the plane and is the same in direction to B_0 in the plane of the ring (Figure 2.2). As a result, nuclei in the region above or below the plane are shielded and the protons in the plane of the ring are deshielded. The shielding effect leads to dispersion of signals of the same nucleus in NMR spectra, opening a possibility for assigning the observed resonance to individual atoms.

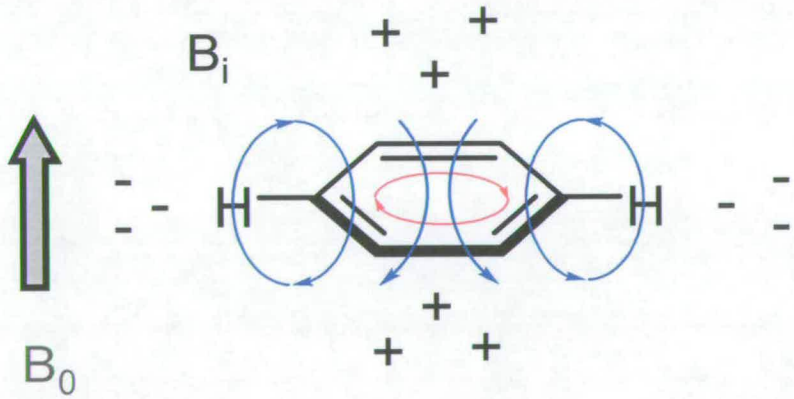

Figure 2.2 Shielding (+) and deshielding (-) effect of a phenyl ring placed in a static magnetic field B_0. The ring current effect (B_i) in the plane and below and above the plane of the ring is shown by red and blue arrows, respectively.

In order to compare spectra acquired at different field strengths, the chemical shift (δ) scale was introduced. This is a relative scale describing the position of a signal relative to the position of a reference compound,

$$\delta(\text{ppm}) = ((\xi - \xi_{ref})/\xi_{ref})10^6$$

where ξ and ξ_{ref}: are the absolute frequencies.

2.1.1.3 Pulsed-field gradients

Pulsed-field gradients (PFG) are short, typically millisecond, pulses during which the static magnetic field B_0 is made inhomogeneous. This disturbance is not random. The strength of a PFG varies linearly along a certain axis, typically the z axis. During PFGs, spins experience different magnetic fields depending on their position in the NMR tube, resulting in a loss of coherence for any magnetization not aligned along the z axis. This magnetization, temporarily lost, can be recovered by applying an identical gradient with opposite sign, or as in polarization transfer experiments, with an appropriately scaled gradient.

Gradients are also used for purging of unwanted magnetization, for example, after storing the useful magnetization along the z-axis or by manipulating selected signals by selective pulses. The latter principle is used for water suppression in the WATERGATE experiment[2] and double-pulse field-gradient spin-echo (DPFGSE) experiment.[3]

2.1.1.4 Experimental methods

All NMR spectra were recorded on either Bruker DPX (^{1}H 360 MHz) equipped with a QNP [^{1}H, ^{13}C, ^{15}N] probe, DMX (500 MHz) equipped with a TBI [^{1}H, ^{13}C, ^{15}N] *z*-gradient probe or AVA (600 MHz) spectrometer equipped with a TXI [^{1}H, ^{13}C, ^{15}N] *x,y,z*-gradient probe. ^{1}H NMR signals were referenced to the residual solvent peak, δ 2.52 (DMSO), δ 7.27 (chloroform) and δ 3.34 (methanol). Spectra for pH titrations were recorded on the Bruker DMX 500 spectrometer, with dioxan as an internal reference (δ 3.75). All spectra were recorded at 25°C unless stated otherwise, using 5 mm diameter tubes and standard pulse sequences modified by Dr Dusan Uhrin and Mr Juraj Bella (The University of Edinburgh). The data were processed using XWIN-NMR (Version 3.6 Bruker UK Ltd).

2.1.2 Ultraviolet-visible (UV-Vis) and fluorescence spectroscopy[4]

UV-Vis spectroscopy (wavelength of 200-800 nm) uses light in the visible (wavelength of 400-700 nm) and adjacent near ultraviolet (UV) and near infrared (NIR) ranges. The UV-Vis spectrum is a graph of light absorbance versus wavelength in a range of the UV-Vis regions of the electromagnetic spectrum, where molecules undergo electronic transitions between different energy levels.

Absorption measures transitions from the ground state to the excited state, while fluorescence spectroscopy deals with transitions from the excited state to the ground state. Excitation is an elevation in energy level above ground energy state (Figure 2.3).

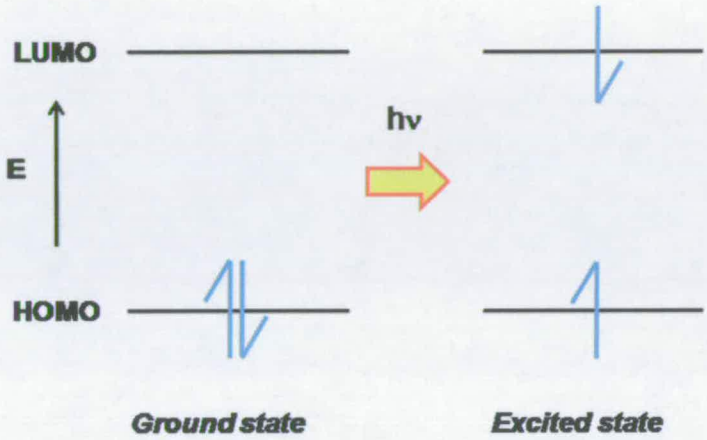

Figure 2.3 Promotion of the electron from the HOMO (highest occupied molecular orbital) to the LUMO (lowest unoccupied molecular orbital), caused by absorption of the photon of the same energy as the gap between the orbitals.

The transitions are classified as allowed and forbidden, dependent on their intensities. The probability of these transitions (intensities of transitions) is represented by ε (molar extinction coefficient):

$$\varepsilon = \log (I_0/I)/cl = A/cl$$

where I_0 and I are intensities of incident and transmitted light, respectively, c concentration, l a path length in cm and A absorbance.

Here some transitions that can occur in metal complexes are discussed. One of them, metal-to-ligand charge-transfer (MLCT) transition involves a MO with metal-like

character and those with ligand-like character. This is most commonly observed in complexes with ligands having low-lying π^* orbitals (aromatic ligands). Ligand-to-metal charge-transfer (LMCT) arises from transfer of electrons from an MO with ligand-like character to those with metal-like character. This type of transfer is predominant in metal complexes that have ligands with relatively high energy lone pairs or the metal with low-lying empty orbitals. These conditions imply that the acceptor level is available and low in energy. π - π^* transitions are ascribed as a promotion of an electron from a `bonding` π orbital of a ligand to an `antibonding` π orbital, designated as π^*. Many metal complexes are coloured due to d-d electronic transitions. Visible light of the correct wavelength is absorbed, promoting a lower energy d-electron to an higher excited state. This absorption of light causes colour. These colours are usually quite faint. This is because of the selection rules.

1) The spin rule: $\Delta S = 0$, the electron should not experience a change in spin. Electronic transitions which experience a change in spin are *spin forbidden* transitions.

2) Laporte's rule: d-d transitions for complexes which have a center of symmetry are forbidden - *symmetry forbidden* or *Laporte-forbidden* transitions.

Laporte-forbidden transitions tend to be more intense than *spin forbidden* transitions.

2.1.2.1 Experimental methods

A Perkin-Elmer Lambda-16 UV-Vis spectrophotometer was used with quartz cuvettes (1 cm path length; 0.5 mL) and PTP1 Peltier temperature controller, unless otherwise stated. Experiments were carried out at 25°C unless otherwise stated, in the range of 200-800 nm and at the scan rate of 420 nm/min (at 1 nm intervals). Spectra were processed using UV-Winlab software for Windows'95.

Fluorescence measurements were performed on a Shimadzu RF 40 spectrofluorophotometer using a 1 cm quartz cell. More details are described in Chapters 3 and 4.

2.1.3 Electrospray ionization mass spectrometry (ESI-MS)[5]

ESI-MS was used in this work to characterize synthesized complexes. ESI-MS is a solution based technique and the sample must be present as an ion in solution. If species is not already charged the addition of a small amount of acid or base can protonate or deprotonate it (positive and negative ESI, respectively).

The details vary with different commercial instruments, but the overall processes are similar. The sample, dissolved in the appropriate volatile solvent, is injected as a fine spray at a low flow rate (typical flow rates are 0.01 mL/min and concentrations required are in ppm) from a capillary held at a high voltage into a chamber at atmospheric pressure. The chamber into which the sample is sprayed is purged with a drying gas (usually nitrogen) which evaporates the solvent from the charged droplets.

As the droplets get smaller the charge density increases and ions are transferred to the gas phase once the charge density exceeds some critical value. The ions formed are then pumped through skimmer cones or similar, each at successively higher vacuum, before transferring to the mass analyzer.

2.1.3.1 Experimental methods

Positive-ion ESI (unless otherwise stated) mass spectra were obtained on a Micromass Platform II mass spectrometer and solutions were infused directly. The capillary voltage was 3.5 V and the cone voltage was either 15 or 25 V. The source temperature was dependent on the solvent used. Data were collected and analyzed on a MASS LYNX V3.5 Windows NT PC data system, unless otherwise stated.

2.1.4 Elemental analysis.

By determining the percentage of C, N and H and comparing these to theoretical values, elemental analysis provides information about the purity of compounds. Elemental analysis was used to characterize complexes described in this work.

2.1.4.1 Experimental methods

Elemental analyses were carried out by the Warwick Analytical Service or the University of Edinburgh, using an Exeter analytical analyser CE 440, or by the University of St. Andrews using a Carlo Erba CHNS analyser.

2.1.5 X-ray crystallography

X-ray crystallography determinates the arrangement of non-hydrogen atoms within a crystal. In this thesis, x-ray crystallography was used as a characterization method, together with other methods described in this Chapter.

2.1.5.1 Experimental methods

Diffraction data were collected and analyzed by Professor Simon Parsons and his research group at the University of Edinburgh. The instrument used, Bruker Smart Apex CCD diffractometer using Mo Kα radiation (λ = 0.71073 Å), is equipped with Oxford Cryosystems device that is operating at 150 K. Absorption corrections for all data sets were applied using the multi-scan procedure SADABS.[6] The details about the methods used are described in the following chapters.

2.1.6 Circular dichroism (CD)[7]

CD spectroscopy can be used to provide the information about molecular structure and about interactions between molecules. CD is used for studying chiral molecules (molecules that cannot be superimposed on their mirror images). All biological systems and many of non-living ones are chiral. A CD spectropolarimeter contains a source of monochromatic (more or less) left and right circularly polarized light and it detects the difference in absorbance of the two polarizations of light. Molecules

absorb energy in units called photons. A chiral molecule has no reflection plane (or other symmetry element) and any rearrangement of its electrons will not have one either, and the electrons would move in some kind of helix. The interaction of chiral molecules in circularly polarized light, with left- and right-handed photons will be different. Every chiral molecule therefore, would have both positive and negative CD signal.

2.1.6.1 CD of DNA

The UV absorbance of nucleic acids from 200 to 300 nm is due to transitions of the planar purine and pyrimidine bases. This band is believed to be composed of more than one transition predominated by π-π^* transitions whose assignment is still a matter of debate. The backbone begins to contribute at about 190 nm. In the CD spectrum, the purine bases have a negative signal, while the pyrimidine bases have a positive signal. The sugar units (D-deoxyribose) and the helix of DNA provide the original chirality. The CD spectrum of DNA arises from the CD induced into the transitions of the bases as a result of their coupling with each other since the bases stack on top of each other in a chiral (helical) fashion.

The signature of B-DNA in the CD spectrum (above 220 nm) is a positive band centered at 275 nm and a negative band at 240 nm, with a zero at 258 nm (Chapter 3). These bands are superimpositions result of all the couplings of the transitions arising from all the DNA bases. A-DNA is characterized by a positive CD band centred at 260 nm, which is larger than the corresponding B-DNA band, a fairly intense negative band at 210 nm, and a very intense positive band at 190 nm. Z-DNA does not readily form for all sequences. It is easily form for poly[d(G-C)]$_2$ in the presence

of highly charged ions. In the CD spectrum (above 200 nm) characteristic is a negative band at 290 nm and a positive band at 260 nm.

2.1.6.2 Experimental methods

CD measurements were performed on a Jasco J-720 spectropolarimeter equipped with a thermoelectrically-controlled cell holder. The cell pathlength was 1 cm and spectra were recorded in the range of 230–500 nm in 0.5 nm increments, with an averaging time of 1 s. The details of the experiments are described in Chapter 3.

2.1.7 Atomic absorption spectrometry (AAS)[8]

AAS is the measurement of the absorption of optical radiation by atoms in the gaseous state. In analytical chemistry, AAS is a technique for determining the concentration of a particular metal element in a sample. The electrons of the atoms in the atomizer of the instrument can be promoted to higher orbitals, by absorbing energy (light of a given wavelength). This amount of energy is specific to a particular electron transition for a particular element, and each wavelength usually corresponds to only one element, which gives selectivity to the technique.

A sample has to be atomized in order to be analyzed and the flame is typically used for this purpose. As the quantity of energy put into the flame is known, and the quantity remaining at the detector is measured, it is possible to calculate how many of these transitions took place, and thus get a signal that is proportional to the concentration of the element. Apart from flame there are other common atomizers,

such as a graphite furnace or plasma (e.g. inductively coupled plasma). The instrument used for the experiments described in this thesis is the FAAS (Flameless Atomic Absorption Spectrometer) equipped with the graphite tube atomizer.

2.1.7.1 Experimental methods

The FAAS (Flameless Atomic Absorption Spectrometry) measurements were carried out on a Varian AA240Z Zeeman atomic absorption spectrometer equipped with a GTA 120 graphite tube atomizer. More details about measurements are reported in Chapters 3 and 4. The measurements were performed with assistance of Dr Olga Novakova in Brno.

2.1.8 Molecular modeling[9]

2.1.8.1 Density Functional Theory (DFT)

Kohn-Sham DFT[10] is an important first-principle computational method for the accurate prediction of chemical and physical properties. The DFT approach provides, in most cases, a "chemical" accuracy of a few kcal/mol for binding energies; the computed orbitals are suitable for the typical MO-theoretical analyses and interpretations.

The major problem with DFT is that the exact functional for exchange and correlation are not known except for the free electron gas. However, approximations exist which permit the calculation of certain physical quantities. In physics the most widely used

approximation is the local-density approximation (LDA),[9] where the functional depends only on the density at the coordinate where the functional is evaluated. Various approximations have been implemented in the Amsterdam Density Functional (ADF, described bellow) program at the level of the LDA, and with corrections of the generalized gradient approximation (GGA) included. At GGA level the first implemented options included the formulas of Becke (excange), Perdew (correlation), Perdew-Wang (both) and Lee-Yang-Parr (correlation).[11-14]

The self-consistent solution of the Kohn-Sham DFT equations is obtained in an interactive self-consistent field (SCF) procedure. From a trial density matrix P^k the Fock matrix F^k is computed and diagonalized to obtain the eigenvectors, i.e. the MOs. The occupied MOs then yield a new trial density matrix P^{k+1}, etc. until P^k and P^{k+1} are identical, and we have reached self-consistency. The first derivatives of the energy with respect to nuclear displacements are calculated analytically for a particular geometry at the end of the SCF procedure.

2.1.8.2 The Amsterdam Density Functional (ADF) program

ADF is a program for electronic structure calculations that makes use of DFT. ADF was developed in the early seventies by the group of E. J. Baerends, working at the University of Amsterdam, and by the Ziegler group from Calgary.[15] At that time the program was named HFS, for Hartree-Fock-Slater. These two research groups with frequent additions and improvements of the program made ADF one of the widely used programs in quantum-chemical research. Recent developments enhance the efficiency and functionality of the program.

DFT is implemented in ADF and all the DFT implementations employ some kind of

numerical integration scheme. ADF uses a Gaussian-type quadrature method, which is based on partitioning of space in atomic cells. ADF exploits Slater-type (ST) functions as basis set elements, in terms the molecular orbitals (MOs) are expanded. The Gaussian-type orbitals (GTOs), in comparison, typically would need a factor of 3 more functions for the same level of basis set quality. The ADF package comprises a database with a large number of basis sets for all elements of the periodic table, ranging from minimum single-ζ (SZ) to doubly-polarised triple- ζ (TZ2P) basis sets. An important aspect of ADF is the (optional) use of a frozen core[16] to trim down the computational time by reducing the size of the variational basis set. Because deep-core atomic orbitals change very little upon bond formation, the frozen core approximation saves time without sacrificing much in quality. ADF supports the incorporation of relativistic effects (used for the heavy elements for which the frozen core approximation is applied), and a recently developed approximation is the zero-order regular approximation (ZORA).[17] In ADF, bonding energies are calculated directly, with respect to the fragments, by one single numerical integral of the difference in energy density between the overall molecule and the constituting fragments. The conductor-like screening model (COSMO)[18] has been implemented in ADF to include solvent effects.

The Veronoi Deformation Density (VDD)[19] method for computing atomic charges is based on the deformation density and a partitioning of space into non-overlapping atomic areas, the so-called Voronoi cells. The Voronoi cell of an atom is the region in space closer to the nucleus of that atom than to any other nucleus. The VDD charge of an atom monitors the flow of charge into, or out of the atomic Voronoi cell as a result of "turning on" the chemical interactions between the atoms.

2.1.8.3 Experimental methods

The coordinates used were obtained directly from the crystal structures unless the modifications were performed using ChemCraft (Version 1.5).[20] The calculations were carried out using DFT at the GGA as implemented in the ADF program (version 2007.01). Geometries and energies were obtained by using the Becke Perdew gradient-corrected functional (BP86) with scalar ZORA relativistic correction, unless otherwise stated. The frozen core approximation was applied using TZP bases. The COSMO as implemented in ADF was used to simulate the aqueous environment, with $\varepsilon = 78.4$ and a probe radius = 1.9 Å. The atomic radii used were Ru = 1.950, Cl = 1.725, O = 1.517, N= 1.608, C = 1.700 and H = 1.350. The VDD method for computing atomic charges was used. Default convergence criteria were applied for self-consistent field (SCF) and geometry optimisation. Further details are described in Chapters 4 and 5. The calculations were carried out with an assistance of Dr Robert J. Deeth.

2.1.9 Cancer cell growth inhibition

Cytotoxicity tests were performed by Emily Jones and Daniel Simpson (Oncosense Ltd). Compounds were tested for inhibitory growth activity against A2780 human ovarian and A549 human lung cancer cell lines, using a previously described protocol.[21] For compounds described in Chapter 3, cytotoxicity tests were performed at the Institute of Biophysics (Academy of Sciences of the Czech Republic; Brno, CR), as described in the appropriate chapter.

2.2 Synthesis and characterization of starting materials

2.2.1 Materials

$RuCl_3 \cdot 3H_2O$ was purchased from Precious Metals Online and used as received. The arenes (*m*- and *p*-terphenyls, biphenyl, dihydroanthacene and hexamethylbenzene) and α-terpinene were purchased from Sigma-Aldrich. Ethanol was dried over Mg/I_2 and THF over Na/benzophenone.

2.2.2 Birch reduction[22]

Birch reduction involves the reaction of benzene or a benzene derivative with an alkali metal in liquid ammonia containing an alcohol as a cosolvent. This is the classical Birch reduction pathway for monocyclic benzene derivatives with relatively low electron affinities, which do not readily form anions. The presence of alcohol is required to protonate the radical anion and shift the unfavorable equilibrium to the right leading to the completion of the reaction (formation of diene product).

On the other hand, the polycyclic aromatic systems generally undergo a transformation to the dianion without the presence of the alcohol as a proton source, and in this case water or ammonium chloride is used as a protonating agent (added to the solution of the already dianionized hydrocarbon). This modified Birch reduction was used for reduction of biphenyl (bip), *p*-terphenyl (*p*-terp) and *m*-terphenyl (*m*-terp) hydrocarbons. In the case of bip, rapid protonation is necessary to prevent its further reduction and isomerisation. Therefore in the reduction of bip ammonium

chloride is used as a source of protons. The details for individual reaction are described in the text bellow. Starting materials as well as the products from the reaction are listed in Table 2.1.

Table 2.1 Arenes used in Birch reductions and dienes obtained as products

Starting materials (arenes)	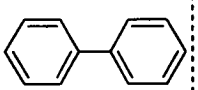 bip	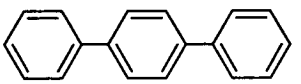 *p*-terp	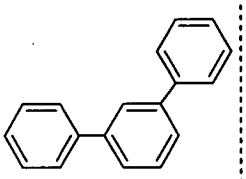 *m*-terp	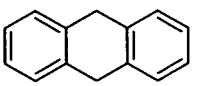 dha
Products from Birch reduction (dienes)	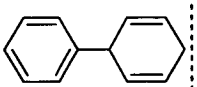 dhbip	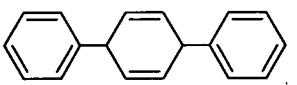 dh′-*p*-terp 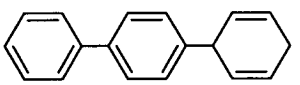 dh-*p*-terp 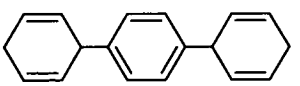 th-*p*-terp	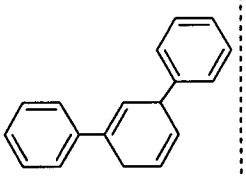 dh-*m*-terp	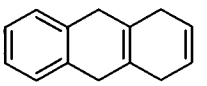 tha 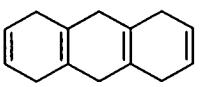 hha

1,4-Dihydrobiphenyl (dhbip).[23] Biphenyl (bip; 17.5 g, 113.6 mmol) was dissolved in a dry, freshly-distilled THF (250 mL) and this was added to 1 L of liquid ammonia, which had been condensed under argon into a 2 L flask equipped with a Dewar condenser, cooling bath (dry ice / acetone) and mechanical stirrer. Li wire (1.99 g, 286 mmol) was added in small pieces to the reaction mixture over ~3 min. The addition of Li was followed by a change of colour of the solution from white, via green to red. After 30 min of stirring and cooling, NH_4Cl (22 g, 412 mmol) was added into the reaction mixture and the solution turned white immediately. The cooling bath was removed and the ammonia was allowed to evaporate overnight. Water was added (350 mL) into the mixture and the pH was adjusted to 3 using HCl. The mixture was extracted with ether (3 × 250 mL) and the combined ether layers were washed with saturated NaCl solution (200 mL), and dried over $MgSO_4$. Removal of ether under reduced pressure afforded a yellowish oily product, which was distilled (58°C / 10^{-2} mbar) to give 14.40 g (81%, 15 mL, d = 0.96 g/cm^3) of pure product. ^{1}H NMR ($CDCl_3$): δ 7.28 (m, 5H), 5.85 (m, 4H), 3.40 (broad t, 1H), 2.77 (broad m, 2H).

1,4,5,8,9,10-Hexahydroanthracene (hha). A modification of the previously published procedure[24] for reducing anthracene to hha in liquid ammonia in the presence of Na, was applied here. 9,10-Dihydroanthracene (dha; 4.5 g, 24.99 mmol), used instead of anthracene, was dissolved in a dry and freshly-distilled mixture of THF (300 mL) and ethanol (130 mL). This was followed by addition of the solution to the refluxing ammonia (1 L), which had been condensed under argon into a 2 L flask equipped with a Dewar condenser, cooling bath (dry ice / acetone) and

mechanical stirrer. Li wire (12 g, 0.5 mols), used here instead of Na, was cut into small pieces and added to the reaction mixture over ~3 min. After 2 h of cooling and stirring, the cooling bath was removed and the ammonia was allowed to evaporate overnight. Water (200 mL) was added into the mixture. The mixture was extracted with ether (4 × 250 mL) and the combined ether layers were washed with saturated NaCl solution (200 mL) and dried over $MgSO_4$. Removal of ether on a rotary evaporator afforded a white solid which was washed with warm petroleum ether (10 × 250 mL) until all 1,4,9,10-tetrahydroanthracene (tha), present as a side product, was removed and only hha remained as white needles. Yield: 2.7 g (65%). ^{1}H NMR ($CDCl_3$): δ 5.68 (s, 4H), 2.51 (s, 8H), 2.37 (s, 4H).

1,4,9,10-Tetrahydroanthracene (tha). A modification of the previously published procedure for the reduction of dha to tha,[25] was used here. Dha (6.5 g, 36.1 mmol) dissolved in 300 mL of dry and freshly-distilled THF was added to refluxing ammonia (1 L) which had been condensed under argon into a 2 L flask equipped with a Dewar condenser, cooling bath (dry ice / acetone) and mechanical stirrer. Li metal wire (0.66 g, 95.1 mmol) was added in small pieces. After refluxing and stirring for 2 h, dry and freshly-distilled ethanol (60 mL) was added to the reaction mixture followed by 130 mL of water, and the ammonia was allowed to evaporate overnight. Additional water (50 mL) was added into the reaction mixture. This was extracted with diethyl ether (3 × 250 mL) and the combined ether layers were washed with saturated NaCl solution (200 mL) and dried over $MgSO_4$. Removal of ether on a rotary evaporator afforded a light yellow solid which was recrystallised (10 ×) from petroleum ether to remove completely hha, formed as a side product as white needles. The residual yellowish solid (0.26 g) contained the starting material dha (40%) and

the product, tha (60%). ^{1}H NMR ($CDCl_3$) of tha: δ 7.11 (m, 4H), 5.78 (s, 2H), 3.25 (s, 4H), 2.70 (s, 4H).

Interaction of Li metal with *p*-terphenyl (*p*-terp) in liquid ammonia leads to formation of 3 different species: 1,4-dihydro-*p*-terphenyl (dh-*p*-terp) containing a reduced terminal ring of the tricyclic ring system, 1′,4′-dihydro-*p*-terphenyl (dh′-*p*-terp) containing a reduced the middle ring of the tricyclic ring system, and 1′,4′,1″,4″-tetrahydro-*p*-terphenyl (th-*p*-terp) that contains both terminal rings reduced. The ratio of the mixture of dh-*p*-terp, dh′-*p*-terp and th-*p*-terp is dependent on the conditions used.[26] When water is used as a source of protons, the inner ring product is repressed.[27] However this requires a small reaction scale, and in this work water could not be used as a quenching agent as 1 L of condensed cold ammonia was present (*vide supra*) and this would create extensive production of the gas, by warming up the solution. Therefore dh-*p*-terp was isolated as a side product from the Birch reduction for obtaining the dh′-*p*-terp. The slight difference in solubility of these two products, allowed the purification of dh-*p*-terp to be carried out (*vide supra*).

1, 4-Dihydro-*p*-terphenyl (dh-*p*-terp). A solution of *p*-terp (25 g, 108.55 mmol) in THF (500 mL) was added to refluxing ammonia (1 L) which had been condensed under argon into a 2 L flask equipped with a Dewar condenser, cooling bath (dry ice / acetone) and mechanical stirrer. Li wire (1.74 g, 251.11 mmol) was added and upon the addition the solution turned deep blue. After 45 min of refluxing the reaction mixture was quenched by addition of NH_4Cl (100 g, 1.87 mol), and the solution turned white. The ammonia was left to evaporate overnight. Products were isolated by

partition between water (400 mL) and ether (4 × 200 mL), followed by separation of the ether layer which was washed with a saturated NaCl solution (200 mL), dried over $MgSO_4$ and the solvent removed under reduced pressure. Fractional recrystallization from petroleum ether led to the purification of the products. The less soluble diene was dh′-*p*-terp and the diene remaining in the filtrate was dh-*p*-terp. This procedure was used to separate and purify the dienes. Yield of dh-*p*-terp: 0.35 g (1%). ^{1}H NMR ($CDCl_3$) of dh-*p*-terp: δ 7.50 (m, 9H), 5.85 (d of d, 4H), 4.05 (broad t, 1H), 2.80 (broad m, 2H) and ^{1}H NMR ($CDCl_3$) of dh′-*p*-terp: δ 7.50 (m, 10H), 5.90 (s, 4H), 4.12 (s, 2H).

The isolation and purification of th-*p*-terp (obtained as a side product) was carried out using fractional recrystallization from ethanol. ^{1}H NMR ($CDCl_3$) of th-*p*-terp: δ 7.20 (s, 4H), 5.80 (d of d, 8H), 4.0 (broad m, 2H), 2.78 (broad m, 4H).

1,4-Dihydro-*m*-terphenyl (dh-*m*-terp). A solution of *m*-terphenyl (*m*-terp; 11.5 g, 49.5 mmol) in THF (350 mL) was added to refluxing ammonia (1 L) which had been condensed under argon into a 2 L flask equipped with a Dewar condenser, cooling bath (dry ice / acetone) and mechanical stirrer. Li wire (0.77 g, 110.77 mmol) was added and upon the addition the solution turned deep blue. After 30 min of stirring and cooling, the reaction mixture was quenched by addition of NH_4Cl (100g, 1.87 mol). The ammonia was left to evaporate overnight. The product was isolated by partition between water (400 mL) and ether (3 × 250 mL) and the separation of ether layer was followed by washing with 200 mL of a saturated NaCl solution, drying over $MgSO_4$ and evaporation of the solvent under reduced pressure. Yield: 5.5 g (47%). ^{1}H NMR ($CDCl_3$): δ 7.50 (m, 10H), 6.25 (m, 1H), 6.03 (m, 1H), 5.90 (m, 1H), 4.23 (broad m, 1H), 3.23 (broad m, 2H).

2.2.3 Preparation of dimers

All the dimers were prepared according to literature methods,[28] using a similar procedure. Typically a different excess of the reduced hydrocarbon (diene) was added to an ethanolic solution of $RuCl_3 \cdot 3H_2O$. Details for individual reactions and characterization of dimers are described below.

[(η^6-*p*-cym)RuCl$_2$]$_2$. $RuCl_3 \cdot 3H_2O$ (3.50g, 16.8 mmol) was dissolved in dried and freshly-distilled ethanol (100 mL). Into this, α-terpinene (30 mL, 25.11 g, 202 mmol) was added drop-wise and the solution was heated to reflux for 24 h. During this time the solution changed color from originally dark brown to red. After the solution was allowed to cool down to room temperature, it was filtered to give a reddish-orange solid, which was washed with diethyl ether until the filtrate was clear and dried overnight in vacuum. Yield: 3.50 g (85%). ^{1}H NMR ($CDCl_3$): δ 5.50 (d, 4H), 5.35 (d, 4H), 2.95 (m, 2H), 2.15 (s, 6H), 1.30 (d, 12H).

[(η^6-hmb)RuCl$_2$]$_2$. The dimer [(η^6-*p*-cym)RuCl$_2$]$_2$ (2.00 g, 3.26 mmol) and hexamethylbenzene (hmb; 20 g, 123 mmol) were placed in a flask and heated up to ca. 180°C for 3 h, and the mixture gradually turned from orange-red to orange-brown. During the heating of the mixture solidified hmb around the top of the flask was continually scraped back down into the melting mixture. The reaction mixture was allowed to cool down, the orange-brown solid was washed with hexane (200 mL), followed by diethyl ether (200 mL) and the excess of hmb was removed by sublimation. The brownish solid left was filtered through celite and washed with

chloroform (400 mL) until the filtrate turned colourless. Chloroform was removed on a rotary evaporator to leave a reddish-brown solid. Yield: 1.05 g (49%). ^{1}H NMR ($CDCl_3$): δ 2.01 (s, 18H).

[(η^6-bip)RuCl$_2$]$_2$. 1,4-Dihydrobiphenyl (dhbip; 4.3 g, 27.5 mmol) was added to a solution of $RuCl_3 \cdot 3H_2O$ (5 g, 19.12 mmol) in dry, freshly-distilled ethanol (60 mL). The reaction mixture was left refluxing under argon for 48 h. The warm reaction mixture was filtered and the brown solid was washed with fresh ethanol (3 mL) followed by ether (4 × 10 mL) and dried under vacuum. Yield: 5.06 g (81%). ^{1}H NMR (DMSO-d$_6$): δ 7.86 (d, 2H), 7.54 (m, 3H), 6.47 (d, 2H), 6.11 (m, 3H).

[(η^6-tha)RuCl$_2$]$_2$. 1,4,5,8,9,10-Hexahydroanthracene (hha; 2.7 g, 14.6 mmol) was added to a solution of $RuCl_3 \cdot 3H_2O$ (1.42 g, 5.37 mmol) in dry, freshly-distilled ethanol (30 mL) and the reaction mixture refluxed under argon for 48 h. Immediately after the refluxing was stopped, the reaction mixture was filtered and yellowish-brown solid washed with fresh ethanol (2 mL) followed by ether (4 × 10 mL) and dried under vacuum. Yield: 1.3 g (67%). ^{1}H NMR (DMSO-d$_6$): δ 5.83 (m, 2H), 5.71 (s, 2H), 5.61 (m, 2H), 3.21 (m, 2H), 3.05 (m, 2H), 2.5 (m, 4H).

[(η^6-dha)RuCl$_2$]$_2$. 1,4,9,10-Tetrahydroanthracene (tha; 0.26 g, 1.44 mmol) was added to a solution of $RuCl_3 \cdot 3H_2O$ (1.28 g, 4.84 mmol) in dry, freshly-distilled ethanol (30 mL). This mixture was left refluxing under argon for 48 h. The warm reaction mixture was filtered and dark brown solid was washed with fresh ethanol (2 mL) followed by ether (4 × 10 mL) and dried under vacuum. Yield: 0.29 g (18%). ^{1}H NMR (DMSO-d$_6$): δ 7.27 (m, 4H), 5.89 (m, 4H), 3.92 (m, 4H).

[(η^6-*p*-terp)RuCl$_2$]$_2$. 1,4-Dihydro-*p*-terphenyl (dh-*p*-terp; 0.35 g; 1.34 mmol) was added to a solution of $RuCl_3 \cdot 3H_2O$ (1.55 g, 6.68 mmol) in dry, freshly-distilled ethanol (60 mL). This mixture was left refluxing under argon for 48 h and was filtered while still warm. The dark brown solid was washed with fresh ethanol (5 mL) followed by ether (2 × 10 mL) and dried under vacuum. Soxhlet extraction was carried out using chloroform as a solvent in order to purify the dimer. The solvent was removed under reduced pressure and brownish solid dried in vacuum. Yield: 0.5 g (20%). ^{1}H NMR ($CDCl_3$): δ 7.95 (d, 2H), 7.80 (d of d, 4H), 7.52 (t, 2H), 7.43 (t, 1H), 6.50 (d, 2H), 6.10 (m, 3H).

[(η^6-*m*-terp)RuCl$_2$]$_2$. 1,4-Dihydro-*m*-terphenyl (dh-*m*-terp; 5.5 g; 23.7 mmol) was added to a solution of $RuCl_3 \cdot 3H_2O$ (1.60 g, 6.12 mmol) in dry, freshly-distilled ethanol (60 mL). This mixture was left refluxing under argon for 48 h. The reaction mixture was filtered while still warm and the dark brown solid was washed with fresh ethanol (5 mL) followed by ether (2 × 10 mL) and dried under vacuum. Soxhlet extraction was carried out using chloroform, in order to purify the dimer. The solvent was removed under reduced pressure and the bright orange solid dried in vacuum. Yield: 1 g (41%). ^{1}H NMR ($CDCl_3$): δ 7.80 (m, 8H), 7.45 (m, 12H), 6.23 (m, 4H), 6.05 (d, 4H).

2.3 References

(1) Hore, P. J., *Nuclear Magnetic Resonance*. Oxford University Press Inc: New York, **1995**.

(2) Piotto, M.; Saudek, V.; Sklenar, V. *J. Biomol. NMR* **1992,** *2*, 661-5.

(3) Hwang, T.-L.; Shaka, A. J. *J. Mag. Reson., Series A* **1995,** *112*, 275-9.

(4) Shriver, D. F.; Atkins, P. W., *Inorganic Chemistry*. Oxford University Press: Belgium, **1999**.

(5) Henderson, W.; Nicholson, B. K.; McCaffrey, L. J. *Polyhedron* **1998,** *17*, 4291-4313.

(6) Sheldrick, G. M. *SADABS*, 2006/1; University of Gottingen: Gottingen, Germany, **2006**.

(7) Rodger, A.; Norden, B., *Circular Dichroism and Linear Dichroism*. Oxford University Press: New York, **1997**.

(8) Welz, B. *Atomic Absorption Spectrometry*. Wiley-VCH, Weinheim, **1985**.

(9) Te Velde, G.; Bickelhaupt, F. M.; Baerends, E. J.; Fonseca Guerra, C.; Van Gisbergen, S. J. A.; Snijders, J. G.; Ziegler, T. *J. Comput. Chem.* **2001,** *22*, 931-967.

(10) Parr, R. G.; Yang, W., *Density-functional Theory of Atoms and Molecules*. Oxford University Press: New York, **1989**; p 333.

(11) Perdew, J. P.; Wang, Y. *Phys. Rev. B* **1986,** *33*, 8800.

(12) Perdew, J. P. *Phys. Rev. B* **1986,** *33*, 8822.

(13) Becke, A. D. *Phys. Rev. A* **1988**, 3098.

(14) Lee, C.; Yang, W.; Parr, R. G.; *Phys. Rev. B* **1988,** *37*, 785.

(15) Baerends, E. J.; Ellis, D. E.; Ros, P. *Chem. Phys.* **1973,** *2*, 41-51.

(16) Baerends, E. J.; Ellis, D. E.; Ros, P. *Theor. Chim. Acta* **1972,** *27*, 339-54.

(17) Van Lenthe, E.; Van Leeuwen, R.; Baerends, E. J.; Snijders, J. G. *Int. J. Quantum Chem.* **1996,** *57*, 281-93.

(18) Klamt, A. *J. Phys. Chem* **1995,** *99*, 2224.

(19) Te Velde, G., *PhD thesis*, Vrije Universiteit, Amsterdam, **1990**.

(20) Horn, A. *Nachricht. Chem.* **2007,** *55*, 415-416.

(21) Dougan, S. J.; Melchart, M.; Habtemariam, A.; Parsons, S.; Sadler, P. J. *Inorg. Chem.* **2007,** *46*, 1508.

(22) Harvey, R. G. *Synthesis* **1970,** *2*, 161-72.

(23) Birch, A. J.; Nadamuni, G. *J. Chem. Soc., Perkin Trans.* **1974**, 545-52.

(24) Birch, A. J.; Fitton, P.; Smith, D. C. C.; Steere, D. E.; Stelfox, A. R. *J. Chem. Soc.* **1963**, 2209-16.

(25) Harvey, R. G. *J. Org. Chem.* **1967,** *32*, 238-40.

(26) Rabideau, P. W. *Tetrahedron* **1989,** *45*, 1579-603.

(27) Harvey, R. G.; Lindow, D. F.; Rabideau, P. W. *J. Am. Chem. Soc.* **1972,** *94*, 5412-20.

(28) Zelonka, R. A.; Baird, M. C. *Can. J. Chem.* **1972,** *50*, 3063.

Chapter 3

Terphenyl Ru^{II} complexes

"The joy of discovery is certainly the liveliest that the mind of man can ever feel."

Claude Bernard

3.1 Introduction

Organoruthenium complexes of the type $[(\eta^6\text{-arene})Ru^{II}(en)Cl]^+$, where arene = benzene (bz) or a benzene derivative, and en = ethylenediamine exhibit anticancer activity, including activity against cisplatin resistant cancer cells.[1, 2] This class of complexes can form strong monofunctional adducts with DNA.[2] The selectivity of pseudo-octahedral Ru^{II} arene en complexes for guanine (G) residues in DNA was found in the studies of reactions of DNA with Ru^{II} arene complexes of the type $[(\eta^6\text{-arene})Ru(en)Cl]^+$, where the arene is biphenyl (bip), dihydroanthracene (dha), tetrahydroanthracene (tha), *p*-cymene (*p*-cym), or bz.[3] $[(\eta^6\text{-bip})Ru(en)Cl]^+$ binds to DNA through coordination to G *N7* as well as noncovalently, through hydrophobic interactions between the arene and DNA. These hydrophobic interactions may include intercalation of the non-coordinated phenyl ring between DNA bases and minor groove binding. Intramolecular π-π arene-nucleobase stacking has been observed in the crystal structure of $[(\eta^6\text{-bip})Ru(en)(9\text{-EtG-}N7)][PF_6]_2$,[4] as well as a strong H-bonding between an NH of en and C6O from G and both contribute to the G-specificity.[5]

In this Chapter the synthesis and characterization of new complexes of the type $[(\eta^6\text{-arene})Ru(en)Cl]^+$, where the arene is *ortho*-, *meta*- or *para*-terphenyl (*o*-, *m*- or *p*-terp) are reported. These complexes were synthesized in order to investigate the effect on cytotoxicity of an additional phenyl ring compared to bip as arene. Such complexes are expected to show enhanced arene intercalation compared to the bip analogue. In the case of *p*-terp complex, Ru is bound to a terminal phenyl ring whereas in the cases

of *o*- and *m*-terp analogues, Ru is bound to the central phenyl ring. Aromatic hydrocarbons consisting of a chain of three benzene rings, terphenyls (terps), have three isomers in which the terminal rings are *o*-, *m*- or *p*-substituents of the central ring. Most of the natural terphenyls are *p*-terp derivatives. Very few *m*-terp derivatives occur naturally, and *o*-terps have not been found in nature.[6] In recent years, it has been reported that some terphenyls exhibit significant biological activity, such as neuroprotective, antithrombotic, anticoagulant, and cytotoxic activity. It has also been found that some popular edible mushrooms are rich in terphenyls, a sign that the toxicity of terphenyls is low.

The potency of the *p*-terp complex (**1**) against A2780 human ovarian cancer cells (IC_{50} = 4 μM, IC_{50} = concentration inhibiting cell growth by 50%), reported in this Chapter, is higher than that of the bip analogue (IC_{50} = 6 μM),[2] whereas, intriguingly, the *o*- and *m*-terp complexes (complexes **2** and **3**) appeared to be much less active (with IC_{50} values of 30 μM for complex **2** and 42 μM for complex **3**).

In this Chapter the relationship between cytotoxicity, cellular uptake and DNA binding of complexes consisting of *p*-, *o*- or *m*-terp arenes (complexes **1**, **2**, and **3**, respectively) is investigated. Their activity towards human ovarian tumor cell lines A2780 (parent, cisplatin-sensitive) and A2780cisR (with acquired cisplatin resistance), human ovarian carcinoma CH1 (cisplatin sensitive) and human mammary carcinoma SKBR3 (intrinsically cisplatin resistant) cell lines was also investigated.

3.2 Experimental section

3.2.1 Materials

The starting dimers $[(\eta^6\text{-arene})RuCl_2]_2$, arene = *p*-terphenyl (*p*-terp, bound to the Ru through the terminal phenyl ring), *o*-terphenyl (*o*-terp, bound to the Ru through the central phenyl ring) and *m*-terphenyl (*m*-terp, bound to the Ru through the central phenyl ring), are prepared as described in Chapter 2. Ethylenediamine (en) and 1,3-propylenediamine (pda) were purchased from Sigma-Aldrich. Methanol was dried over Mg/I_2. Cisplatin and dimethylsulfoxide (DMSO) were obtained from Sigma-Aldrich. [PtCl(dien)]Cl (dienPt) was a generous gift of Professor G. Natile from University of Bari. All other reagents were obtained from commercial suppliers.

Stock solutions of complexes for the biophysical and biochemical studies were prepared at the concentration of 5×10^{-4} M in water, filtered and stored at room temperature in the dark. Stock solutions of metal complexes for the cytotoxicity and cellular uptake studies (performed by Anna Halamikova at University of Brno, Czech Republic) were prepared in DMSO and used immediately after dissolution. The concentrations of ruthenium or platinum in the stock solutions were determined by Flameless Atomic Absorption Spectrometry (FAAS), which is described in Chapter 2. CT DNA (42% G + C, mean molecular mass ca. 2×10^7) was prepared and characterized as described previously.[7, 8] pSP73KB (2455 bp) plasmid (superhelical density -0.036) was isolated according to standard procedures. EtBr was obtained from Merck KgaA and agarose purchased from FMC BioProducts.

3.2.2 Preparation of complexes

All complexes were synthesized using a similar procedure. Typically the ligand (2 mol equiv) was added to a methanolic solution of $[(\eta^6\text{-arene})RuCl_2]_2$, where arene = *p*-terp, *o*-terp or *m*-terp. Details for individual reactions are described below.

$[(\eta^6$-*p*-terp)Ru(en)Cl][PF_6] (1). To a suspension of $[(\eta^6$-*p*-terp)$RuCl_2]_2$ dimer (0.10 g, 0.125 mmol) in dry, freshly-distilled methanol (50 mL) en (17 μL, 0.250 mmol) was added. The reaction mixture was stirred at ambient temperature under argon, overnight and the resulting clear yellow solution was filtered. NH_4PF_6 (0.061 g, 0.375 mmol) was added and the flask shaken. A precipitate started to appear almost immediately. The flask was kept at -20°C overnight, and the product was collected by filtration, washed with cold methanol and ether, and dried in air to give an orange solid. Yield: 0.061 g (43%).

Crystals suitable for x-ray analysis were obtained by slow evaporation of a methanolic solution at ambient temperature and the complex crystallized as $[(\eta^6$-*p*-terp)Ru(en)Cl][PF_6]. ESI-MS: calcd for $C_{20}H_{22}ClRuN_2^+$ $[M]^+$ m/z 426.9, found 427.0. ^{1}H NMR in DMSO-d_6: δ 7.87 (d, 2H), 7.80 (d, 2H), 7.74 (d, 2H), 7.52 (t, 2H), 7.42 (t, 1H), 6.50 (d, 2H; NH), 6.22 (d, 2H), 5.90 (t, 1H), 5.82 (t, 2H), 4.20 (d, 2H; NH), 2.31 (m, 2H), 2.22 (m, 2H). Anal. calcd for $C_{20}H_{22}ClRuN_2PF_6$: C, 42.00; H, 3.88; N, 4.90. Found: C, 42.75; H, 3.97; N, 4.90.

[(η^6-*o*-terp)Ru(en)Cl][PF_6] (2). Complex **2** was prepared by Dr Abraha Habtemariam. To a suspension of [(η^6-*o*-terp)$RuCl_2$]$_2$ dimer (0.05 g, 0.06 mmol) in dry, freshly-distilled methanol (50 mL) en (8 μL, 0.12 mmol) was added. The rest of the procedure was the same as described for complex **1**. After addition of NH_4PF_6 (0.03 g, 0.18 mmol) the fine yellow solid was isolated as described for complex **1** and recrystallized from methanol/ether. Yield: 0.023 g (32%).

ESI-MS: calcd for $C_{20}H_{22}ClRuN_2^+$ $[M]^+$ m/z 426.9, found 427.0. ^{1}H NMR in DMSO-d_6: δ 7.43 (m, 4H), 7.31 (m, 2H), 7.26 (m, 4H), 6.49 (d, 2H; NH), 5.95 (m, 4H), 4.31 (d, 2H; NH), 2.36 (m, 2H), 2.23 (m, 2H). Anal. calcd for $C_{20}H_{22}ClRuN_2PF_6$: C, 42.00; H, 3.88; N, 4.90. Found: C, 42.06; H, 3.75; N, 4.17.

[(η^6-*m*-terp)Ru(en)Cl][PF_6] (3). To a suspension of [(η^6-*m*-terp)$RuCl_2$]$_2$ dimer (0.053 g, 0.065 mmol) in dry, freshly-distilled methanol (50 mL) en (8.7 μL, 0.13 mmol) was added. The rest of the procedure was the same as described above. After addition of NH_4PF_6 (0.032 g, 0.19 mmol) brownish solid was isolated as described for complex **1** and recrystallized from methanol. Yield: 0.024 g (32%).

ESI-MS: calcd for $C_{20}H_{22}ClRuN_2^+$ $[M]^+$ m/z 426.9, found 427.0. ^{1}H NMR in DMSO-d_6: δ 7.92 (d of d, 4H), 7.52 (m, 6H), 6.60 (s, 1H), 6.43 (d of d, 2H), 6.35 (d, 2H; NH), 5.85 (t, 1H), 4.17 (d, 2H; NH), 2.30 (m, 2H), 2.15 (m, 2H). Anal. calcd for $C_{20}H_{22}ClRuN_2PF_6$: C, 42.00; H, 3.88; N, 4.90. Found: C, 42.14; H, 4.11; N, 4.93.

[(η^6-*m*-terp)Ru(pda)Cl][PF_6] (4). To a suspension of [(η^6-*m*-terp)$RuCl_2$]$_2$ dimer (0.050 g, 0.06 mmol) in dry, freshly-distilled methanol (50 mL) pda (10 μL, 0.124 mmol) was added. The rest of the procedure was the same as described above. After

addition of NH_4PF_6 (0.03 g, 0.18 mmol) fine orange solid was isolated as described for complex **1** and recrystallized from methanol/ether. Yield: 0.026 g (36%).

Crystals suitable for x-ray analysis were obtained by slow evaporation of a methanolic/ether solution at ambient temperature and the complex crystallized as [(η^6-*m*-terp)Ru(pda)Cl][PF_6]. ESI-MS: calcd for $C_{21}H_{24}ClRuN_2^+$ $[M]^+$ m/z 440.9, found 441.1. ^{1}H NMR in DMSO-d_6: δ 8.00 (d of d, 4H), 7.54 (m, 6H), 6.80 (s, 1H), 6.50 (d of d, 2H), 6.20 (d, 2H; NH), 6.05 (t, 1H), 3.10 (m, 2H), 2.70 (d, 2H; NH), 2.12 (m, 2H), 1.4 (m, 2H).

3.2.3 X-ray crystallography

The details of the instrumentation used, are described in Chapter 2. The structure of complex **1** was solved by Professor Simon Parsons by Patterson method (DIRDIF)[9], while the structure of **4** was solved by Stephen Moggach by direct method (SIR92)[10]. The structures were refined by full-matrix least squares against $|F|^2$ using SHELXL[11] for the structure of **1** and CRYSTALS[12] for the structure of **4**. Hydrogen atoms were placed in calculated positions, and all non-H atoms were modelled with anisotropic displacement parameters. The final conventional *R* factor (based on *F* and 3564 out of 4590 with $F > 4\sigma(F)$) was 0.0479 for the structure of **1**, and the final conventional *R* factor (based on *F* and 4982 out of 6331 with $F > 4\sigma(F)$) was 0.0297 for the structure of **4**. Other crystal and refinement data are summarized in Table 3.1. The crystal structure of **1** has been deposited in the Cambridge Crystallographic Data Centre under the accession number CCDC 681045.

3.2.4 Cytotoxicity

The cytotoxicity tests were performed at the Institute of Biophysics in Brno (CR). The tumour cell lines A2780, A2780cisR, CH1 and SKBR3 were cultured in RPMI 1640 medium (Gibco) (A2780 and A2780cisR) and Dulbecco's Modified Eagle's Medium (DMEM) (CH1 and SKBR3), supplemented with 10% FBS, 50 μg/mL gentamycin at 37°C in an atmosphere of 95% of air and 5% CO_2. Cell death was evaluated by using a system based on the tetrazolium compound MTT [3-(4,5-dimethyl-2-thiazolyl)-2,5-diphenyl-2H-tetrazolium bromide] which is reduced by living cells to yield a soluble formazan product that can be detected colorimetrically.[13] Cells were seeded in 96-well sterile plates at a density of 10^4 cells/well in 100 μL of medium and were incubated 16 h. The final concentration of DMSO in cell culture medium did not exceed 0.25%. Complexes **1**, **2** and **3** were added to final concentrations from 0 to 256 μM in a volume of 100 μL/well. Seventy-two hours later 10 μL of a freshly diluted MTT solution (2.5 mg/mL) was pipetted into each well and the plate was incubated at 37°C in a humidified 5% CO_2 atmosphere. After 5 h the medium was removed and the formazan product was dissolved in 100 μL of DMSO. The cell viability was evaluated by measurement of the absorbance at 570 nm, using an Absorbance Reader Sunrice Tecan Schoeller. IC_{50} values (complex concentration that produces 50% of cell growth inhibition) were calculated from curves constructed by plotting cell survival (%) versus drug concentration (μM). All experiments were made in quadruplicate.

3.2.5 Cellular ruthenium complex uptake

The cellular uptake experiments were performed at the Institute of Biophysics in Brno (CR). Cellular uptake of complexes **1-3**, and cisplatin was measured in A2780 and A2780cisR cells (sensitive and resistant to cisplatin, respectively). The cells were seeded in 60 mm tissue culture dishes (30 000/cm^2). After overnight incubation, the cells were treated with the ruthenium complex for 72 h at the concentrations corresponding to the IC_{50} values (these concentrations were verified by the measurement of ruthenium in the growing medium by FAAS). The attached cells were washed twice with PBS (4°C), the pellet stored at -80°C and ruthenium content determined by FAAS. For other details, see the results section. All experiments were performed in quadruplicate.

3.2.6 Metalation reactions in cell-free media

Calf thymus (CT) and plasmid DNAs were incubated with ruthenium or platinum complexes in 10 mM $NaClO_4$ (pH = 6) at 37°C for 24 h in the dark, if not stated otherwise. The values of r_b were determined by FAAS.

3.2.7 Fluorescence measurements

The details of instrumentation are described in Chapter 2. Fluorescence measurements of CT DNA modified by Ru^{II} arene complexes **1**, **2** and **3**, in the presence of EtBr were performed at an excitation wavelength of 546 nm, and the emitted fluorescence was analyzed at 590 nm. The fluorescence intensity was measured at 25°C in 0.4 M NaCl to avoid secondary binding of EtBr to DNA.[14, 158] The concentrations were 0.01 mg/mL for DNA and 0.04 mg/mL for EtBr, which corresponded to the saturation of all intercalation sites of EtBr in DNA.[14]

3.2.8 DNA melting

The melting curves of CT DNA were recorded by measuring the absorbance at 260 nm. The melting curves of unmodified or ruthenated DNA were recorded in a medium containing 10 mM $NaClO_4$ with 1 mM Tris-HCl/0.1 mM EDTA, pH= 7.4. The value of t_m (melting temperature) was determined as a temperature corresponding to a maximum on the first-derivative profile of the melting curves. The t_m values could be thus determined with an accuracy of ± 0.3°C.

3.2.9 Unwinding of negatively supercoiled DNA

The unwinding experiments were performed by Dr Jana Kasparkova at the Institute of Biophysics in Brno (CR). Unwinding of closed circular supercoiled pSP73KB plasmid DNA was assayed by an agarose gel mobility shift assay.[16] The unwinding angle Φ, induced per ruthenium-DNA adduct was calculated upon the determination of the r_b value (r_b values are defined as the number of atoms of the metal bound per nucleotide residue) at which the complete transformation of the supercoiled to relaxed form of the plasmid was attained. Samples of plasmid DNA were incubated with complexes **1**, **2** or **3** at 37°C in the dark for 24 h. All samples were precipitated by ethanol and redissolved in the TAE (Tris-acetate/EDTA) buffer. One aliquot of the precipitated sample was subjected to electrophoresis on 1% agarose gels running at 25°C in the dark with TAE buffer and the voltage set at 25 V. The gels were then stained with EtBr, followed by photography with a transilluminator. The other aliquot was used for the determination of r_b values by FAAS.

3.2.10 Other Physical Methods

Absorption spectra were measured with a Beckman DU 7 4000 spectrophotometer equipped with a thermoelectrically controlled cell holder and quartz cells with the path length of 1 cm. For FAAS analysis, DNA was precipitated with ethanol and

dissolved in 0.1 M HCl. The gels were visualized by using a BAS 2500 FUJIFILM bioimaging analyzer.

3.3 Results

3.3.1 Synthesis and characterization

Complexes reported in this Chapter are shown in Figure 3.1.

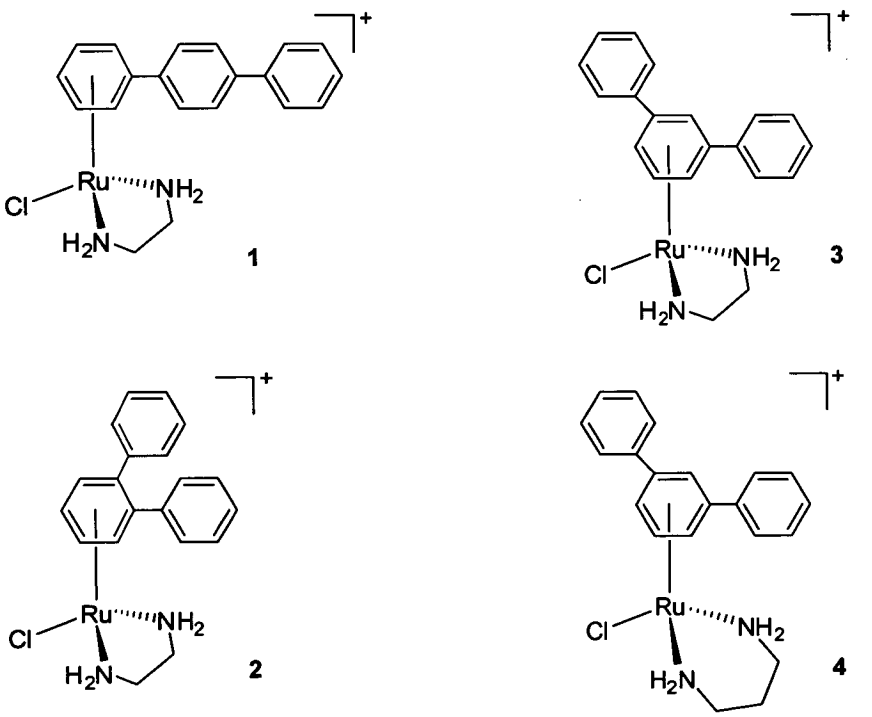

Figure 3.1 Chemical structures of Ru^{II} arene complexes **1**, [(η^6-*p*-terp)Ru(en)Cl]$^+$; **2**, [(η^6-*o*-terp)Ru(en)Cl]$^+$; **3** [(η^6-*m*-terp)Ru(en)Cl]$^+$ and **4** [(η^6-*m*-terp)Ru(pda)Cl]$^+$.

Synthesis and characterization of these complexes are reported in the experimental section. UV-Vis spectra of complexes **1**, **2** and **3** are shown in Figure 3.2A. The UV-Vis spectrum of complex **1** in water shows a shoulder at 260 nm (ε = 13497 $M^{-1}cm^{-1}$) and a band at 285 nm (ε = 19263 $M^{-1}cm^{-1}$), complex **2** has bands at 233 nm (ε = 14595 $M^{-1}cm^{-1}$) and 260 nm (ε = 6761 $M^{-1}cm^{-1}$), and complex **3** at 260 nm (ε = 11100 $M^{-1}cm^{-1}$) and 447 nm (ε = 1350 $M^{-1}cm^{-1}$). The lower energy bands (at 285, 260 and 447 nm for **1**, **2** and **3**, respectively) correspond to MLCT,[17] assigned to Ru ($4d^6$) $\rightarrow$ π^* (arene) transitions. The difference in the energy of these bands is not surprising as the free arenes (*o*-, *m*- and *p*-terp) exhibit different absorption spectra as well, due to the different electronic interactions between the first and the third phenyl ring of *o*-, *m*- and *p*-terp.[18] The higher energy bands (at 260, 233 and again 260 nm for **1**, **2** and **3**, respectively) are assigned to the arene $\pi \rightarrow \pi^*$ transitions.[17] Figure 3.2B shows the difference in absorbance (at 260 nm) of DNA modified by complexes **1**, **2** and **3** (24 h incubation) and the absorbance of unmodified DNA. The table in Figure 3.2 shows the dependence of these differences in absorbance (ΔA^{260}) on the concentration of **1**, **2** and **3** (determined by FAAS).

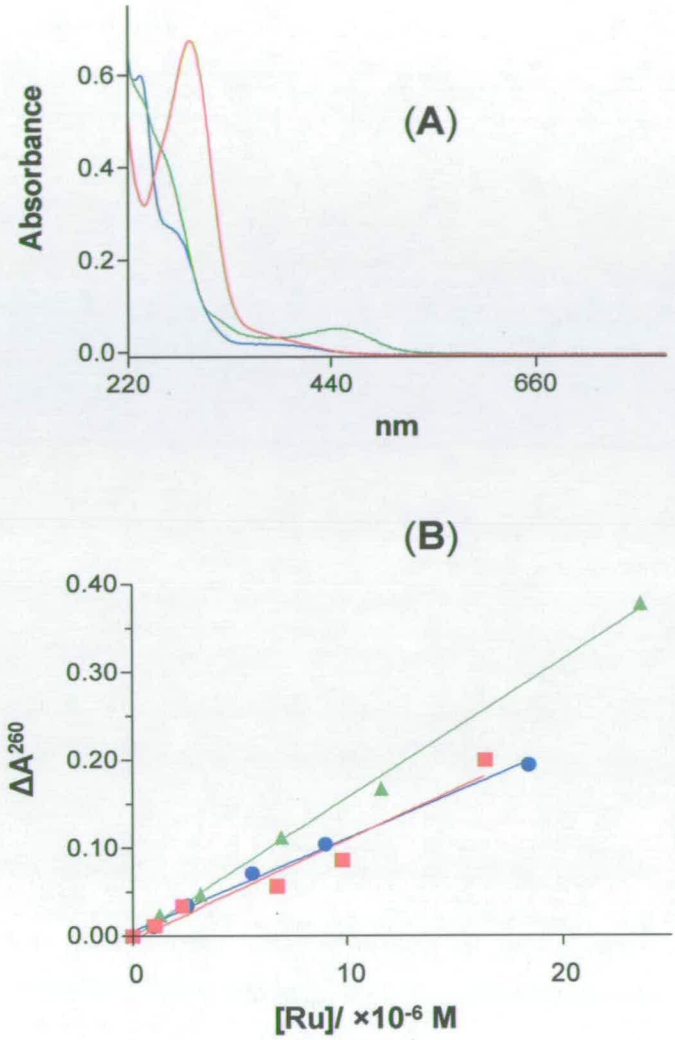

[Ru]/ ×10^{-6} M	ΔA^{260} 1	2	3
0.00	0.000	0.000	0.000
1.00	0.012	-	-
0.95	-	0.011	-
1.25	-	-	0.024
2.30	0.034	-	-
2.50	-	0.035	-
3.20	-	-	0.048
6.80	0.057	-	-
5.60	-	0.071	-
7.00	-	-	0.112
9.80	0.086	-	-
9.00	-	0.104	-
11.6	-	-	0.168
16.4	0.200	-	-
18.4	-	0.195	-
23.6	-	-	0.378

Figure 3.2 (**A**) UV-Vis spectra of complexes **1**, **2** and **3** in water at concentrations of 3.5, 4.1 and 3.8 x 10^{-5} M, respectively. (**B**) The difference in absorbance (at 260 nm) of DNA modified by complexes **1**, **2** and **3** (24 h incubation) and the absorbance of unmodified DNA; concentrations of **1**, **2** and **3** are determined by FAAS.

3.3.2 Crystal structures

The x-ray crystal structures of the cations of complexes [(η^6-*p*-terp)Ru(en)Cl][PF_6] (**1**) and [(η^6-*m*-terp)Ru(pda)Cl][PF_6] (**4**) are shown in Figure 3.3. Both complexes crystallized as PF_6 salts. The crystallographic data are listed in Table 3.1, and selected bond lengths and angles in Table 3.2. In both complexes, Ru^{II} adopts the familiar 'three-legged piano-stool' geometry with an η^6 π-bonded arene, forming the seat of the stool. The legs of the stool form σ-bonded Cl and N atoms of the en or pda chelating ligands, respectively.

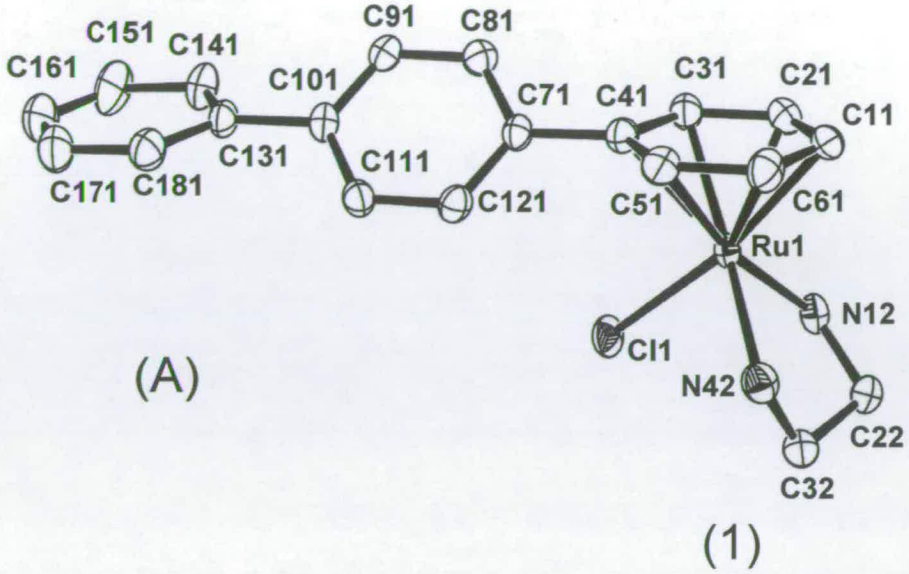

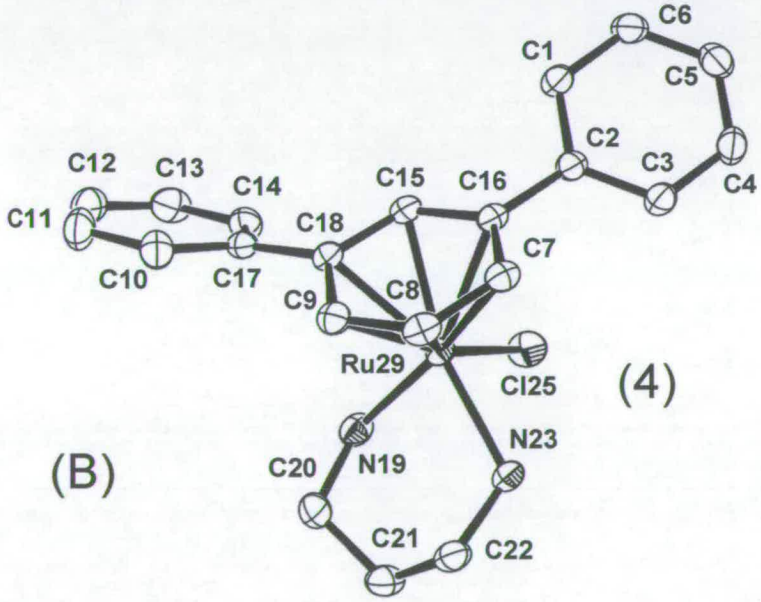

Figure 3.3 ORTEP diagrams for cations of (A) [(η^6-*p*-terp)Ru(en)Cl][PF_6] (**1**) and (B) [(η^6-*m*-terp)Ru(pda)Cl][PF_6] (**4**), with 50% probability thermal ellipsoids. All hydrogen atoms have been omitted for clarity.

Table 3.1 X-ray crystal structure data for complexes **1** and **4**

Complex	**1**	**4**
Formula	$C_{20}H_{22}ClF_6N_2PRu$	$C_{21}H_{24}ClF_6N_2PRu$
Molar mass	571.89	585.92
Crystal system	monoclinic	monoclinic
Crystal size /mm	0.27 × 0.21 × 0.21	0.56 × 0.22 × 0.16
Space group	*P21/c*	*P121/c1*
Crystal	yellow / block	yellow / rod
a / Å	19.0359(10)	11.0450(3)
b / Å	10.1405(5)	10.6507(3)
c / Å	11.2966(5)	19.2317(5)
α / deg	90	90
β / deg	105.218(3)	98.737(2)
γ / deg	90	90
T / K	150(2)	150
Z	4	4
R [F > 4σ (F)][a]	0.0479	0.0297
R_w[b]	0.1256	0.0778
GOF[c]	1.041	0.9572
Δρ max and min, /eÅ^{-3}	1.557, -0.814	0.80, -0.92

[a] $R = \sum||F_o| - |F_c||/\sum|F_o|$. [b] $R_w = [\sum w(F_o^2 - F_c^2)^2/\sum wF_o^2)]^{1/2}$. [c] $GOF = [\sum w(F_o^2 - F_c^2)^2/(n-p)]^{1/2}$, where n = number of reflections and p = number of parameters.

Table 3.2 Selected bond lengths (Å) and angles (°) for complexes **1** and **4**

Bond/Angle	**1**	**4**
Ru-Cl	2.3929(11)	2.3894(5)
Ru-N12/ N19	2.125(4)	2.1370(18)
Ru-N42/ N23	2.126(4)	2.1231(16)
Ru-C11/ C7	2.174(4)	2.210(2)
Ru-C21/ C8	2.152(5)	2.1669(19)
Ru-C31/ C9	2.190(4)	2.1817(19)
Ru-C41/ C15	2.225(4)	2.2067(18)
Ru-C51/ C16	2.191(4)	2.2237(19)
Ru-C61/ C18	2.157(5)	2.2182(18)
N12/ N19-Ru-N42/ N23	78.76(14)	83.14(7)
N12/ N19-Ru-Cl	83.65(10)	83.29(5)
N42/ N23-Ru-Cl	84.57(11)	83.66(5)

Twisting of the phenyl rings is present in the crystal structure of **1.** The twist angle between the bound and the middle ring is 43.21°, and between the middle and the terminal ring 38.47°. The planes, in which the terminal and bound rings lay, are twisted by 5.62°. The twisting between the phenyl rings has been previously observed for [(η^6-bip)Ru(en)Cl][PF_6] (twist angle 24.6°).[2] CH/ π interaction is present between the C61H proton of the bound ring of *p*-terp from one molecule and the centre of the π-system of the middle ring of *p*-terp from another molecule (2.6 Å; Figure 3.4). The distances between carbons of the bound arene ring and the metal centre range from 2.152(5) to 2.225(4) Å. The bond between Ru and the substituted carbon (Ru-C41 with the value of 2.225(4) Å; Table 3.2) is 0.034 Å longer than any other Ru-C bond in the molecule. This pattern has been reported previously for the bip analogue [(η^6-bip)Ru(en)Cl][PF_6], where the bond between Ru and the substituted carbon, of 2.244(6) Å, is 0.054 Å longer than any other Ru-C bond in that molecule.[2]

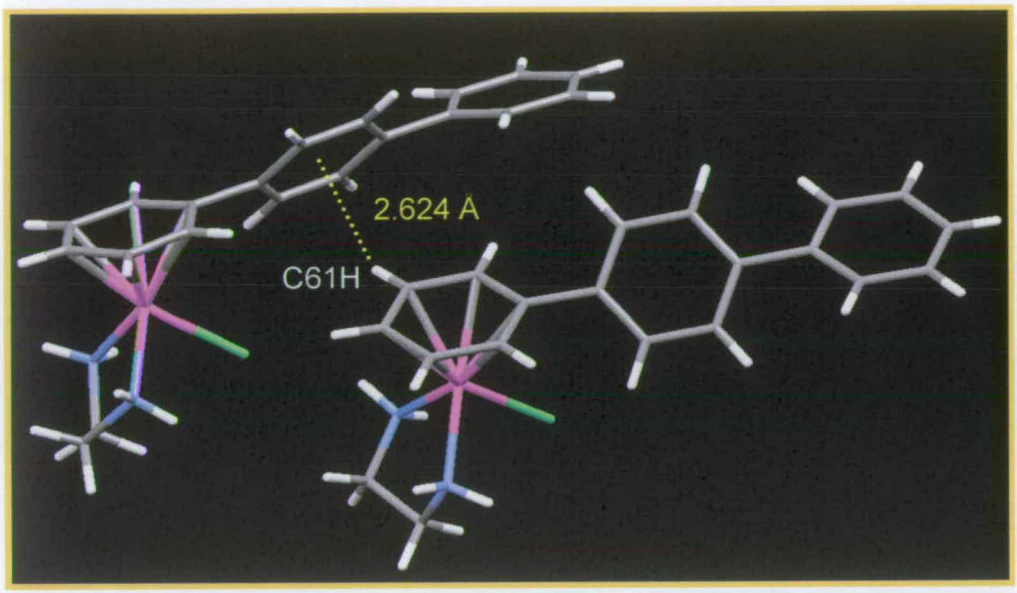

Figure 3.4 Capped-stick model of the crystal structure of complex **1**, showing interactions between C61H proton of the bound ring of *p*-terp from one molecule and the centre of the π-system of the middle ring of *p*-terp from another molecule.

In the crystal structure of **4** the common chair conformation is adopted by the six-membered ring formed between pda chelating ligand and Ru. The twisting of the phenyl rings of *m*-terp is present. The twist angles between middle (bound) phenyl ring and terminal rings are 32.07° and 36.84°. The twist angle between the two terminal phenyl rings of *m*-terp is 58.24°. The Ru carbon (of the bound phenyl ring) distances range from 2.1669(19) to 2.2237(19) Å. The bond length between Ru and the substituted carbons (Ru-C16/C18 with the values of 2.2237(19) and 2.2182(18) Å; Table 3.2) are 0.014 and 0.008 Å (for C16 and C18, respectively) longer than any other Ru-C bond in the molecule.

3.3.3 Cytotoxicity

The cytotoxicity of *m*-terp pda complex **4** was determined against A2780 ovarian (IC_{50} = 12 μM) and A549 lung (IC_{50} = 18 μM) cancer cell lines, by Oncosence Ltd using the procedure from Chapter 2 (24 h exposure). The cytotoxic activity of Ru^{II} arene complexes **1-3** was determined against four different cisplatin-sensitive and cisplatin-resistant cancer cell lines. The human ovarian carcinoma cell lines A2780, CH1 (both cisplatin sensitive), A2780cisR (with acquired cisplatin resistance) and human mammary carcinoma cell line SKBR3 (intrinsically cisplatin resistant) were employed. A2780cisR cells are resistant to cisplatin through a combination of decreased uptake, enhanced DNA repair/tolerance, and elevated glutathione (GSH) levels.[19] The tumor cell lines were incubated for 72 h with complexes **1**, **2** and **3** or cisplatin and the cell survival in the culture was evaluated as described in the experimental section. All complexes show activity and their corresponding IC_{50} values (IC_{50} = concentration inhibiting cell growth by 50%) are reported in Table 3.3. In general activity follows the order **1**, cisplatin >> **2** > **3**, with all Ru complexes lacking cross-resistance with cisplatin.

Table 3.3 IC_{50} values (μM) for Ru^{II} en complexes described in this Chapter[a,b]

Complex	CH1	SKBR3	A2780	A2780cisR (RF)[c]
cisplatin	0.9±0.1	8±2	2.8±0.7	18.6±0.4 (6.7)
1	2.2±0.3	8±1	4±1	1.4±0.6 (0.4)
2	23±1	13±3	30±4	18.3±0.8 (0.6)
3	51±9	80±5	42±4	31±4 (0.7)

[a] Drug-treatment period was 72 h.

[b] The experiments were performed in quadruplicate.

[c] Resistance factor (RF), defined as IC_{50} (resistant) / IC_{50} (sensitive), is given in parentheses.

3.3.4 Cellular ruthenium complex uptake

An important factor that usually contributes to transition metal-based drug cytotoxicity is cellular uptake. To examine accumulation of complexes **1-3**, the cellular levels of these complexes were measured after a 72 h exposure of the A2780 and A2780cisR cells to **1**, **2** and **3** at equitoxic concentrations (i.e. at the concentrations corresponding to the IC_{50} values shown in Table 3.3). The amount of ruthenium found in cells (in pmol/10^6 cells, Table 3.4): **2** >> **3** > **1**, does not correlate with their cytotoxicity (IC_{50} value). Since complexes **1-3** were tested at their equitoxic doses, the results shown in Table 3.4 imply that notably less molecules of complex **1** inside the cells, in comparison with complexes **2** and **3**, are necessary to induce the same cytotoxic effect.

Table 3.4 Uptake of Ru^{II} arene en complexes and cisplatin into cells[a,b]

Cell line	Uptake (pmol/10^6 cells)			
	cisplatin	complex **1**	complex **2**	complex **3**
A2780	30±2	350±20	2130±130	630±50
A2780cisR	47±3	150±10	1010±90	490±80

[a] Table shows the uptake of cisplatin and complexes **1-3** at their equitoxic concentrations (corresponding to the IC_{50} values shown in Table 3.3) into A2780 or A2780cisR cells after 72 h. Each value shown in the Table 3.4 is in pmol of Ru or Pt/10^6 cells.

[b] The experiments were performed in triplicate.

3.3.5 DNA binding in cell-free media

DNA is an important potential biological target for many metal-based anticancer agents.[20] Distortions of DNA structure often correlate with anticancer activity.[21, 22] Hence, it is of great importance to understand in detail DNA binding properties of complexes **1**, **2** and **3** and their possible relationship to cytotoxicity in tumor cell lines.

3.3.5.1 Kinetics of binding to calf thymus (CT) DNA

The rate of binding of Ru^{II} arene complexes **1**, **2** and **3** to CT DNA was determined at an r_i (molar ratio of free Ru^{II} arene complex to nucleotide phosphate) ratio of 0.08 in 10 mM $NaClO_4$. Ru^{II} arene complexes were incubated with CT DNA (at 37°C in the dark) and aliquots removed at various time intervals, and rapidly cooled. DNA with a bound complex was precipitated out by addition of ethanol, and the concentration of free complex in the supernatant determined by flameless atomic absorption spectrometry (FAAS; Figure 3.5). Complexes **1** and **3** bind rapidly to DNA ($t_{1/2}$ ca. 5 and 9 min for **1** and **3**, respectively), while $t_{1/2}$ for complex **2** is ca. 31 min. Complex **1** binds to CT DNA almost quantitatively, whereas only ca. 90% of complex **2** and 80% of complex **3** are bound after 48 h.

The binding experiments carried out in this Chapter indicated that modification reactions resulted in the irreversible coordination of complexes **1**, **2** and **3** to CT DNA, which thus facilitated sample analysis. Hence, it was possible to prepare samples of DNA modified by Ru^{II} complexes at a preselected value of r_b. Thus, except where stated, samples of DNA modified by Ru^{II} arene complexes **1**, **2** and **3** and analyzed further by biophysical or biochemical methods were prepared in 10 mM $NaClO_4$ at 37 °C. After 24 h of the reaction of DNA with a complex, the samples were precipitated in ethanol and dissolved in the medium necessary for a particular analysis, and the r_b value in an aliquot of this sample was checked by FAAS. In this way, all analyses described in this Chapter were performed in the absence of unbound (free) Ru^{II} arene complex.

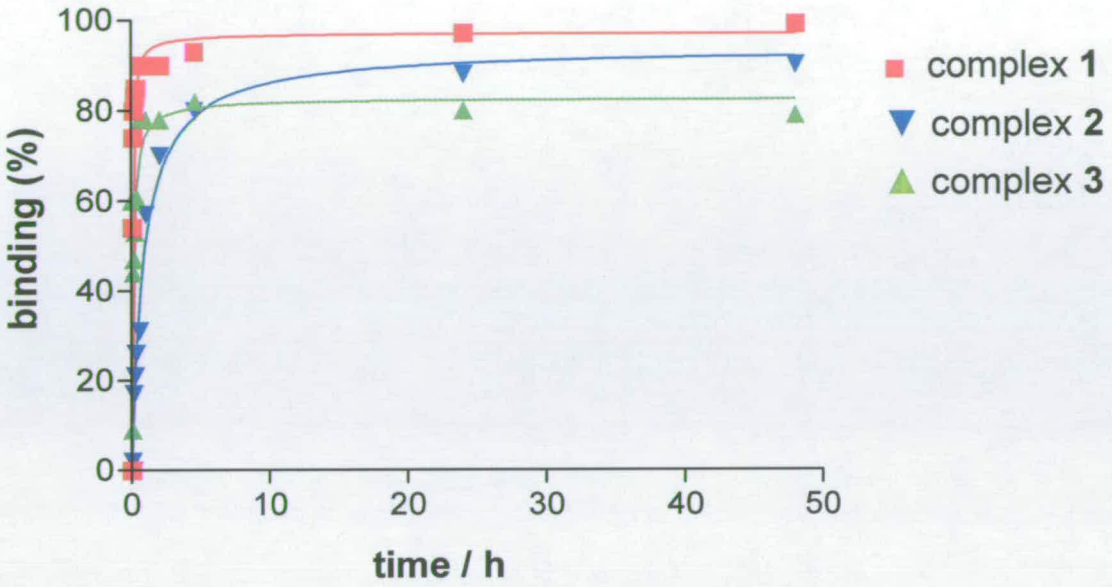

Figure 3.5 Kinetics of the binding (studied by ethanol precipitation method) of complexes **1** (■), **2** (▼) and **3** (▲) to calf-thymus (CT) DNA in the medium of 10 mM $NaClO_4$, at 37 °C and pH = 6. The concentration of DNA was 3×10^{-4} M and r_i was 0.08 (concentration of complexes was 2.4×10^{-5} M).

3.3.5.2 Circular Dichroism (CD)

To gain further information, CD spectra of DNA modified by complexes **1**, **2** and **3** (at 25 °C in 10 mM $NaClO_4$, for more details see Chapter 2) were also recorded. These complexes have no intrinsic CD signals as they are achiral and any CD signal above 300 nm is, therefore, attributed to the interaction of complexes with DNA. Below 300 nm any change in the spectrum of B-DNA (see Chapter 2) is due either to the DNA induced CD (ICD) of the metal complex or the metal-complex-induced

perturbation of the DNA spectrum. The signature of complex **1** bound to CT DNA is a strong negative ICD at around 308 nm and a strong positive ICD centered at 376 nm with the crossover at 351 nm (Figure 3.6). On the other hand, the signature of complex **3** bound to CT DNA is only very weak and broad positive ICD centered at 376 nm. Complex **2** bound to CT DNA does not have any signature in the region above 300 nm. These results reflect different binding modes of complexes **2** and **3** to DNA, compare to that of complex **1**. Unfortunately these complexes also absorb in the DNA region (Chapter 2 and Figure 3.2B), leading to the interpretation of the CD spectra (below 300 nm) in terms of alterations of DNA conformation or the DNA binding mode of complexes.

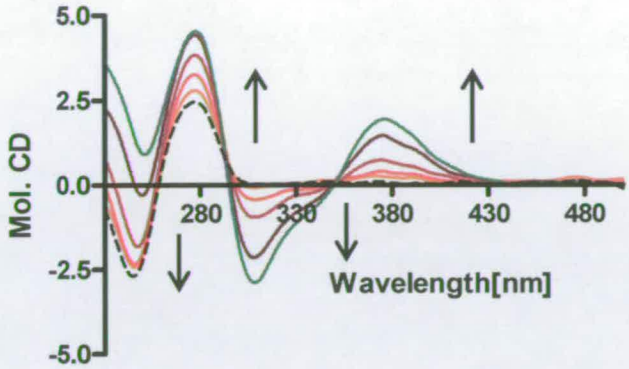

Figure 3.6 Circular dichroism (CD) spectrum of CT DNA (1×10^{-4} M) modified by complex **1**; the medium was 10 mM $NaClO_4$, pH = 6. DNA was modified by complex **1** at r_i = 0, 0.01, 0.02, 0.04, 0.08 and 0.12 (r_i = molar ratio of free Ru complex to nucleotide phosphates at the onset of incubation with DNA). The arrows show changes in CD spectrum with increasing the r_i value.

The changes in CD spectra of CT DNA modified by Ru^{II} terphenyl complexes (at different r_b values) are shown in Figure 3.7. The changes in the CD spectrum of CT DNA modified by complex **1** were monitored at 244, 278, 308 and 378 nm, and for the modification by complexes **2** and **3** at 244 and 278 nm and at 244, 278 and 376 nm, respectively.

r_b	wavelength /nm			
	244	278	308	376
	mol. CD			
0.000	-2.600	2.370	0.000	0.000
0.013	-1.900	2.800	-0.460	0.330
0.029	-1.400	3.000	-0.970	0.530
0.087	-0.300	3.200	-1.840	1.000
0.125	0.600	3.170	-2.380	1.360
0.209	0.900	2.420	-1.950	1.270

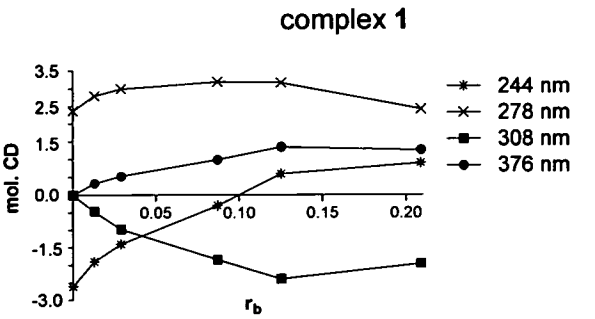

r_b	wavelength /nm	
	244	278
	mol. CD	
0.000	-2.600	2.370
0.009	-1.700	2.360
0.027	-1.090	2.320
0.044	-0.040	1.870
0.080	0.920	1.470
0.128	1.830	0.670

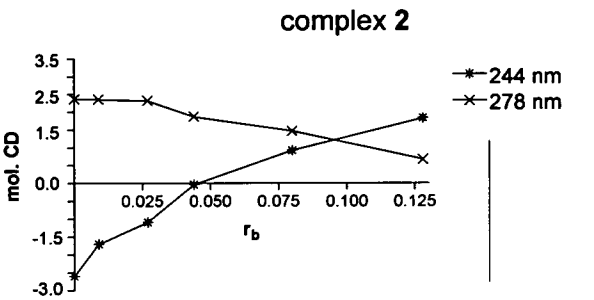

r_b	wavelength /nm		
	244	278	376
	mol. CD		
0.000	-2.600	2.370	0.000
0.010	-2.400	2.300	0.170
0.027	-2.400	2.260	0.240
0.055	-2.100	1.900	0.340
0.078	-1.900	1.500	0.360
0.120	-1.900	0.740	0.230

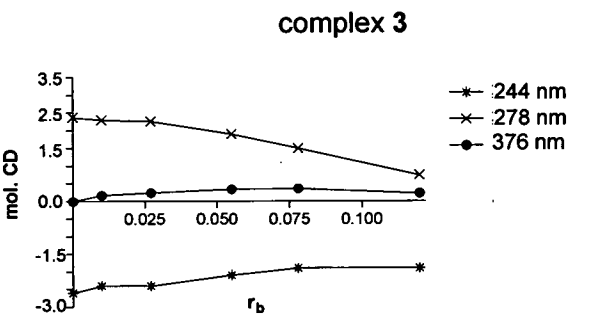

Figure 3.7 The changes induced in CD spectra of CT DNA modified by Ru^{II} complexes **1**, **2** and **3** at different r_b values.

3.3.5.3 Ethidium bromide (EtBr) fluorescence

The ability of complexes to displace the DNA intercalator EtBr from CT DNA was probed by monitoring the relative fluorescence of the EtBr-DNA adduct after treating the DNA with varying concentrations of **1**, **2** and **3**. Figure 3.8 shows a plot of relative fluorescence vs r_b for complexes **1**, **2** and **3**, cisplatin and monofunctional dienPt. The adducts of Ru^{II} arene complexes **1** and **3** competitively replaced intercalated EtBr markedly more effectively than the adducts of monofunctional dienPt and even slightly more than the adducts of bifunctional cisplatin. The replacement of EtBr by the adducts of complex **2** was closer to that observed for monofunctional dienPt, than observed for the other two complexes. Notably, the ability of complex **1** to displace DNA intercalator EtBr from CT DNA was considerably greater than that of complexes **2** and **3** (Figure 3.8).

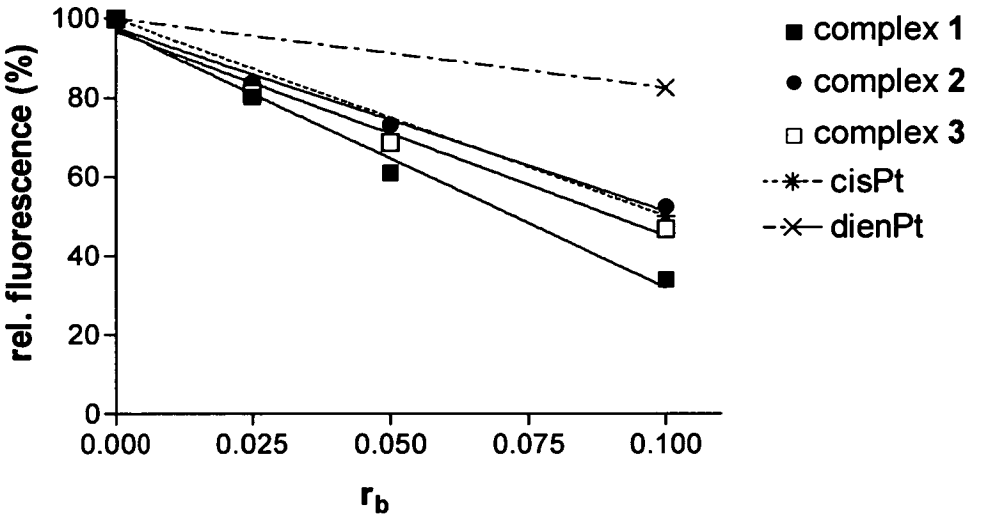

r_b	rel. fluorescence (%)				
	1	2	3	cisPt	dienPt
0.000	100.0	100.0	100.0	100.0	100.0
0.025	80.4	83.9	81.3	-	-
0.050	61.0	73.2	68.7	-	-
0.100	34.0	52.5	49.6	50.0	82.50

Figure 3.8 Plots of the EtBr fluorescence versus r_b for DNA modified by cisplatin, dienPt and Ru^{II} arene complexes **1**, **2** and **3** in 10 mM $NaClO_4$ at 37°C (incubation for 24 h): (x), dienPt; (•), cisplatin; (■), complex **1**; (●), complex **2** and (□), complex **3**.

3.3.5.4 DNA melting

CT DNA was modified by Ru^{II} arene complexes **1**, **2** and **3** at various r_b values (Figure 3.9) in 10 mM $NaClO_4$ at 37°C for 24 h. The salt concentration was then further adjusted by addition of $NaClO_4$ to values in the range 0.01-0.205 M (Figure 3.9). The DNA melting temperature (t_m) is dependent both on the amount of ruthenium bound and on the salt concentration. At low concentrations of $NaClO_4$ (0.01 M) an increase in t_m was observed for DNA modified by complex **1** compared to that of unmodified DNA, and this became more pronounced with increasing r_b values (Figure 3.9). With increasing ionic strength, the enhancement of t_m (Δt_m, defined as the difference between the values of ruthenated and nonmodified DNAs) due to the presence of the complex decreased. CT DNA modified by complexes **2** and **3** exhibited a different melting behavior. At higher concentrations of $NaClO_4$ (0.055-0.205 M) a decrease in t_m was observed for modification by complexes **2** and **3**, and this became more pronounced with increasing r_b values (Figure 3.9). With increasing ionic strength, the Δt_m due to the modification by **2** and **3** decreased. At a concentration of $NaClO_4$ as low as 0.01 M for DNA modified by complex **2** an increase in t_m was observed with increasing r_b value, while for the modification by complex **3**, a slight increase in t_m was first observed with increasing r_b ($r_b < 0.078$), but at higher r_b values Δt_m decreased with increasing r_b.

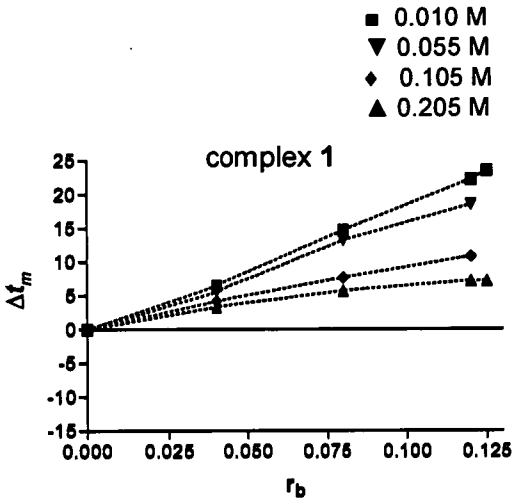

r_b	[ClO_4^-]/M 0.010	0.055	0.105	0.205
	Δt_m			
0.000	0.000	0.000	0.000	0.000
0.040	6.500	5.600	4.200	3.400
0.080	14.700	13.200	7.700	5.750
0.120	22.200	18.500	10.800	7.220
0.125	23.500	-	-	7.220

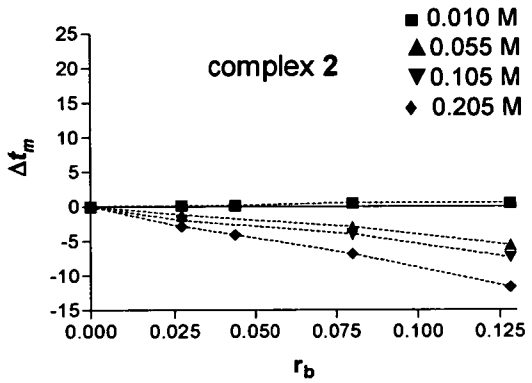

r_b	[ClO_4^-]/M 0.010	0.055	0.105	0.205
	Δt_m			
0.000	0.000	0.000	0.000	0.000
0.027	0.200	-1.200	-2.000	-2.900
0.044	0.200	-	-	-4.100
0.080	0.500	-3.000	-4.000	-6.800
0.128	0.500	-5.600	-7.300	-11.600

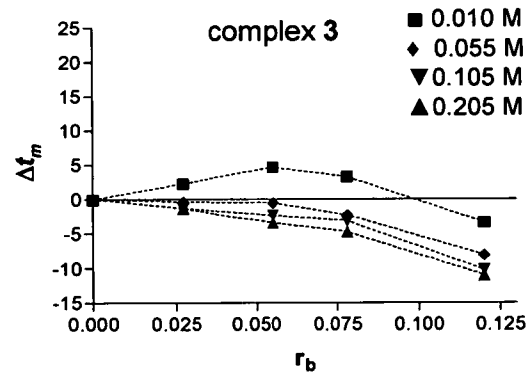

r_b	[ClO_4^-]/M 0.010	0.055	0.105	0.205
	Δt_m			
0.000	0.000	0.000	0.000	0.000
0.027	2.300	-0.400	-1.250	-1.300
0.055	4.700	-0.500	-2.300	-3.400
0.078	3.300	-2.250	-3.100	-4.700
0.120	-3.300	-8.050	-10 .200	-11.000

Figure 3.9 Plots showing the dependence of Δt_m values on r_b for calf thymus (CT) DNA modified by Ru^{II} arene complexes **1**, **2** and **3**. The melting curves were measured in of 1 mM Tris-HCl with 0.1 mM EDTA, at pH = 7.4 and varying concentrations of $NaClO_4$: 0.01 M, 0.055 M, 0.105 M and 0.205 M. Δt_m is defined as the difference between the t_m values of ruthenated and nonmodified DNAs.

3.3.5.5 Unwinding of supercoiled DNA

As being the most and the least cytotoxic of the terphenyl complexes, **1** and **3**, respectively, were chosen for studies of the unwinding of supercoiled DNA. The unwinding of supercoiled plasmid pSP73KB DNA induced on binding complexes **1** and **3** was determined by incubating the plasmid with **1** or **3** for 24 h at 37°C at various r_b values (different lanes in the gel). The native agarose gels, resulting from DNA modified by Ru^{II} terphenyl complexes **1** and **3**, are shown in Figure 3.10 (top and bottom panels, respectively). A decrease in the rate of migration is the result of unwinding the DNA as this reduces the number of supercoils. The mean unwinding angle can be calculated from the equation $\Phi = -18\sigma/r_b(c)$, where σ is the superhelical density (represents the number of turns added or removed relative to the total number of turns in the relaxed plasmid, indicating the level of supercoiling) and $r_b(c)$ is the r_b at which the supercoiled and nicked forms comigrate.[16] It can be seen in Figure 3.10 (top) that complex **1** causes a significant unwinding of DNA (Φ = 14±1°, the comigration point of the modified supercoiled and nicked DNA, $r_b(c)$, was reached at r_b = 0.047). In contrast, complex **3** unwinds the DNA significantly less (Φ = 8±1°, the comigration point of the modified supercoiled and nicked DNA, $r_b(c)$, was reached at r_b = 0.083). The high level of unwinding induced by complex **1** is similar to that induced by bifunctional cisplatin (Φ = 13±1°).

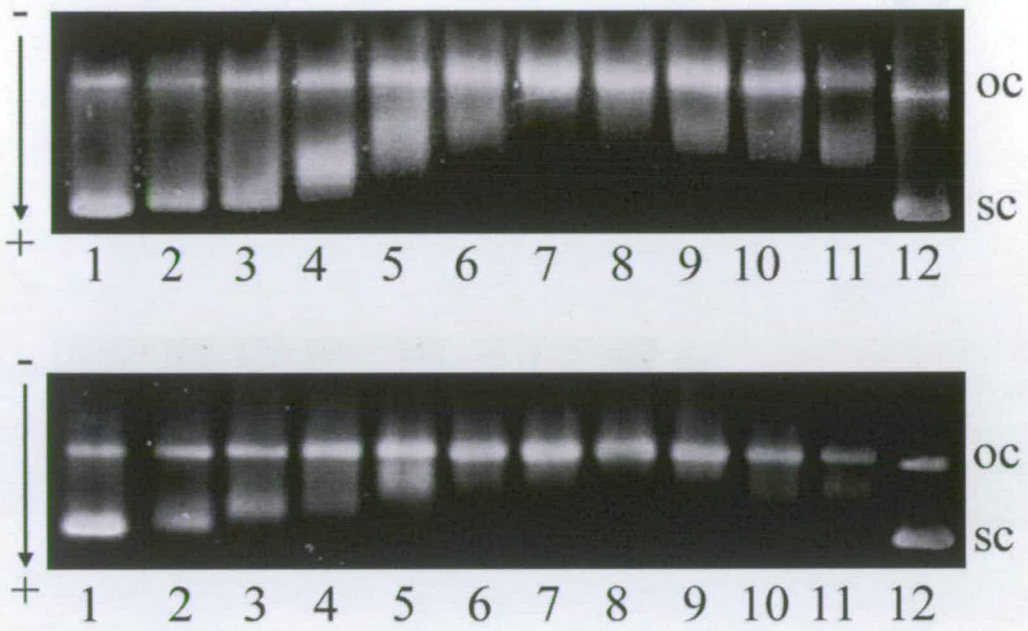

Figure 3.10 The unwinding of supercoiled pSP73KB plasmid DNA by complexes **1** (top) and **3** (bottom). The plasmid was incubated with Ru^{II} arene complexes in 10 mM $NaClO_4$, at pH = 6 for 24 h at 37 °C. Lanes in the top panel: 1 and 12, control, unmodified DNA; 2, r_b = 0.008; 3, r_b = 0.016; 4, r_b = 0.024; 5, r_b = 0.031; 6, r_b = 0.039; 7, r_b = 0.047; 8, r_b = 0.055; 9, r_b = 0.063; 10, r_b = 0.071; 11, r_b = 0.079. Lanes in the bottom panel: 1 and 12, control, unmodified DNA; 2, r_b = 0.017; 3, r_b = 0.033; 4, r_b = 0.050; 5, r_b = 0.058; 6, r_b = 0.066; 7, r_b = 0.074; 8, r_b = 0.083; 9, r_b = 0.091; 10, r_b = 0.099; 11, r_b = 0.108. The top bands in each panel correspond to the form of nicked plasmid, and the bottom bands, to the closed, negatively supercoiled plasmid.

3.4 Discussion

New complexes of the type $[(\eta^6\text{-arene})Ru(N,N)Cl]^+$, where arene = *ortho-*, *meta-* or *para*-terphenyl (*o-*, *m-* or *p*-terp) and N,N = ethylenediamine (en) or 1,3-propylenediamine (pda), reported in this Chapter are shown in Figure 3.1.

In the reported crystal structure of the *p*-terp complex **1** the twisting of the phenyl rings is shown to be caused by the presence of inter-molecular CH/ π interaction between the C61H proton of the bound ring of *p*-terp (Figure 3.4) from one molecule and the center of the π-system of the central ring of *p*-terp from another molecule. With a value of 2.6 Å this interaction is classified as weak.[23] This suggests that in the solution the CH/ π interaction could be absent and the *p*-terp arene of **1** could possibly become well positioned for the intercalation into DNA (*vide supra*).

DNA binding mode, the effect on cytotoxicity and cellular Ru^{II} complex uptake were investigated for terphenyl complexes that contain en as the chelating ligand (complexes **1**, **2** and **3**). The cytotoxic activity of Ru^{II} arene complexes **1-3** was determined against different cisplatin-sensitive and cisplatin-resistant cancer cell lines (Table 3.3). The highest activity in all cell lines is exhibited by the *p*-terp complex **1**. Interestingly, in A2780, CH1 and SKBR3 cells, complex **1** shows potency comparable with that of conventional cisplatin. Importantly, the cytotoxicity of all Ru^{II} arene en complexes, tested in this Chapter in the cisplatin-resistant line A2780cisR, is characterized by remarkably low resistance factors, less than 1 (Table 3.3); complex **1** shows the best circumvention of cisplatin resistance (lowest value of resistance factor). On the other hand, complex **3** is the least potent in all cell lines with IC_{50}

values in the range of 31 - 75 μM. Notably all Ru^{II} arene en complexes **1-3** show higher potency towards cisplatin-resistant compared to cisplatin-sensitive A2780 cells, indicating a mechanism of cytotoxicity of this class of Ru^{II} complexes different from that of cisplatin.

The ruthenium complexes uptake does not correlate with their cytotoxicity (IC_{50} value). Since complexes **1-3** were tested at their equitoxic doses, the results imply that notably less molecules of complex **1** inside the cells are needed, in comparison with complexes **2** and **3**, to induce the same cytotoxic effect. This means that intracellular damage induced by complex **1** and responsible for cytotoxic effects is more efficient than those induced by complexes **2** and **3**.

The results of studies of the binding of **1**, **2** and **3** to natural double-helical CT DNA (in a cell-free medium) are summarized in Table 3.5.

Table 3.5 Summary of DNA binding studies for complexes **1**, **2** and **3**

Study	Complex **1**	Complex **2**	Complex **3**
DNA binding	rapid ($t_{1/2}$=5 min)/ quantitative	moderate ($t_{1/2}$=31 min)/ 90% (48 h)	rapid ($t_{1/2}$=9 min)/ 80% (48 h)
CD	strong ICD negative (308 nm)/ positive (376 nm)	no signature in the region above 300 nm	weak and broad ICD positive (376 nm)
DNA unwinding	14°	–	8°
DNA melting, Δt_m (r_b = 0.120 or 0.128; 0.205 M $NaClO_4$)	+7.2°C	-11.6°C	-11°C
EtBr displacement	greater replacement	less replacement	less replacement

The results show (Table 3.5) that the reactions with CT DNA of complexes **1** and **3** are significantly faster than that of complex **2**. The rate of binding is dependent on the type of arene ligand: complex **2** containing *o*-terp shows the slowest binding to CT DNA, while complex **3** containing *m*-terp binds to CT DNA faster than **2**, but still slower than **1** (a complex with *p*-terp arene). The binding is quantitative in the case of complex **1**, but not quantitative in the case of complexes **2** and **3** (~90 and 80% for **2** and **3**, respectively after 48 h). Different rates of reactions between CT DNA and Ru^{II} arene complexes were also observed in the case of analog Ru^{II} complexes of the type $[(\eta^6\text{-arene})Ru(en)Cl]^+$, where the arene is biphenyl, dihydroanthracene, tetrahydroanthracene, *p*-cymene, or benzene.[3] It has been deduced that hydrophobic

interactions contribute to the driving force for the binding of chlorido Ru^{II} arene complexes to double-helical DNA. Hence, a faster reaction between CT DNA and complex **1** suggests that DNA binding mode of complex **1** involves not only its coordination to the base residues in DNA, but also hydrophobic interactions, such as intercalation of the *p*-terp arene. This interpretation also implies that the significance of these hydrophobic interactions in DNA binding mode of complex **3** is diminished, and for complex **2** these interactions might be completely absent, due to the most compact, bulky arene (*o*-terp).

The CD measurements are consistent with different binding modes of complexes **1**, **2** and **3** to DNA and support the hypothesis that the DNA binding mode, particularly of complex **1**, may involve its interaction in specific orientations. The CD spectra of DNA modified by complexes **1**, **2** or **3** (the changes in spectra are shown in Figure 3.7) indicate that the binding of these complexes results in conformational alterations in double-helical DNA. Complex **1** bound to CT DNA yields a strong negative ICD at around 308 nm and a strong positive ICD centered at 376 nm (Figure 3.6). On the other hand, complex **3** bound to CT DNA yields only a very weak and broad positive ICD centered at 376 nm, while the CD spectrum of CT DNA modified by complex **2** shows no band in the region above 300 nm.

The CD changes observed for double-helical DNA modified by complexes **1**, **2** and **3** also correlate with the results of competitive EtBr displacement (Figure 3.8) and DNA unwinding (Figure 3.10) experiments. The adducts of *p*-terp complex **1** are considerably more efficient in DNA-EtBr fluorescence quenching than those of *o*-terp complex **2** and *m*-terp complex **3**. A greater efficiency of DNA unwinding for complex **1** compared to **3** is also observed. The large unwinding angle of 14° was produced by complex **1** while complex **3** unwinds DNA only by 8° (Figure 3.10), a

similar behavior to that of the monofunctional adducts of dienPt (unwinding angle 6°)[16] or of $[(\eta^6\text{-arene})Ru(en)Cl]^+$, where the arene is non-intercalating *p*-cymene (unwinding angle 7°)[3]. This observations may be explained by additional contribution to fluorescence quenching and unwinding from intercalation of the extended arene ligand of **1** into the duplex upon its monofunctional binding. It seems reasonable to suggest that *o*-terp and *m*-terp arenes in complexes **2** and **3** do not interact with the double helix in a similar way to that of *p*-terp arene of complex **1**. Hence, the results of DNA-EtBr fluorescence quenching and unwinding experiments strengthen the theory based on combined intercalative and monofunctional binding mode of complex **1**.

Melting of DNA modified by complex **1**, **2** or **3** (Figure 3.9) also deserves discussion. The following factors can be invoked to account for the thermal stability of DNA modified by Ru^{II} arene complexes:[3]

(1) Stabilizing effects of the positive charge on ruthenium, favorable stacking interactions between the base residues and the arene, and the separation of negative backbone charges inherent to intercalating arene residue (due to elongation and unwinding of DNA). The changes in solvent structure and the counterion distribution around the phosphate groups may help to overcome electrostatics unfavorable for the hybridization of the strands of the duplex.[24, 25]

(2) A destabilizing effect of conformational distortions induced in DNA by ruthenium coordination. The dependence of the t_m value of DNA modified by non-intercalating ruthenium drugs on ionic strength can be explained by competing electrostatic effects as the salt concentration is varied.[26]

Thus, the observed change in t_m will reflect the relative proportion and contribution of all limiting binding modes.

At low ionic strength (0.01 M), it is reasonable to conclude that the increase in t_m due to the modification of DNA by complex **1** (Figure 3.9) is caused by positive charges on ruthenium $[(\eta^6\text{-arene})Ru(en)Cl]^+$ complex and by the intercalation. The smaller increase in t_m due to the modification by complex **1** observed at high ionic strength is a consequence of reduced stabilizing effects, since the electrostatic stabilizing effects of this complex are apparently lowered with increasing concentration of Na^+ counterions from $NaClO_4$.

The melting behavior of DNA modified by complexes **2** and **3** is different (Figure 3.9). Modification by these complexes already decreases t_m at concentrations of Na^+ as low as 0.055 M. This indicates that the effects of the factors responsible for the thermal stabilization of DNA (the positive charge on ruthenium and intercalation of the arene into the duplex) are noticeably reduced (in general more for complex **2** compare to **3**) so that the destabilization effect of conformational alterations induced by these complexes predominates already at low salt concentrations. Thus, the results of DNA melting experiments are consistent with the formation of a monofunctional adducts of *o*- and *m*-terp complexes **2** and **3** with DNA (coordination to G *N7*) and the absent or reduced intercalation.

3.5 Summary

In summary, complex **1** containing *p*-terp arene exhibits promising cytotoxic activity in several human tumor cell lines including those resistant to conventional cisplatin and its DNA binding mode involves combined intercalative and monofunctional (coordination) binding modes. In contrast, complexes **2** and **3** containing *o*- and *m*-terp arenes are much less cytotoxic and bind to DNA via preferentially monofunctional coordination to DNA bases. In the case of complex **1**, ruthenium is bound to a terminal phenyl ring whereas in the case of complexes **2** and **3**, ruthenium is bound to the central phenyl ring. It is therefore possible that the distances between marginal phenyl rings in complexes **2** and **3** and Ru coordinated to DNA bases is too short to allow these marginal phenyl rings to adopt configurations which allow intercalation into DNA. In complex **1**, the distance between distant marginal phenyl ring and Ru coordinated to DNA bases is greater allowing this phenyl ring to adopt a configuration appropriate for intercalation. In any case, the results of this Chapter further support the view that the presence of the arene ligand in $[(\eta^6\text{-arene})\text{Ru(en)Cl}]^+$ complexes capable of noncovalent, hydrophobic interaction with DNA considerably enhances cytotoxicity in tumor cell lines. Thus, these results represent a further improvement in the structure-activity relationship needed for the design of new antitumour ruthenium drugs.

3.6 References

(1) Aird, R.; Cummings, J.; Ritchie, A.; Muir, M.; Morris, R.; Chen, H.; Sadler, P.; Jodrell, D. *British J. Cancer* **2002,** *86*, 1652-1657.

(2) Morris, R. E.; Aird, R. E.; Murdoch, P. D.; Chen, H. M.; Cummings, J.; Hughes, N. D.; Parsons, S.; Parkin, A.; Boyd, G.; Jodrell, D. I.; Sadler, P. J. *J. Med. Chem.* **2001,** *44*, 3616-3621.

(3) Novakova, O.; Chen, H.; Vrana, O.; Rodger, A.; Sadler, P. J.; Brabec, V. *Biochemistry* **2003,** *42*, 11544 -11554.

(4) Chen, H. M.; Parkinson, J. A.; Parsons, S.; Coxall, R. A.; Gould, R. O.; Sadler, P. J. *J. Am. Chem. Soc.* **2002,** *124*, 3064-3082.

(5) Liu, H. K.; Berners-Price, S. J.; Wang, F. Y.; Parkinson, J. A.; Xu, J. J.; Bella, J.; Sadler, P. J. *Angew. Chem.-Int. Ed.* **2006,** *45*, 8153-8156.

(6) Liu, J.-K. *Chem. Rev.* **2006,** *106*, 2209-2223.

(7) Brabec, V.; Palecek, E. *Biophysik* **1970,** *6*, 290-300.

(8) Brabec, V.; Palecek, E. *Biophys. Chem.* **1976,** *4*, 76-92.

(9) Beurskens, P. T.; Beurskens, G.; Bosman, W. P.; Gelder, R. d.; Garcia-Granda, S.; Gould, R. O.; and, R. I.; Smits, J. M. M. *Crystallography Laboratory*, University of Nijmegen: Nijmegen, The Netherlands, **1999**.

(10) Altomare, A.; Cascarano, G.; Giacovazzo, C.; Guagliardi, A.; Polidori, G.; Camalli, M. *J. Appl. Crystallogr.* **1994,** *27*, 435.

(11) Sheldrick, G. M. *SHELXTL*, 6.10; University of Gottingen: Gottingen, Germany, **2001**.

(12) Betteridge, P. W.; Carruthers, J. R.; Cooper, R. I.; Prout, K.; Watkin, D. J. *J. Appl. Crystallogr.* **2003,** *36*, 1487.

(13) Alley, M. C.; Scudiero, D. A.; Monks, A.; Hursey, M. L.; Czerwinski, M. J.; Fine, D. L.; Abbott, B. J.; Mayo, J. G.; Shoemaker, R. H.; Boyd, M. R. *Cancer Res.* **1988,** *48*, 589-601.

(14) Butour, J. L.; Macquet, J. P. *Eur. J. Biochem.* **1977,** *78*, 455-463.

(15) Butour, J. L.; Alvinerie, P.; Souchard, J. P.; Colson, P.; Houssier, C.; Johnson, N. P. *Eur. J. Biochem.* **1991,** *202*, 975-980.

(16) Keck, M. V.; Lippard, S. J. *J. Am. Chem. Soc.* **1992,** *114*, 3386-3390.

(17) Hung, Y.; Kung, W.-J.; Taube, H. *Inorg. Chem.* **1981,** *20*, 457-63.

(18) Teply, J.; Bursik, J. *J. Radioanal. Nucl. Chem.* **1986,** *101*, 369-75.

(19) Behrens, B. C.; Hamilton, T. C.; Masuda, H.; Grotzinger, K. R.; Whang-Peng, J.; Louie, K. G.; Knutsen, T.; McKoy, W. M.; Young, R. C.; Ozols, R. F. *Cancer Res.* **1987,** *47*, 414-418.

(20) Zhang, C. X.; Lippard, S. J. *Curr. Opin. Chem. Bio.* **2003,** *7*, 481–489.

(21) Brabec, V. *Prog. Nucleic Acid Res. Mol. Biol.* **2002,** *71*, 1-68.

(22) Brabec, V.; Novakova, O. *Drug Resist. Updates* **2006,** *9*, 111-122.

(23) Bogdanovic, G. A.; Spasojevic-de Bire, A.; Zaric, S. D. *Eur. J. Inorg. Chem.* **2002,** *2002*, 1599-1602.

(24) Maeda, Y.; Nunomura, K.; Ohtsubo, E. *J. Mol. Biol.* **1990,** *215*, 321-329.

(25) Bjorndal, M. T.; Fygenson, D. K. *Biopolymers* **2002,** *65*, 40-44.

(26) Zaludova, R.; Kleinwächter, V.; Brabec, V. *Biophys. Chem.* **1996,** *60*, 135-142.

Chapter 4

Bipyridine Ru^{II} arene complexes

"Happy is he who gets to know the reasons for things."

Virgil

4.1 Introduction

Structure-activity relationships for Ru^{II} arene complexes containing N,N-chelating ligands have been reported previously.[1] It was notable that although complexes containing ethylenediamine (en) as chelating ligand were active (cytotoxic to cancer cells), complexes containing tetramethyl-en or bipyridine as chelating ligands were inactive. This suggests that NH groups on the chelating ligand (en) play a role in the activity, perhaps stabilizing guanine (G) adducts on DNA via H-bonding. Indeed stereospecific H-bonding has been observed between en NH···C6O of 9-ethylguanine (9-EtG) in the crystal structures of $[(\eta^6\text{-tha})Ru^{II}(en)(9\text{-EtG})]^{2+}$ and $[(\eta^6\text{-dha})Ru^{II}(en)(9\text{-EtG})]^{2+}$ (distances of 1.9 Å and 2.1 Å, respectively).[2]

In the work reported in this Chapter, the presence of hydroxyl groups at the 3,3′-positions of 2,2′-bipyridine (2,2′-bipyridine-3,3′-diol) is found to dramatically alter the activity profile of these Ru^{II} arene complexes. Unlike en, which is purely a σ-donor, the bipyridine derivatives are σ-donors and π-acceptors, and as π-acceptors make the metal center more acidic. The 3,3′-positions in 2,2′-bipyridine are different from the other positions on the ligand; for example, they have been reported to introduce steric strain upon the 3,3′-protons in $[Ru(bipy)_3]^{2+}$.[3] When 2,2′-bipyridine-3,3′-diol chelates to a metal, steric constraint is introduced[4] by the proximity of the two hydroxyl substituents and the strain is released upon the formation of O–H···O H-bond and a deprotonation of one of the OH groups.

It was of interest here to compare the aqueous solution chemistry, solid-state structures and cytotoxicity of Ru^{II} arene complexes containing bipyridine (bipy),

bipyridinediol (bipy$(OH)_2$) or deprotonated bipyridinediol (bipy(OH)O) as N,N-chelating ligands. Eight chlorido Ru^{II} arene complexes containing bipy, bipy$(OH)_2$ or bipy(OH)O with a variety of arenes were synthesized and the structures of complexes [(η^6-tha)Ru(bipy)Cl][PF_6] (**1**), [(η^6-tha)Ru(bipy(OH)O)Cl] (**2**) and [(η^6-ind)Ru(bipy$(OH)_2$)Cl][PF_6] (**8**) were determined by x-ray crystallography. The effects of hydroxylation and methylation of the bipy ligand on the electron distribution were studied using DFT calculations. The aqueous solution chemistry of these complexes (hydrolysis, arene loss and acidity of OH protons of bound bipy$(OH)_2$ and bipy(OH)O) has been investigated, as well as interactions with the DNA model nucleobase 9-EtG both in solution and by x-ray crystallography, and cytotoxicity towards human ovarian (A2780) and human lung (A549) cancer cells. In addition DNA binding studies were performed with complexes [(η^6-ind)Ru(bipy$(OH)_2$)Cl][PF_6] (**8**) and [(η^6-ind)Ru(bipy)Cl][PF_6] (**16**).

4.2 Experimental section

4.2.1 Materials

The starting materials $[(\eta^6\text{-arene})RuCl_2]_2$, arene = biphenyl (bip), *p*-terphenyl (*p*-terp, bound to Ru through the terminal phenyl ring), tetrahydroanthracene (tha), or dihydroanthracene (dha), were prepared as described in Chapter 2. $[(\eta^6\text{-bz})RuCl_2]_2$, $[(\eta^6\text{-ind})RuCl_2]_2$ and $[(\eta^6\text{-thn})RuCl_2]_2$, where bz = benzene, ind = indan and thn = tetrahydronaphthalene were donated from Dr Abraha Habtemariam. 2,2′-Bipyridine-3,3′-diol, 2,2′-bipyridine, N-methylimidazole (N-MeIm) and 9-ethylguanine (9-EtG) were purchased from Sigma-Aldrich. Methanol was dried over Mg/I_2. Complexes $[(\eta^6\text{-ind})Ru(4,4'\text{-}Me_2\text{-bipy})Cl][PF_6]$ (**13**), $[(\eta^6\text{-ind})Ru(phen)Cl][PF_6]$ (**14**), $[(\eta^6\text{-bip})Ru(bipy)Cl][PF_6]$ (**15**) and $[(\eta^6\text{-ind})Ru(bipy)Cl][PF_6]$ (**16**) were prepared as previously described,[1] by Dr Abraha Habtemariam. Cisplatin was obtained from Sigma-Aldrich and [PtCl(dien)]Cl (dienPt) was a generous gift of Professor G. Natile from University of Bari. Ethidium bromide (EtBr) was obtained from Merck KgaA. All other reagents were obtained from commercial suppliers.

Stock aqueous solutions of metal complexes (5×10^{-4} M) for the biophysical and biochemical studies were filtered and stored at room temperature in the dark. The concentrations of ruthenium or platinum in stock solutions were determined by flameless atomic absorption spectrometry (FAAS). Calf thymus (CT) DNA (42 % G + C, mean molecular mass ca. 2×10^7) was also prepared and characterized as described previously.[5, 6]

4.2.2 Synthesis of ruthenium complexes

All chlorido complexes were synthesized in methanol using a similar procedure. Typically the ligand (2 mol equiv) was added to a methanolic solution of the ruthenium dimer $[(\eta^6\text{-arene})RuCl_2]_2$. Details for individual reactions are described below.

$[(\eta^6\text{-tha})Ru(bipy)Cl][PF_6]$ (1). To a suspension of $[(\eta^6\text{-tha})RuCl_2]_2$ (0.053 g, 0.075 mmol) in dry, freshly-distilled methanol (25 mL) bipyridine (0.023 g, 0.150 mmol) was added. The reaction mixture was stirred at ambient temperature under argon, overnight. The resulting clear yellow solution was filtered, NH_4PF_6 (0.060 g, 0.374 mmol) was added and the flask was shaken. A precipitate started to appear almost immediately. The flask was kept at -20°C overnight, and the product was collected by filtration, washed with cold methanol and ether, and dried in air to give a brownish solid. Yield: 0.036 g (39%).

Crystals suitable for x-ray analysis were obtained by slow evaporation of a methanolic solution at ambient temperature and the complex crystallized as $[(\eta^6\text{-tha})Ru(bipy)Cl][PF_6] \cdot H_2O$. ^1H NMR in DMSO-d_6: δ 9.55 (d, 2H), 8.6 (d, 2H), 8.3 (d of d, 2H), 7.85 (m, 2H), 6.4 (d of d, 2H), 6.1 (d of d, 2H), 5.45 (s, 2H), 3.12 (m, 2H), 2.43 (m, 4H), 1.5 (m, 2H). Anal. Calcd for $C_{24}H_{24}ClF_6N_2PORu$ (**1** · H_2O): C, 45.33; H, 3.80; N, 4.41. Found: C, 45.43; H, 3.40; N, 4.55.

[(η^6-tha)Ru(bipy(OH)O)Cl] (2). To a suspension of [(η^6-tha)$RuCl_2$]$_2$ (0.050 g, 0.070 mmol) in dry, freshly-distilled methanol (25 mL), 2,2′- bipyridine- 3,3′-diol (0.026 g, 0.140 mmol) was added. The reaction mixture was stirred at ambient temperature under argon overnight, filtered and the volume was reduced until the onset of precipitation. It was kept at -4°C for 24 h to allow further precipitation to occur. The fine yellow solid was collected by filtration, washed with methanol followed by ether, and dried in vacuum. It was recrystallized from methanol/ether. Yield: 0.036 g (51%).

A portion of the complex (1 mg) was dissolved in methanol (1 mL) and filtered to yield a clear yellow solution. Slow diffusion of diethyl ether into this solution resulted in the formation of yellow crystals suitable for x-ray diffraction. ESI-MS: calcd for $RuClN_2O_2C_{24}H_{22}^+$ $[M+H]^+$ m/z 507.0, found 507.3. ^{1}H NMR in DMSO-d_6: δ 17.92 (s, 1H, OH), 8.62 (d, 2H), 7.22 (d of d, 2H), 7.06 (d, 2H), 6.08 (d of d, 2H), 5.91 (d of d, 2H), 5.56 (s, 2H), 3.12 (m, 2H), 2.43 (m, 4H), 1.92 (m, 2H).

[(η^6-dha)Ru(bipy(OH)O)Cl] (3). To a suspension of [(η^6-dha)$RuCl_2$]$_2$ (0.028 g, 0.040 mmol) in dry, freshly-distilled methanol (30 mL), 2,2′- bipyridine- 3,3′-diol (0.015 g, 0.080 mmol) was added. The rest of the procedure was the same as described for **2**. The fine yellow solid was recrystallized from methanol/ether. Yield: 0.016 g (41%).

ESI-MS: calcd for $RuClN_2O_2C_{24}H_{20}^+$ $[M+H]^+$ m/z 504.9, found 504.8. ^{1}H NMR in MeOD-d_4: δ 17.69 (s, 1H, OH), 8.62 (d, 2H), 7.14 (d of d, 2H), 6.95 (d, 2H), 6.89 (d, 2H), 6.63 (t, 2H), 6.30 (d, 2H), 5.96 (t, 2H), 4.17 (d, 2H), 3.77 (d, 2 H).

[(η^6-thn)Ru(bipy(OH)O)Cl] (4). To a suspension of [(η^6-thn)$RuCl_2$]$_2$ (0.030 g, 0.050 mmol) in dry, freshly-distilled methanol (30 mL), 2,2′- bipyridine- 3,3′-diol (0.018 g, 0.100 mmol) was added. The rest of the procedure was the same as described for **2**, the only difference was that the reaction mixture was stirred for 4 h instead of overnight. The fine yellow solid was recrystallized from methanol/ether. Yield: 0.030 g (68%).

ESI-MS: calcd for $RuClN_2O_2C_{20}H_{20}^+$ $[M+H]^+$ m/z 456.9, found 457.3. ^1H NMR in DMSO-d_6: δ 17.92 (s, 1H, OH), 8.66 (d, 2H), 7.27 (d of d, 2H), 7.10 (d, 2H), 5.96 (t, 2H), 5.84 (d, 2H), 2.54 (m, 2H), 2.20 (m, 2H), 1.52 (m, 2H), 1.20 (m, 2H).

[(η^6-bz)Ru(bipy(OH)O)Cl] (5). To a suspension of [(η^6-bz)$RuCl_2$]$_2$ (0.052 g, 0.106 mmol) in dry, freshly-distilled methanol (30 mL), 2,2′-bipyridine- 3,3′-diol (0.040 g, 0.213 mmol) was added. The rest of the procedure was the same as described for **2**, the only difference was that the reaction mixture was stirred for 3 h instead of overnight. The fine yellow solid was recrystallized from methanol/ether. Yield: 0.060 g (72%).

^1H NMR in DMSO-d_6: δ 17.89 (s, 1H, OH), 8.78 (d, 2H), 7.21 (d of d, 2H), 7.09 (d, 2H), 6.05 (s, 6H). Anal. Calculated for $C_{16}H_{13}ClN_2O_2Ru \cdot 0.5\ H_2O$ (**5** · 0.5 H_2O): C, 46.77; H, 3.43; N, 6.82. Found: C, 46.72; H, 2.83; N, 6.68.

[(η^6-*p*-terp)Ru(bipy(OH)O)Cl] (6). To a suspension of [(η^6-*p*-terp)$RuCl_2$]$_2$ (0.050 g, 0.062 mmol) in dry, freshly-distilled methanol (50 mL), 2,2′- bipyridine- 3,3′-diol (0.023 g, 0.124 mmol) was added. The rest of the procedure was the same as

described for **2**. The fine yellow solid was recrystallized from acetone/ether. Yield: 0.051 g (75%).

^{1}H NMR in DMSO-d_6: δ 17.91 (s, 1H, OH), 8.5 (d, 2H), 7.75 (m, 6H), 7.5 (t, 2H), 7.4 (t, 1H), 7.1 (m, 4H), 6.5 (d, 2H), 6.2 (t, 2H), 6.1 (t, 1H). Anal. Calculated for $C_{28}H_{23}ClN_2O_3Ru$ (**6** · H_2O): C, 58.79; H, 4.05; N, 4.89. Found: C, 59.22; H, 3.41; N, 4.69.

[(η^6-bip)Ru(bipy(OH)O)Cl] (7). To a suspension of [(η^6-bip)$RuCl_2$]$_2$ (0.053 g, 0.08 mmol) in dry, freshly-distilled methanol (30 mL), 2,2′- bipyridine-3,3′-diol (0.030 g, 0.16 mmol) was added. The rest of the procedure was the same as described for **2**. The fine yellow solid was recrystallized from acetone/ether. Yield: 0.049 g (63%).

^{1}H NMR in DMSO-d_6: δ 17.85 (s, 1H, OH), 8.5 (d, 2H), 7.7 (t, 1H), 7.6 (d, 2H), 7.4 (t, 2H), 7.00 (m, 4H), 6.5 (d, 2H), 6.2 (t, 2H), 6.1 (t, 1H). Anal. Calculated for $C_{22}H_{17}ClN_2O_2Ru$: C, 55.29; H, 3.58; N, 5.86. Found: C, 55.36; H, 3.27; N, 5.88.

[(η^6-ind)Ru(bipy(OH)$_2$)Cl][PF_6] (8). Complex **8** was prepared by Dr Abraha Habtemariam. To a suspension of [(η^6-ind)$RuCl_2$]$_2$ (0.075g, 0.13 mmol) in dry, freshly-distilled methanol (10 mL), 2,2′- bipyridine-3,3′-diol (0.050g, 0.26 mmol) dissolved in methanol (3 mL) was added dropwise. The reaction mixture was left stirring at ambient temperature for 1 h. It was then filtered and to the filtrate NH_4PF_6 (0.128 g, 0.80 mmol) was added and the flask shaken. A precipitate started to appear almost immediately. The flask was kept at -20°C overnight. The solid obtained was collected by filtration, washed with cold methanol and ether and dried in air to give an intense bright yellow solid. Yield: 0.079 g (52%).

Crystals suitable for x-ray analysis were obtained by slow evaporation of a methanolic solution at ambient temperature and complex crystallized as [(η^6-ind)Ru(bipy(OH)$_2$)Cl][PF_6] · CH_3OH. ^{1}H NMR in DMSO-d_6: δ 8.60 (d, 2H), 7.27 (d of d, 2H), 7.05 (d, 2H), 6.10 (m, 2H), 5.82 (m, 2H), 2.67-2.50, 2.05-1.85 (m, 6H), Anal. Calcd for $C_{19}H_{18}ClF_6N_2O_2PRu$: C, 39.73; H, 3.67; N, 4.63. Found: C, 39.03; H, 3.66; N, 4.66.

[(η^6-tha)Ru(bipy)(9-EtG-*N7*)][PF_6]$_2$ (9). To a suspension of [(η^6-tha)Ru(bipy)Cl][PF_6] (0.020 g, 0.030 mmol) in water (30 mL), 9-ethylguanine (0.006 g, 0.030 mmol) was added. The reaction mixture was left stirring for 2 h at 37°C. The clear yellow solution was then filtered and to the filtrate NH_4PF_6 (0.026 g, 0.160 mmol) was added. The volume was reduced until the onset of precipitation. The flask was sealed and placed on ice for 2 h for further precipitation to occur. The precipitate was filtered off, washed with water followed by ethanol and ether, and dried in vacuum to give a brown solid.

ESI-MS: calcd for $RuN_7OC_{31}H_{31}^+$ $[M-H]^+$ m/z 618.7, found 619.0. ^{1}H NMR in DMSO-d_6 (90 % of complex **9**): δ 11.1 (broad, 1H, NH), 10.0 (d, 2H), 8.6 (d, 2H), 8.3 (d of d, 2H), 7.9 (m, 2H), 7.4 (s, 1H), 7.0 (broad, 2H, NH), 6.65 (d of d, 2H), 6.10 (d of d, 2H), 5.4 (s, 2H), 3.8 (q, 2H), 3.18 (d, 2H), 2.30 (m, 4H), 1.3 (d, 2H), 1.15 (t, 3H).

[(η^6-tha)Ru(bipy(OH)O)(9-EtG-*N7*)][PF_6] (10). To a suspension of [(η^6-tha)Ru(bipy(OH)O)Cl] (0.020 g, 0.030 mmol) in water (30 mL), 9-ethylguanine (0.006 g, 0.030 mmol) was added. The reaction mixture was left stirring for 2 h at

37°C. The clear yellow solution was filtered and to the filtrate NH_4PF_6 (0.020 g, 0.150 mmol) was added. The rest of the procedure was the same as for **9**. The complex (1 mg) was dissolved in methanol (1 mL) and filtered to yield a clear yellow solution. Slow diffusion of diethyl ether into this solution resulted in the formation of brown crystals suitable for x-ray diffraction. The complex crystallized as [(η^6-tha)Ru(bipy(OH)O)(9-EtG-*N7*)][PF_6] · CH_3OH (**10** · CH_3OH).

ESI-MS: calcd for $RuN_7O_3C_{31}H_{30}^+$ $[M]^+$ m/z 649.7, found 650.0. ^1H NMR in MeOD-d_4 (98 % of complex **10**): δ 17.88 (s, 1H, OH), 9.14 (d, 2H), 7.39 (d of d, 2H), 7.26 (d, 2H), 7.12 (s, 1H), 6.25 (d of d, 2H), 6.00 (d of d, 2H), 5.53 (s, 2H), 3.95 (q, 2H), 3.18 (d, 2H), 2.45 (m, 4H), 1.79 (d, 2H), 1.25 (t, 3H).

[(η^6-thn)Ru(bipy(OH)O)(N-MeIm)][PF_6] (11). To a suspension of [(η^6-thn)Ru(bipy(OH)O)Cl] (0.014 g, 0.023 mmol) in water (30 mL), $AgNO_3$ (0.0039 g, 0.023 mmol) was added. The reaction mixture was left stirring overnight at ambient temperature covered with aluminium foil. It was then filtered to remove AgCl, and to the filtrate N-methylimidazole (1.85 μL, 0.023 mmol) dissolved in methanol (5 mL) was added. The reaction mixture was left stirring for 3 h at 37°C. The clear yellow solution was then filtered and the volume reduced to ~5 mL. NH_4PF_6 was added (0.058 g, 0.35 mmol) and the flask sealed and placed on ice for 2 h for further precipitation to occur. The yellow precipitate was filtered off, washed with a little water followed by ethanol and ether, and dried in vacuum. It was recrystallized from methanol. Yield: 0.013 g (67%).

The complex (1 mg) was dissolved in methanol (1 mL) and filtered to yield a clear yellow solution. Slow evaporation of this solution resulted in the formation of yellow

crystals suitable for x-ray diffraction. ^{1}H NMR in DMSO: δ 17.88 (s, 1H, OH), 8.82 (d, 2H), 7.70 (s, 1H), 7.39 (t, 2H), 7.21 (d, 2H), 6.65 (d of d, 2H), 6.19 (t, 2H), 6.00 (d, 2H), 3.65 (s, 3H), 2.67 (m, 2H), 2.06 (m, 2H), 1.60 (m, 2H), 1.16 (m, 2H).

[(η^6-bz)Ru(bipy(OH)O)(9-EtG-*N*7)][PF_6] (12). To a suspension of [(η^6-bz)Ru(bipy(OH)O)Cl] (0.030 g, 0.060 mmol) in water (30 mL), 9-ethylguanine (0.011 g, 0.06 mmol) was added. The reaction mixture was left stirring for 2 h at 37°C. The clear yellow solution was filtered and to the filtrate NH_4PF_6 (0.029 g, 0.180 mmol) was added. The rest of the procedure was the same as for **9**. It was recrystallized from methanol to give a bright yellow solid.

ESI-MS: calcd for $RuN_7O_3C_{23}H_{22}^+$ $[M]^+$ m/z 545.6, found 545.9. ^{1}H NMR in DMSO-d_6 (100 % of complex **12**): δ 17.6 (s, 1H, OH), 11.0 (broad, 1H, NH), 9.1 (d, 2H), 7.35 (d of d, 2H), 7.15 (d, 2H), 7.05 (s, 1H), 6.9 (broad, 2H, NH), 6.2 (s, 6H), 4.0 (d of d, 2H), 1.2 (t, 3H).

4.2.3 X-ray crystallography

The details of the instrumentation are described in Chapter 2. x-ray crystal structures of complexes **1**, **2** and **11** are solved by Professor Simon Parsons, **8** by Mr Andrew Parkin and **10** by Mr Alessandro Prescimone. Structures **1** and **10** were solved by direct methods (SIR92)[7] and refined using CRYSTALS,[8] while **2**, **8** and **11** were solved using Patterson methods (SHELXS-97[9] or DIRDIF)[10] and refined with SHELXL-97.[11] In most cases H atoms were placed in idealised positions. In complex **1**, H-atoms belonging to the water of crystallisation were located in a difference map

and the positions refined subject to the restraint that the OH distance was equal to 0.85(1) Å. In complex **2**, H52 was located in a difference map in a bridging position between O52 and O82; it was refined freely with an isotropic displacement parameter. H-atoms in complex **8** attached to methyl and hydroxyl groups were located in a difference synthesis and refined using the Sheldrick rigid rotating group model. In complex **10**, the H-atoms were located in a difference map, idealised, and then allowed to ride on their parent atoms; H231 is involved in a hydrogen bond, and its position was refined freely. In complex **11**, the thn ligand is disordered at C81 over two positions in the ratio 0.85 : 0.15. Similarity restraints were applied to the geometry about the part-weight atoms. Only the major component (C81) was refined with anisotropic displacement parameters. The expected formula for a protonated $bipy(OH)_2$ chelating ligand had 2 PF_6^- per formula unit, but only one was located in the crystal structure. A difference map in the region of the two O-atoms attached to the bipy showed one peak in a bridging position between the two O-atoms, bonded predominantly to O52. This was interpreted as a bridging O···H···O H-bond, with the overall charge on the ligand being -1, thus ensuring change balance. The hydroxyl group O52-H52 was treated as a variable metric rigid group. The crystal structures of **1**, **2**, **8**, **10** and **11** have been deposited in the Cambridge Crystallographic Data Center under the accession numbers CCDC 676256, 676253, 611053, 676255 and 676254, respectively.

4.2.4 pH measurement

The pH values of NMR samples in D_2O were measured at 25°C directly in the NMR tube before and after recording NMR spectra using a Corning pH meter 145 calibrated with pH 4, pH 7 and pH 10 buffer solutions (Sigma Aldrich) and equipped with Aldrich microcombination electrode. No corrections have been made for the effect of deuterium on the glass electrode and these are termed as pH* values. The pH* values were adjusted with NaOD and DCl of varying concentrations.

4.2.5 Hydrolysis

Hydrolysis of the chlorido complexes was monitored by UV/Vis spectroscopy or by ^{1}H NMR spectroscopy, without explicit control of pH or chloride concentrations. For UV/Vis spectroscopy: complexes were dissolved in methanol and diluted with H_2O to give ca. 50 μM solutions (95% H_2O, 5% MeOH). The absorbance was recorded at 30 or 60 s intervals at the selected wavelength over ca. 4 h at 37°C. Plots of the change in absorbance with time were computer-fitted to the first-order rate equation: $A = C_0 + C_1e^{-kt}$ (C_0 and C_1 are computer-fitted constants and A is the absorbance corresponding to time t) using Origin version 7.5 (Microcal Software Ltd) to give the half-lives ($t_{1/2}$) and rate constant values (k). For ^{1}H NMR spectroscopy: complexes were dissolved in MeOD-d_4 and diluted in D_2O to give ca. 100 μM solutions (95% D_2O, 5% MeOD-d_4). The ^{1}H NMR spectra were recorded at various time intervals at 37°C. The relative

amounts of chlorido species or aqua adducts (determined by integration of peaks in ^1H NMR spectra) versus time were fitted to appropriate equations for pseudo-first-order kinetics using Origin version 7.5 (Microcal Software Ltd) to give the half-lives and rate constants.

4.2.6 Rate of arene loss

The complexes were dissolved in MeOD-d_4 and diluted with D_2O to give ca. 100 μM solutions (95% D_2O, 5% MeOD-d_4). Arene loss with time was followed by ^1H NMR.

4.2.7 Computation

The details are described in Chapter 2. Single point calculations were carried out for the tha fragment of the cation of complex **10** $[(\eta^6\text{-tha})Ru(bipy(OH)O)(9\text{-EtG-}N7)]^+$ and the fragment of the cation without tha. The energies of these two separate fragments were subtracted from the energy of the entire 1+ cation of complex **10**, in the single point calculation of cation of **10** $[(\eta^6\text{-tha})Ru(bipy(OH)O)(9\text{-EtG-}N7)]^+$, to obtain the total bonding energy of tha. The total bonding energy of tha is a sum of the bonding energy of the arene and Ru and the energy of the CH/π interaction between the arene and the chelating ligand (bipy(OH)O). The tha ligand in the crystal structure of **10** was rotated so as to allow π-π interaction with the purine ring of 9-EtG fragment and the geometry was optimized to give the minimum energy structure. After geometry optimization a single point calculation was carried out again on the tha

fragment of the modified cation of **10** and the fragment of the cation without tha. The energies of these two separate fragments were subtracted, in the single point calculation of the 1+ cation of modified **10**, from the energy of the entire cation of modified **10** $[(\eta^6\text{-tha})\text{Ru(bipy(OH)O)(9-EtG-}N7)]^+$. The total bonding energy of tha obtained is in this case a sum of the bonding energy of the arene and Ru and the energy of the π-π interaction. Upon geometry optimization, the atomic coordinates of the minimum energy structures were used in single point calculations.

4.2.8 Metallation reactions

CT DNA was incubated with ruthenium or platinum complex in 10 mM $NaClO_4$ (pH = 6) at 37°C for 48 h in the dark, if not stated otherwise. The values of r_b (defined as the number of atoms of the metal bound per nucleotide residue) were determined by FAAS.

4.2.9 Circular dichroism (CD)

Isothermal CD spectra of CT DNA modified by ruthenium complexes were recorded at 25°C in 10 mM $NaClO_4$.

4.2.10 DNA melting

The melting curves of CT DNA were recorded by measuring the absorbance at 260 nm. The melting curves of unmodified or ruthenated DNA were recorded in the medium containing 10 mM $NaClO_4$ with 1 mM Tris-HCl/0.1 mM EDTA, pH = 7.4 and 0.01 M or 0.1 M $NaClO_4$. The value of melting temperature (t_m) was determined as the temperature corresponding to a maximum on the first-derivative profile of the melting curves. The t_m values could be thus determined with an accuracy of ± 0.3°C.

4.2.11 Fluorescence measurements

The details of the instrumentation are described in Chapter 2. Fluorescence measurements of CT DNA modified by Ru^{II} arene complexes, in the presence of EtBr were performed at an excitation wavelength of 546 nm, and the emitted fluorescence was analyzed at 590 nm. The fluorescence intensity was measured at 25°C in 0.4 M NaCl to avoid secondary binding of EtBr to DNA.[12, 13] The concentrations were 0.01 mg/mL for DNA and 0.04 mg/mL for EtBr, which corresponded to the saturation of all intercalation sites for EtBr in DNA.[12]

4.3 Results

4.3.1 Synthesis and characterization

The ligands used in this work are shown in Figure 4.1. The chlorido Ru^{II} arene complexes **1-8** (Figure 4.1) were synthesized as PF_6 salts or as neutral complexes in good yields (39.0-74.6%) by the reaction of $[(\eta^6\text{-arene})RuCl_2]_2$ dimers and the appropriate chelating ligand in methanol. All the synthesized complexes were fully characterized by ^1H NMR and the OH proton resonance from bipy(OH)O was shifted to very low field, at ~ 18 ppm. The ^1H NMR resonances of the coordinated η^6-arenes are shifted upfield compared to the uncoordinated arenes.

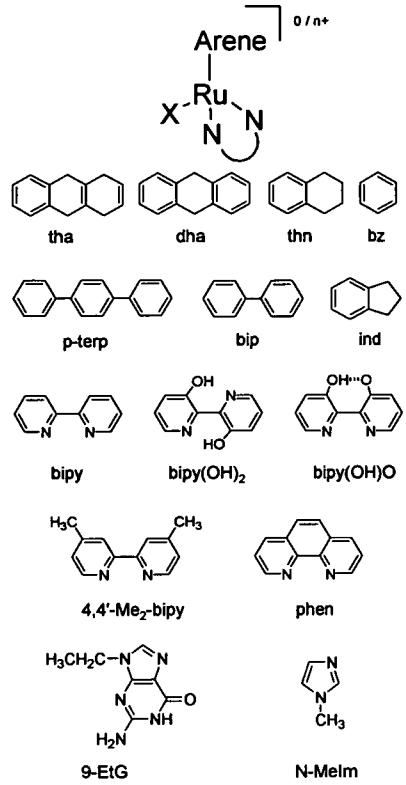

Complex	Arene	N-N	X
1	tha	bipy	Cl
2	tha	bipy(OH)O	Cl
3	dha	bipy(OH)O	Cl
4	thn	bipy(OH)O	Cl
5	bz	bipy(OH)O	Cl
6	p-terp	bipy(OH)O	Cl
7	bip	bipy(OH)O	Cl
8	ind	$bipy(OH)_2$	Cl
9	tha	bipy	9-EtG
10	tha	bipy(OH)O	9-EtG
11	thn	bipy(OH)O	N-MeIm
12	bz	bipy(OH)O	9-EtG
13	ind	$4,4'\text{-}Me_2\text{-bipy}$	Cl
14	ind	phen	Cl
15	bip	bipy	Cl
16	ind	bipy	Cl

Figure 4.1 General structures of complexes studied in this Chapter, as neutral or PF_6 salts.

4.3.2 Crystal structures

The crystal structures of [(η^6-tha)Ru(bipy)Cl][PF_6] (**1**), [(η^6-tha)Ru(bipy(OH)O)Cl] (**2**) and [(η^6-ind)Ru(bipy(OH)$_2$)Cl][PF_6] (**8**) are shown in Figure 4.2. The crystal structures of N-MeIm and 9-EtG adducts [(η^6-thn)Ru(bipy(OH)O)(N-MeIm)][PF_6] (**11**) and [(η^6-tha)Ru(bipy(OH)O)(9-EtG-*N7*)][PF_6] (**10**) are shown in Figure 4.3. The crystallographic data are listed in Table 4.1 and Table 4.2, and selected bond lengths and angles in . In all the complexes, Ru^{II} adopts the familiar 'three-legged piano-stool' geometry. It is π-bonded to the appropriate arene ligand and σ-bonded to the N atoms of the chelating ligand and Cl, or N-MeIm, or *N7* of 9-EtG. The Ru-Cl bond lengths in all the chlorido Ru^{II} complexes are almost the same (~ 2.4 Å). In the crystal structure of [(η^6-tha)Ru(bipy)Cl][PF_6] · H_2O (**1** · H_2O), the Ru-N (bipy) distances (2.085(2) and 2.0796(19) Å; Table 4.3) are significantly longer than Ru-N (bipy(OH)O) distances in [(η^6-tha)Ru(bipy(OH)O)Cl] (complex **2**; 2.0701(14) and 2.0659(13) Å; Table 4.3). In all the crystal structures, the Ru – arene centroid distances are similar (~ 1.7 Å).

From the crystal structure of [(η^6-tha)Ru(bipy)Cl][PF_6] · H_2O (**1** · H_2O), it can be seen (Figure 4.2A) that the outer ring of tha is tilted (tilt angle 41.41°) towards the chelating ligand. The space-filling and capped-stick models of **1** · H_2O (Figure 4.4A and 4.4D, respectively) clearly show the presence of intramolecular CH/π interactions between CH protons of the outer ring of tha and the centres of the pyridine rings of the chelating ligand (distances 2.7 Å and 2.8 Å).

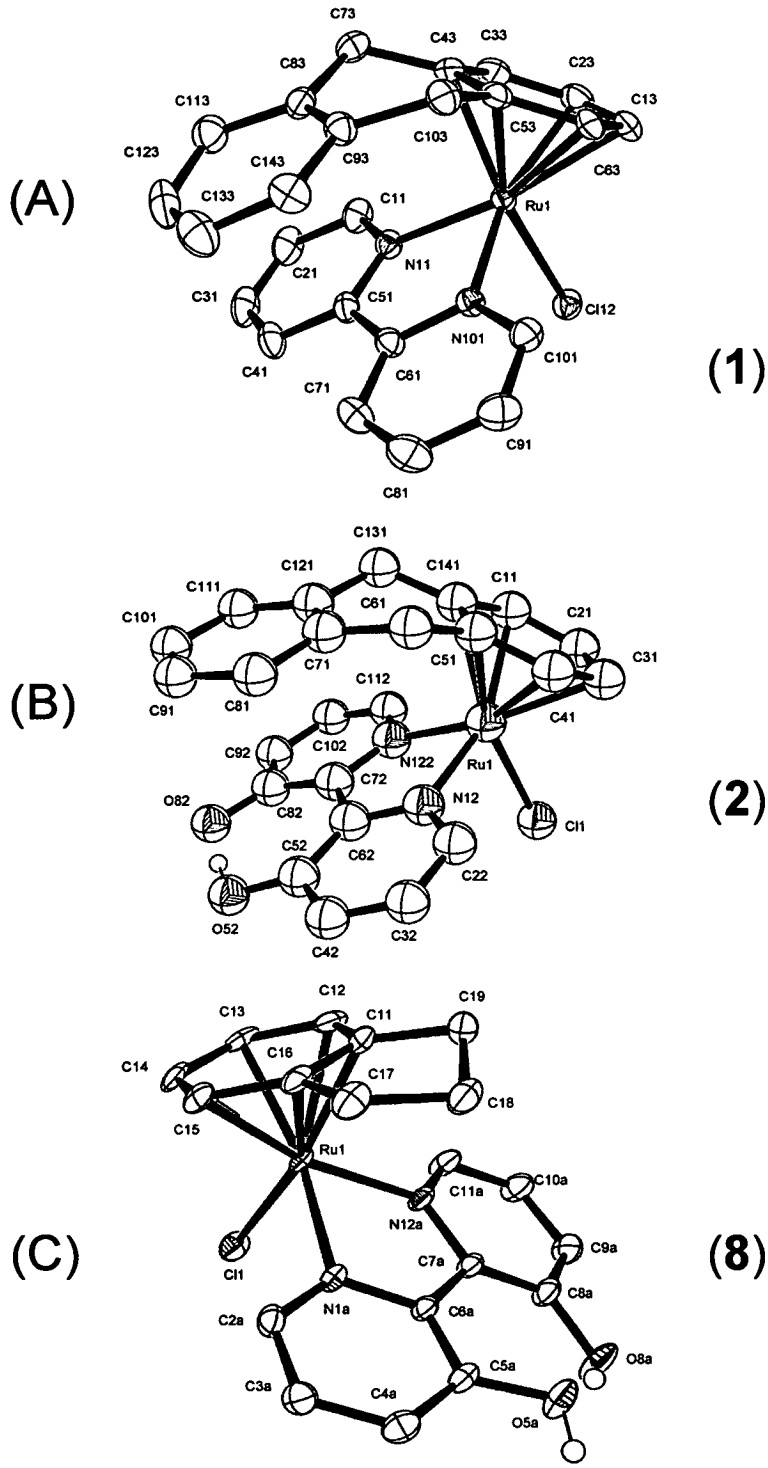

Figure 4.2 ORTEP diagrams for (**A**) cation of $[(\eta^6\text{-tha})Ru(bipy)Cl][PF_6] \cdot H_2O$ (**1** · H_2O), (**B**) $[(\eta^6\text{-tha})Ru(bipy(OH)O)Cl]$ (**2**), and (**C**) cation of $[(\eta^6\text{-ind})Ru(bipy(OH)_2)Cl][PF_6] \cdot CH_3OH$ (**8** · CH_3OH), with 50% probability thermal ellipsoids. All hydrogens apart from OH hydrogen atoms from chelating ligands, $bipy(OH)_2$ and bipy(OH)O, have been omitted for clarity.

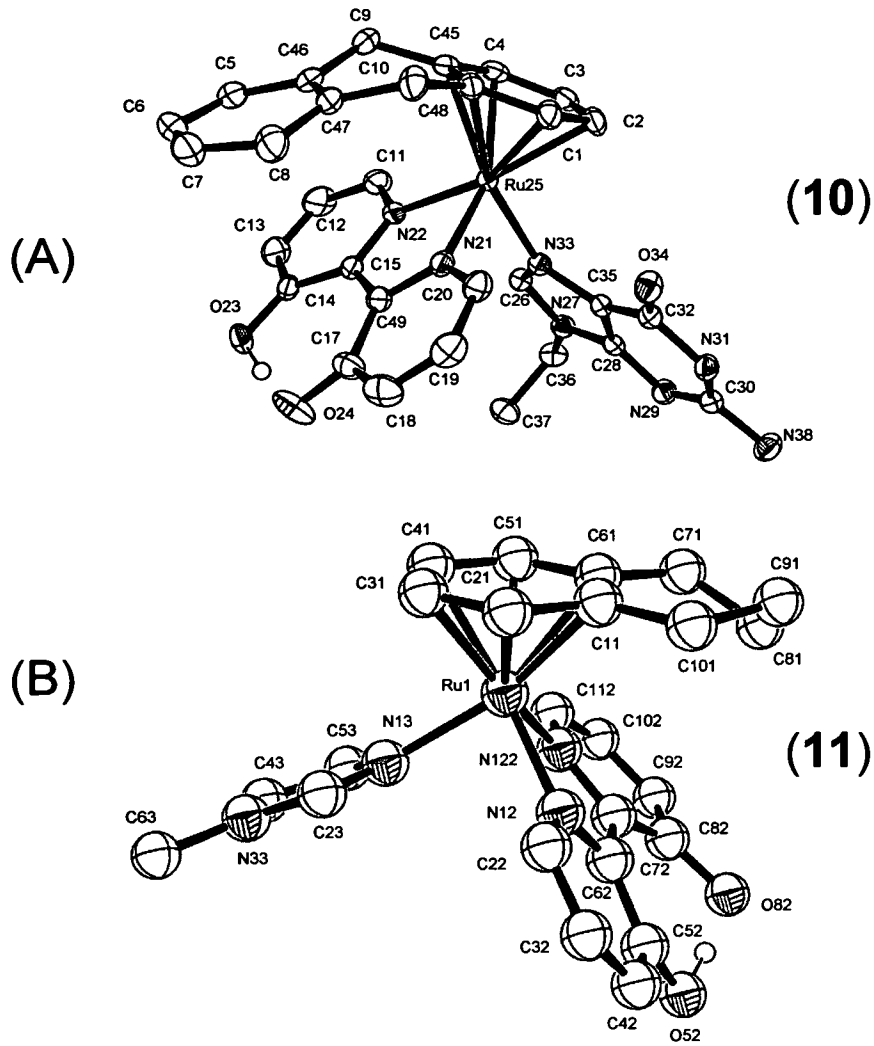

Figure 4.3 ORTEP diagrams for cations of (**A**) [(η^6-tha)Ru(bipy(OH)O)(9-EtG-*N7*)][PF_6] · CH_3OH (**10** · CH_3OH), and (**B**) [(η^6-thn)Ru(bipy(OH)O)(N-MeIm)][PF_6] (**11**), with 50% probability thermal ellipsoids. All hydrogens apart from OH hydrogen atom from the chelating ligand (bipy(OH)O), have been omitted for clarity.

Table 4.1 X-ray crystal structure data for **1** · H_2O, **2** and **8** · CH_3OH

	1 · H_2O	**2**	**8 · CH_3OH**
Formula	$C_{24}H_{24}ClF_6N_2OPRu$	$C_{24}H_{21}ClN_2O_2Ru$	$C_{20}H_{22}ClF_6N_2O_3PRu$
Molar mass	637.95	505.95	619.89
Crystal system	triclinic	monoclinic	triclinic
Crystal size /mm	0.42 × 0.25 × 0.14	0.40 × 0.18 × 0.11	0.37 × 0.25 × 0.12
Space group	*P-1*	*P21/n*	*P-1*
Crystal	Yellow / block	Yellow / block	Orange / block
a / Å	7.4422(3)	7.2697(2)	7.9858(10)
b / Å	11.8685(5)	16.7711(4)	12.1538(15)
c / Å	13.7805(6)	16.0993(4)	12.5825(16)
α / deg	94.960(2)	90	67.843(2)
β / deg	101.341(2)	99.6900(10)	83.718(2)
γ / deg	91.580(2)	90	83.549(2)
T / K	150	150(2)	150(2)
Z	2	4	2
R [F > 4σ (F)][a]	0.0336	0.0250	0.0464
R_w[b]	0.0868	0.0656	0.1248
GOF[c]	0.9159	1.077	1.051
Δρ max and min, / eÅ^{-3}	0.81, -0.78	0.599, -0.380	2.784, -1.723

[a]$R = \Sigma||F_o| - |F_c||/\Sigma|F_o|$. [b]$R_w = [\Sigma w(F_o^2 - F_c^2)^2/\Sigma wF_o^2)]^{1/2}$. [c]$GOF = [\Sigma w(F_o^2 - F_c^2)^2/(n-p)]^{1/2}$, where n = number of reflections and p = number of parameters.

Table 4.2 X-ray crystal structure data for **10** · CH_3OH and **11**

	10 · CH_3OH	**11**
Formula	$C_{32}H_{34}F_6N_7O_4PRu$	$C_{24}H_{25}F_6N_4O_2PRu$
Molar mass	826.70	647.52
Crystal system	monoclinic	monoclinic
Crystal size /mm	0.23 × 0.12 × 0.09	0.44 × 0.40 × 0.18
Space group	*P 1 21 / n 1*	*P21 / n*
Crystal	Brown / block	Yellow / block
a / Å	9.5526(2)	12.7776(2)
b / Å	10.8630(2)	13.4949(3)
c / Å	31.6240(7)	14.4729(3)
α / deg	90	90
β / deg	95.1740(10)	90.7780(10)
γ / deg	90	90
T / K	150	150(2)
Z	4	4
R [F > 4σ (F)][a]	0.0408	0.0331
R_w[b]	0.0427	0.0845
GOF[c]	1.0967	1.034
Δρ max and min, / eÅ^{-3}	0.90, -0.57	0.879, -0.540

[a]$R = \sum||F_o| - |F_c||/\sum|F_o|$. [b]$R_w = [\sum w(F_o^2 - F_c^2)^2/\sum wF_o^2)]^{1/2}$. [c]$GOF = [\sum w(F_o^2 - F_c^2)^2/(n-p)]^{1/2}$, where n = number of reflections and p = number of parameters.

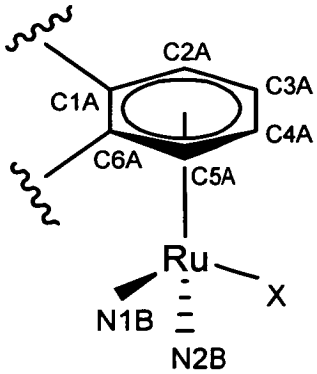

Table 4.3 Selected bond lengths (Å) and angles (°) for complexes **1, 2, 8, 10** and **11**

Bond/angle[a]	**1**	**2**	**8**	**10**	**11**
Ru-Cl	2.4047(6)	2.3958(4)	2.4118(8)	-	-
Ru-N13	-	-	-	-	2.0971(17)
Ru-N33	-	-	-	2.1233(19)	-
Ru-N1B	2.085(2)	2.0701(14)	2.080(3)	2.0786(19)	2.0706(16)
Ru-N2B	2.0796(19)	2.0659(13)	2.070(3)	2.077(2)	2.0736(16)
Ru-C1A	2.191(2)	2.1928(15)	2.200 (3)	2.195(2)	2.234(2)
Ru-C2A	2.215(2)	2.2083(15)	2.230(3)	2.225(2)	2.185(2)
Ru-C3A	2.215(2)	2.2073(16)	2.221(3)	2.220(2)	2.188(2)
Ru-C4A	2.199(2)	2.2189(17)	2.215(3)	2.217(2)	2.203(2)
Ru-C5A	2.192(2)	2.2124(16)	2.204(3)	2.206(2)	2.204(2)
Ru-C6A	2.193(2)	2.1934(15)	2.195(3)	2.201(2)	2.2270(19)
N2B-Ru-	76.89(8)	76.49(5)	76.52(10)	76.27(7)	77.09(6)
N1B-Ru-Cl	85.85(6)	85.06(4)	87.15(7)	-	-
N1B-Ru-N13	-	-	-	-	88.08(6)
N1B-Ru-N33	-	-	-	85.71(7)	-
N2B-Ru-Cl	85.44(5)	87.03(4)	85.55(8)	-	-
N2B-Ru-N13	-	-	-	-	89.23(7)
N2B-Ru-N33	-	-	-	85.87(7)	-

[a]Atom labelling scheme used for purposes of comparison only. The crystallographic atom labelling schemes for individual complexes are different. X = Cl, N13 or N33.

In the crystal structure of **2** (Figure 4.2B), one of the bipyridinediol oxygens is deprotonated, an intramolecular hydrogen bond forms (O82···H···O52; O-O distance 2.3886(19) Å), and the complex is neutral. The outer ring from the tricyclic-ring system of tha, in the crystal structure of **2**, is tilted by 36.90° towards the chelating ligand (Figure 4.2B). The space-filling and capped-stick models (Figure 4.4B and 4.4E) clearly show the presence of intramolecular CH/π interactions between CH protons of the outer ring of tha and the centres of the pyridine rings of the chelating ligand, bipy(OH)O (distances 2.8 Å and 2.9 Å).

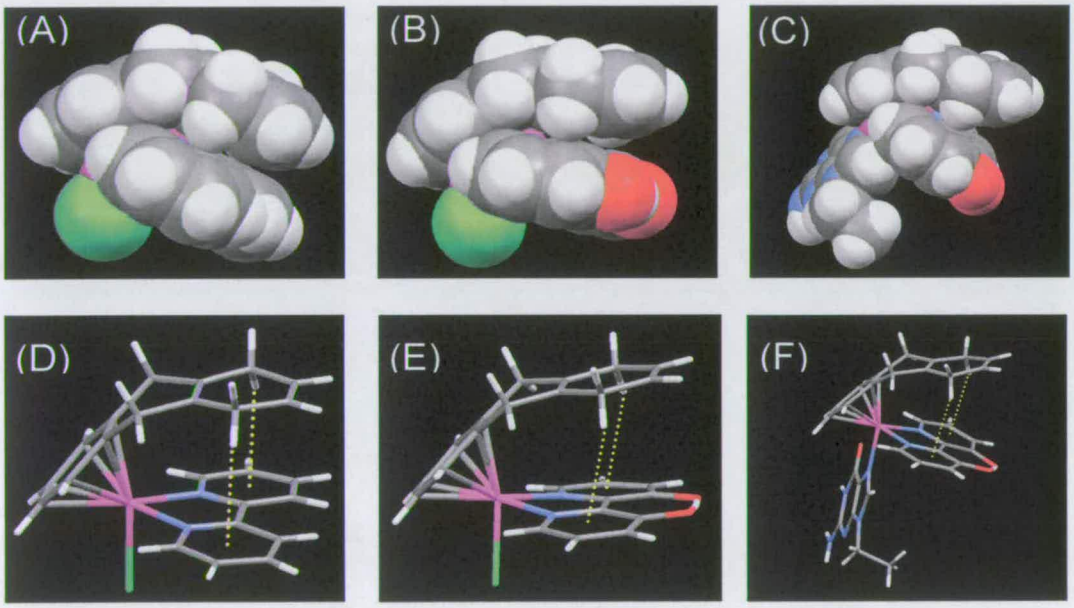

Figure 4.4 CH/π interactions in tha complexes **1**, **2** and **10**. Space-filling and capped-stick models (**A**) and (**D**) the cation of $[(\eta^6\text{-tha})Ru(bipy)Cl][PF_6] \cdot H_2O$ (**1** · H_2O), (**B**) and (**E**) $[(\eta^6\text{-tha})Ru(bipy(OH)O)Cl]$ (**2**) and (**C**) and (**F**) the cation of $[(\eta^6\text{-tha})Ru(bipy(OH)O)(9\text{-EtG-}N7)][PF_6] \cdot CH_3OH$ (**10** · CH_3OH), showing interaction between CH protons from the outer ring of tha and the centres of the π-systems of the chelating ligands.

The x-ray crystal structure of the cation of $[(\eta^6\text{-ind})Ru(bipy(OH)_2)Cl][PF_6] \cdot CH_3OH$ (**8** · CH_3OH, Figure 4.2C) shows a twisting of the pyridine rings of bipyridinediol (twist angle 17.31°) as well as intramolecular H-bonding involving the OH groups and intermolecular H-bonding involving methanol to give dimers in the unit cell (Figure 4.5A). The two oxygen atoms of the $bipy(OH)_2$ ligand (O5A and O8A) are 2.532(4) Å apart.

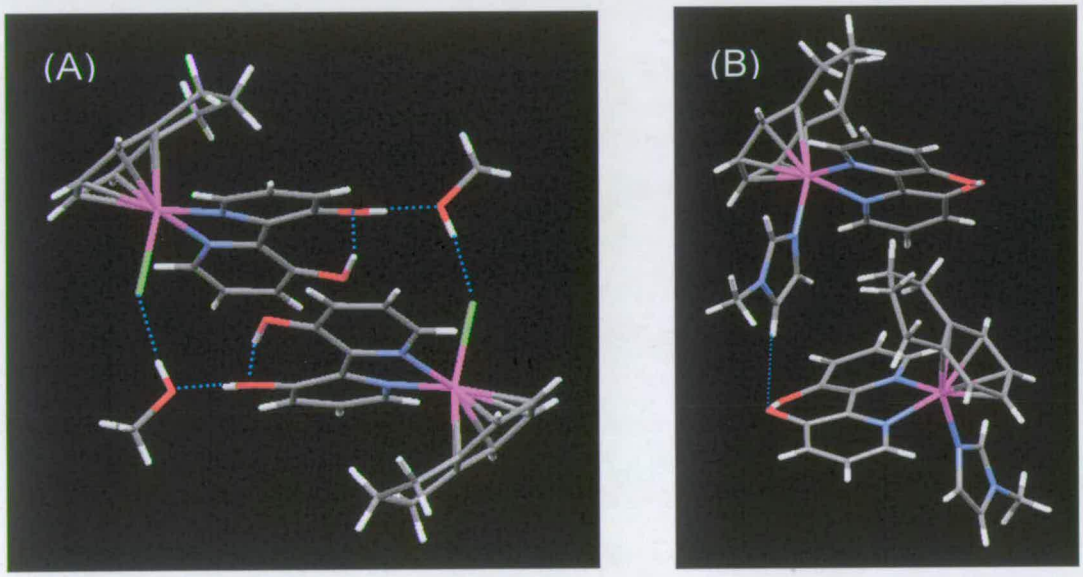

Figure 4.5 (**A**) H-bonding involving the OH groups of $[(\eta^6\text{-ind})Ru(bipy(OH)_2)Cl][PF_6] \cdot CH_3OH$ (**8** · CH_3OH) giving rise to dimers in the unit cell. (**B**) Twisting of the bipy(OH)O ligand in $[(\eta^6\text{-thn})Ru(bipy(OH)O)(N\text{-MeIm})][PF_6]$ (**11**) as a result of H-bond formation between O82 from bipy(OH)O of one molecule and C43H from N-MeIm of another molecule.

[(η^6-tha)Ru(bipy(OH)O)(9-EtG-*N7*)][PF_6] (**10**) crystallized with one molecule of solvent (CH_3OH) in the lattice per molecule of complex. One of the oxygens of the chelating ligand in the crystal structure of **10** · CH_3OH is deprotonated and an intramolecular hydrogen bond is formed between this oxygen (O24) and the hydrogen from the other oxygen (O23; Figure 4.3A). The two oxygen atoms are 2.389(3) Å apart. The outer ring from the coordinated tricyclic-ring system of tha is tilted (tilt angle 37.21°) towards the chelating bipy(OH)O ligand. The space-filling and capped-stick models (Figure C and 4.4F) show the presence of intramolecular CH/π interactions between CH protons of the outer ring of tha and the centres of the pyridine rings of bipy(OH)O (distances 2.8 Å and 3.0 Å).

In the crystal structure of [(η^6-thn)Ru(bipy(OH)O)(N-MeIm)][PF_6] (**11**) one of the oxygens of the bipydiol ligand (O82) is again deprotonated (Figure 4.3B) and an intramolecular hydrogen bond is formed between this oxygen and the hydrogen from the other oxygen (O52). The two oxygen atoms are 2.390(3) Å apart. Ru is σ-bonded to N13 of N-methylimidazole. Neither intra- nor inter-molecular π-π stacking nor CH/π interactions are observed in the crystal structure of **11**. The non-coordinated ring of thn is disordered and bipy(OH)O ligand is twisted (by 14.43°), as a result of the hydrogen bond formed between O82 of bipy(OH)O of one molecule and the C43H hydrogen of N-methylimidazole of another molecule (2.474 Å, Figure 4.5B).

4.3.3 pH dependence

In order to determine the pK_a values of the OH protons of bipyridinediol chelating ligand without the complication of deprotonation of coordinated water (aquation of chlorido complex), the N-MeIm adduct $[(\eta^6\text{-thn})Ru(bipy(OH)O)(N\text{-MeIm})][PF_6]$ (complex **11**) was prepared. ^1H NMR spectra of **11** in DMSO-d_6 showed a peak at 17.88 ppm corresponding to the O-H···O proton from bipy(OH)O. ^1H NMR spectra of complex **11** in D_2O were recorded over the pH* range 2-10. None of the peaks shifted as a function of pH within this range, indicating that the form of the chelated ligand does not change. Therefore, it is reasonable to assume that at physiological pH (pH = 7), the ligand is present in the deprotonated form, bipy(OH)O.

4.3.4 Aqueous solution chemistry

The hydrolysis of complexes **4, 7, 8, 13-16** were studied at 37°C, using UV-Vis or by ^1H NMR spectroscopy (complex **4**). Due to the small amount of sample required, in general it was more convenient to follow hydrolyses by UV-Vis spectroscopy.

The time dependence of the absorbance of the complexes followed first-order kinetics (Figure 4.6A) in each case. ESI-MS spectra were consistent with the formation of the aqua complex as the product (observed peaks: $[(\eta^6\text{-thn})Ru(bipy(OH)O)H_2O]^{1+}$ $-H_2O$ calc. m/z 421.1, found m/z 421.3; $[(\eta^6\text{-bip})Ru(bipy(OH)O)H_2O]^{1+}$ $-H_2O$ calc. m/z 443.0, found m/z 443.1; $[(\eta^6\text{-ind})Ru(bipy(OH)O)H_2O]^{1+}$ $-H_2O$ calc. m/z 407.0, found

m/z 407.2; $[(\eta^6\text{-ind})Ru(4,4'\text{-}Me_2\text{-bipy})H_2O]^{2+}$ $-H_2O$ $-H^+$ calc. m/z 403.1, found m/z 403.2; $[(\eta^6\text{-ind})Ru(phen)H_2O]^{2+}$ $-H_2O$ $-H^+$ calc. m/z 399.0, found m/z 399.1; $[(\eta^6\text{-bip})Ru(bipy)H_2O]^{2+}$ $-H_2O$ $-H^+$ calc. m/z 411.0, found m/z 411.1; $[(\eta^6\text{-ind})Ru(bipy)H_2O]^{2+}$ $-H_2O$ $-H^+$ calc. m/z 375.0, found m/z 375.1 for the aqua adducts of complexes **4**, **7**, deprotonated **8**, **13**, **14**, **15** and **16**, respectively).

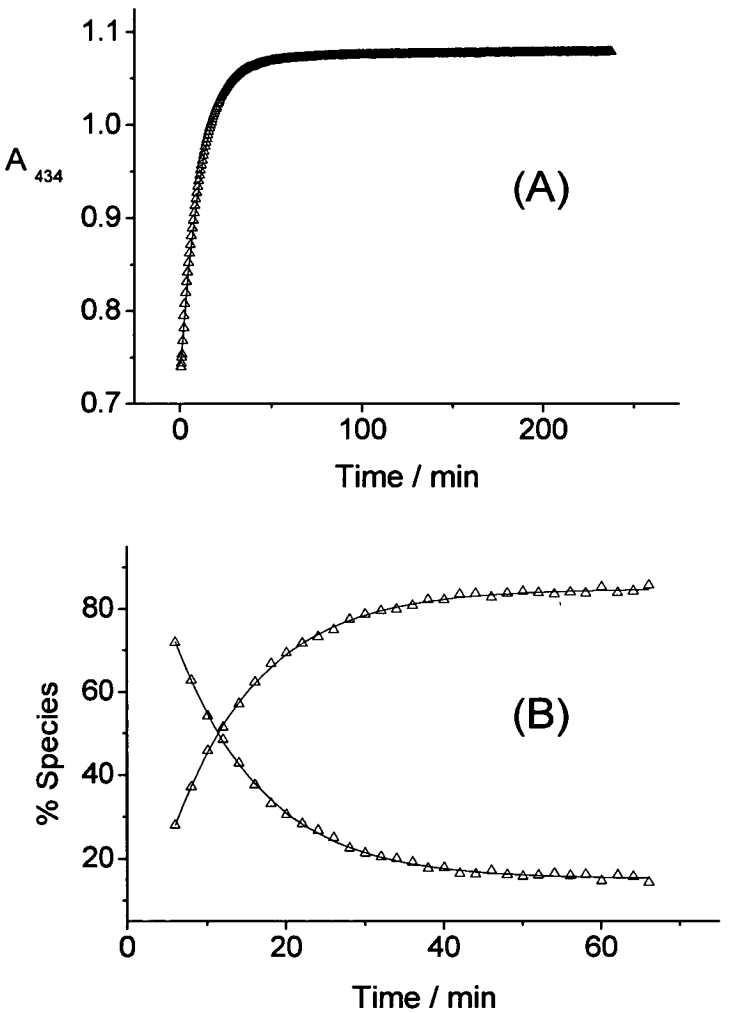

Figure 4.6 (**A**) Dependence of the absorbance at 434 nm over ca. 4 h during aquation of complex **4** at 37°C. (**B**) Time dependence of the percentage of chlorido and aqua species during aquation of complex **4** at 37°C followed by ^1H NMR.

^1H NMR spectra of **4** in 5% MeOD-d_4 / 95% D_2O (for which hydrolysis was also monitored using UV-Vis spectroscopy) initially contained one major set of peaks (chlorido species), and then a second set of peaks increased in intensity with time. The new set of peaks has the same chemical shifts as those of the aqua adduct under the same conditions (37°C, 100 μM solution in 5% MeOD-d_4 / 95% D_2O). The aqua adduct was prepared by treating **4** with $AgNO_3$ in water at room temperature overnight and removal of AgCl by filtration. The time dependence of the increase in concentration of aqua adduct or decrease in concentration of chlorido species followed first-order kinetics (Figure 4.6B), and the corresponding rate constant is listed in Table 4.4 together with rate constants determined using UV-Vis spectroscopy.

For complexes [(η^6-bip)Ru(bipy(OH)O)Cl] (**7**) and [(η^6-bip)Ru(bipy)Cl][PF_6] (**15**), separate sets of peaks were observed in ^1H NMR spectra (in 5% MeOD-d_4 / 95% D_2O) for products which had undergone arene-loss during the aquation. After 24 h, 33% of **7** and 46% of **15** had undergone arene loss.

The hydrolysis rates for the complexes which did not undergo arene loss, were determined over a period of 4 h. The rate constants for bip complexes that underwent arene loss were determined over the period of time before the onset of arene loss (80 min, detected by NMR). It can be seen that hydrolysis of the neutral bip complex **7** containing bipy(OH)O as chelating ligand ($t_{1/2}$ = 14.95 min) is twice as slow as for the positively-charged bip complex **15** containing bipy as chelating ligand ($t_{1/2}$ = 7.43 min), Table 4.4.

Aqueous solutions of [(η^6-ind)Ru(bipy$(OH)_2$)Cl][PF_6] (**8**) were found to be acidic immediately after dissolution (1 mM, pH ~ 3) consistent with the release of a proton

from $bipy(OH)_2$. Aqueous solutions of [(η^6-thn)Ru(bipy(OH)O)Cl] (**4**) were approximately neutral in pH, consistent with a lack of proton dissociation.

Table 4.4 Hydrolysis data for complexes **4**, **7**, **8**, **13**, **14**, **15** and **16** at 37°C

Complex		$10^3 \cdot k_{obs}$ (min^{-1})[a]	$t_{1/2}$ (min)
[(η^6-thn)Ru(bipy(OH)O)Cl]	(**4**)	91.8±0.4[b]	7.55
		91.6±1.4[c]	7.57
[(η^6-bip)Ru(bipy(OH)O)Cl]	(**7**)	46.3±0.2[b]	14.95
[(η^6-ind)Ru(bipy(OH)O)Cl][d]	(**8**)	164.6±1.0[b]	4.21
[(η^6-ind)Ru(4,4′-Me_2-bipy)Cl][PF_6]	(**13**)	113.0±2.0[b]	6.30
[(η^6-ind)Ru(phen)Cl][PF_6]	(**14**)	75.1±1.2[b]	9.24
[(η^6-bip)Ru(bipy)Cl][PF_6]	(**15**)	93.3±0.8[b]	7.43
[(η^6-ind)Ru(bipy)Cl][PF_6]	(**16**)	121.0±1.0[b]	5.73

[a]The errors quoted are fitting errors. [b]Determined by UV-Vis spectroscopy for a 50 μM solution in 95% H_2O, 5% MeOH. [c]Determined by ^1H NMR spectroscopy in 95% D_2O, 5% MeOD-d_4 [d]Species present in aqueous solution; synthesized as [(η^6-ind)Ru($bipy(OH)_2$)Cl][PF_6].

4.3.5 Interactions with 9-EtG

Attempts were made to prepare 9-EtG adducts of the bipy complex **1** and the bipy(OH)O complexes **2** and **5**. Reactions were carried out in water for 2 h at 37°C. The ^{1}H NMR spectrum of the product from the reaction of complex **1** with 9-EtG, in DMSO-d_6 showed that 90 % of complex **1** had reacted with 9-EtG to form [(η^6-tha)Ru(bipy)(9-EtG-*N7*)][PF_6]$_2$ (complex **9**). Peaks assigned to bound 9-EtG in complex **9** are shifted to high field in comparison to those of free 9-EtG, the H8 peak (7.4 ppm) by 0.35 ppm. The ^{1}H NMR spectrum of the product in MeOH-d_4 showed that 98% of complex **2** had reacted with 9-EtG to form [(η^6-tha)Ru(bipy(OH)O)(9-EtG-*N7*)][PF_6] (complex **10**). Peaks assigned to bound 9-EtG in complex **10** were again shifted to high field compared to those of free 9-EtG, the H8 peak (7.12 ppm) by 0.63 ppm. The ^{1}H NMR spectrum of complex **5** in DMSO-d_6 is shown in Figure 4.7 and the ^{1}H NMR spectrum of the product from reaction of **5** with 9-EtG ([(η^6-bz)Ru(bipy(OH)O)(9-EtG-*N7*)][PF_6], complex **12**) in DMSO-d_6 in Figure 4.8. Under the conditions of this reaction almost complete binding of 9-EtG to complex **5** occurred. Peaks assignable to bound 9-EtG in complex **12** are again shifted to high field compared to the peaks of free 9-EtG, the H8 peak (7.01 ppm) by 0.74 ppm.

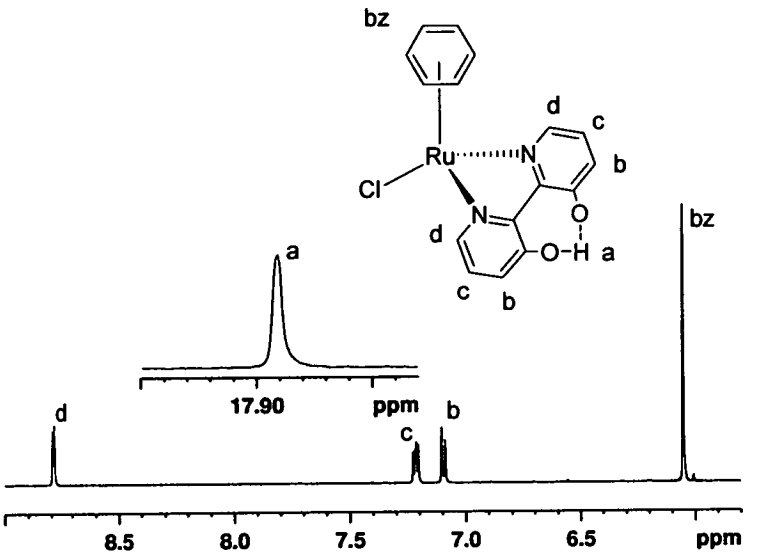

Figure 4.7 Low field region of the ^{1}H NMR spectrum of [(η^6-bz)Ru(bipy(OH)O)Cl] (**5**) in DMSO-d_6. Inset: shows resonance of H-bonded proton from bipy(OH)O ligand.

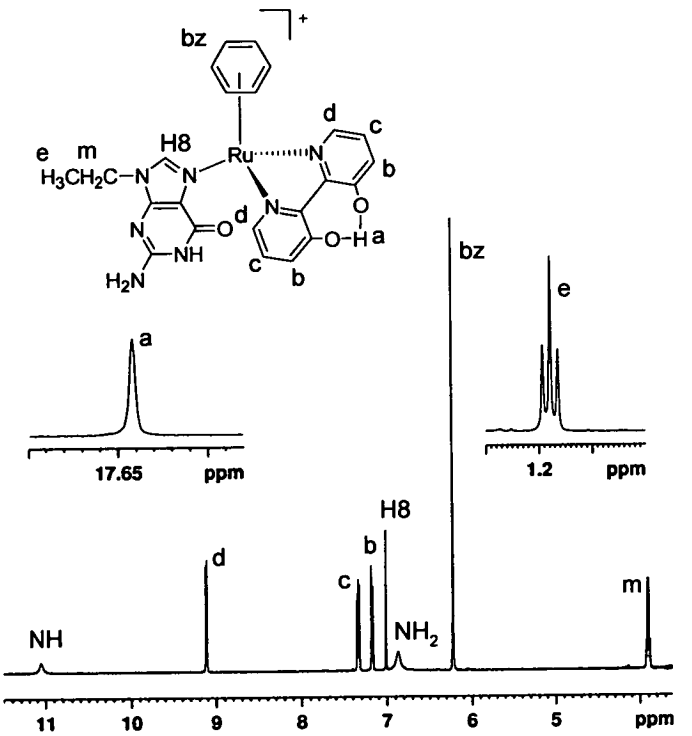

Figure 4.8 Low field region of the ^{1}H NMR spectrum of [(η^6-bz)Ru(bipy(OH)O)(9-EtG-*N7*)][PF_6] (**12**) in DMSO-d_6. Low field inset: resonance of H-bonded proton from the chelating ligand. High field inset: CH_3 resonance of 9-EtG.

4.3.6 Computation

The minimum energy structures of chlorido complexes [(η^6-ind)Ru(bipy(OH)$_2$)Cl][PF$_6$] (**8**), [(η^6-ind)Ru(bipy(Me)$_2$)Cl][PF$_6$] (**13**) and [(η^6-ind)Ru(bipy)Cl][PF$_6$] (**16**) obtained from DTF calculations are shown in Figure 4.9.

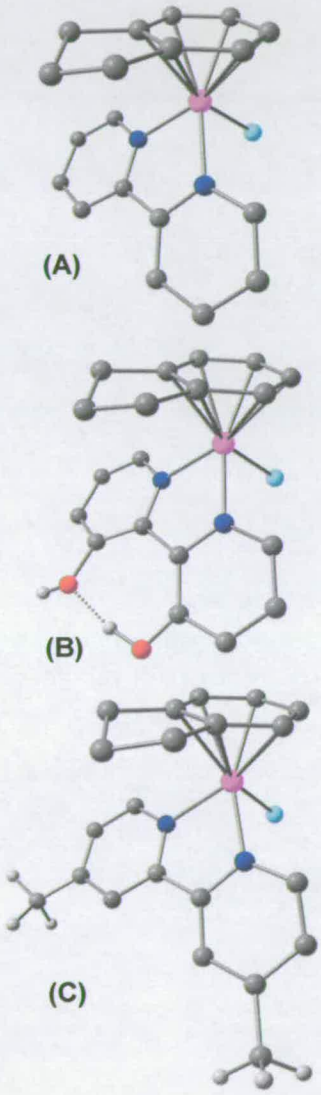

Figure 4.9 Optimized geometries of cations of complexes (**A**) [(η^6-ind)Ru(bipy)Cl][PF$_6$] (**16**), (**B**) [(η^6-ind)Ru(bipy(OH)$_2$)Cl][PF$_6$] (**8**) and (**C**) [(η^6-ind)Ru(bipy(Me)$_2$)Cl][PF$_6$] (**13**). All H-atoms were omitted for clarity apart from the H-atoms of the substituents on bipy.

The total bonding energy of tha in the optimized structure of $[(\eta^6$-tha)Ru(bipy(OH)O)(9-EtG-*N7*)$]^+$ (cation of **10**, where the arene is interacting with the chelating ligand through the intramolecular CH/ π interaction) is -313.4 kJ/mol, which is 7.5 kJ/mol lower than the bonding energy of tha in the optimized structure of modified cation of **10** (-305.9 kJ/mol), in which there is an arene/9-EtG intramolecular π-π interaction. The minimum energy structures of complex **10** and modified complex **10** are shown in Figure 4.10.

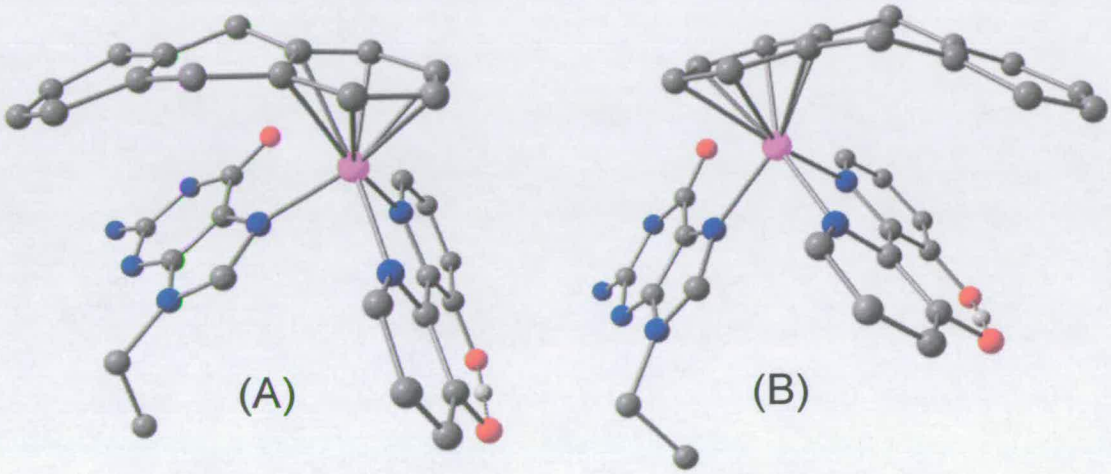

Figure 4.10 Optimized geometries of cations of complexes (**A**) modified **10**, where tha is interacting with 9-EtG through the π-π interaction and (**B**) $[(\eta^6$-tha)Ru(bipy(OH)O)(9-EtG-*N7*)$][PF_6]$ (**10**), where tha exhibits a CH/π interaction with bipy(OH)O.

To determine the effect of bipy substituents on the electron density on ruthenium, the Voronoi Deformation Density (VDD) method for computing atomic charges was used. This method has been used previously for transition metals such as Cr and Fe, in

complexes $Cr(CO)_6$ and $Fe(CO)_5$.[14] Charges on Ru in the $bipy(OH)_2$ complex **8**, $bipy(Me)_2$ complex **13** and bipy complex **16** were found to be similar, with values of +0.268 a.u. for **8** and **13** and +0.270 a.u. for complex **16**. For deprotonated complex **8**, [(η^6-ind)Ru(bipy(OH)O)Cl] the charge on Ru was +0.271 a.u.

4.3.7 Cancer cell growth inhibition

The IC_{50} values for chlorido complexes (**1-8**) against the A2780 human ovarian and A549 human lung cancer cell lines are given in Table 4.2. In general the complexes were more active against the A2780 human ovarian cancer cells than against A549 human lung cancer cells (IC_{50} values 7-65 μM for A2780 ovarian cells, and 21-62 μM for A549 lung cells). The most potent complex against A2780 cells [(η^6-thn)Ru(bipy(OH)O)Cl] (**4**) had an IC_{50} value of 7 μM, comparable to that of cisplatin (5 μM) under the same conditions. In general the most active complexes in ovarian cancer cell line contain the most extended arene ring systems in the order thn, tha > dha, ind > *p*-terp > bip > bz, a notable exception is the tha/ bipy complex **1**, which is inactive not only against A2780 cells but also against A549 cells (IC_{50} values >100 μM, Table 4.2). Complexes **5** and **7** containing bz and bip as arenes, respectively, and bipy(OH)O as chelating ligand were also inactive against A549 cells. The most active complex in this cell line was [(η^6-tha)Ru(bipy(OH)O)Cl] (**2**) with an IC_{50} value of 21 μM. The IC_{50} values for bipy(OH)O complexes showed the following dependence on the arene: thn, tha < dha, ind < *p*-terp (Table 4.2).

Table 4.2 IC_{50} values for ruthenium(II) arene complexes against the A2780 human ovarian and A549 human lung cancer cell lines

Complex		IC_{50} (μM)		% arene loss (24 h, 37°C)[a]
		A2780	A549	
[(η^6-tha)Ru(bipy)Cl][PF_6]	**(1)**	> 100	> 100	0
[(η^6-tha)Ru(bipy(OH)O)Cl]	**(2)**	8	21	0
[(η^6-dha)Ru(bipy(OH)O)Cl]	**(3)**	17	38	0
[(η^6-thn)Ru(bipy(OH)O)Cl]	**(4)**	7	24	0
[(η^6-bz)Ru(bipy(OH)O)Cl]	**(5)**	65	> 100	0
[(η^6-*p*-terp)Ru(bipy(OH)O)Cl]	**(6)**	21	62	–[b]
[(η^6-bip)Ru(bipy(OH)O)Cl]	**(7)**	40	> 100	33
[(η^6-ind)Ru(bipy(OH)O)Cl][c]	**(8)**	18	39	0
[(η^6-bip)Ru(bipy)Cl][PF_6]	**(15)**	> 100[d]	–	46
cisplatin		5	5	–

[a]Determined by ^{1}H NMR spectroscopy in 95% D_2O, 5% MeOH-d_4. [b]Solubility too low to determine arene loss by NMR. [c]Species present under test conditions; synthesized as [(η^6-ind)Ru(bipy(OH)$_2$)Cl][PF_6]. [d]Previously reported.[1]

4.3.8 Binding to calf thymus (CT) DNA

The experiments were performed at the Institute of Biophysics in Brno (CR) by Professor Victor Brabec's research group.

4.3.8.1 Kinetics of binding

The extent of binding of complexes [(η^6-ind)Ru(bipy)Cl][PF_6] (**16**) and [(η^6-ind)Ru(bipy$(OH)_2$)Cl][PF_6] (**8**, under the experimental conditions as neutral [(η^6-ind)Ru(bipy(OH)O)Cl]) to CT DNA was determined at r_i (molar ratio of free complex to nucleotide phosphate) ratios of 0.02 – 0.16 in 10 mM $NaClO_4$ at 37°C, after 48 h of the reaction in the dark. Complexes **16** and **8** were incubated with CT DNA for 48 h, rapidly cooled, DNA containing bound complex precipitated out by addition of ethanol, and the content of free Ru in the supernatant determined by FAAS. Intriguingly, both complexes bind to a relatively small extent (only 43% and 11% of **16** and **8**, respectively, after 48 h).

The binding experiments indicated that modification reactions resulted in the irreversible coordination of Ru^{II} arene complexes to CT DNA, which thus facilitated sample analysis. Hence, it was possible to prepare samples of DNA modified by complexes **16** or **8** at a preselected value of r_b. Thus, except where stated, samples of DNA modified by Ru^{II} arene complexes and analyzed further by biophysical or biochemical methods were prepared in 10 mM $NaClO_4$ at 37°C. After 48 h of the

reaction of DNA with complexes, the samples were precipitated in ethanol and dissolved in the medium necessary for a particular analysis, and the r_b value in an aliquot of this sample was checked by FAAS. In this way, all analyses described in this Chapter were performed in the absence of unbound (free) complex.

4.3.8.2 Circular dichroism (CD)

To gain further information, CD spectra were also recorded of CT DNA modified by **16** and **8** (Figure 4.11). CD spectral characteristics were compared for CT DNA in the absence and in the presence of **16** and **8** at r_b values in the range of 0.006 - 0.056 and 0.017-0.084, respectively. Upon binding of these complexes to CT DNA, the conservative CD spectrum normally found for DNA in canonical B-conformation transforms at wavelengths below 300 nm. There was a slight, but significant increase or decrease in the intensity of the positive band around 280 nm if DNA was modified by **16** or **8**, respectively.

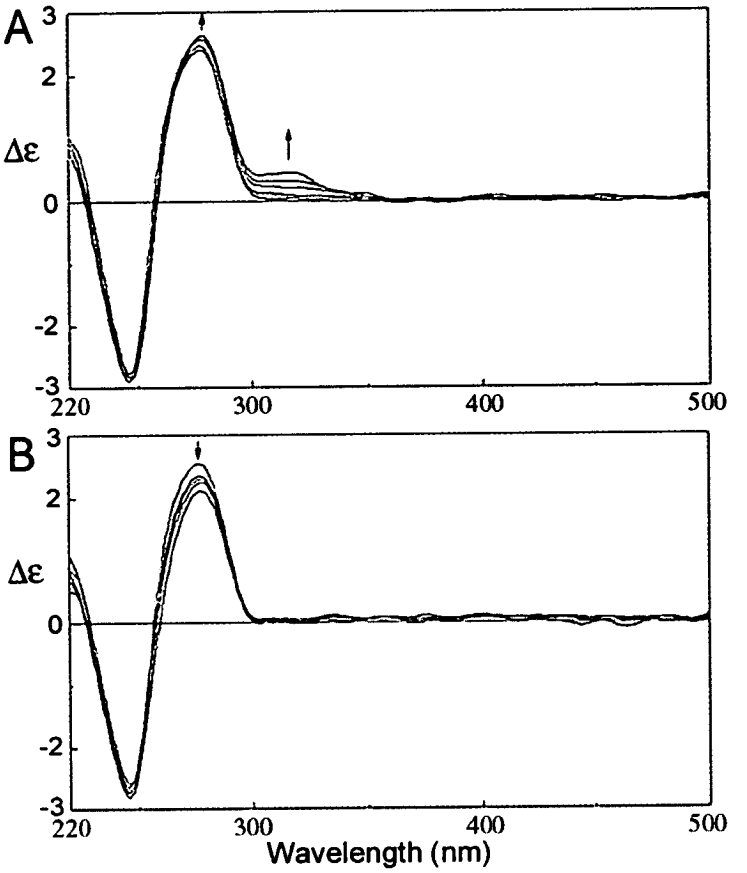

Figure 4.11 CD spectra of CT DNA (1×10^{-4} M, the concentration is related to the phophorus content) modified by complexes **16** or **8**; the medium was 10 mM $NaClO_4$, pH = 6. (**A**) DNA was modified by complex **16** at r_b = 0, 0.006, 0.026, 0.040, 0.056. (**B**) DNA was modified by complex **8** at r_b = 0, 0.017, 0.031, 0.044, 0.084 (curves 1-5, respectively). The arrows show a change of CD with increasing r_b value.

Complexes **16** and **8** have no intrinsic CD signals as they are achiral so that any CD signal above 300 nm can be attributed to the interaction of complexes with DNA. Below 300 nm any change from the DNA spectrum is due either to the DNA induced CD (ICD) of the metal complex or the metal complex induced perturbation of the DNA spectrum. The signature of complex **16** bound to CT DNA is a strong positive

ICD centered at 320 nm (Figure 4.11A). On the other hand, the signature of complex **8** bound to CT DNA includes no such ICD (Figure 4.11B).

4.3.8.3 DNA melting

CT DNA was modified by [(η^6-ind)Ru(bipy)Cl][PF_6] (**16**) and [(η^6-ind)Ru(bipy($OH)_2$)Cl][PF_6] (**8**, under the experimental conditions as neutral [(η^6-ind)Ru(bipy(OH)O)Cl]) to the value of r_b = 0.06 and 0.08, respectively in 10 mM $NaClO_4$ at 37°C for 48 h. The samples were divided into two parts and in one part the salt concentration was further adjusted by addition of $NaClO_4$ to 0.1 M. Hence, the melting curves for DNA modified by **16** and **8** were measured in the two different media, at low and high salt concentrations. The effect on the melting temperature (t_m) is dependent on the salt concentration. At both high and low salt concentration (0.01 M and 0.1 M) modification of DNA by **16** and **8** affected t_m only very slightly (t_m was changed by less than 1°C). Thus, the melting behavior of DNA was affected by **16** and **8** only negligibly.

4.3.8.4 Ethidium bromide (EtBr) fluorescence

The ability of complexes to displace the DNA intercalator EtBr from CT DNA was probed by monitoring the relative fluorescence of the EtBr-DNA adduct after treating the DNA with varying concentrations of **16** or **8**. Figure 4.12 shows a plot of relative fluorescence vs. r_b for complexes **16** and **8**, cisplatin and monofunctional dienPt. The adducts of both Ru^{II} arene complexes competitively replaced intercalated EtBr

markedly more effectively than the adducts of monofunctional dienPt and the adducts of **16** even more than the adducts of bifunctional cisplatin. Thus, the ability of complex **16** to displace the DNA intercalator EtBr from CT DNA was considerably greater than that of complex **8**.

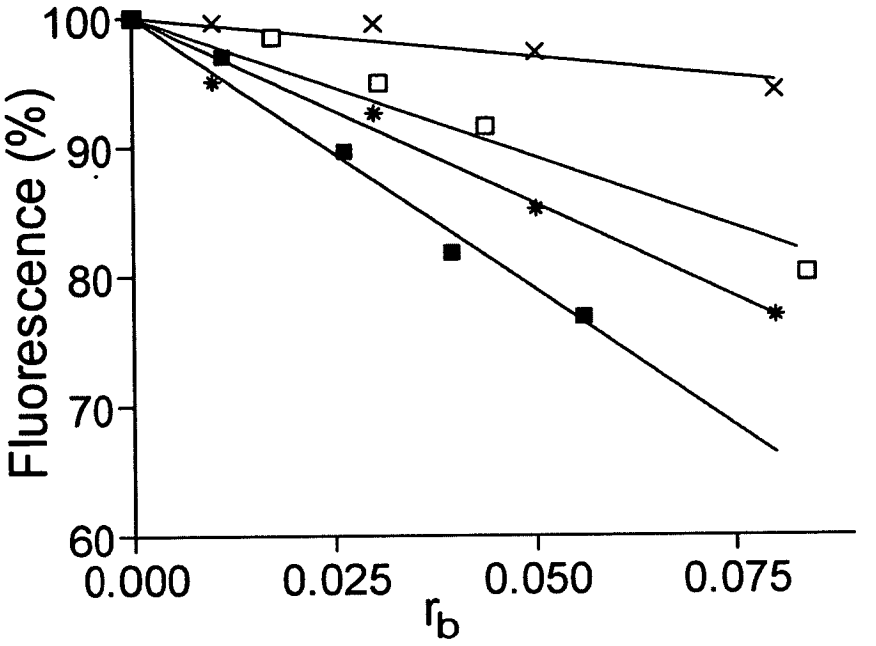

Figure 4.12 Plots of the EtBr fluorescence versus r_b for DNA modified by cisplatin, dienPt and Ru^{II} arene complexes in 10 mM $NaClO_4$ at 37°C for 48 h: (×), dienPt; (*), cisplatin; (■), complex **16**; (□), complex **8**. Data points measured in triplicate varied on average ± 3% from their mean.

4.4 Discussion

It has been observed previously, a loss of cytotoxicity towards cancer cells for complexes of the type $[(\eta^6\text{-arene})Ru(en)Cl]^+$ when en, a σ-donor, is replaced by 2,2′-bipyridine.[1] Bipyridines contain two σ-donor nitrogens, and a fully conjugated π-system which makes them strong π-acceptors. Incorporation of methyl, hydroxymethyl or methylester groups in the 4,4′ positions of bipyridine did not restore activity. Loss of activity could arise from the absence of NH groups, which are known to stabilize nucleobase adducts through strong H-bonding between an NH of en and C6O from the guanine (G) nucleobase,[15] or from the back-donation of electron density from Ru^{II} onto bipyridine as a π-acceptor, that would make the metal centre more acidic compared to en analogues. This could have an effect on the binding of these complexes to DNA.

Complexes containing 2,2′-bipyridine-3,3′-diol ($bipy(OH)_2$) as the chelating ligand showed a dramatic increase in anticancer activity compared to the other bipyridine analogues (Table 4.2). N,N-chelation of $bipy(OH)_2$ without deprotonation creates steric-crowding and distortion of ligand planarity, as observed in the crystal structure of $[(\eta^6\text{-ind})Ru(bipy(OH)_2)Cl]^+$ (**8**), where the pyridine rings are twisted by 17.31°, and previously for complexes of 3,3′-dimethyl-2,2′-bipyridine.[16] Chelation of bipyridine derivatives to a metal lowers the energy of the form in which the rings of the bipyridine are coplanar,[17-19] and the deprotonation of $bipy(OH)_2$ as a chelating ligand is favoured as it leads to planarity of the ligand. Furthermore, for 2,2′-bipyridines with substituents in the 3,3′-positions, cyclization can occur when substituents are able to

react, as observed for $-CO_2CH_2CF_3$ and $-CONHCH_2C_6H_5$ substituents that form $-CO(NCH_2C_6H_5)OC-$ with release of CF_3CH_2OH.[20]

Very stable H-bonding within the deprotonated 2,2′-bipyridine-3,3′-diol (bipy(OH)O) ligand gives rise to a large downfield shift of the resonance for the H-bonded proton (δ~18). "Soft" and "borderline" metal ions usually prefer coordination via nitrogens of the heterocycle rather than via oxygens.[21] If the bipy(OH)O ligand was N,O-chelated instead of N,N-chelated, the resonance from the proton involved in the O–H···N hydrogen-bond would be expected to appear at δ~15,[22-24] as observed in the ^1H NMR spectrum of 2,2′-bypyridine-3,3′-diol itself, where both hydrogens form O–H···N hydrogen bonds. The absence of a resonance with this chemical shift, suggests that N,N-chelation is more favourable than N,O-chelation for deprotonated bipy(OH)O. The presence of the strong O–H···O intramolecular hydrogen bond stabilizes the negative charge on the oxygen of bipy(OH)O and prevents further deprotonation/protonation within the pH range studied by NMR (2-10). It has been found previously for $[Ru(bipy)_2(bipy(OH)O)]^+$ that protonation requires pH values of ≤ ca. 0.4, and of ca. 13.6 for deprotonation.[4] The close contact between two oxygens (O82 and O52) in the crystal structure of complex **2** confirms formation of a strong symmetrical O···H···O hydrogen bond, as observed previously in $[Ni(Hdmg)]_2$ (Hdmg = dimethylglyoxime)[25] and $[Ru(bipy)_2(bipy(OH)O)]^+$.[4] In the crystal structure of $[(\eta^6\text{-ind})Ru(bipy(OH)_2)Cl][PF_6]$ (**8**), where the chelating ligand is $bipy(OH)_2$, the distance between the two oxygens (O5A and O8A) is significantly longer than that observed in the crystal structures of $[(\eta^6\text{-tha})Ru(bipy(OH)O)Cl]$ (**2**), $[(\eta^6\text{-tha})Ru(bipy(OH)O)(9\text{-EtG-}N7)][PF_6]$ (**10**) and $[(\eta^6\text{-thn})Ru(bipy(OH)O)(N\text{-MeIm})][PF_6]$ (**11**), where the chelating ligands are in the deprotonated, bipy(OH)O form (see the results section).

CH/π interactions between the arene and the bipyridine ligand were observed in the crystal structures of [(η^6-tha)Ru(bipy)Cl][PF_6] (**1**), [(η^6-tha)Ru(bipy(OH)O)Cl] (**2**) and [(η^6-tha)Ru(bipy(OH)O)(9-EtG-*N7*)][PF_6] (**10**). The phenomenon of CH/π interactions is now well established[26] and the interaction ranges from weak (CH···π center 2.6-3.0 Å) to very strong (CH···π center < 2.6 Å).[27] Such interactions can play an important role in protein stability,[26] and in recognition processes. The CH···π interactions observed for complex **1** (2.7 Å and 2.8 Å), where the chelating ligand is bipy (Figure 4.2A), are stronger (0.1 Å shorter in each case) than in complex **2** (2.8 Å and 2.9 Å) where the chelating ligand is bipy(OH)O (Figure 4.2B). This can be attributed to the greater delocalization of the π-electrons in bipy(OH)O through two possible tautomeric forms (Figure 4.13).

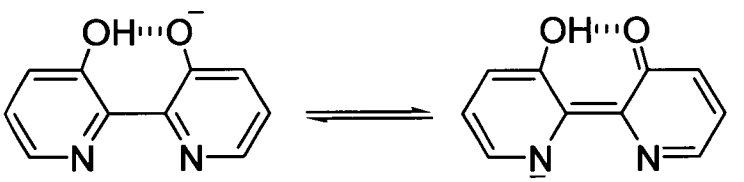

Figure 4.13 Tautomeric forms of bipy(OH)O.

The space-filling and capped-stick models of [(η^6-tha)Ru(bipy(OH)O)Cl] (**2**) (Figure 4.4B and 4E) show the tilting of the arene towards the chelating ligand in the crystal structure, possibly due to an intramolecular CH/π interaction[26-30] between CH protons from the outer non-coordinated ring of tha and the centers of the pyridine rings of the chelating ligand (*vide infra*). In such interactions the hydrogen atoms tend to lie above the centres of the aromatic rings.[29] In the previously-reported crystal structure of [(η^6-

tha)Ru(en)Cl][PF_6],[2] where en = ethylenediamine, the tricyclic ring system of tha is nearly flat and the outer ring of the arene is slightly bent away from the Cl ligand. Intramolecular π-π arene-nucleobase stacking, observed previously in [(η^6-tha)Ru(en)(9-EtG-*N7*)][PF_6]$_2$,[2] is not present in the crystal structure of complex **10**. The space-filling and capped-stick models of **10** (Figure 4.4C and 4.4F) clearly show that intramolecular CH/π interactions between protons from the outer ring of tha and the centres of the π-system of the chelating ligand (distances 2.8 Å and 3.0 Å), are present for the 9-EtG adduct as they are for the chlorido adduct (complex **2**).

DFT calculations show that the total bonding energy of tha in the optimized structure of [(η^6-tha)Ru(bipy(OH)O)(9-EtG-*N7*)]$^+$ (**10**), where the arene is interacting with the chelating ligand through the intramolecular CH/ π interaction (Figure 4.10B), is 7.5 kJ/mol lower than the total bonding energy of tha in the optimized structure of modified complex **10**, in which there is an arene/9-EtG intramolecular π-π interaction (Figure 4.10A). This result shows that the π-π interaction between the arene and 9-EtG observed[2] for [(η^6-tha)Ru(en)(9-EtG-*N7*)][PF_6]$_2$, which might play a role in stabilizing DNA adducts, is less favoured compared to CH/ π interactions in complex **10**. This may lead to less stable DNA adducts.

Hydrolysis of chlorido complexes also deserves discussion as an important step in binding to DNA. Complexes **4**, **7**, **8** and **13-16** undergo relatively fast hydrolysis with half-lives of the order of minutes at 37°C (Table 4.4). The reported half-lives for aquation of the chlorido en Ru^{II} arene complexes, [(η^6-dha)Ru(en)Cl][PF_6], [(η^6-tha)Ru(en)Cl][PF_6] and [(η^6-bip)Ru(en)Cl][PF_6],[31] are 1.4 - 8.8 times shorter than those of complexes mentioned in this Chapter, under comparable conditions. The presence of bipy as a π-acceptor in [(η^6-arene)Ru(bipy)Cl]Cl complexes where arene = benzene (bz), *p*-cymene (*p*-cym) and hexamethylbenzene (hmb), has been reported

to decrease the rate of hydrolysis by 2 orders of magnitude compared to analogues in which bipy is replaced with two aqua ligands.[32] The π-acceptor ligand bipy withdraws electron density from Ru and increases the positive charge on the metal, making it less favourable for Cl^- to leave, slowing down the hydrolysis.

For complexes which contain bip as the arene (**7** and **15**), loss of the arene is observed in aqueous solution (33 and 46%, after 24 h for complexes **7** and **15**, respectively). The same arene loss was previously observed for Ru^{II} bip complexes containing phenylazo-pyridines as π-acceptor ligands (22-50% loss of bip after 24 h in aqueous solution).[33] No arene loss was observed for the other arene complexes. Biphenyl (bip) has a high aromaticity, and competes as a π-acceptor[34] with the π-acceptor chelating ligands (bipy(OH)O and bipy in complexes **7** and **15**, respectively) for electron density. This leads to a weakening of the Ru-arene bonds and loss of bip, which is not the case for the other arenes. In **7**, the hydroxyl substituents on the chelating ligand are electron donors,[35] and the chelating ligand can exist in two tautomeric forms (Figure 4.13) one of which places a negative charge on the nitrogen atom. These features could make bipy(OH)O a weaker π-acceptor than bipy and stabilize the Ru^{II}-arene bonds by π-back-donation. As in both complexes (**7** and **15**) arene loss was observed there seems to be no significant difference in the π-acceptor abilities of bipy and bipy(OH)O. Attempts to detect arene loss from the *p*-terp complex (**6**) were hampered by its very low solubility.

Substituents on bipy have no significant influence on the rates of hydrolysis which suggests that their electronic effects on the metal are small. This statement is consistent with the DFT calculations. After the geometry optimization of [(η^6-ind)Ru(bipy$(OH)_2$)Cl][PF_6] (**8**), [(η^6-ind)Ru(bipy$(Me)_2$)Cl][PF_6] (**13**) and [(η^6-ind)Ru(bipy)Cl][PF_6] (**16**, Figure 4.9), VDD charges on Ru showed no significant

differences among complexes (with values of +0.268 a.u. for complexes **8** and **13** and +0.270 a.u. for complex **16**). Therefore these results prove that substituents on bipy have no significant effect on the charge on the metal. Deprotonation of $bipy(OH)_2$ and chelation as bipy(OH)O is expected to reduce the positive charge on Ru^{II} since electron density from the oxygen (O^-) of one pyridine ring can be transferred onto the nitrogen of the other pyridine ring (Figure 4.13). However because the H-bonded proton stabilises the tautomer in which the negative charge is localised on the oxygen atom, this effect is weak,[4, 36] as indicated by the VDD charge on Ru in deprotonated complex **8** [(η^6-ind)Ru(bipy(OH)O)Cl] of +0.271 a.u., similar to the charges for **8**, **13** and **16**.

Consistent with the results from hydrolysis studies and DFT calculations, no significant difference in extent of binding to 9-EtG was observed for bipy and bipy(OH)O complexes. As DNA is a potential target for transition metal anticancer complexes,[37] reactions of the complexes with 9-EtG as a model nucleobase are studied in this Chapter. Ru^{II} complexes [(η^6-tha)Ru(bipy)Cl][PF_6] (**1**), [(η^6-tha)Ru(bipy(OH)O)Cl] (**2**) and [(η^6-bz)Ru(bipy(OH)O)Cl] (**5**) react relatively rapidly with *N7* of 9-EtG (90, 98 and 100% of binding of **1**, **2** and **5**, respectively after 2 h in water at 37°C). 9-EtG binds to a greater extent to complexes **2** and **5** containing bipy(OH)O than to complex **1** containing bipy. In all three 9-EtG adducts (complexes **9**, **10** and **12**), the ^{1}H NMR peaks corresponding to H8 are shifted to high field relative to free 9-EtG (making the difference of 0.35, 0.63 and 0.74 ppm for complexes **9**, **10** and **12**, respectively). Usually metallation at the *N7* site of purine bases produces a low field shift of the H8 resonance by about 0.3 - 1 ppm.[38] Previously it was observed for en Ru^{II} and Os^{II} arene complexes that 9-EtG H8 peaks for bound 9-EtG are shifted to low field relative to those of free 9-EtG.[1, 39] However

for 9-EtG in $[(\eta^6\text{-}p\text{-cym})Ru(acac)(9\text{-EtG-}N7)]^+$ (acac = acetylacetonate) the H8 peak is shifted to high field compared to the free model nucleobase.[40] The similar H8 chemical shift behaviour of 9-EtG in complexes **9**, **10** and **12** might result from the shielding of H8 by one of the pyridine rings from the bipyridine ligands (Figure 4.3A; H8 = C26H).

The polarization of C-H bonds of the bipy rings of bipy(OH)O and bipy chelating ligands could lead to the formation of C-H (of chelating ligand)···O (of 9-EtG) hydrogen bonds. In the crystal structure of complex **10** (Figure 4.3A), a hydrogen bond was observed between C20H from bipy(OH)O and O34 from 9-EtG (2.46 Å). Such C-H···O H-bonds observed in other systems commonly have bond lengths of 2.1 - 2.6 Å.[41] The observed hydrogen bond could lead to the additional stabilization of 9-EtG adducts.

Showing no significant difference in extent of binding to 9-EtG bipy and bipy(OH)O complexes surprisingly show a significant difference in anti-cancer activity. Complex **1**, containing tha as the arene and bipy as the chelating ligand, showed no activity in either the A2780 human ovarian or A549 human lung cancer cell lines, consistent with the previous report of the inactivity of bipy/ind and bipy/bip complexes.[1] Complexes containing bipy(OH)O as the chelating ligand show a dramatic increase in cytotoxicity compare to their bipy analogues (Table 4.2).[1] The higher IC_{50} (lower cytotoxicity) value for $[(\eta^6\text{-bip})RuCl(bipy(OH)O)]$ (complex **7**; 40 μM in A2780 cells), compared to most of the other complexes containing bipy(OH)O, may be related to the facile loss of arene in this case.

DNA binding studies performed with the bipy complex **16** and the bipy(OH)O complex **8** do not explain the significant difference in anti-cancer activity of these complexes. Complexes **16** and **8** both bind to DNA to a relatively small extent (43 and

11% after 48 h, respectively). CD spectra showed (Figure 4.11) that the binding of **16** results in conformational alterations in double-helical DNA of a non-denaturational character, similar to those induced in DNA by conventional antitumor cisplatin. In contrast, the binding of **8** results in conformational alterations in DNA of a denaturational character, similar to those induced in DNA by clinically ineffective transplatin.[42] The melting behavior of DNA was affected by **16** and **8** only negligibly (t_m was changed by less than 1°C) and the ability of complex **16** to displace DNA intercalator EtBr from CT DNA was considerably greater than that of complex **8** (Figure 4.12). These results do not explain the dramatic difference in anti-cancer activity of **8** (Table 4.2; IC_{50} = 18 and 39 μM, against A2780 and A549 cells, respectively) and **16** (IC_{50} > 100 μM against A2780 cells)[1] and so it seems likely that DNA is not a major target for these complexes.

4.5 Summary

In this Chapter it is shown that half-sandwich Ru^{II} arene complexes containing deprotonated 2,2′-bipyridine-3,3′-diol (bipy(OH)O) as the chelating ligand can exhibit significant cytotoxic activity towards cancer cells, in contrast to analogous complexes containing bipyridine or bipyridine with 4,4′-substituents such as Me. X-ray crystal structures and ^1H NMR spectroscopy have shown that deprotonated $bipy(OH)_2$ (bipy(OH)O) can form a strong intraligand H-bonding system which enforces planarity on bipy(OH)O. It is shown that strong binding to 9-EtG can occur for complexes containing bipy(OH)O as well as for those containing bipy. An interesting feature of the structures of complexes with tha as arene is the presence of arene CH···π

(bipy(OH)O and bipy) interactions. Using DFT calculations, these interactions were found to be more stable compared to π-π interactions between the arene and 9-EtG. The latter are known to stabilize DNA adducts. The work in this Chapter illustrates that subtle features in organometallic complexes can exert major effects on biological activity. However, DNA binding studies suggest that neither bipy nor bipy(OH)O complexes bind strongly to DNA, suggesting that DNA is not the major target for these complexes.

4.6 References

(1) Habtemariam, A.; Melchart, M.; Fernandez, R.; Parsons, S.; Oswald, I. D. H.; Parkin, A.; Fabbiani, F. P. A.; Davidson, J. E.; Dawson, A.; Aird, R. E.; Jodrell, D. I.; Sadler, P. J. *J. Med. Chem.* **2006,** *49*, 6858-6868.

(2) Chen, H.; Parkinson, J. A.; Parsons, S.; Coxall, R. A.; Gould, R. O.; Sadler, P. J. *J. Am. Chem. Soc.* **2002,** *124*, 3064-3082.

(3) Constable, E. C.; Seddon, K. R. *J. Chem. Soc., Chem. Commun.* **1982**, 34-6.

(4) Thompson, A. M. W. C.; Jeffery, J. C.; Liard, D. J.; Ward, M. D. *J. Chem. Soc., Dalton Trans.* **1996**, 879-84.

(5) Brabec, V.; Palecek, E. *Biophys. Chem.* **1976,** *4*, 79-92.

(6) Brabec, V.; Palecek, E. *Biophysik* **1970,** *6*, 290-300.

(7) Altomare, A.; Cascarano, G.; Giacovazzo, C.; Guagliardi, A.; Polidori, G.; Camalli, M.; *J. Appl. Crystallogr.* **1994,** *27*, 435.

(8) Betteridge, P. W.; Carruthers, J. R.; Cooper, R. I.; Prout, K.; Watkin, D. J. *J. Appl. Crystallogr.* **2003,** *36*, 1487.

(9) Sheldrick, G. M. *SHELXS-97*, University of Göttingen: Göttingen, Germany, **1997**.

(10) Beurskens, P. T; Beurskens., G.; Bosman, W. P.; de Gelder, R.; Garcia-Granda, S.; Gould, R. O.; Israel, R. and Smits, J. M. M., *The DIRDIF96 Program System*. University of Nijmegen: Nijmegen, The Netherlands, **1996**.

(11) Sheldrick, G. M. *SHELXL-97*, University Of Göttingen: Göttingen, Germany, **1997**.

(12) Butour, J. L.; Macquet, J. P. *Eur. J. Biochem.* **1977,** *78*, 455-463.

(13) Butour, J. L.; Alvinerie, P.; Souchard, J. P.; Colson, P.; Houssier, C.; Johnson, N. P. *Eur. J. Biochem.* **1991,** *202*, 975-980.

(14) Guerra, C. F.; Handgraaf, J.-W.; Baerends, E. J.; Bickelhaupt, F. M. *J. Comput. Chem.* **2003,** *25*, 189-210.

(15) Liu, H. K.; Berners-Price, S. J.; Wang, F. Y.; Parkinson, J. A.; Xu, J. J.; Bella, J.; Sadler, P. J. *Angew. Chem.-Int. Ed.* **2006,** *45*, 8153-8156.

(16) Nakamaru, K. *Bull. Chem. Soc. Jpn.* **1982,** *55*, 2697-705.

(17) Rebek, J., Jr.; Costello, T. *Heterocycles* **1984,** *22*, 2191-4.

(18) Rebek, J., Jr.; Trend, J. E. *J. Am. Chem. Soc.* **1978,** *100*, 4315-16.

(19) Rebek, J., Jr.; Costello, T.; Wattley, R. V. *Tetrahedron Lett.* **1980,** *21*, 2379-80.

(20) Rebek, J., Jr.; Costello, T.; Wattley, R. *J. Am. Chem. Soc.* **1985,** *107*, 7487-93.

(21) Hancock, R. D.; Martell, A. E. *Chem. Rev.* **1989,** *89*, 1875-914.

(22) Holligan, B. M.; Jeffery, J. C.; Norgett, M. K.; Schatz, E.; Ward, M. D. *J. Chem. Soc., Dalton Trans.* **1992,** 3345-51.

(23) Holligan, B. M.; Jeffery, J. C.; Ward, M. D. *J. Chem. Soc., Dalton Trans.* **1992,** 3337-44.

(24) Jeffery, J. C.; Schatz, E.; Ward, M. D. *J. Chem. Soc., Dalton Trans.* **1992,** 1921-7.

(25) Chakravorty, A. *Coord. Chem. Rev.* **1974,** *13*, 1-46.

(26) Brandl, M.; Weiss, M. S.; Jabs, A.; Suhnel, J.; Hilgenfeld, R. *J. Mol. Biol.* **2001,** *307*, 357-377.

(27) Bogdanovic, G. A.; Spasojevic-de Bire, A.; Zaric, S. D. *Eur. J. Inorg. Chem.* **2002**, 1599-1602.

(28) Hunter, C. A.; Lawson, K. R.; Perkins, J.; Urch, C. J. *J. Chem. Soc., Perkin Trans. 2* **2001**, 651-669.

(29) Takahashi, O.; Kohno, Y.; Iwasaki, S.; Saito, K.; Iwaoka, M.; Tomoda, S.; Umezawa, Y.; Tsuboyama, S.; Nishio, M. *Bull. Chem. Soc. Jpn.* **2001,** *74*, 2421-2430.

(30) Janiak, C. *Dalton* **2000**, 3885-3896.

(31) Wang, F.; Chen, H.; Parsons, S.; Oswald, I. D. H.; Davidson, J. E.; Sadler, P. J. *Chem.-A Eur. J.* **2003,** *9*, 5810-5820.

(32) Dadci, L.; Elias, H.; Frey, U.; Hoernig, A.; Koelle, U.; Merbach, A. E.; Paulus, H.; Schneider, J. S. *Inorg. Chem.* **1995,** *34*, 306-15.

(33) Dougan, S. J.; Melchart, M.; Habtemariam, A.; Parsons, S.; Sadler, P. J. *Inorg. Chem.* **2007,** *46*, 1508.

(34) Koefod, R. S.; Mann, K. R. *J. Am. Chem. Soc.* **1990,** *112*, 7287-93.

(35) Kunkely, H.; Vogler, A. *Inorg. Chim. Acta* **2003,** *343*, 357-360.

(36) Himeda, Y.; Onozawa-Komatsuzaki, N.; Sugihara, H.; Arakawa, H.; Kasuga, K. *Stu. Surf. Sci. Cat.* **2004,** *153*, 263-266.

(37) Zhang, C. X.; Lippard, S. J. *Curr. Opin. Chem. Bio.* **2003,** *7*, 481-489.

(38) Scheller, K. H.; Scheller-Krattiger, V.; Martin, R. B. *J. Am. Chem. Soc.* **1981,** *103*, 6833-9.

(39) Peacock Anna, F. A.; Habtemariam, A.; Fernandez, R.; Walland, V.; Fabbiani Francesca, P. A.; Parsons, S.; Aird Rhona, E.; Jodrell Duncan, I.; Sadler Peter, J. *J. Am. Chem. Soc.* **2006,** *128*, 1739-48.

(40) Fernandez, R.; Melchart, M.; Habtemariam, A.; Parsons, S.; Sadler, P. J. *Chem.-A Eur. J.* **2004,** *10*, 5173-5179.

(41) Steiner, T. *Chem. Comm.* **1997**, 727-734.

(42) Brabec, V.; Kleinwächter, V.; Butour, J. L.; Johnson, N. P. *Biophys. Chem.* **1990,** *35*, 129-141.

Chapter 5

Ru^{II} arene complexes with redox active diamine ligands

"It's an experience like no other experience I can describe, the best thing that can happen to a scientist, realizing that something that's happened in your mind exactly corresponds to something that happens in nature. It's startling every time it occurs. One is surprised that a construct of one's own mind can actually be realized in the honest-to-goodness world out there. A great shock, and a great, great joy."

Professor Leo Kadanoff

5.1 Introduction

The nature of the chelating ligand can play a crucial role in anticancer activity of the Ru^{II} arene complexes.[1] In this Chapter complexes in which the chelating ligand is *o*-phenylenediamine (*o*-pda) are investigated. Transition-metal complexes with the *o*-pda as a chelating ligand are of particular interests due to their oxidation properties. Dichlorido Pt^{II} complexes containing *o*-pda were among the first cisplatin analogues showing antitumor activity.[2-4] Recently good activity for *o*-pda complexes of the type $[(\eta^6\text{-arene})Ru^{II}(o\text{-pda})Cl]^+$, containing a range of mono-, di- and tri-cyclic hydrocarbons (arenes), has been reported.[1] Complexes containing mono- or di-methylated *o*-pda and indan as the arene also exhibit good activity. The incorporation of OH groups onto the chelating ligand (*o*-pda) decreased the activity. It has been found that these complexes have the ability to overcome cross-resistance with adriamycin (doxorubicin). The reduction in resistance factor (RF) achievable by replacing ethylenediamine (en) by *o*-pda can be dramatic (RF = $IC_{50}(A2780^{AD})/IC_{50}(A2780)$ for $[(\eta^6\text{-tha})Ru^{II}(en)Cl]^+$, tha = tetrahydroanthracene, reduces from > 100 to 2 when en is replaced with *o*-pda to form $[(\eta^6\text{-tha})Ru^{II}(o\text{-pda})Cl]^+$ and from 92 to 2 for the analogous dihydroanthracene (dha) complex).

In this Chapter the preparation and characterization of six Ru^{II} arene complexes containing *o*-pda, *o*-benzoquinonediimine (*o*-bqdi) or 4,5-dimethyl-*o*-phenylenediamine (dmpda) as chelating ligands, with a variety of arenes and halides as other ligands, are reported. The effect of variation of the arene and halides on oxidation of coordinated *o*-pda is investigated, as well as their effect on cytotoxicity

against A2780 human ovarian and A549 human lung cancer cell lines. The aqueous solution chemistry of complexes containing *o*-pda and its oxidized form *o*-bqdi, as chelating ligands, is compared. The difference in the solid state structures of the diamine and diimine complexes is investigated. The x-ray crystal structures of complexes [(η^6-*p*-cym)Ru(*o*-pda)Cl][PF_6] (**1**) and [(η^6-hmb)Ru(*o*-bqdi)Cl][PF_6] (**3**) are reported. The stability of 9-EtG adducts of complexes **1** and **3** is studied using DFT calculations. The ability of complex [(η^6-*p*-cym)Ru(*o*-bqdi)I][PF_6] (**4**) to undergo ligand-based reduction by glutathione (GSH) in water, to give complex [(η^6-*p*-cym)Ru(*o*-pda)I][PF_6] (**8**), is also studied in this Chapter.

5.2 Experimental section

5.2.1 Materials

The starting materials [(η^6-arene)$RuCl_2$]$_2$ (arene = *p*-cymene (*p*-cym), hexamethylbenzene (hmb) or biphenyl (bip)) are prepared as described in Chapter 2. [(η^6-*p*-cym)RuI_2]$_2$ was donated by Dr Holm Petzold. *o*-Phenylenediamine (*o*-pda) and 4,5-dimethyl-*o*-phenylenediamine (dmpda) were purchased from Sigma-Aldrich, and glutathione (GSH) from Acros Organics. Methanol was dried over Mg/I_2. All other reagents were obtained from commercial suppliers.

5.2.2 Synthesis of ruthenium complexes

Complexes **1-4** and **6** were synthesized using a similar procedure. Typically the ligand, *o*-pda or dmpda (2 mol equiv), respectively, was added to a methanolic solution of the ruthenium dimer $[(\eta^6\text{-arene})RuCl_2]_2$ and the reaction mixture stirred at ambient temperature for 30 min. Iodido and bromido complexes **4** and **5** were synthesized in the halide exchange reaction, using the chlorido complex **1** and ca. 5 mol equiv of KX (X = I or Br). The products were isolated as PF_6 salts. Details for individual reactions are described below.

$[(\eta^6$-*p*-cym)Ru(*o*-pda)Cl][PF_6] (1). To a suspension of $[(\eta^6$-*p*-cym)$RuCl_2]_2$ (0.05 g, 0.08 mmol) in dry, freshly-distilled methanol (30 mL) *o*-pda (0.02 g, 0.16 mmol) was added. The reaction mixture turned yellow immediately after addition of *o*-pda. It was stirred at ambient temperature in air for 30 min. The clear yellow solution was filtered, NH_4PF_6 (0.06 g, 0.40 mmol) was added and the flask shaken. A precipitate started to appear almost immediately. The fine yellow precipitate was collected by filtration, washed with cold methanol and ether, and dried in air. Yield: 0.038 g (89%).

Crystals suitable for x-ray analysis were obtained by slow evaporation of a methanolic solution at ambient temperature. The complex crystallized as $[(\eta^6$-*p*-cym)Ru(*o*-pda)Cl][PF_6]. ESI-MS: calcd for $RuClN_2C_{16}H_{22}^+$ $[M]^+$ m/z 378.9, found 379.1. Anal. calcd for $C_{16}H_{22}ClF_6N_2PRu$ (**1**): C, 36.68; H, 4.23; N, 5.35. Found: C, 36.56; H, 4.16; N, 5.32. ^1H NMR in DMSO-d_6: δ 8.01 (d, 2H, NH), 7.21 (m, 4H), 6.34 (d, 2H, NH), 5.75 (d, 2H), 5.52 (d, 2H), 2.28 (m, 1H), 2.21 (s, 3H), 1.18 (d, 6H).

[(η^6-hmb)Ru(o-pda)Cl][PF_6] (2). To a suspension of [(η^6-hmb)$RuCl_2$]$_2$ (0.05 g, 0.07 mmol) in dry, freshly-distilled methanol (30 mL) *o*-pda (0.02 g, 0.15 mmol) was added. The reaction mixture was stirred at ambient temperature under argon for 30 min. The resultant red solution was filtered, NH_4PF_6 (0.06 g, 0.39 mmol) added and the flask shaken. The precipitate, which started to appear almost immediately, was collected by filtration, washed with cold methanol and ether, and dried in air to give a red solid. Yield: 0.030 (73%).

^{1}H NMR in DMSO-d_6: δ 7.11 (m, 4H), 6.71 (d, 2H, NH), 6.51 (d, 2H, NH), 2.01 (s, 18H).

[(η^6-hmb)Ru(*o*-bqdi)Cl][PF_6] (3). To a suspension of [(η^6-hmb)$RuCl_2$]$_2$ (0.05 g, 0.07 mmol) in dry, freshly-distilled methanol (30 mL) *o*-pda (0.02 g, 0.15 mmol) was added. The reaction mixture was stirred at ambient temperature in air for 30 min. After removing methanol under reduced pressure, the ^{1}H NMR spectrum of the remaining solid in DMSO-d_6, showed a mixture of complexes **2** and **3** in the ratio 1:1. The mixture was redissolved in methanol, NH_4PF_6 (0.06 g, 0.39 mmol) was added and this left in air overnight. The purple solid which formed was filtered, washed with cold methanol, followed by ether, and was dried in air. Yield: 0.028 (67%).

Crystals suitable for x-ray analysis were obtained by slow evaporation of a methanolic solution of **3** at ambient temperature, and the complex crystallized as [(η^6-hmb)Ru(*o*-bqdi)Cl][PF_6]. ESI-MS: calcd for $RuClN_2C_{18}H_{24}^+$ $[M]^+$ m/z 404.9, found 405.1. ^{1}H NMR in DMSO-d_6: δ 13.97 (s, 2H, NH), 7.11 (m, 4H), 2.03 (s, 18H).

[(η^6-*p*-cym)Ru(*o*-bqdi)I][PF_6] (4). Two methods were used in the preparation of **4**.

Method A: To a suspension of [(η^6-*p*-cym)RuI_2]$_2$ (0.05 g, 0.05 mmol) in dry, freshly-distilled methanol (30 mL), *o*-pda (0.01 g, 0.10 mmol) was added. The reaction mixture turned purple immediately and was stirred at ambient temperature in air for 30 min. The clear dark purple solution was filtered, NH_4PF_6 (0.04 g, 0.25 mmol) added and the flask shaken. The precipitate that appeared was collected by filtration, washed with cold methanol and ether, and dried in air to give a dark purple solid. Yield: 0.023 g (73%).

Method B: To a suspension of [(η^6-*p*-cym)Ru(*o*-pda)Cl][PF_6] (**1**, 0.01 g, 0.02 mmol) in dry, freshly-distilled methanol (30 mL), KI (0.02 g, 0.09 mmol) was added. The reaction mixture was stirred at ambient temperature in air for 30 min. The yellow solution turned dark purple and a dark purple precipitate appeared. The precipitate was collected by filtration, washed with cold methanol and ether, and dried in air to give a dark purple solid. Yield: 0.004 g (36%).

ESI-MS: calcd for $RuIN_2C_{16}H_{20}^+$ $[M]^+$ m/z 468.3, found 468.9. ^1H NMR in DMSO-d_6: δ 14.68 (s, 2H, NH), 7.09 (m, 4H), 6.33 (d, 2H), 6.11 (d, 2H), 2.95 (m, 1H), 2.43 (s, 3H), 1.20 (d, 6H).

[(η^6-*p*-cym)Ru(o-bqdi)Br][PF_6] (5). To a suspension of [(η^6-*p*-cym)Ru(*o*-pda)Cl][PF_6] (**1**, 0.01 g, 0.02 mmol) in dry, freshly-distilled methanol (30 mL), KBr (0.01 g, 0.12 mmol) was added. The reaction mixture was stirred at ambient temperature in air for 30 min. The yellow solution turned purple and a dark purple precipitate started to appear. The dark purple precipitate was collected by filtration, washed with cold methanol and ether, and dried in air. Yield: 0.003 g (32%).

ESI-MS: calcd for $RuBrN_2C_{16}H_{20}^+$ $[M]^+$ m/z 421.3, found 421.3. ^1H NMR in DMSO-d_6: δ 14.70 (s, 2H, NH), 7.08 (m, 4H), 6.30 (d, 2H), 6.07 (d, 2H), 2.87 (m, 1H), 2.33 (s, 3H), 1.19 (d, 6H).

[(η^6-bip)Ru(dmpda)Cl][PF_6] (6). To a suspension of [(η^6-bip)$RuCl_2]_2$ (0.05 g, 0.08 mmol) in dry, freshly-distilled methanol (30 mL), dmpda (0.02 g, 0.15 mmol) was added. The reaction mixture was stirred at ambient temperature in air for 30 min. The dark violet solution was filtered, NH_4PF_6 (0.06 g, 0.38 mmol) added, and the flask shaken. The precipitate that appeared almost immediately, was collected by filtration, washed with cold methanol and ether, and dried in air to give a violet solid. Yield: 0.022 g (49%).

ESI-MS: calcd for $RuClN_2C_{20}H_{22}^+$ $[M]^+$ m/z 426.9, found 426.9. Anal. calcd for $C_{20}H_{26}ClF_6N_2PO_2Ru$ (**6** · 2 H_2O): C, 39.51; H, 4.31; N, 4.61. Found: C, 39.11; H, 3.86; N, 4.44. ^1H NMR in DMSO-d_6: δ 8.20 (d, 2H, NH), 7.84 (d, 2H), 7.50 (m, 3H), 6.98 (s, 2H), 6.30 (d, 2H, NH), 6.26 (d, 2H), 6.00 (t, 1H), 5.88 (t, 2H), 2.15 (s, 6H).

5.2.3 X-ray crystalography

Details of the instrumentation used are described in Chapter 2. Structure **1** was solved by Professor Simon Parsons by Patterson method (DIRDIF)[5] and refined with SHELXL-97[6], while structure **3** was solved by Dr Francesca Fabbiani by direct method (SIR92)[7] and refined using CRYSTALS.[8] Hydrogen atoms were placed in calculated positions, and all non-H atoms were modelled with anisotropic displacement parameters. The final conventional *R* factor (based on *F* and 4930 out of 5671 with $F > 4\sigma(F)$) was 0.0340 for the structure of **1**, and the final conventional *R*

factor (based on F and 2449 out of 4304 with $F > 4\sigma(F)$) was 0.0407 for the structure of **3**. Other crystal and refinement data are summarized in Table 5.1.

5.2.4 Hydrolysis

The hydrolysis of chlorido Ru^{II} arene complexes was monitored by UV-Vis spectroscopy, without explicit control of pH or chloride concentrations. Complexes were dissolved in H_2O to give ca. 50 μM solutions. The absorbance was recorded at 30 s intervals at the selected wavelength over ca. 30 min at 37°C. Plots of the change in absorbance with time were computer-fitted to the first-order rate equation: $A = C_0 + C_1e^{-kt}$ (C_0 and C_1 are computer-fitted constants and A is the absorbance corresponding to time t) using Origin version 7.5 (Microcal Software Ltd) to give the half-lives ($t_{1/2}$) and rate constant values (k).

5.2.5 Oxidation in methanol

Oxidation of complex [(η^6-*p*-cym)Ru(*o*-pda)Cl][PF_6] (**1**) was monitored in methanol (50 μM solution) in the absence, and in the presence of KI (1 mol equiv), by UV-Vis spectroscopy. The absorbance was recorded at 30 s intervals at the selected wavelength over ca. 4 h at 37°C. Plots of the change in absorbance with time were computer-fitted to the first-order rate equation: $A = C_0 + C_1e^{-kt}$ (C_0 and C_1 are computer-fitted constants and A is the absorbance corresponding to time t) using Origin version 7.5 (Microcal Software Ltd) to give the half-lives ($t_{1/2}$) and rate constant values (k).

5.2.6 Reaction with GSH

UV-Vis spectra of complex [(η^6-*p*-cym)Ru(*o*-bqdi)I][PF_6] (**4**) in water (50 μM), in the presence of 15 mol equiv GSH, were recorded at 5 min intervals for 1 h, at 37°C. The ^{1}H NMR spectra of D_2O solution of **4** (200 μM), in the presence of 15 mol equiv GSH, were recorded 15 min, 2 h, 4 h, 24 h and 72 h after dissolution at 37°C.

5.2.7 Computation

The details are described in Chapter 2. The 9-EtG adducts of complexes **1** and **3** (**1EtG** and **3EtG**, respectively) were created by substituting the chlorido ligand with 9-EtG in the crystal structures of **1** and **3** in Chemcraft (Version 1.5). 9-EtG used in substitution was imported into the database of Chemcraft from the previously determined x-ray crystal structure of 9-EtG adduct of the Ru^{II} arene complex similar in structure to complexes **1** and **3**. The coordinates used for the calculations were obtained directly from ChemCraft. Estimates of the Ru-{9-EtG} bonding energies in **1EtG** and **3EtG** were obtained by subtracting the energies of the separate fragments from that of the whole molecule.

5.3 Results

5.3.1 Syntheses and characterization

The ligands used in this Chapter are shown in Figure 5.1. Ru^{II} arene complexes **1-4** and **6** (Figure 5.1) were synthesized as PF_6 salts by the reaction of $[(\eta^6\text{-arene})RuX_2]_2$ (X = Cl or I) and the appropriate chelating ligand, in methanol. The synthesized complexes (**1-6**) were fully characterized by 1D ^{1}H NMR, ESI-MS and CHN analysis. Experimental values obtained for CHN analyses of complexes $[(\eta^6\text{-hmb})Ru(o\text{-pda})Cl]^+$ (**2**), $[(\eta^6\text{-hmb})Ru(o\text{-bqdi})Cl]^+$ (**3**), $[(\eta^6\text{-}p\text{-cym})Ru(o\text{-bqdi})I]^+$ (**4**) and $[(\eta^6\text{-}p\text{-cym})Ru(o\text{-bqdi})Br]^+$ (**5**) differ from the calculated values by > 1% for C in each case, possibly due to the complexes containing a mixture of counter ions, especially in the cases of **4** (Cl^-, I^- or PF_6^-) and **5** (Cl^-, Br^- or PF_6^-). The synthesis of complex **1** as a BF_4 salt was reported previously.[9] A simplified procedure which isolates the complex as a PF_6 salt is reported here.

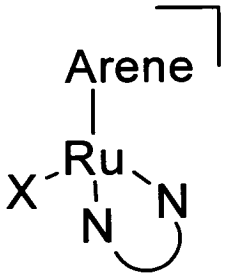

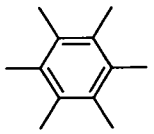
hmb

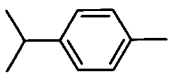
p-cym

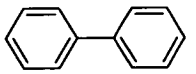
bip

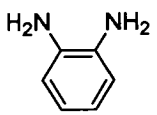

o-pda

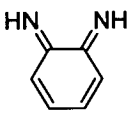

o-bqdi

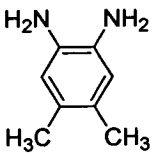

dmpda

Complex	Arene	N-N	X
1	*p*-cym	*o*-pda	Cl
1a	*p*-cym	*o*-pda	H_2O
2	hmb	*o*-pda	Cl
3	hmb	*o*-bqdi	Cl
4	*p*-cym	*o*-bqdi	I
5	*p*-cym	*o*-bqdi	Br
6	bip	dmpda	Cl
7	*p*-cym	*o*-bqdi	Cl
7a	*p*-cym	*o*-bqdi	H_2O
8	*p*-cym	*o*-pda	I

Figure 5.1 General structures of complexes studied in this Chapter as PF_6 salts.

All the Ru^{II} imine complexes described in this Chapter (complexes **3-5**), exhibit a characteristic broad singlet imine NH resonance at low field (δ ca. 14 – 15) in ^1H NMR spectra in DMSO-d_6 (e.g. δ 14.68 for complex **4**, Figure 5.2). For all the Ru^{II}

amine complexes studied in this Chapter (**1**, **2** and **6**), a characteristic doublet amine NH_2 resonance was observed (δ ca. 6-8).

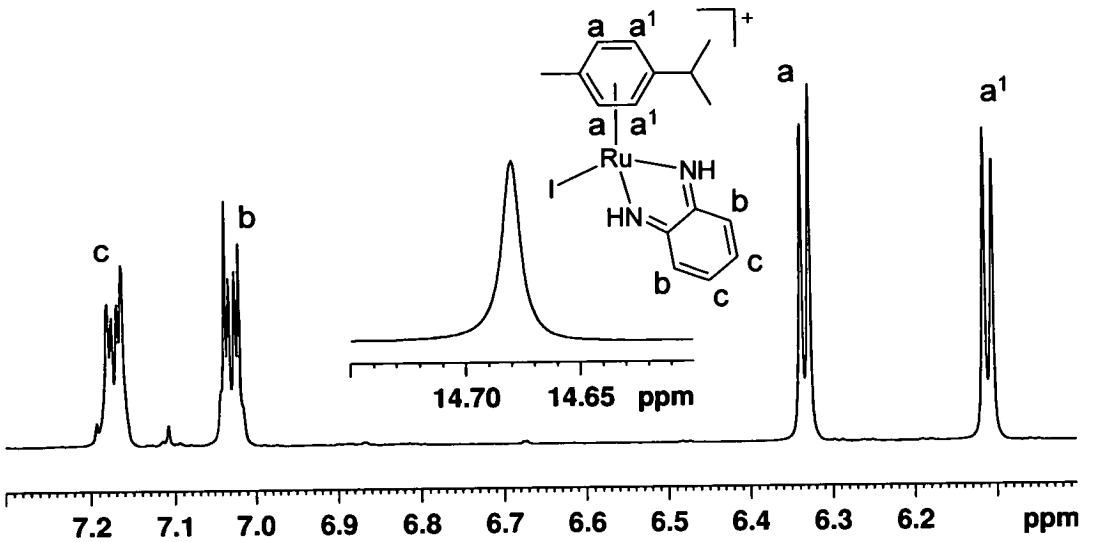

Figure 5.2 Low field region of ^1H NMR spectrum of complex [(η^6-*p*-cym)Ru(*o*-bqdi)I][PF_6] (**4**) in DMSO-d_6. Inset: shows resonance of imine NH protons from *o*-bqdi.

The chlorido complex **1** underwent ligand-based oxidation in the presence of ca. 5 mole equiv of KI or KBr in methanol, to afford the diimine iodido and bromido complexes **4** and **5**, respectively.

5.3.2 Crystal structures

The x-ray crystal structures of complexes [(η^6-*p*-cym)Ru(*o*-pda)Cl][PF_6] (**1**) and [(η^6-hmb)Ru(*o*-bqdi)Cl][PF_6] (**3**) are determined and their ORTEP diagrams are shown in Figure 5.3. The crystallographic data are listed in Table 5.1, and selected bond lengths

and angles in Table 5.2. The crystal structures of complexes **1** and **3** show the typical pseudo-octahedral `piano-stool´ geometry. The `seat´ of the stool (π-bonded arene) occupies three coordination sites and the two N atoms and Cl fill the remaining three sites.

The distance between the arene centroid and Ru in *p*-cym complex **1** (1.66 Å) is shorter than in hmb complex **3** (1.71 Å). The Ru-Cl bond lengths in these two chlorido Ru^{II} complexes are significantly different, with a values of 2.4039(8) Å for **1** and 2.3936(13) Å for **3**. In complex **3**, which contains *o*-bqdi as a chelating ligand, the Ru-N distances are significantly shorter (2.033(4) Å and 2.025(4) Å) than those in the diamine complex **1** (2.141(2) Å and 2.156(2) Å).

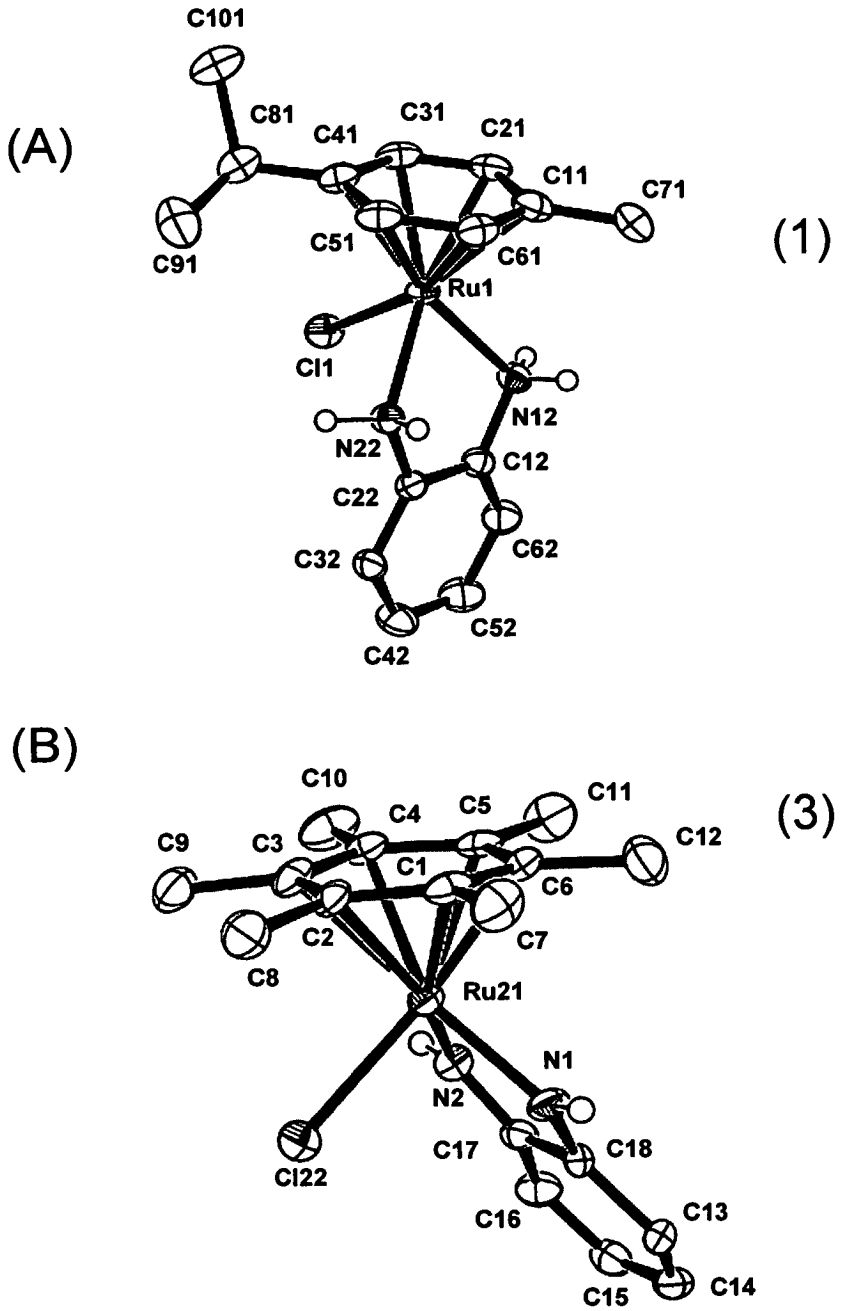

Figure 5.3 ORTEP diagrams for cations of (**A**) complex [(η^6-*p*-cym)Ru(*o*-pda)Cl][PF_6] (**1**), and (**B**) complex [(η^6-hmb)Ru(*o*-bqdi)Cl][PF_6] (**3**) at 50% probability thermal ellipsoids. All hydrogens, apart from NH hydrogen atoms from *o*-pda and *o*-bqdi, have been omitted for clarity.

Table 5.1 X-ray crystal structure data for complexes **1** and **3**

	1	**3**
Formula	$C_{16}H_{22}ClF_6N_2PRu$	$C_{18}H_{24}ClF_6N_2PRu$
Molar mass	523.85	549.89
Crystal system	orthorhombic	monoclinic
Crystal size /mm	0.48 × 0.19 × 0.08	0.35 × 0.14 × 0.06
Space group	*Pna21*	*P121/c1*
Crystal	Orange / needle	red / plate
a / Å	10.6876(4)	12.7647(6)
b / Å	17.0748(8)	10.8910(5)
c / Å	10.8625(5)	15.8629(7)
α / deg	90	90
β / deg	90	113.431(3)
γ / deg	90	90
T / K	150(2)	150
Z	4	4
R [F > 4σ (F)][a]	0.0340	0.0407
R_w[b]	0.0838	0.0948
GOF[c]	1.056	0.6189
Δρ max and min, /eÅ^{-3}	0.893, -0.450	1.39, -1.31

[a] $R = \sum||F_o| - |F_c||/\sum|F_o|$. [b] $R_w = [\sum w(F_o^2 - F_c^2)^2/\sum wF_o^2)]^{1/2}$. [c] $GOF = [\sum w(F_o^2 - F_c^2)^2/(n-p)]^{1/2}$, where n = number of reflections and p = number of parameters.

Table 5.2 Selected bond lengths (Å) and angles (°) for complexes **1** and **3**

Bond/Angle	1	3
Ru-Cl	2.4039(8)	2.3936(13)
Ru-N12/ N2	2.156(2)	2.025(4)
Ru-N22/ N1	2.141(2)	2.033(4)
Ru-C11/ C1	2.188(4)	2.263(4)
Ru-C21/ C2	2.195(4)	2.253(4)
Ru-C31/ C3	2.166(4)	2.252(4)
Ru-C41/ C4	2.207(4)	2.245(5)
Ru-C51/ C5	2.163(4)	2.176(5)
Ru-C61/ C6	2.186(4)	2.175(5)
N22/ N2-Ru-N12/ N1	76.18(9)	75.06(15)
N12/ N1-Ru-Cl	86.02(8)	87.90(11)
N22/ N2-Ru-Cl	83.56(8)	86.71(11)

The C – C and C – N bonds of *o*-pda in complex **1**, and *o*-bqdi in complex **3**, are shown in Figure 5.4. It can be seen that the C – C bond lengths of *o*-bqdi from **3** are in the range 1.35 – 1.44 Å consistent with the presence of C – C single (average 1.440(6) Å) and C = C double (average 1.347(6) Å) bonds. All C – C bond lengths of *o*-pda from **1** are very similar (1.37 – 1.41 Å), average 1.387(5) Å. The C – N bonds of *o*-bqdi are significantly shorter (1.295(5) Å and 1.300(6) Å) compared to those of *o*-pda (1.448(4) Å and 1.452(4) Å). The observed differences in C – C and C – N bond lengths can be diagnostic for assignment of the oxidation state of the chelating ligand.

(A)

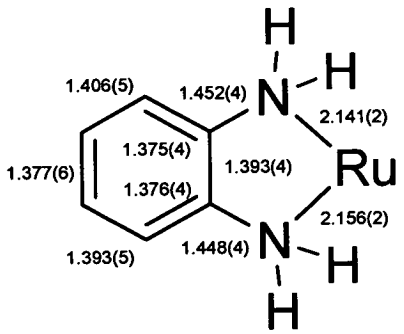

(1)

(B)

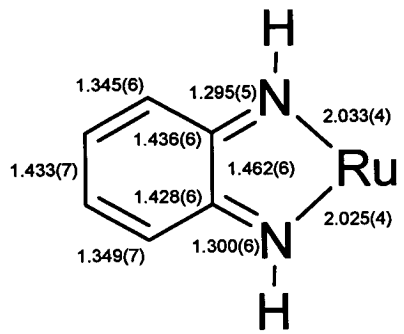

(3)

Figure 5.4 Bond distances for (**A**) Ru^{II}(*o*-pda) unit of complex [(η^6-*p*-cym)Ru(*o*-pda)Cl][PF_6] (**1**), and (**B**) Ru^{II}(*o*-bqdi) unit of complex [(η^6-hmb)Ru(*o*-bqdi)Cl][PF_6] (**3**).

5.3.3 Ligand based-oxidation

Complex [(η^6-*p*-cym)Ru(*o*-pda)Cl][PF_6] (**1**) is formed as a product of the reaction of the dimer ([(η^6-*p*-cym)$RuCl_2$]$_2$) with *o*-pda, at ambient temperature in air and methanol as a solvent. Complex [(η^6-hmb)Ru(*o*-pda)Cl][PF_6] (**2**), however, was prepared in methanol from the reaction of [(η^6-hmb)$RuCl_2$]$_2$ with *o*-pda, under an argon atmosphere at ambient temperature. When the preparation of **2** was attempted under the same reaction conditions as **1** (in air), the result was the formation of a

mixture. The ^{1}H NMR spectrum in DMSO-d_6 showed a mixture of **2** and [(η^6-hmb)Ru(*o*-bqdi)Cl][PF_6] (**3**) in a 1:1 ratio indicating that changing the arene from *p*-cym to hmb has made *o*-pda more sensitive towards ligand-based oxidation in the presence of molecular oxygen from air.

The extent of ligand-based oxidation process in [(η^6-*p*-cym)Ru(*o*-pda)Cl]$^+$ (**1**) and formation of [(η^6-*p*-cym)Ru(*o*-bqdi)Cl]$^+$ (**7**) in methanol was followed by UV-Vis spectroscopy. The data were fitted to the appropriate equation for pseudo-first-order kinetics giving the $k_{obs} = 10 \pm 0.2 \times 10^{-3}$ min^{-1} and $t_{1/2} = 68$ min. This is ca. 2 × slower than observed for ligand-based oxidation of the same complex in the presence of 1 mol equiv of KI ($k_{obs} = 24 \pm 0.2 \times 10^{-3}$ min^{-1}; $t_{1/2} = 29$ min). The formation of **7** and [(η^6-*p*-cym)Ru(*o*-bqdi)I]$^+$ (**4**) was confirmed by ESI-MS (for complex **7**: m/z calc. 376.9, found 377.2; for complex **4**: m/z calc. 468.3, found 468.9) and by ^{1}H NMR (for complex **7**; Figure 5.5). The resonances of the aromatic protons of *p*-cym in **7** (two doublets at 6.00 ppm and 6.23 ppm) are shifted to lower field, compared to those of complex **1** (two doublets at 5.56 ppm and 5.76 ppm).

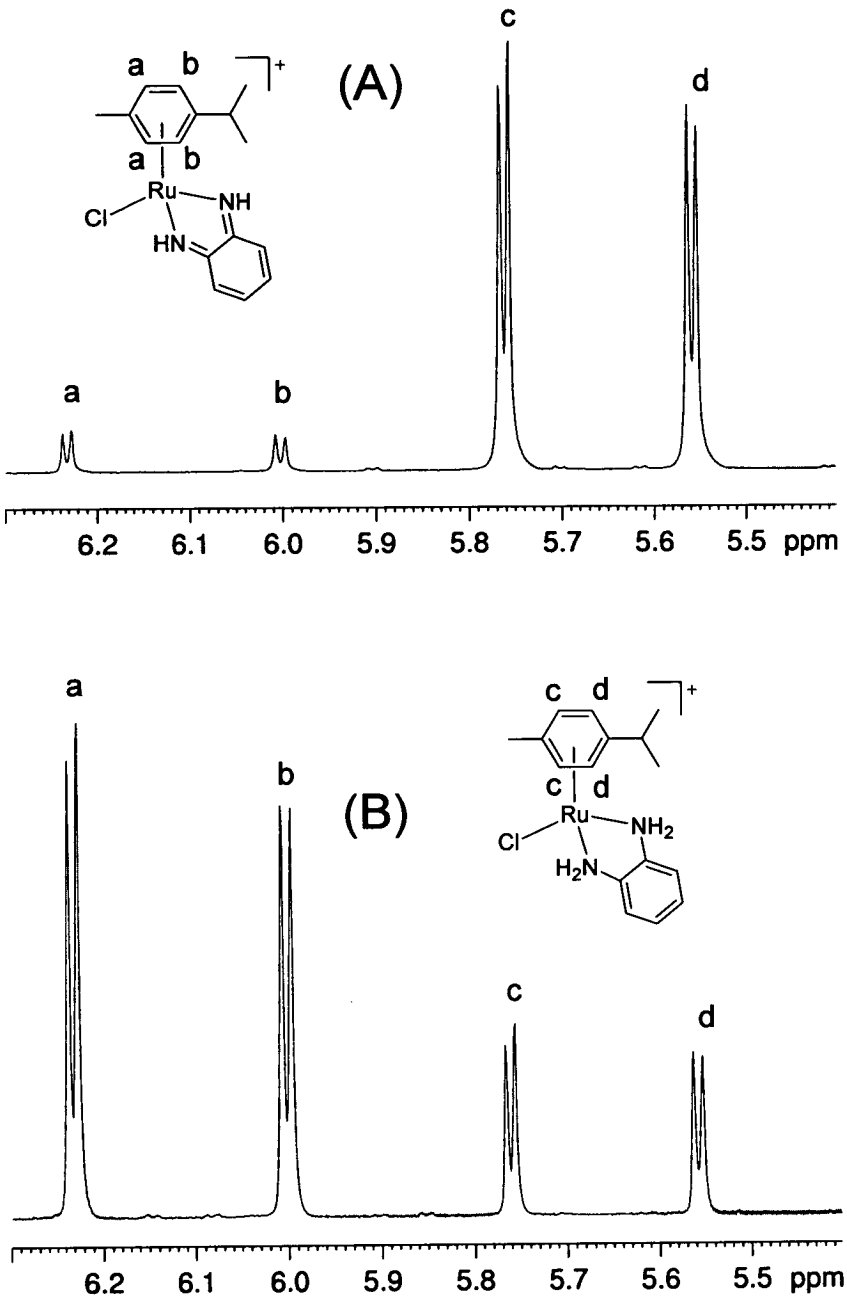

Figure 5.5 Low field region in ^{1}H NMR spectrum of [(η^6-*p*-cym)Ru(*o*-pda)Cl][PF_6] (**1**) in MeOH-d_4 (**A**) 10 min after dissolution, and (**B**) 4 hours after dissolution.

Initially the UV-Vis spectrum of **1** in methanol showed no bands in the visible region; new bands appeared after 5 min, at 248 nm, 357 nm, 485 nm and 690 nm, which increased in intensity with time and can be assigned to **7**.

5.3.4 Aquation

Complex $[(\eta^6\text{-hmb})Ru(o\text{-bqdi})Cl][PF_6]$ (**3**) showed relatively fast hydrolysis, k_{obs} = 92.5 ± 1.36×10^{-3} min^{-1} and $t_{1/2}$ = 7.49 min (Figure 5.6). The presence of the aqua adduct was confirmed by ESI-MS. The ion peak observed at m/z 369.7 is assignable to $[(\eta^6\text{-hmb})Ru(o\text{-bqdi})H_2O]^{2+}$ after loss of the aqua ligand and a proton (calc. m/z 369.4 for $[(\eta^6\text{-hmb})Ru(o\text{-bqdi})H_2O]^{2+}$ $-H_2O$ $-H^+$).

The ^1H NMR spectrum of complex $[(\eta^6\text{-}p\text{-cym})Ru(o\text{-pda})Cl][PF_6]$ (**1**) in D_2O, after 2 h showed peaks consistent with the presence of 4 species, corresponding to the chlorido species **1** (5%) and $[(\eta^6\text{-}p\text{-cym})Ru(o\text{-bqdi})Cl][PF_6]$ (**7**, 9%), together with peaks for the aqua adducts $[(\eta^6\text{-}p\text{-cym})Ru(o\text{-pda})H_2O]^{2+}$ (**1a**, 38%) and $[(\eta^6\text{-}p\text{-cym})Ru(o\text{-bqdi})H_2O]^{2+}$ (**7a** , 48%, Figure 5.7). This is consistent with the formation, and increase in concentration of the aqua adducts with time.

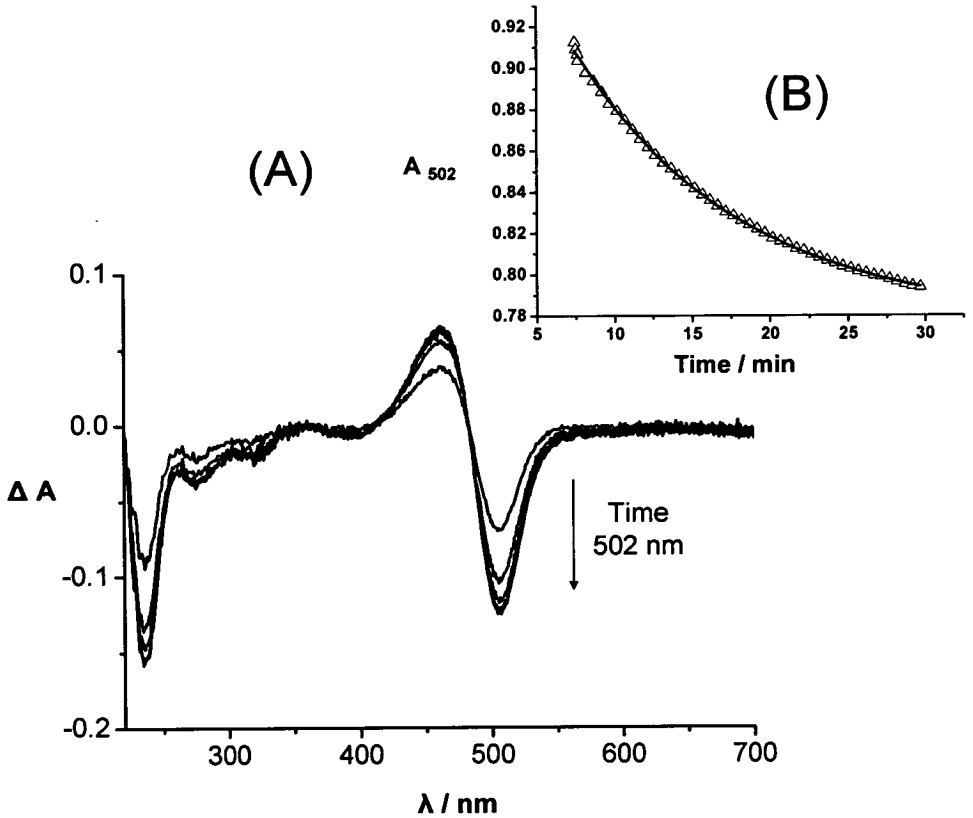

Figure 5.6 Hydrolysis studies of complex $[(\eta^6\text{-hmb})Ru(o\text{-bqdi})Cl][PF_6]$ (**3**) at 37°C. (**A**) the UV-Vis difference spectrum shows that the largest change in absorbance occurs at 502 nm. (**B**) The change in absorbance at 502 nm over 30 min during the aquation of **3**, from which the kinetic data were derived.

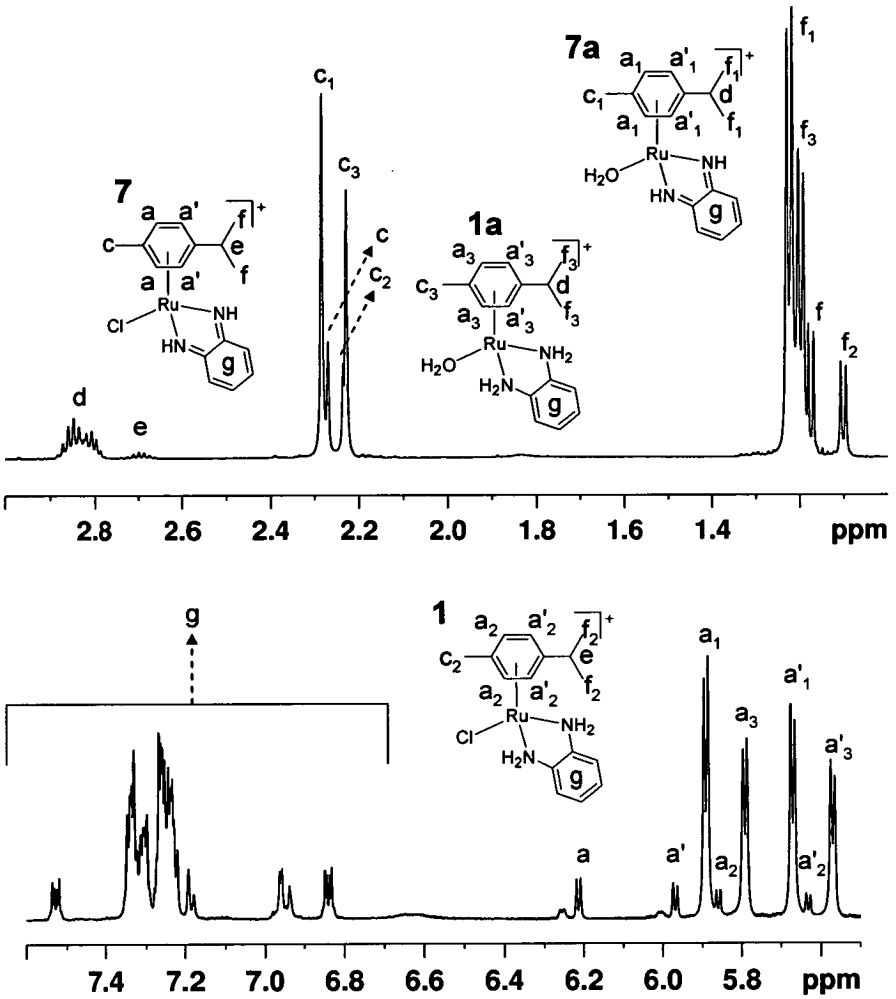

Figure 5.7 ^{1}H NMR spectrum of complex [(η^6-*p*-cym)Ru(*o*-pda)Cl][PF_6] (**1**) in D_2O, 2 h after dissolution, showing formation of [(η^6-*p*-cym)Ru(*o*-bqdi)Cl][PF_6] (**7**) and formation of aqua adducts of both chlorido species (**1a** and **7a**).

The ESI-MS of the same solution in D_2O also showed ion peaks that are consistent with the presence of 4 species. The peaks corresponding to the two aqua adducts **1a** and **7a** (calc. m/z 345.4 for {**1a** -H_2O –D}$^+$, found m/z 345.5; calc. m/z 341.4 for {**7a** -H_2O –D}$^+$, found m/z 341.5; in which the NH protons of *o*-pda and *o*-bqdi exchanged with D) overlapped, but a close analysis showed that there were two sets

of peaks. The less intense peaks corresponding to two chlorido species **1** and **7** (Figure 5.8) are still present in solution, again overlapped (calc. m/z 383.0 for **1**, with ND_2, found m/z 383.5; calc. m/z 379.1 for **7**, with ND, found m/z 379.4). Thus, complex **1** in D_2O undergoes hydrolysis as well as ligand-based oxidation, leading to the formation of $[(\eta^6\text{-}p\text{-cym})Ru(o\text{-bqdi})Cl]^+$ (**7**). The formation and increase in intensity of bands at: 251 nm, 350 nm, 468 nm and 686 nm in the UV-Vis spectrum of **1** in water over 1 h is attributable to ligand based oxidation.

o-Bqdi complexes $[(\eta^6\text{-hmb})Ru(o\text{-bqdi})Cl]^+$ (**3**) and $[(\eta^6\text{-}p\text{-cym})Ru(o\text{-bqdi})I]^+$ (**4**) in water show similar bands in the UV-Vis spectra: at 224, 350, 502 and 678 nm for **3** and at 260, 397, 493 and 680 nm for complex **4** (Figure 5.9).

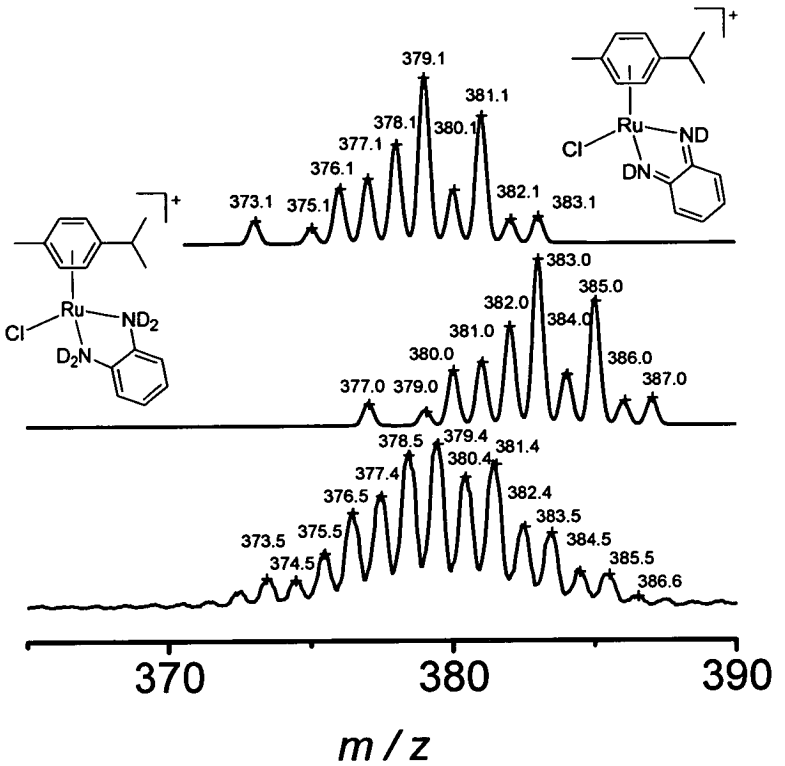

Figure 5.8 ESI-MS spectrum of D_2O solution of $[(\eta^6\text{-}p\text{-cym})Ru(o\text{-pda})Cl][PF_6]$ (**1**, lowest spectrum), and isotopic patterns (upper spectra) showing peaks corresponding to two species: intact complex **1** (where the NH_2 protons have been exchanged with D to give ND_2) and its oxidized form $[(\eta^6\text{-}p\text{-cym})Ru(o\text{-bqdi})Cl][PF_6]$ (**7**, again with ND, instead of NH).

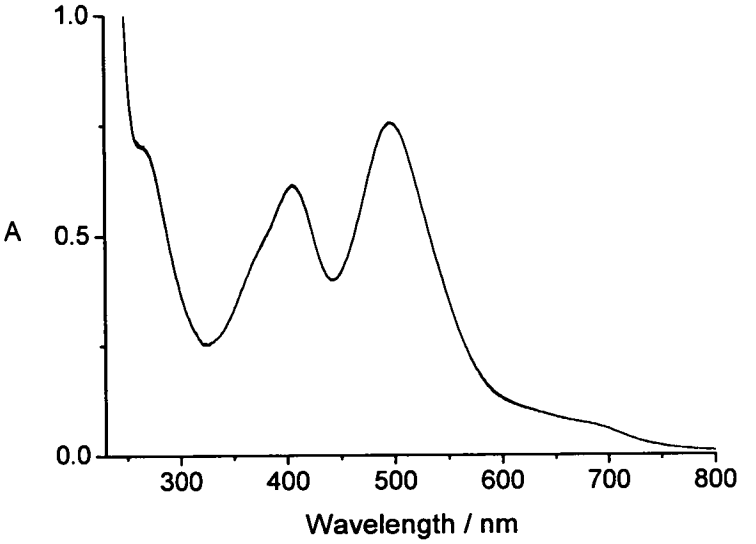

Figure 5.9 UV-Vis spectra of an aqueous solution of $[(\eta^6\text{-}p\text{-cym})Ru(o\text{-bqdi})I][PF_6]$ (**4**), showing no changes during 24 h.

The appearance and increase in intensity of bands at 251, 347, 475 and 662 nm in the UV-Vis spectrum of $[(\eta^6\text{-bip})Ru(dmpda)Cl]^+$ (**6**) in water over 1 h suggested that ligand-based oxidation had occurred, as the species formed absorb at the similar wavelengths as complexes **3** and **4**. In the ^1H NMR spectrum obtained 10 min after dissolution of **6** in D_2O, peaks for free biphenyl were observed (Figure 5.10) indicating arene dissociation from the complex. Complex **4** did not undergo hydrolysis over a period of 24 h.

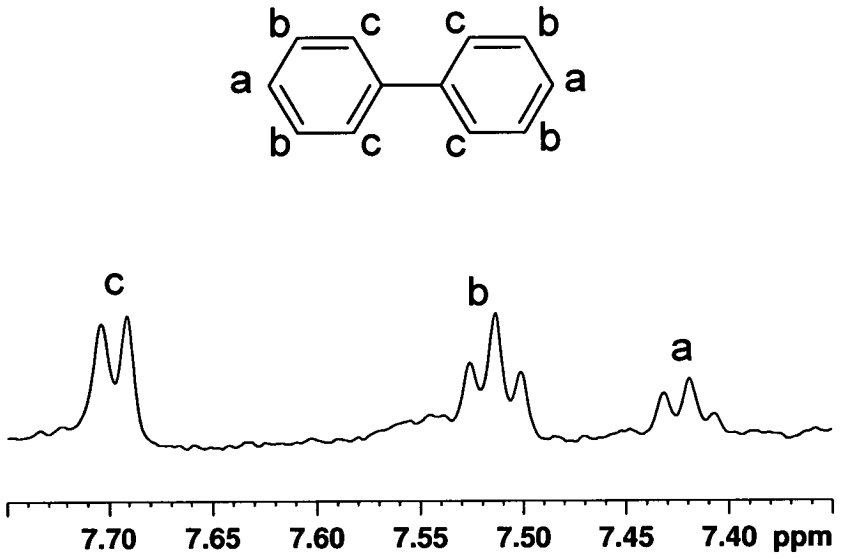

Figure 5.10 Low field region of the ^{1}H NMR spectrum of [(η^6-bip)Ru(dmpda)Cl][PF_6] (**6**) in D_2O, showing release of bip.

5.3.5 Reaction with GSH

UV-Vis spectra of complex [(η^6-*p*-cym)Ru(*o*-bqdi)I][PF_6] (**4**) in water, in the presence of 15 mol equivalents GSH, showed complete disappearance of the bands corresponding to **4** after 1 h, and the appearance of an isosbestic point at 299 nm (Figure 5.11). This indicated the reduction of *o*-bqdi to *o*-pda and the formation of [(η^6-*p*-cym)Ru(*o*-pda)I]$^+$ (**8**), as confirmed by ESI-MS (calc. for [M]$^+$ m/z 470.3, found 470.9). The resulting colourless solution became purple in colour after more than 72 h. Complex **4** dissolved in water gives a purple solution and the UV-Vis spectrum showed the complete restoration of bands for **4**.

The ^{1}H NMR spectrum of **4** in D_2O and the presence of 15 mol equiv GSH, showed resonance peaks at 3.30 (d of d) and 3.00 ppm (d of d, overlapped with the peaks of

GSH in the same region, two d of d at 2.95 and 2.98 ppm), corresponded to the β-CH_2 protons of GSSG. This suggested that oxidation of GSH to GSSG had occurred.[10] The intensity of this peaks increased with time.

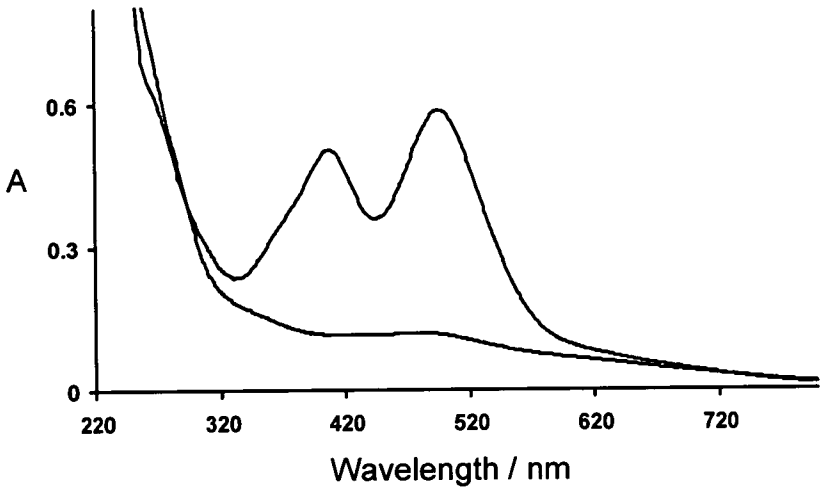

Figure 5.11 UV-Vis spectra of complex **4** in water 5 min after dissolution (top spectra), in the presence of 15 mole equiv GSH, and spectra (bottom) recorded 1h after dissolution, showing complete disappearance of the bands in the visible region and the isobestic point at 299 nm, indicating the conversion of the *o*-bqdi to *o*-pda and formation of $[(\eta^6\text{-}p\text{-cym})Ru(o\text{-pda})I]^+$ (**8**).

No GSH adduct of **4** in an aqueous solution was detectable by ESI-MS. In negative-ion mode ion peaks corresponding to GSS^- (calc. m/z 611.2, found 611.1) and GS^- (calc. m/z 305.1, found 304.9) were observed, confirming the formation of GSSG. Further confirmation of the origin of the peak at m/z 304.9 was achieved by fragmentation. The MS/MS spectrum of this peak showed fragmentation peaks consistent with the presence of a glutathionyl unit.[11]

5.3.6 Computation

The optimized geometries of the 2+ cations $[(\eta^6\text{-}p\text{-cym})Ru(o\text{-pda})(9\text{-EtG-}N7)]^{2+}$ (**1EtG**) and $[(\eta^6\text{-hmb})Ru(o\text{-bqdi})(9\text{-EtG-}N7)]^{2+}$ (**3EtG**) are shown in Figure 5.12. A hydrogen bond of 1.69 Å was formed between O6 of 9-EtG and NH proton (Ha) of *o*-pda (Figure 5.12A) in the optimized structure of **1EtG**. The distance between O6 from 9-EtG and Hi from NH of *o*-bqdi (Figure 5.12B) in the optimized structure of **3EtG** is 2.22 Å. The binding energy of 9-EtG to the metal fragment in **1EtG** is -328.1 kJ/mol, which is 23.8 kJ/mol lower than the corresponding value for **3EtG** (-304.3 kJ/mol).

Voronoi Deformation Density (VDD) charges on Ru in **1EtG** and **3EtG** revealed differences in electron density on the metal. In complex **1EtG** the atomic charge on Ru is +0.25 a.u. and +0.31 a.u. in **3EtG**, a difference of 0.06 a.u.

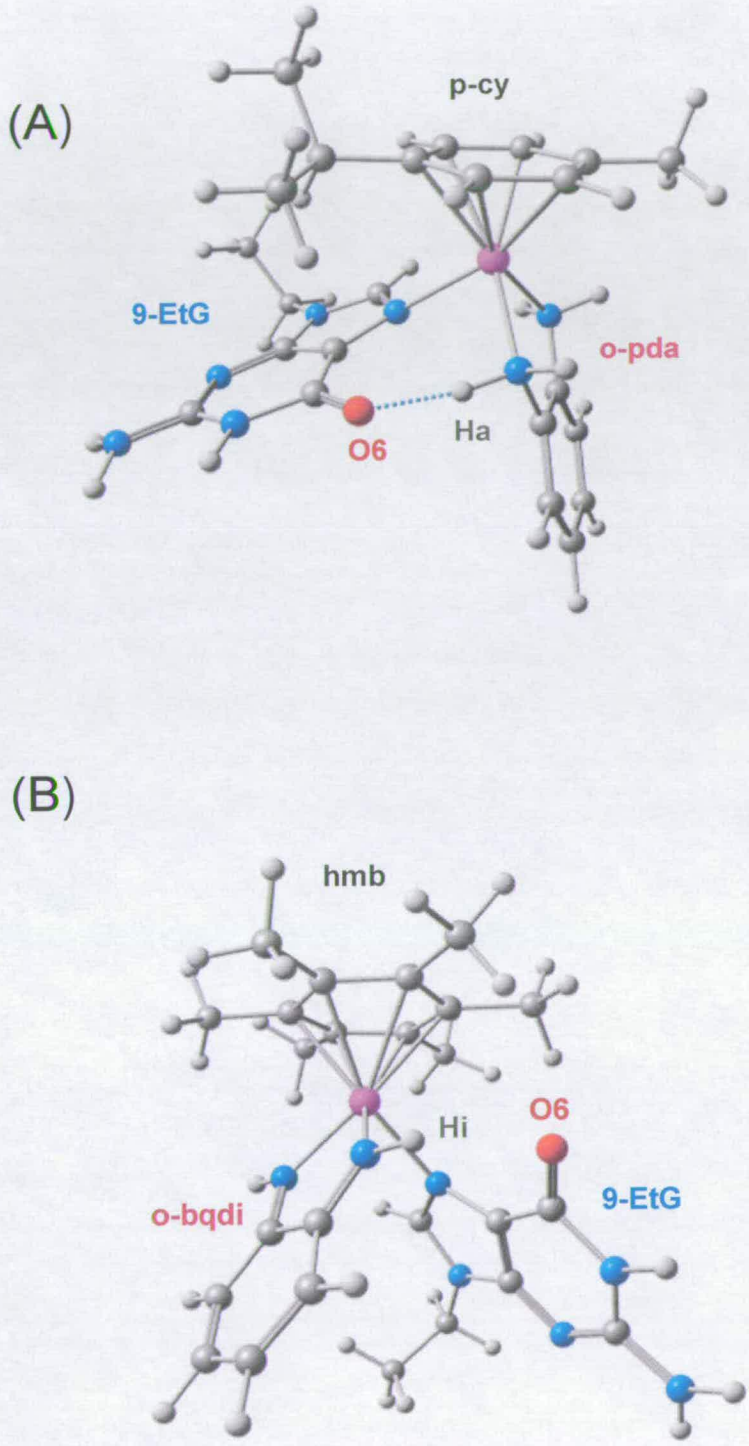

Figure 5.12 Optimized geometries of 9-EtG adducts of complexes (**A**) **1** and (**B**) **3**.

5.3.7 Cytotoxicity

None of the complexes tested (**1**, **3**, **4** or **6**) showed activity against A549 human lung cancer cells (IC_{50} > 100 μM; Table 5.3). Complex **1** containing *o*-pda as a chelating ligand, showed the highest activity against A2780 human ovarian cancer cells (IC_{50} = 11 μM). In contrast, complexes containing the oxidized form of *o*-pda (*o*-bqdi) as a chelating ligand (complexes **3** and **4**), showed no activity (IC_{50} > 100 μM) against the A2780 cell line. Complex **6** containing dmpda as a chelating ligand showed moderate activity against A2780 cells (IC_{50} = 49 μM). Although the activity of complex [(η^6-*p*-cym)Ru(*o*-bqdi)Br][PF_6] (**5**), was not determined, it would be predicted to be inactive. It is likely that both bromido and iodido ligands in these complexes would be substituted by chloride in an extracellular biological media where the concentration of chloride is ~ 104 mM, so that these complexes would in any case act as prodrugs.[12] IC_{50} of complex **2** in A2780 cells was found to be > 50 μM.

Table 5.3 IC_{50} values for Ru^{II} complexes described in this Chapter against the A2780 human ovarian and A549 human lung cancer cell lines

Complex		IC_{50} (μM)	
		A2780	A549
[(η^6-*p*-cym)Ru(*o*-pda)Cl][PF_6]	(**1**)	11[a]	> 100
[(η^6-hmb)Ru(*o*-pda)Cl][PF_6][b]	(**2**)	> 50[c]	ND[d]
[(η^6-hmb)Ru(*o*-bqdi)Cl][PF_6]	(**3**)	> 100	> 100
[(η^6-*p*-cym)Ru(*o*-bqdi)I][PF_6]	(**4**)	> 100	> 100
[(η^6-bip)Ru(dmpda)Cl][PF_6]	(**6**)	49	> 100

[a]The IC_{50} data of **1** against A2780 human ovarian cancer cell line were previously reported.[1]

[b]Complex **2** is believed to be unstable in solution towards the ligand-based oxidation and to be present in the test medium as the oxidized product, complex [(η^6-hmb)Ru(*o*-bqdi)Cl][PF_6] (**3**).

[c]Complex **2** was tested following the same procedure as for the rest of complexes, except that this complex was not tested for activity above 50 μM and other complexes were tested for activity up to 100 μM.

[d]ND = not determined.

5.4 Discussion

In this Chapter the oxidation of the diamine ligand *o*-pda to its diimino form *o*-bqdi in Ru^{II} arene complexes has been investigated, as well as its affect on cytotoxicity towards cancer cells. The control of oxidation through changes in the electronic properties of the arene and substitution of the halide ligand has also been studied.

The *o*-bqdi diimino ligand has been found to exist in solution[13] but has never been isolated in any form. For example, *o*-bqdi was observed as a product from the reaction of *o*-pda with lead dioxide, giving a deep red colour in organic solvents.[14] This reactive ligand can be stabilized by coordination to metal ions. For tris(α-diimine)Fe^{II} complexes, theoretical considerations have shown that a significant π-electron back-donation takes place in the ground state and, as a result, unusually stable Fe^{II} complexes are formed.[15] Similarly low-spin d^6 Ru^{II} complexes containing *o*-bqdi as the α-diimine ligand, are particularly stable.[16] Ru^{II} complexes containing *o*-bqdi have previously been synthesized[16] and structurally characterized.[17-19] The oxidation of *o*-pda and formation of *o*-bqdi has an effect on the overall physical and chemical properties of Ru^{II} arene complexes, including absorption spectra, hydrolysis rates, and cytotoxic activity.

The *o*-pda complex $[(\eta^6\text{-hmb})Ru(o\text{-pda})Cl]^+$ (**2**) contains a strong electron-donating arene (hmb) and in methanol solution the absence of oxygen is necessary to prevent the formation of the *o*-bqdi species. On the other hand the less electron-donating arene (*p*-cym) in $[(\eta^6\text{-}p\text{-cym})Ru(o\text{-pda})Cl]^+$ (**1**) makes it less sensitive to oxidation. Therefore the oxidation of *o*-pda and formation of an 'electron-poor' ligand (*o*-bqdi) is favoured in complexes where the metal center is more 'electron rich'. The stability of

the 'electron-poor' *o*-bqdi ligand in $[Ru^{II}(bpy)_2(o\text{-bqdi})][PF_6]_2$ has been ascribed to its π-accepting ability in conjunction with a low-spin 'electron-rich' Ru^{II} as a π-donor.[17] In contrast rhenium complexes with the oxidation states up to +7 containing $(o\text{-pda})^{2-}$ ligands contain a combination of an 'electron-rich' diamine ligand and an 'electron-poor' metal ion.[20]

The ^{1}H NMR peaks of NH protons from *o*-bqdi appeared in the low field region of the spectra (δ ca. 14-15) compared to those of NH_2 protons from *o*-pda (δ ca. 6-8). The resonances of the NH protons from *o*-bqdi were observed at 11.96 ppm for $[Ru(o\text{-bqdi})_3][PF_6]_2$ and at 7.0 ppm the resonances of the aromatic protons from the same chelating ligand.[16] This chemical shift is close to that observed for the aromatic protons of *o*-bqdi in complexes **3-5** (δ ca. 7.1). The ^{1}H NMR NH (*o*-bqdi) peaks of $[Ru(o\text{-pda})(o\text{-bqdi})_2]^{2+}$ have different chemical shifts δ, 11.20 and 14.24, as a result of different environments of these protons.[21]

o-Pda and o-bqdi species don't only show the difference in ^{1}H NMR spectra; the oxidation state can be distinguished by x-ray crystallography as well. The significantly shorter Ru-Cl bond in the crystal structure of $[(\eta^6\text{-hmb})Ru(o\text{-bqdi})Cl][PF_6]$ (**3**) compared to that of **1** can be attributed to the strong π-acceptor *o*-bqdi in **3**. As a consequence of the reduced electron density on the Ru centre, the negatively charged chlorido ligand is bound strongly. It has been found that the π-accepting ability of the ligand L in $[Ru(NH_3)_nL]^{2+}$, where n = 4 or 5 and L = pyrazine (pyz), 2,2'-bipyridine (bpy), imidazole (im) or *o*-bqdi, follows the order: o-bqdi >> pyz > bpy > im.[22] Therefore the effective charge on Ru in *o*-bqdi complexes is the highest in the series. The presence of significantly shorter Ru-N bonds in the crystal structure of **3** (average bond length of 2.029(4) Å; Table 5.2) compared to those of **1**

(average bond length of 2.148(2) Å; Table 5.2) again indicates strong π-acceptor ability of *o*-bqdi.

Structural parameters obtained from several crystal structure determinations can be used to assign the oxidation levels of the chelating ligand and enable comparisons to be made.[23] The lengths of C = N (av. 1.298(8) Å) and C = C (av. 1.347(6) Å) bonds of *o*-bqdi in complex **3** (Figure 5.4) are consistent with their identification as localized double bonds and are close to C = N (av. 1.300(8) Å) and C = C (av. 1.339(9) Å) bond lengths observed in $[(o\text{-bqdi})_3Fe^{II}][PF_6]$.[23] The lengths of C – C bonds of *o*-bqdi in the crystal structures of $[(o\text{-bqdi})_3Fe^{II}][PF_6]$ (av. 1.437(10) Å) and **3** (av. 1.440(6) Å; Figure 5.4) are very close.

In the crystal structure of complex **3**, the Ru-arene centroid distance is 1.71 Å and the distance in the crystal structure of $[(\eta^6\text{-hmb})Ru(en)Cl][PF_6]$ is 1.67 Å.[24] This indicates slightly weaker π-back-bonding between Ru and the arene in complex **3**, in which more electron density is withdrawn from the metal by *o*-bqdi than by hmb.

The two oxidation forms can be distinguished by UV-Vis spectroscopy as well. All the *o*-bqdi complexes studied (**3**, **4**, **7** and the oxidation product of **6**) exhibit two MLCT bands in UV-Vis spectra (in the range of 468-502 and 224-260 nm in water or methanol). The low and high energy MLCT transitions are assigned to Ru ($4d^6$) → π_1* (*o*-bqdi) and Ru ($4d^6$) → π_2* (*o*-bqdi) transitions by analogy with the assignment of the bands at 480 and 255 nm for $[Ru^{II}(edta)(o\text{-bqdi})]^{2-}$,[25] and at 470 and 258 nm for $[Ru^{II}(NH_3)_4(o\text{-bqdi})]^{2+}$.[26] The d-d transition bands for the chlorido complexes (**3**, **7** and the oxidation product of **6**) in water or methanol appeared in the range of 350-360 nm, while for the iodido complex **4** (Figure 5.9) the same transition comes at lower energy (397 nm). π-Donation increases in the order X = Cl < Br < I for $CpRu(PH_3)X$ complexes (Cp = cyclopentadiene).[27] This should make the d-d transition energy

higher for chlorido Ru^{II} complexes compared to the iodido complexes resulting in hypsochromic (blue) shift in the UV-Vis spectrum.[28] All the complexes show a band in the UV-Vis spectra in the region 662-690 nm in water or methanol. This low intensity band was similar to that observed previously for $[Ru^{II}(edta)(o\text{-bqdi})]^{2-}$ at ca. 575 nm in aqueous solution; its assignment is unclear at the moment, but it is suggested that it could be associated with the low energy MLCT transition.[25]

After being able to distinguish between *o*-pda and its oxidized form (*o*-bqdi) an important next step is the control of the oxidation. Methanol and aqueous solutions of $[(\eta^6\text{-hmb})Ru(o\text{-pda})Cl][PF_6]$ (**2**) are more sensitive to molecular oxygen (from air) compared to the solutions of $[(\eta^6\text{-}p\text{-cym})Ru(o\text{-pda})Cl][PF_6]$ (**1**), due to the difference in the arene (*vide infra*). These solutions react with O_2 to yield very intense purple products. In the ^1H NMR spectrum of **1** in MeOH-d_4 (Figure 5.5), the formation of $[(\eta^6\text{-}p\text{-cym})Ru(o\text{-bqdi})Cl][PF_6]$ (**7**) was detected. The intensity of the peaks corresponding to the protons of **7** increased with time, indicating increase in the concentration of the oxidized product (**7**). After 4 h the ratio of **7** and **1** was 3:1 (Figure 5.5B). For **7**, the aromatic *p*-cym peaks are shifted to low field due to the deshielding of these protons by the π-accepting *o*-bqdi ligand (6.00 and 6.23 ppm). The aquation of **1**, followed by UV-Vis spectroscopy showed the formation of **7**. Isobestic points were not apparent, indicated a multi-step reaction pathway, as suggested by Bednarski for the ligand based oxidation of *o*-pda Pt^{II} chlorido complexes in water.[29]

The ease with which **2** is oxidized compared to **1** is related to the increased number of electron-donating substituents on the arene in **2**. The presence of electron-pushing alkyl groups on the arene has been found to strengthen the Ru-arene bond[30] and effectively increase the electron density on the Ru centre. The same effect is observed

when substituting Cl with the less electronegative Br or I (in complexes **4** and **5**), resulting in less polarized Ru – Br/I bonds. Therefore the increased electron density on the Ru centre makes the chelating ligand in complexes **4** and **5**, more susceptible towards oxidation (*vide infra*).

Simultaneous oxidation and arene loss occurred during the aquation of complex [(η^6-bip)Ru(dmpda)Cl][PF_6] (**6**), even though the replacement of the arene (*p*-cym, hmb) by more electron-deficient bip,[31, 32] should make the Ru centre even more acidic and this should stabilize the chelating ligand and make the oxidation less likely. Arene loss (detected in ^{1}H NMR in D_2O; Figure 5.10) occurs possibly due to the oxidation of the chelating ligand resulting in a strong π-acceptor (dmbqdi), which competes with the bip arene (weak π-acceptor) for electron density from Ru. This destabilizes the Ru – arene bond through lack of π-back donation resulting in the dissociation of the arene from Ru. Arene loss was not observed for other complexes studied here.

The difference in behaviour of *o*-pda and *o*-bqdi species in aqueous solutions deserves discussion as well. ^{1}H NMR spectrum of [(η^6-*p*-cym)Ru(*o*-pda)Cl][PF_6] (**1**), in D_2O (Figure 5.7) showed the formation of [(η^6-*p*-cym)Ru(*o*-bqdi)Cl][PF_6] (**7**), as well as formation of aqua adducts [(η^6-*p*-cym)Ru(*o*-pda)H_2O]$^{2+}$ (**1a**) and [(η^6-*p*-cym)Ru(*o*-bqdi)H_2O]$^{2+}$ (**7a**). Thus complex **1** hydrolyses as it undergoes ligand based oxidation (*vide infra*).

For Ru^{II} complexes, the presence of π-acceptors as chelating ligands decreases the rate of hydrolysis compared to the ethylenediamine analogues,[33] by decreasing the electron density on Ru and reducing Cl^- lability. Thus the hydrolysis of [(η^6-hmb)Ru(*o*-bqdi)Cl][PF_6] (**3**) was found to be 17 times slower than previously observed for [(η^6-hmb)Ru(en)Cl][PF_6].[24] The iodido complex [(η^6-*p*-cym)Ru(*o*-bqdi)I][PF_6] (**4**) was found not to undergo hydrolysis. The absence of hydrolyses for

iodido [(η^6-arene)Ru(azpy)I][PF_6] complexes, where arene = bip or *p*-cym and azpy = N,N-dimethylphenyl- or hydroxyphenyl-azopyridine, had also been reported.[34]

The stabilization of the divalent Ru centre by the π-acceptor *o*-bqdi[35] suggests that reduction of *o*-bqdi back to *o*-pda is not favourable. However the ligand-based reduction of *o*-bqdi complex **4** occurred in the presence of glutathione (GSH). GSH is the primary cellular antioxidant and is present in cells in concentrations of ca. 2-10 mM. In many cases cancer cell resistance to drugs is correlated with an increased level of GSH in cancer cells compare to the healthy ones.[12] For this reason, reactions of Ru^{II} arene complexes with GSH are of particular importance. In the presence of 15 mol equiv GSH, complex [(η^6-*p*-cym)Ru(*o*-bqdi)I][PF_6] (**4**) underwent ligand-based reduction to form [(η^6-*p*-cym)Ru(*o*-pda)I][PF_6] (**8**). Leaving the aqueous solution for over 72 h, resulted in the complete conversion of **8** back to complex **4**, indicating that once all the GSH has been oxidized to GSSG, dissolved oxygen in water goes on to cause ligand-based oxidation and formation of stable complex **4**. The rate of oxidation of GSH is probably too slow to be important under physiological conditions (complete oxidation of GSH to GSSG requires more than 72 h).

The stability of 9-EtG adducts of *o*-pda and *o*-bqdi complexes, as an important feature for potential DNA binding, was examined using DFT calculations. The *o*-bqdi ligand in the crystal structure of [(η^6-hmb)Ru(*o*-bqdi)Cl]$^+$ (**3**, Figure 5.3B), and the optimized structure of [(η^6-hmb)Ru(*o*-bqdi)(9-EtG-*N7*)]$^{2+}$ (**3EtG**, Figure 5.12B) has a planar geometry and the H atoms of NH lie in the same plane. This results in the O6 atom of 9-EtG in **3EtG** being farther away from the NH protons of *o*-bqdi. The H-bond formed between Hi and O6 is weaker (Figure 5.12B; 2.22 Å) compared to the one formed between NH proton of *o*-pda and O6 of 9-EtG in [(η^6-*p*-cym)Ru(*o*-pda)(9-EtG-*N7*)]$^{2+}$ (**1EtG**). The tetrahedral geometry around the N donors of *o*-pda in **1EtG**

(Figure 5.12A) resulted in one hydrogen (Ha) pointing towards O6 making the H-bond strong (1.69 Å). The H-bond between Ha and O6 in **1EtG** appears to be stronger than observed in en complexes of the type $[(\eta^6\text{-arene})Ru(en)(9\text{-EtG-}N7)]^{2+}$, where arene = bip, tetrahydroanthracene (tha) and dihydroanthracene (dha). H-bonds in en complexes had values of 1.868 Å for the bip complex, 1.919 Å for the tha complex and 2.081 Å for the dha complex.[36] The H-bond in **1EtG** is similar in length to the H-bond between the NH proton of en and O6 in the energy minimized structure of $[(\eta^6\text{-}p\text{-cym})Ru(en)(9\text{-EtG-}N7)]^{2+}$ (1.67 Å).[37]

The total bonding energy of 9-EtG in the structure of **1EtG** (-328.1 kJ/mol) is 23.8 kJ/mol lower than the bonding energy of 9-EtG in **3EtG** (-304.3 kJ/mol). This could mainly be attributed to the more stabilized 9-EtG adduct of **1** through the stronger H-bond described above. The charge on the metal centre in **3EtG** (+0.31 a.u.) is 0.06 more positive than in **1EtG** (+0.25 a.u.) which is consistent with *o*-bqdi acting as a π-acceptor. Considering the arenes, hmb in **3EtG** with 6 CH_3 groups would have more electron pushing effect compared to the *p*-cym of **1EtG**. Still the effect of the arene is noticeably smaller compared to the effect of the chelating ligand, and this leaves Ru in complex **3EtG** with higher positive charge compared to Ru in **1EtG**.

For complexes containing *o*-bqdi as the chelating ligand, no cytotoxic activity was achieved. Inactive $[(\eta^6\text{-hmb})Ru(o\text{-bqdi})Cl]^+$ (**3**) showed relatively fast hydrolysis and potential ability to bind to DNA. However as the 9-EtG adduct of **3** was found to be not as stable as the adduct of **1**, the stability of the adduct formed contributes more towards cytotoxic activity than the actual ability of binding. Complex **2** is believed to be unstable in solution towards the ligand based oxidation, and tested as the oxidized product, complex **3**, or at least partially. This explains the inactivity of **2**. The inactivity of iodido complex $[(\eta^6\text{-}p\text{-cym})Ru(o\text{-bqdi})I]^+$ (**4**) could be attributed to the

absence of hydrolysis. This could be a good reason for loss of ability of binding to DNA and loss of cytotoxic activity. The relatively fast hydrolysis of $[(\eta^6\text{-}p\text{-cym})Ru(en)I]^+$ ($t_{1/2}$ = 12.2 min)[24] resulted in relatively good cytotoxic activity of the complex (IC_{50} = 9 μM against A2780 cells).[38] Complexes containing mono- or dimethylated *o*-pda and indan as arene, exhibited good activity, with IC_{50} values of 4 and 14 μM, respectively.[1] The loss of activity for **6**, which contains dimethylated *o*-pda, might arise from the dissociation of the bip arene from the complex (*vide infra*).

5.5 Summary

In this Chapter it is shown, for the first time, that Ru^{II} arene complexes containing *o*-pda as the chelating ligand can lose cytotoxic activity towards cancer cells upon oxidation of the chelating ligand to *o*-bqdi. This oxidation can be controlled through changes in electronic properties of the other ligands in the complex. The ligand based oxidation can be followed by UV-Vis and ^{1}H NMR spectroscopy and the oxidation state of the diamine/diimine ligand can be distinguished in the x-ray crystal structure. The loss of anticancer activity for the dmpda complex containing bip as the arene is attributed to the dissociation of the arene ligand from the complex. It is suggested that the loss of activity for *o*-bqdi complexes can be attributed to the absence of hydrolysis or as well to the formation of the less stable adducts with 9-EtG, which would lead to the weakened binding to DNA. π-Accepting ability of the *o*-bqdi ligand is confirmed by the higher charge on Ru in the *o*-bqdi complex compared to that in the *o*-pda complex. It is shown that *o*-bqdi complexes can be reduced back to the original *o*-pda form by an excess of the intracellular reducing agent GSH. Once all the GSH is oxidized to form GSSG, the *o*-pda complex again undergoes ligand-based oxidation to form very stable *o*-bqdi Ru^{II} species.

5.6 References

(1) Habtemariam, A.; Melchart, M.; Fernandez, R.; Parsons, S.; Oswald, I. D. H.; Parkin, A.; Fabbiani, F. P. A.; Davidson, J. E.; Dawson, A.; Aird, R. E.; Jodrell, D. I.; Sadler, P. J. *J. Med. Chem.* **2006,** *49*, 6858-6868.

(2) Connors, T. A.; Jones, M.; Ross, W. C.; Braddock, P. D.; Khokhar, A. R.; Tobe, M. L. *Chem. Biol. Interact.* **1972,** *5*, 415-24.

(3) Gale, G. R.; Atkins, L. M.; Walker, E. M., Jr.; Smith, A. B.; Meischen, S. J. *Proc. Soc. Exp. Biol. Med.* **1973,** *142*, 1349-54.

(4) Meischen, S. J.; Gale, G. R.; Lake, L. M.; Frangakis, C. J.; Rosenblum, M. G.; Walker, E. M., Jr.; Atkins, L. M.; Smith, A. B. *J. Nat. Cancer Inst.* **976,** *57*, 841-5.

(5) Beurskens, P. T. B., G.; Bosman, W. P.; de Gelder, R.; Garcia-Granda, S.; Gould, R. O.; Israel, R. and Smits, J. M. M., *The DIRDIF96 Program System.* University of Nijmegen: Nijmegen, The Netherlands, **1996.**

(6) Sheldrick, G. M. *SHELXL-97*, University Of Göttingen: Göttingen, Germany, **1997.**

(7) Altomare, A.; Cascarano, G.; Giacovazzo, C.; Guagliardi, A.; Polidori, G.; Camalli, M.; *J. Appl. Crystallogr.* **1994,** *27*, 435.

(8) Betteridge, P. W.; Carruthers, J. R.; Cooper, R. I.; Prout, K.; Watkin, D. J. *J. Appl. Crystallogr.* **2003,** *36*, 1487.

(9) Govindaswamy, P.; Mozharivskyj, Y. A.; Kollipara, M. R. *Polyhedron* **2004,** *23*, 3115-3123.

(10) Nakayama, T.; Isobe, T.; Nakamiya, K.; Edmonds, J. S.; Shibata, Y.; Morita, M. *Magn. Reson. Chem.* **2005,** *43*, 543-550.

(11) Dieckhaus, C. M.; Fernandez-Metzler, C. L.; King, R.; Krolikowski, P. H.; Baillie, T. A. *Chem. Res. Toxicol.* **2005,** *18*, 630-638.

(12) Kennedy, R. S.; Konok, G. P.; Bounous, G.; Baruchel, S.; Lee, T. D. G. *Anticancer Res.* **1995,** *15*, 2643-9.

(13) Christoph, G. G.; Goedken, V. L. *J. Am. Chem. Soc.* **1973,** *95*, 3869-75.

(14) Willstatter, R.; Pfannenstiel, A. *Ber. Deu. Chem. Gesell.* **1905,** *38*, 2348-52.

(15) Ito, T.; Tanaka, N.; Hanazaki, I.; Nagakura, S. *Bull. Chem. Soc. Jpn.* **1968,** *41*, 365-73.

(16) Warren, L. F. *Inorg. Chem.* **1977,** *16*, 2814-19.

(17) Belser, P.; Von Zelewsky, A.; Zehnder, M. *Inorg. Chem.* **1981,** *20*, 3098-103.

(18) Milliken, B.; Borer, L.; Russell, J.; Bilich, M.; Olmstead, M. M. *Inorg. Chim. Acta* **2003,** *348*, 212-216.

(19) Rusanova, J.; Rusanov, E.; Gorelsky, S. I.; Christendat, D.; Popescu, R.; Farah, A. A.; Beaulac, R.; Reber, C.; Lever, A. B. P. *Inorg. Chem.* **2006,** *45*, 6246-6262.

(20) Danopoulos, A. A.; Wong, A. C. C.; Wilkinson, G.; Hursthouse, M. B.; Hussain, B. *J. Chem. Soc., Dalton Trans.* **1990**, 315-31.

(21) Cheng, H. Y.; Peng, S. M. *Inorg. Chim. Acta* **1990,** *169*, 23-4.

(22) Baranovski, V. I.; Sizova, O. V. *Chem. Phys. Lett.* **1999,** *315*, 130-134.

(23) Peng, S. M.; Chen, C. T.; Liaw, D. S.; Chen, C. I.; Wang, Y. *Inorg. Chim. Acta* **1985,** *101*, L31-L33.

(24) Wang, F.; Habtemariam, A.; van der Geer Erwin, P. L.; Fernandez, R.; Melchart, M.; Deeth Robert, J.; Aird, R.; Guichard, S.; Fabbiani Francesca, P. A.; Lozano-Casal, P.; Oswald Iain, D. H.; Jodrell Duncan, I.; Parsons, S.; Sadler Peter, J. *Proc. Natl. Acad. Sci. U. S. A.* **2005,** *102*, 18269-74.

(25) Rein, F. N.; Rocha, R. C.; Toma, H. E. *Electrochem. Comm.* **2002,** *4*, 436-441.

(26) Metcalfe, R. A.; Lever, A. B. P. *Inorg. Chem.* **1997,** *36*, 4762-4771.

(27) Reddy, A. R.; Ranjini, A. S.; Das, P. K.; Samuelson, A. G. *Inorg. Chim. Acta* **2007,** *360*, 2778-2782.

(28) Bickford, C. C.; Johnson, T. J.; Davidson, E. R.; Caulton, K. G. *Inorg. Chem.* **1994,** *33*, 1080-6.

(29) Kockerbauer, R.; Bednarski, P. J. *J Inorg. Biochem.* **1996,** *62*, 281-98.

(30) Dadci, L.; Elias, H.; Frey, U.; Hoernig, A.; Koelle, U.; Merbach, A. E.; Paulus, H.; Schneider, J. S. *Inorg. Chem.* **1995,** *34*, 306-15.

(31) Peacock, A. F. A.; Parsons, S.; Sadler, P. J. *J. Am. Chem. Soc.* **2007,** *129*, 3348-3357.

(32) Hung, Y.; Kung, W.-J.; Taube, H. *Inorg. Chem.* **1981,** *20*, 457-63.

(33) Dougan, S. J.; Melchart, M.; Habtemariam, A.; Parsons, S.; Sadler, P. J. *Inorg. Chem.* **2007,** *46*, 1508.

(34) Dougan, S. J.; Habtemariam, A.; McHale, S. E.; Parsons, S. *Proc. Natl. Acad. Sci. U. S. A., in press.*

(35) Juestel, T.; Bendix, J.; Metzler-Nolte, N.; Weyhermueller, T.; Nuber, B.; Wieghardt, K. *Inorg. Chem.* **1998,** *37*, 35-43.

(36) Chen, H.; Parkinson, J. A.; Parsons, S.; Coxall, R. A.; Gould, R. O.; Sadler, P. J. *J. Am. Chem. Soc.* **2002,** *124*, 3064-3082.

(37) Gossens, C.; Tavernelli, I.; Rothlisberger, U. *J. Chem. Theory Comp.* **2007,** *3*, 1212-1222.

(38) Aird, R. E.; Cummings, J.; Ritchie, A. A.; Muir, M.; Morris, R. E.; Chen, H.; Sadler, P. J.; Jodrell, D. I. *Br. J. Cancer* **2002,** *86*, 1652-1657.

Chapter 6

Isomer separation by ion mobility mass spectrometry

"Man's mind, once stretched by a new idea, never regains its original dimensions."

Oliver Wendell Holmes

6.1 Introduction

In this Chapter the separation of isomeric terphenyl complexes of the type $[(\eta^6\text{-arene})Ru(en)Cl]^+$, where en = ethylenediamine and arene = *para*- (**1**), *ortho*- (**2**) or *meta*-terphenyl (**3**) (*p*-, *o*- or *m*-terp; Figure 6.1, synthesis and characterization are reported in Chapter 3) is studied by ion mobility in combination with mass spectrometry.

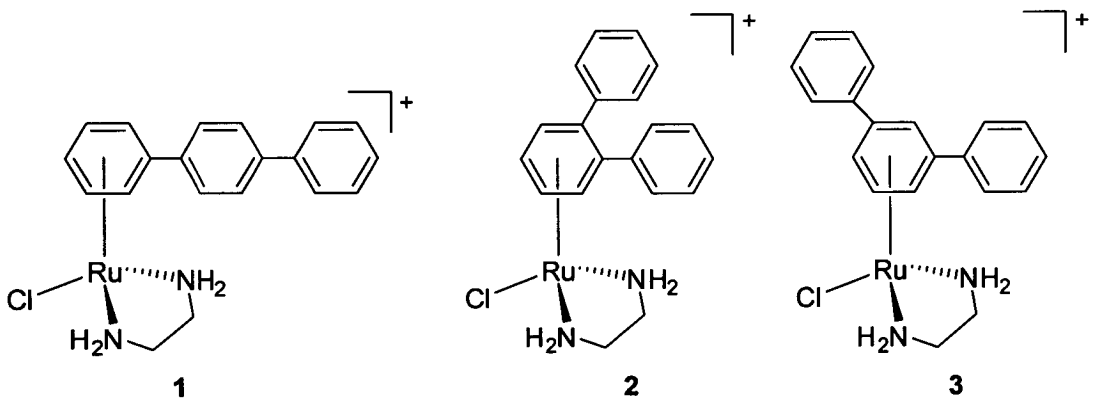

Figure 6.1 Chemical structures of terphenyl complexes **1**, **2** and **3**.

6.1.1 Ruthenium(II) terphenyl complexes

DNA binding properties of **1**, **2** and **3** were investigated in Chapter 3, and the data are consistent with a combined intercalative and monofunctional (coordination) binding mode of complex **1**, while the two other complexes showed preferential binding

through the coordination. Intercalative binding mode of **1** seems therefore to make a major contribution to the high potency of this complex (IC_{50} = 4 μM against A2780 ovarian cancer cell line) compared to complexes **2** and **3** (IC_{50} = 30 and 42 μM, respectively against A2780 cells; Chapter 3).

6.1.2 Mass Spectrometry (MS)

Due to its speed, selectivity and sensitivity modern mass spectrometry (MS) is becoming an essential tool for chemical, biological and medical research. Recent applications have allowed the stoichiometry of heterogeneous protein complexes to be defined based on their differences in mass-to-charge ratios (*m/z*).[1, 2] The application of electrospray mass spectrometry (ES-MS) to organometallic chemistry and its development towards the characterization of organometallic compounds have been discussed in the literature.[3-5] Electrospray ionization mass spectrometry (ESI-MS) is described in Chapter 2.

MS however cannot separate isomeric species as a stand-alone technique. It is often common to distinguish isomers using tandem MS since differences in the relative abundance of product ions, formed by fragmentation of individual selected isomeric precursor ions, may often be observed. It would be highly advantageous if the separation of isomeric species could be achieved on a time-scale compatible with the MS acquisition time-scale, and also provide an insight into the physical dimension of the separated species.

6.1.3 Ion mobility (IM)

Ion mobility (IM) has the ability to rapidly separate isomeric and isobaric species based on differences in their collision cross-sections (physical size and shape) in the gas-phase and thus provide specific information on ionic conformation. IM separates ionic species based on their drift time through a gas-filled cell under the influence of an applied electric field (Figure 6.2). Drift time is dependent on factors such as mass, charge, together with physical size and shape (collision cross-section) and instrumental operating parameters. It is therefore possible to separate isomeric and isobaric species using IM if they have sufficiently different collision cross-sections.[6, 7]

6.1.4 Ion mobility (IM) in combination with mass spectrometry (MS)

In combination with MS, IM represents a powerful analytical tool since *m/z* and structural information can rapidly be obtained from a single experiment. A variety of IM methods are commonly used in combination with MS but they cannot all provide absolute collision cross-section (CCS) measurements directly from kinetic theory (attempts to explain macroscopic properties such as pressure, temperature, or volume, by considering the molecular composition and motion).[2]

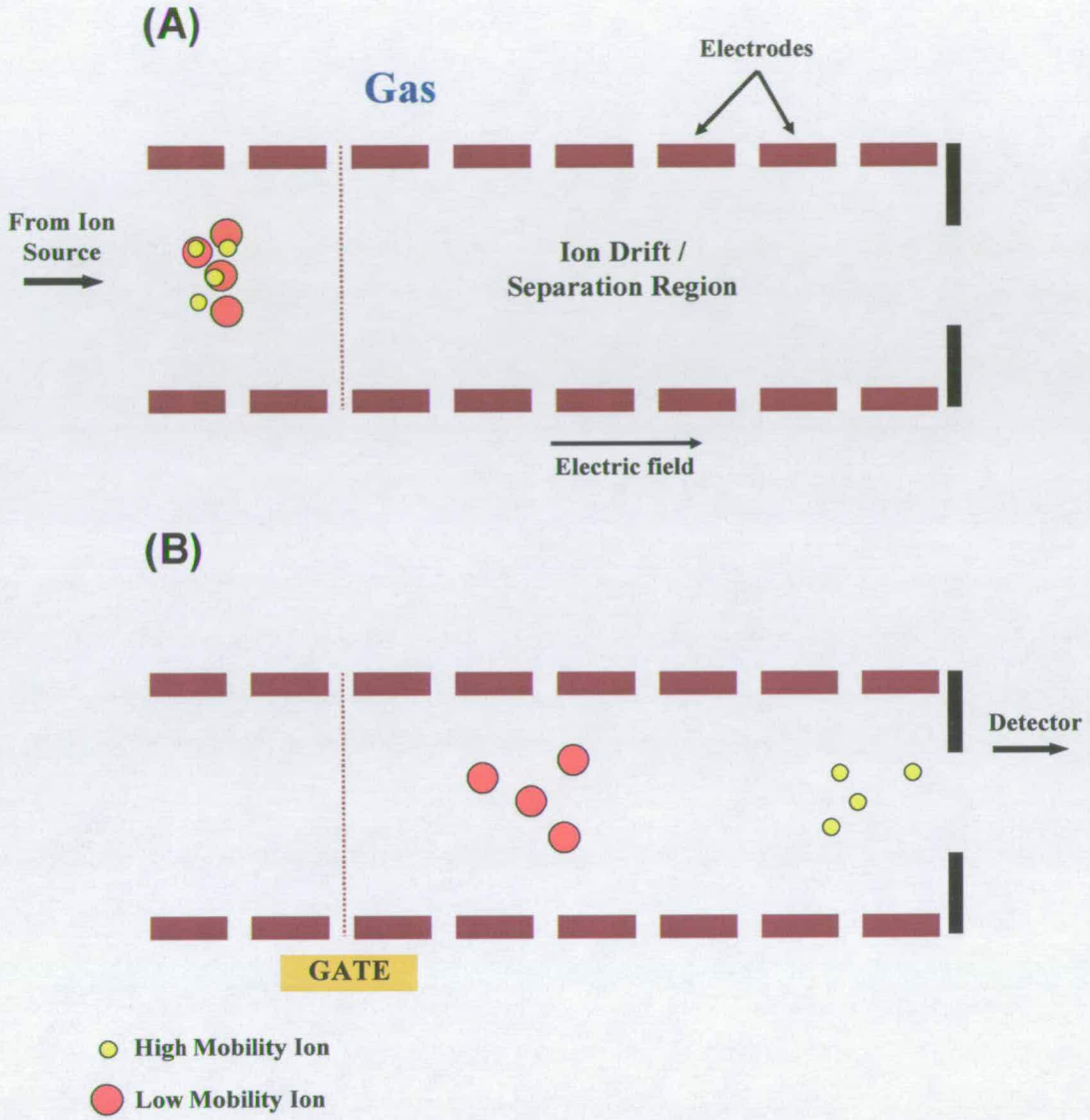

Figure 6.2 Schematic diagram illustrating ion mobility separation (**A**) starting point (**B**) the achieved separation (based on the previously published scheme).[8]

To take advantage of the IM-MS technique, an instrument based on 'travelling-wave' (T-Wave) technology has been developed.[7-9] The instrument (Synapt HDMS, Waters UK; Figure 6.3) uses a radio-frequency (RF) stacked ring ion guide (consists of a series of ring electrodes and adjacent rings have opposite phases of RF voltage

applied to them; Figure 6.4) as the mobility cell with a continuous train of transient voltages (travelling waves) to propel ions through the N_2 drift gas (*vide supra*). The lower mobility ion rolls over the wave more often and takes longer to traverse the cell (Figure 6.2). For more details see Experimental section.

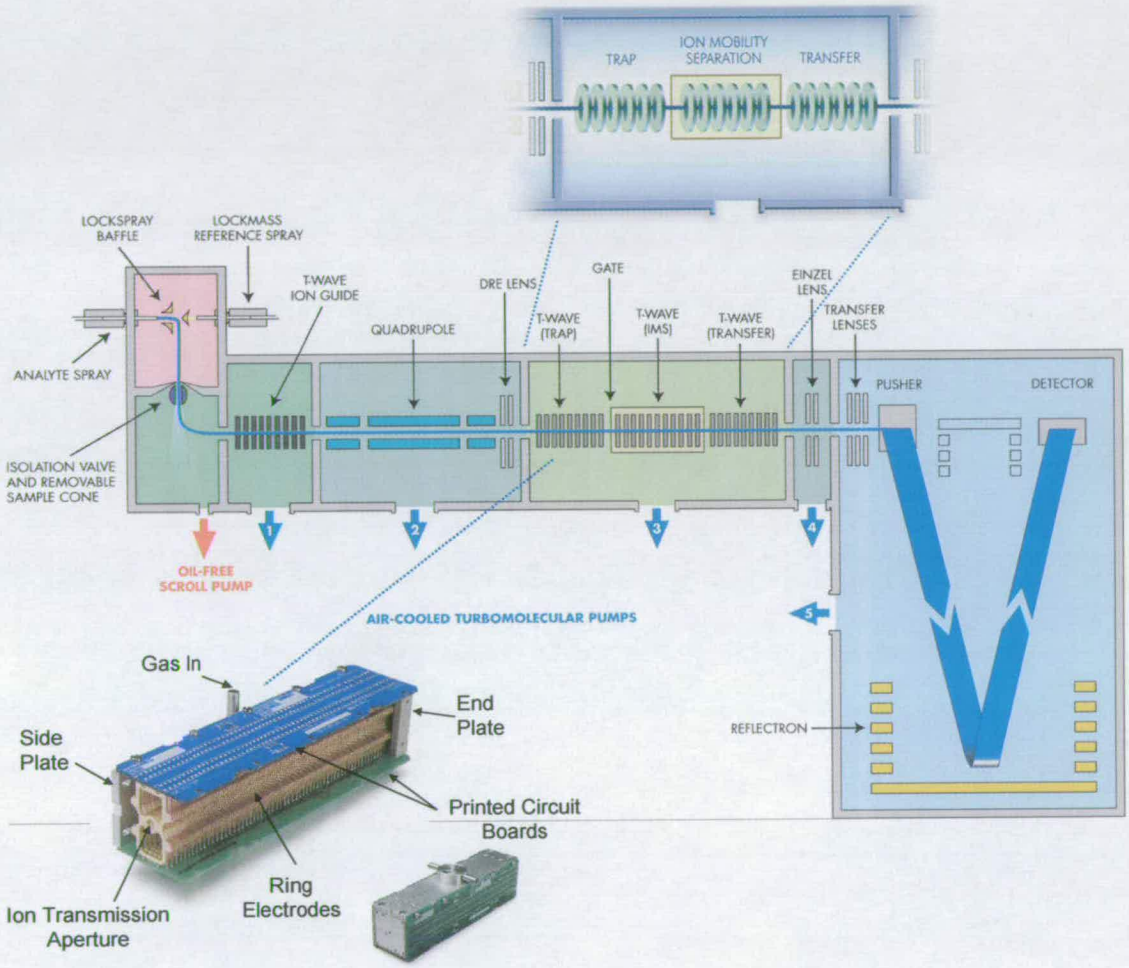

Figure 6.3 A schematic diagram of the Synapt HDMS system (reproduced from the previously published scheme).[7] All the turbomolecular pumps have pumping speed of 2201/s and are backed by 35 m^3/h scroll pump.

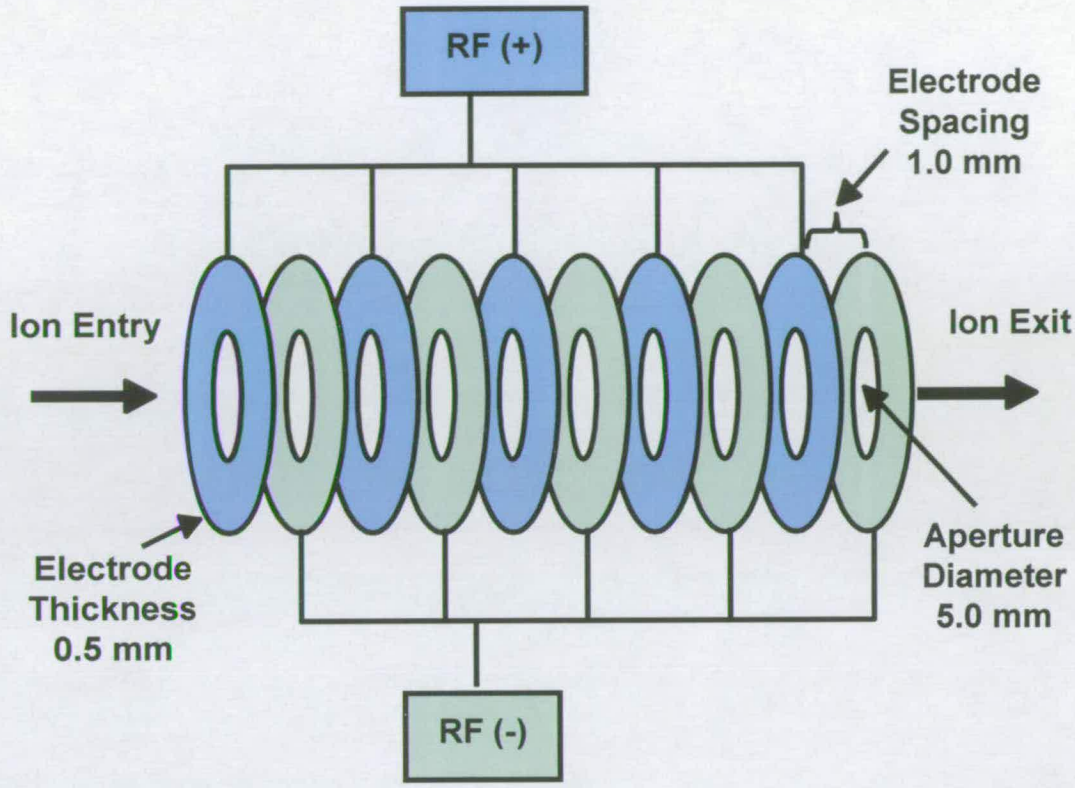

Figure 6.4 A schematic diagram of an RF-only stacked ring ion guide (based on the previously published scheme).[8]

6.2 Experimental Section

6.2.1 Preparation of Complexes

All complexes were synthesized using a similar procedure. Typically 2 mol equiv of en was added to a methanolic solution of $[(\eta^6\text{-arene})RuCl_2]_2$, where arene = *o*-terphenyl (*o*-terp), *m*-terphenyl (*m*-terp) or *p*-terphenyl (*p*-terp). Details for individual reactions and characterization of complexes (**1** $[(\eta^6\text{-}p\text{-terp})Ru(en)Cl]^+$, **2** $[(\eta^6\text{-}o\text{-terp})Ru(en)Cl]^+$ and **3** $[(\eta^6\text{-}m\text{-terp})Ru(en)Cl]^+$) are described in Chapter 3.

6.2.2 Preparation of samples

Complexes **1**, **2** and **3** were dissolved in methanol to a concentration of 1 ng/μL (ca. 2 μM) prior for analysis.

6.2.3 Hybrid quadrupole/ion mobility/oa-ToF MS instrumentation

Experiments were performed using the Waters (Manchester, UK) Synapt HDMS (high definition mass spectrometer) instrument shown in Figure 6.3. This instrument has been described in detail elsewhere.[7, 8] In brief, the instrument has a hybrid quadrupole/ion mobility/orthogonal acceleration time-of-flight (oa-ToF) geometry. Ions are transported to the mobility separation section through the quadrupole analyser, which in this work was operated in both resolving and non-resolving mode depending on the experiment. The mobility section comprises three consecutive, gas filled, travelling wave (T-Wave) RF ion guides. Ions are accumulated in the first (Trap) T-Wave and periodically released into the second (Mobility) T-Wave, where they separate according to their mobility through action of a continuous train of transient voltage pulses (travelling waves; *vide infra*). The separated ions are then propelled through the third (Transfer) T-Wave into the oa-ToF analyser for mass analysis.

The Mobility T-Wave consists of 61 electrode pairs, while Trap and Transfer T-Waves consist of 33 electrode pairs each. Ion drift times or arrival time distributions (ATDs) are recorded by synchronisation of the oa-ToF mass spectral acquisition with

the release of ions from the Trap to the Mobility device. In this study ions were released from the Trap for 100 μs every 10 ms. Mass spectra were acquired in positive ion mode. The instrument was operated with a capillary voltage of 3.0 kV. The ion source block and nitrogen desolvation gas temperature were set to 80°C and 150°C, respectively. The Trap and Transfer T-Waves were operated at approximately 10^{-2} mbar of argon and the ion mobility T-Wave optimised between 2.05 mbar of nitrogen. The Mobility T-wave was operated at 300 m/s and the pulse height optimised between 28.4 V for separation.

Data acquisition and processing were carried out using MassLynx (V4.1) software supplied with the instrument. The data were acquired and processed by Dr. Jonathan P. Williams (University of Warwick) and Kevin Giles (Waters MS Technologies Centre, Micromass UK Ltd., Manchester).

6.2.4 Estimation of collision cross-section (CCS) measurement using the T-Wave based ion mobility device

The experiments were performed by Dr Jonathan P. Williams. Instrument mobility calibration was performed by measuring the arrival times of ionic species whose absolute CCS have previously been determined using drift-cell technology as explained in detail previously.[9, 10] CCS calibration of the Synapt was undertaken using the tryptic peptide ions produced from human hemoglobin whose absolute CCS values are known from drift-tube studies.[11] Drift time measurements obtained from a single pulse height were normalised with respect to the square root of the reduced mass and charge. Reduced mass is defined as, $\mu = (M_{ion} \times m_{gas} / M_{ion} + m_{gas})$. A

correction factor is applied to the ATDs for ions obtained from the reference tryptic peptides such that their differences correspond to those measured using a DC system. This corrects for potential non-linear relationships between an ion's ATD and collision cross-section together with flight time offsets in the system as previously discussed.[12]

6.3 Results

IM in combination with MS has been used in this study to probe the differences in size and shape of the isomeric ruthenium terphenyl complexes **1**, **2** and **3**. The difference in size and shape of complexes could influence, for example, their diffusion into cells and cellular uptake. If complexes are entering the cell by passive diffusion smaller size should aid uptake.[13]

Isomeric complexes **1**, **2** and **3** were detected at *m/z* 427.06 (Figure 6.5) corresponding to $[M]^+$ (calcd for $C_{20}H_{22}ClRuN_2^+$ $[M]^+$ m/z 426.90). The peak observed at *m/z* 391.08 corresponded to $[M\text{-}HCl]^+$ (calcd for $C_{20}H_{21}RuN_2^+$ $[M\text{-}HCl]^+$ m/z 390.44).

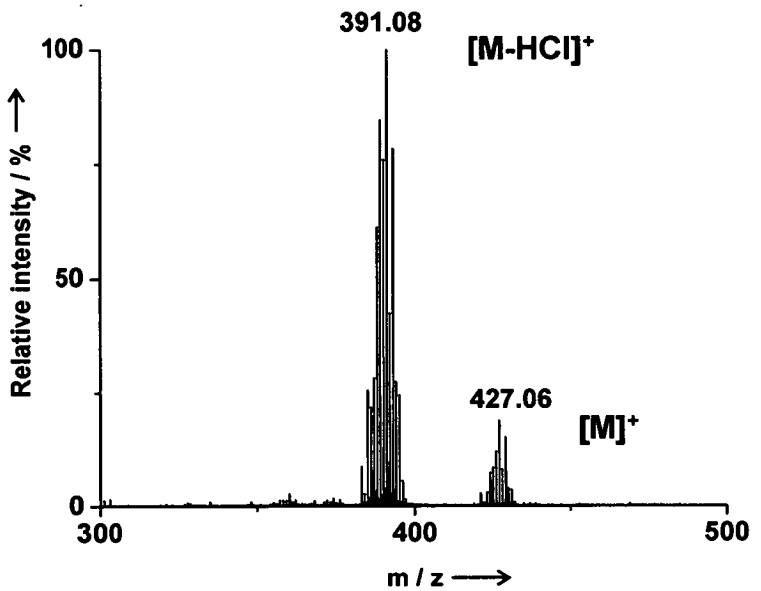

Figure 6.5 ESI mass spectrum of a 1 ng/μL (ca. 2 μM) methanol solution of complex **1**.

Arrival-time distributions (ATDs) of *m/z* 427.1 from a mixture of complexes **2** and **1** showed a significant difference in arrival time of 550 μs (4.17 ms for **2** and 4.72 ms for **1**; Figure 6.6A). A slightly smaller difference of 500 μs in arrival time was observed for the mixture of **3** and **1** (4.22 ms for **3** and 4.72 ms for **1**; Figure 6.6B). When all three isomeric complexes are mixed together, **2** and **3** merge into one peak and have an ATD centred around 4.22 ms. The ATD for complex **2** (dashed line; Figure 6.6C) is compared with the ATD of the mixture of **3** and **1** in Figure 6.6C highlighting the small but reproducible difference in arrival time of complexes **2** and **3**. For a more detailed analysis of the IM data the arrival times were converted into CCS values, shown in Table 6.1.

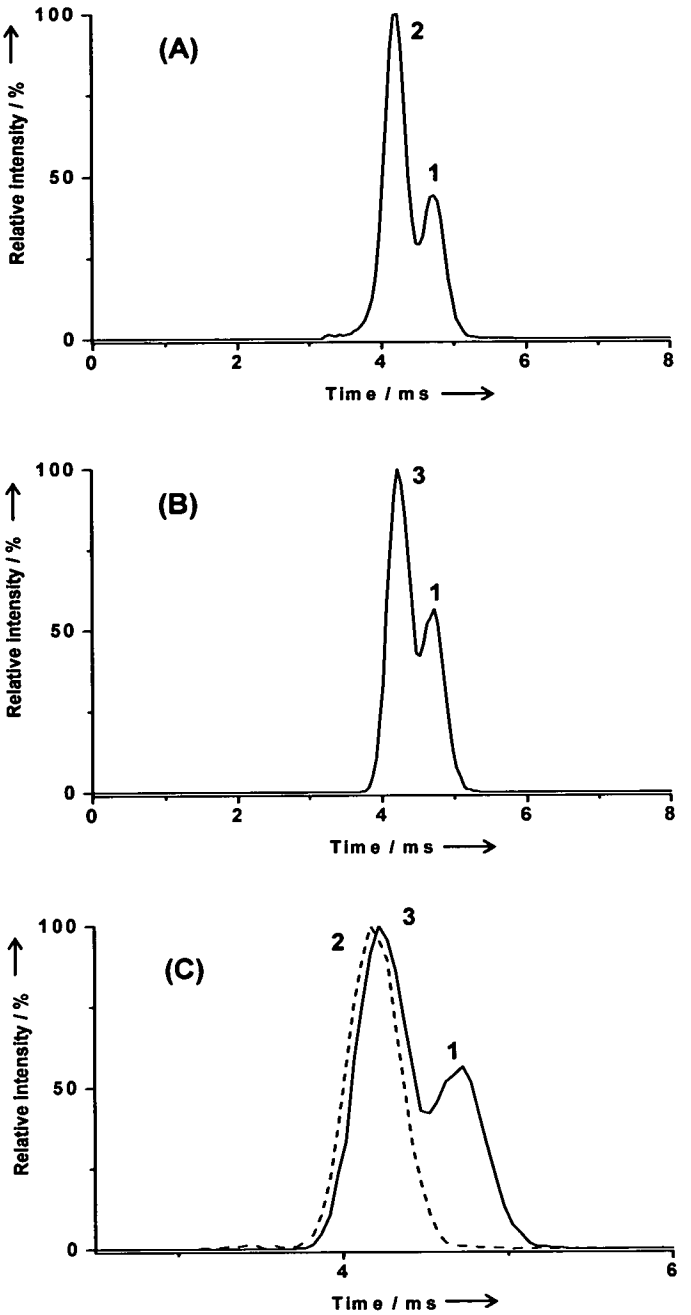

Figure 6.6 (A) Ion mobility (IM) arrival time distribution (ATD) of 1 ng/μL (methanol) solution of the mixture of complexes **2** and **1** (1:1) (**B**) IM ATD of 1 ng/μL (methanol) solution of complexes **3** and **1** (1:1 mixture) and (**C**) IM ATD of the mixture (1:1) of complexes **3** and **1** (solid line) in methanol (1ng/μL) overlaid with IM ATD of the solution (1 ng/μL in methanol) of complex **2** (dotted line), highlighting the subtle differences in arrival times of **2** and **3**.

Table 6.1 The estimated collision cross-section (CCS) measurements of complexes **1**, **2** and **3**, obtained using ion mobility (IM)

Complex	Estimated CCS ($Å^2$)
1	120.6
2	113.0
3	113.6

6.4 Discussion

The separation of some isomeric aromatic hydrocarbons (arenes) has been explored previously with a differential mobility spectrometer without MS.[1] IM-MS data obtained previously for $Cu(DAC)^{2+}$, where DAC = 1,8-bis(9-methylanthracyl)cyclam and cyclam = 1,4,8,11-tetraazacyclotetradecane, showed that this powerful technique can be used to probe the shape and number of existing conformers of the complex, which can be separated as a function of differences in collision cross-section.[14]

Here it has been possible for the first time, to separate a mixture of Ru^{II} isomeric arene anticancer complexes **1** and **3**, and **1** and **2**, but similarities in conformation (shape) of complexes **2** and **3** render them difficult to separate using the present ion mobility approach. Furthermore, similar in their size and shape complexes **2** and **3** (more compact) showed reduced anti-cancer activity, while the complex that differs

the most in size and shape (complex **1**, more elongated) showed the best potency (Chapter 3).

6.5 Summary

Ruthenium(II) anti-cancer isomer complexes have the same mass and charge and measured differences in ion mobility arrival times were a result of differences in collision cross-section (CCS), which relates to structural conformation in the gas-phase. Overall, here we have shown that isomeric Ru^{II} terphenyl anticancer complexes can be separated as a function of a difference in CCS. Arrival-time distributions of *m/z* 427.1 from a mixture of isomeric complexes **2** and **1**, and **3** and **1** showed significant differences, while similarities in conformation of **2** and **3** render them difficult to separate. These observations correlate with the fact that the differences in shape of these complexes cause differences in anticancer activity. More similar in shape, complexes **2** and **3** showed reduced anti-cancer activity, and the one that differs the most in shape (complex **1**) showed the best potency (Chapter 3).

6.6 References

(1) Borsdorf, H.; Nazarov, E. G.; Miller, R. A. *Anal. Chim. Acta* **2006,** *575*, 76-88.

(2) Kanu, A. B.; Dwivedi, P.; Tam, M.; Matz, L.; Hill, H. H., Jr. *J. Mass Spectrom.* **2008,** *43*, 1-22.

(3) Colton, R.; D'Agostino, A.; Traeger, J. C. *Mass Spectrom. Rev.* **1995,** *14*, 79-106.

(4) Henderson, W.; Nicholson, B. K.; McCaffrey, L. J. *Polyhedron* **1998,** *17*, 4291-4313.

(5) Traeger, J. C. *Int. J. Mass Spec.* **2000,** *200*, 387-401.

(6) Wu, C.; Siems, W. F.; Klasmeier, J.; Hill, H. H., Jr. *Anal. Chem.* **2000,** *72*, 391-395.

(7) Pringle, S. D.; Giles, K.; Wildgoose, J. L.; Williams, J. P.; Slade, S. E.; Thalassinos, K.; Bateman, R. H.; Bowers, M. T.; Scrivens, J. H. *Int. J. Mass Spectrom.* **2007,** *261*, 1-12.

(8) Giles, K.; Pringle, S. D.; Worthington, K. R.; Little, D.; Wildgoose, J. L.; Bateman, R. H. *Rapid Commun. Mass Spectrom.* **2004,** *18*, 2401-2414.

(9) Williams, J. P.; Scrivens, J. H. *Rapid Commun. Mass Spectrom.* **2008,** *22*, 187-196.

(10) Ruotolo, B. T.; Giles, K.; Campuzano, I.; Sandercock, A. M.; Bateman, R. H.; Robinson, C. V. *Science* **2005,** *310*, 1658-1661.

(11) Valentine, S. J.; Counterman, A. E.; Clemmer, D. E. *J. Am. Soc. Mass Spectrom.* **1999,** *10*, 1188-211.

(12) Ruotolo, B. T.; Hyung, S.-j.; Robinson, P. M.; Giles, K.; Bateman, R. H.; Robinson, C. V. *Angew. Chem.-Int. Ed.* **2007,** *46*, 8001-8004.

(13) Puckett Cindy, A.; Barton Jacqueline, K. *J. Am. Chem. Soc.* **2007,** *129*, 46-7.

(14) Baker, E. S.; Bushnell, J. E.; Wecksler, S. R.; Lim, M. D.; Manard, M. J.; Dupuis, N. F.; Ford, P. C.; Bowers, M. T. *J. Am. Chem. Soc.* **2005,** *127*, 18222-18228.

Chapter 7

Conclusions and Future work

"The real voyage of discovery consists not in seeking new landscapes but in having new eyes."

Marcel Proust

7.1 Conclusions

This thesis is concerned with synthesis and characterization of ruthenium(II) arene complexes of the general formula $[(\eta^6\text{-arene})Ru(N,N)X]^{0/+}$, where arene = benzene or benzene derivative, N,N = chelating ligand and X = leaving group. Synthesis and characterization of starting materials, ruthenium dimers of the type $[(\eta^6\text{-arene})RuCl_2]_2$, reduction of arenes as well as purification of diene products used in synthesis of the dimmers, are reported. The focus is on the synthesis of novel Ru^{II} arene complexes containing features such as arene ligands capable of intercalation into DNA bases or redox active chelating ligands. The control of stereochemistry of chelating ligands and examination of solid and solution state structures are attempted. Determination of the cytotoxicity and potential cellular targets for these complexes are attempted as well. The structure-activity relationships are investigated.

Preparation and characterization of complexes $[(\eta^6\text{-arene})Ru(en)Cl]^+$, where arene = *ortho-*, *meta-* or *para*-terphenyl (*o-*, *m-* or *p*-terp) are reported, together with those of appropriate dimers and diene ligands used in their preparation. The separation and purification of dienes are reported as well. The cancer cell cytotoxicity, cell uptake and DNA binding properties of the terphenyl complexes are investigated. The complex containing *p*-terp showed higher activity against cancer cell lines, compared to the analogues where arene = *o-* or *m*-terp. The extent of the complex uptake into A2780 or A2780cis cells shows that higher amounts of $[(\eta^6\text{-}o\text{-terp})Ru(en)Cl]^+$ or $[(\eta^6\text{-}m\text{-terp})Ru(en)Cl]^+$ complexes are needed compared to the *p*-terp analogue in cells to induce the same cytotoxic effect. $[(\eta^6\text{-}p\text{-terp})Ru(en)Cl]^+$ binds to DNA rapidly and

quantitatively, and causes significant DNA unwinding. Circular dichroism, competitive binding experiments with ethidium bromide and DNA melting data are consistent with combined intercalative and monofunctional (coordination) binding mode of *p*-terp complex, while *o*- and *m*-terp analogues bind preferentially through the coordination. The unusual DNA binding mode of $[(\eta^6\text{-}p\text{-terp})\text{Ru(en)Cl}]^+$ therefore makes a major contribution towards the high potency of the complex.

Arrival-time distributions of *m/z* 427.1 from mixtures of these isomeric terphenyl complexes showed that similarities in conformation of $[(\eta^6\text{-}o\text{-terp})\text{Ru(en)Cl}]^+$ and $[(\eta^6\text{-}m\text{-terp})\text{Ru(en)Cl}]^+$ render them difficult to separate using ion mobility in combination with mass spectrometry. Both *o*- and *m*-terp complexes are well separated from the *p*-terp analogue.

Changing the en chelating ligand in $[(\eta^6\text{-arene})\text{Ru(en)Cl}]^+$ to bipyridine (bipy) or deprotonated 2,2′-bipyridine-3,3′-diol (bipy(OH)O) and the arene from terphenyl to indane, leads to reduction in extent of binding of these complexes to DNA. DNA binding studies of $[(\eta^6\text{-indane})\text{Ru(N,N)Cl}]^{0/+}$, where N,N = bipy or bipy(OH)O, suggest that DNA is not the major target for this type of complexes. Neither $[(\eta^6\text{-indane})\text{Ru(bipy)Cl}]^+$ nor $[(\eta^6\text{-indane})\text{Ru(bipy(OH)O)Cl}]$ bind strongly to DNA. In general Ru^{II} arene bipy(OH)O complexes showed the significant cytotoxic activity towards cancer cells, in contrast to analogous complexes containing bipy or bipy with 4,4′-substituents such as Me. X-ray crystal structures and ^{1}H NMR spectroscopy has shown that deprotonated 2,2′-bipyridine-3,3′-diol (bipy (OH)O) can form a strong intraligand H-bonding system which enforces planarity on bipy(OH)O. Strong binding to 9-EtG can occur for complexes containing bipy(OH)O as well as for those containing bipy. An interesting feature of the structures of complexes with tetrahydroanthracene (tha) as arene is the presence of arene CH···π (bipy(OH)O and

bipy) interactions. Using DFT calculations these interactions were found to be more stable compared to π-π interactions between the arene and 9-EtG. As the latter are known to stabilize DNA adducts, this contributes towards the statement that the DNA adducts of the tha complexes wouldn't be additionally stabilized.

The stability of 9-EtG adducts was as well investigated for complexes containing *o*-benzoquinonediimine (*o*-bqdi) and *o*-phenylenediamine (*o*-pda) as chelating ligands. The formation of less stable 9-EtG adducts of [(η^6-hmb)Ru(*o*-bqdi)Cl][PF_6] compared to the adducts of [(η^6-*p*-cym)Ru(*o*-pda)Cl][PF_6] is suggested to be a reason for the inactivity of [(η^6-hmb)Ru(*o*-bqdi)Cl][PF_6]. The formation of the less stable adduct would lead to the weakened binding to DNA, which explains inactivity of the complex. In general complexes containing *o*-pda as the chelating ligand have shown loss of cytotoxic activity towards cancer cells when the chelating ligand is oxidized to *o*-bqdi. It is shown that the loss of activity can be attributed as well to the absence of hydrolysis, as found for [(η^6-*p*-cym)Ru(*o*-bqdi)I][PF_6] and loss of ability of binding to DNA, as a potential target. The ligand-based oxidation can be controlled through changes in electronic properties of the other ligands in the complex. The ligand-based oxidation can be followed by UV-Vis and ^{1}H NMR spectroscopy and the oxidation form can be distinguished in the x-ray crystal structure, based on differences in bond lengths within *o*-pda and *o*-bqdi ligands. *o*-Bqdi complex [(η^6-*p*-cym)Ru(*o*-bqdi)I][PF_6] is involved in redox reactions with glutathione, and as a result glutathione is oxidized and the complex reduced to form [(η^6-*p*-cym)Ru(*o*-pda)I][PF_6]. Once all glutathione is oxidized, [(η^6-*p*-cym)Ru(*o*-pda)I][PF_6] undergoes ligand-based oxidation under oxygen from air and [(η^6-*p*-cym)Ru(*o*-bqdi)I][PF_6] is recovered.

7.2 Future work

The following experiments would lead to the synthesis of novel mono- and di-nuclear complexes, to further insight into the cellular mechanism of action of Ru^{II} arene complexes and further exploration of the structure-activity relationships.

7.2.1 DNA structural distortion induced by terphenyl Ru^{II} arene complexes

Studies of the interactions of terphenyl complexes (*o*-, *m*- and *p*-terp, Chapter 3) with double-stranded DNA and the characterization of the resulting structural perturbations could be performed by *ab initio* and classical molecular dynamics simulations. This could provide more information on differences in induced structural distortions in DNA by $[(\eta^6\text{-}o\text{-terp})Ru(en)Cl]^+$, $[(\eta^6\text{-}m\text{-terp})Ru(en)Cl]^+$ and $[(\eta^6\text{-}p\text{-terp})Ru(en)Cl]^+$. Previously, the binding processes were investigated for $[(\eta^6\text{-}p\text{-cymene})Ru(en)X]^+$ and $[(\eta^6\text{-}p\text{-cymene})Ru(pta)X_2]$ complexes, where X = leaving group, en = ethylenediamine and pta = monodentate phosphine 1,3,5-triaza-7-phosphaadamantane, by the means of *ab initio* and classical molecular dynamics simulations. It was found that both complexes bind easily through the Ru centre to the *N7* of guanine (G) bases, but once bound these two complexes induce different structural distortions. It was found that the strain induced in the DNA backbone from en complex is released by a local break of a Watson-Crick base-pair (local denaturation). The bulkier pta complex bends the DNA helix towards the major

groove, resembling the characteristic DNA distortion like that induced by cisplatin.[1] As *o*- and *m*-terp complexes are bulkier compared to the *p*-terp analogue, the expected differences in structural distortion of DNA induced by these complexes would be of a great importance to confirm.

7.2.2 Sandwich bis-p-terp complex

$[(\eta^6\text{-}p\text{-terp})Ru(en)Cl]^+$ is the most potent complex in the series of isomeric terphenyl complexes, and the one that shows combined coordinative and intercalative binding modes (Chapter 3). Therefore, it would be of a great interest to prepare bis-*p*-terp complex $[(\eta^6\text{-}p\text{-terp})_2Ru]^{2+}$, study DNA binding properties and examine the contribution of only intercalative mode of binding versus the combined (coordination and intercalation) observed for $[(\eta^6\text{-}p\text{-terp})Ru(en)Cl]^+$. Sandwich $FeCp^+$ complexes of *o*-, *m*-, and *p*-terp have been synthesized previously by ligand exchange reactions[2] between ferrocene and terphenyl.[3]

7.2.3 Dinuclear terphenyl complexes

1′,4′,1″,4″-Tetrahydro-*p*-terphenyl (th-*p*-terp, Chapter 2) can be used in the synthesis of dinuclear Ru^{II} complex $[(\eta^6\text{-}p\text{-terp})Ru_2(en)_2Cl_2]^{2+}$. As there is a possibility for Ru being coordinated to only one terminal ring of th-*p*-terp, forming a mononuclear $[(\eta^6\text{-dh-}p\text{-terp})Ru(en)Cl]^+$ (dh = dihydro) complex, the separation of these might be required. This should not create additional problems as these two complexes would

have a different charge, which would lead to differences in their solubility. Mass spectra of $FeCp^+$ *o*-, *m*-, and *p*-terp complexes showed the existence of mononuclear and dinuclear complexes for all isomers. The mononuclear and dinuclear products have been isolated by using the difference in solubility; the mononuclear complex is soluble in dichloromethane, while the dinuclear complex is soluble in acetone.[3]

The DNA binding studies of $[(\eta^6\text{-}p\text{-terp})Ru_2(en)_2Cl_2]^{2+}$ could be performed in order to examine a possibility of interstrand cross links. The Ru^{III} *mer*-[Ru(terpy)Cl_3] (terpy = 2,2′:6′,2″-terpyridine) is reported to be exceptionally cytotoxic in comparison to Ru^{II} complexes [Ru(terpy)(bpy)Cl]Cl and *cis*-[Ru(bpy)$_2$Cl$_2$] (bpy = 2,2′-bipyridine).[4] The reason for such behaviour is suggested to be that in a cell-free medium, the Ru^{III} trichlorido complex coordinates to DNA preferentially at guanine residues forming interstrand cross-links. Thus, an important feature for biological activity of ruthenium complexes can be DNA interstrand cross-linking.

7.2.4 Cellular uptake studies of bipyridine complexes

For positively charged $[(\eta^6\text{-indane})Ru(bipy)Cl]^+$ and neutral $[(\eta^6\text{-indane})Ru(bipy(OH)O)Cl]$, cellular uptake studies could provide additional information to help understand the difference in activity (Chapter 4). The cellular uptake of small molecules can be critical to their application as drugs. The cellular uptake of $[Ru(bipy)_2(N,N)]Cl_2$, where N,N = bipyridine (bipy), phenantralene or other bipy derivatives (with more extended aromatic system), by human cancer cells in general showed that enlargement of the aromatic ring system results in an increase in the cellular uptake.[5] This is in agreement with the higher affinity of the more

hydrophobic systems for the cell membrane. If complexes are entering the cell by passive diffusion, neutral charge, smaller size and greater hydrophobicity should aid uptake.[6] For cisplatin analogues, the complexes with the greatest lipophilicity exhibit the highest uptake (all the complexes studied were hydrophilic, with octanol/water partition coefficients of <1).[7] It has been reported that ligand hydrophobicity outweighs the influence of the charges.[8] Subtle features in organometallic complexes can exert major effects on cellular uptake. Therefore it would be of a great interest to determine the uptake of $[(\eta^6\text{-indane})\text{Ru(bipy)Cl}]^+$ and its bipy(OH)O analogue, to examine the effect of the overall charge of the complex, influence of the substituents and differences in π-systems of the chelating ligands.

7.2.5 o-Semiquinonediimine (o-sqdi) as a possible intermediate in the oxidation of o-phenylenediamine

7.2.5.1 Detection of the o-sqdi species

The mechanism of the oxidation of *o*-phenylenediamine (*o*-pda) to *o*-benzoquinonediimine (*o*-bqdi) in water is believed to occur via a multi-step mechanism (Chapter 5) as suggested for *o*-pda Pt^{II} chlorido complexes.[9] This behaviour is not apparent in methanol, and the different oxidation mechanism pathways might arise from the difference in oxygen solubility in these two solvents; oxygen is around 25 times more soluble in methanol than in water.[10] The oxidation pathway in water, therefore, might involve the formation of *o*-semiquinonediimine (*o*-sqdi) as an intermediate. In the literature there are several examples of complexes

containing *o*-sqdi.[11, 12] The existence of *o*-sqdi in water, could be examined by EPR spectroscopy. As the oxidation in water is relatively slow (Chapter 5), the detection of *o*-sqdi as an intermediate, could be possible. The EPR spectra of the previously described [Ru^{II}(bipy)$_2$(*o*-sqdi)] showed that the unpaired electron is located primarily on the *o*-sqdi ligand and therefore the description of the Ru-ligand species is Ru^{II}-*o*-sqdi.[12] An EPR study in water could confirm the presence of *o*-sqdi species, and provide the information on where the unpaired electron is located. Another technique for the examination of the mechanism of the oxidation is cyclic voltammetry (CV). With CV it could be distinguished if the process is a one or two electron process and if the oxidation is reversible.

7.2.5.2 The ability of o-phenylenediamine (o-pda) complexes to overcome cross-resistance towards A2780^{AD} cell line

o-Pda complexes have the ability to overcome cross-resistance with adriamycin (doxorubicin).[13] The reduction in resistance factor (RF) achievable by replacing ethylenediamine (en) in Ru^{II} arene complexes by *o*-pda can be dramatic (Chapter 5). Multi-drug resistance A2780^{AD} cells over-express the plasma membrane transporter P-170 glycoprotein. Proteins of the p-glycoprotein class, which are responsible for pumping drugs out of cells, appear to possess binding cavities lined on opposite faces with nonpolar (e.g. Phe) and negatively charged (e.g. Asp) residues.[14] Such a cavity might accommodate favourably positively charged complexes. Neutral or negatively charged compounds have a better chance to overcome cross-resistance towards A2780^{AD} cells. Therefore it is of particular importance to understand the mechanism

of *o*-pda oxidation (Chapter 5), in order to further investigate the mechanism of cross-resistance towards $A2780^{AD}$ cells.

7.2.6 Dinuclear mixed valent Ru complexes

The use of the 3,3′,4,4′-tetraimino-3,3′,4,4′-tetrahydrobiphenyl (L, Figure 7.1), as a chelating ligand for a dinuclear Ru complex of the type $[(\eta^6\text{-arene})_2Ru_2(L)Cl_2]^{n+}$ could possibly lead to the mixed valent complex as observed previously for $\{Ru^{III}(L)Ru^{II}\}\leftrightarrow\{Ru^{IV}(L^{2-})Ru^{III}\}$ species.[15] The evidence for the presence or the absence of the mixed valent situation usually comes from EPR spectroscopy.

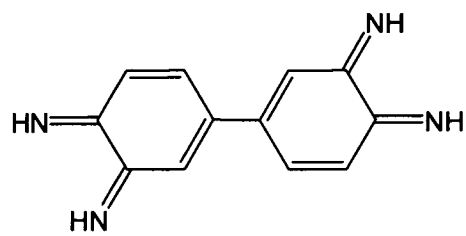

Figure 7.1 Chemical structure of 3,3′,4,4′-tetraamino-3,3′,4,4′-tetrahydrobiphenyl (L).

7.3 References

(1) Gossens, C.; Tavernelli, I.; Rothlisberger, U. *J. Am. Chem. Soc.* **2008,** *published on web 07/24/2008.*

(2) Lacoste, M.; Rabaa, H.; Astruc, D.; Ardoin, N.; Varret, F.; Saillard, J.; Le Beuze, A. *J. Am. Chem. Soc.* **1990,** *112*, 9548-9557.

(3) Masuhara, N.; Kamigaki, Y.; Nakashima, S.; Okuda, T. *Polyhedron* **2005,** *24* 1798–1802.

(4) Novakova, O.; Kasparkova, J.; Vrana, O.; Vliet, P. M.; Reedijk, J.; Brabec, V. *Biochemistry* **1995,** *34*, 12369-12378.

(5) Schatzschneider, U.; Niesel, J.; Ott, I.; Gust, R.; Alborzinia, H.; Woelfl, S. *Chem. Med. Chem.* **2008,** *3*, 1104-1109.

(6) Puckett Cindy, A.; Barton Jacqueline, K. *J. Am. Chem. Soc.* **2007,** *129*, 46-7.

(7) Ghezzi, A.; Aceto, M.; Cassino, C.; Gabano, E.; Osella, D. *J. Inorg. Biochem.* **2004,** *98*, 73-78.

(8) Schaefer, S.; Ott, I.; Gust, R.; Sheldrick, W. S. *Eur. J. Inorg. Chem.* **2007,** 3034-3046.

(9) Kockerbauer, R.; Bednarski, P. J. *J. Inorg. Biochem.* **1996,** *62*, 281-98.

(10) Hosono, E.; Fujihara, S.; Honma, I.; Zhou, H. *J. Mater. Chem.* **2005,** *15*, 1938-1945.

(11) Peng, S. M.; Chen, C. T.; Liaw, D. S.; Chen, C. I.; Wang, Y. *Inorg. Chim. Acta* **1985,** *101*, L31-L33.

(12) Masui, H.; Lever, A. B. P.; Auburn, P. R. *Inorg. Chem.* **1991,** *30*, 2402-10.

(13) Habtemariam, A.; Melchart, M.; Fernandez, R.; Parsons, S.; Oswald, I. D. H.; Parkin, A.; Fabbiani, F. P. A.; Davidson, J. E.; Dawson, A.; Aird, R. E.; Jodrell, D. I.; Sadler, P. J. *J. Med. Chem.* **2006,** *49*, 6858-6868.

(14) Yu, E. W.; McDermott, G.; Zgurskaya, H. I.; Nikaido, H.; Koshland, D. E., Jr. *Science* **2003,** *300*, 976-980.

(15) Kaim, W.; Lahiri, G. K. *Angew. Chem.* **2007,** *46*, 1778-1796.

Conferences Attended

(1) *Third International Symposium on Bioorganometallic Chemistry, Milan-Italy July 5th-8th, 2006., Book of Abstracts p. 61 and p. 74.-oral and poster presentations.*

Tijana Bugarčić, Abraha Habtemariam, Simon Parsons, Peter J. Sadler

Ruthenium(II) arene complexes containing bipyridines as chelating ligands: Chemistry and cancer cell cytotoxicity.

(2) *13th International Conference on Biological Inorganic Chemistry, Vienna-Austria July 15th-20th, 2007., Book of Abstracts p. S25.-poster presentation*

Tijana Bugarčić, Abraha Habtemariam, Peter J. Sadler

Contrasting aqueous chemistry and cancer cell cytotoxicity of ruthenium(II) arene complexes containing bipyridine derivatives.

Publications

(1) Bugarčić, T.; Novakova, O.; Halamikova, A.; Zerzankova, L.; Vrana, O.; Kasparkova, J.; Habtemariam, A.; Parsons, S.; Sadler, P. J.; Brabec, V. **Cytotoxicity, Cellular Uptake, and DNA Interactions of New Monodentate Ruthenium(II) Complexes Containing Terphenyl Arenes.** *Journal of Medicinal Chemistry*, ACS ASAP. CODEN: JMCMAR ISSN:0022-2623. AN 2008:990607 CAPLUS.

(2) Habtemariam, A.; Bugarčić, T.; Sadler, P. J.

Preparation of organometallic ruthenium(II) compounds and their cytotoxic activity. PCT Int. Appl. (2007), 46pp. CODEN: PIXXD2 WO 2007135410 A1 20071129 CAN 148:11346 AN 2007:1364145 CAPLUS-*patent.*

(3) Bugarčić T., Habtemariam A., Stepankova J., Heringova P., Kasparkova J., Deeth R. J., Johnstone R. D. L., Prescimone A., Parkin A., Parsons S., Brabec V., Sadler P. J.

The contrasting chemistry and cancer cell cytotoxicity of bipyridine and bipyridinediol ruthenium(II) arene complexes-*accepted for Inorganic Chemistry (front cover).*

(4) Bugarčić T., Habtemariam A., Deeth R. J., Fabbiani F., Parsons S. and Sadler P. J.

Ruthenium(II) arene anticancer complexes with redox-active diamine ligands-*in preparation.*

(5) Williams J. P., Bugarčić T., Habtemariam A. Gilles K., Rodger P. M. and Sadler P. J.

Separation of isomeric ruthenium(II) arene terphenyl complexes by ion mobility mass spectrometry-*submitted.*